EVALUATION OF AN AIR-TO-AIR CROSS FLOW PLATE HEAT EXCHANGER USING A NEW HEAT RECOVERY TEST FACILITY

Ian Ball

A Thesis

In

The Department of Building, Civil, and Environmental Engineering

Presented in Partial Fulfillment of the Requirements
for the Degree of Master of Applied Science (Building Engineering) at
Concordia University
Montreal, Quebec, Canada

September, 2003

Your file Votre référence
ISBN: 0-612-90999-9
Our file Notre référence
ISBN: 0-612-90999-9

ABSTRACT

EVALUATION OF AN AIR-TO-AIR CROSS FLOW PLATE HEAT EXCHANGER USING A NEW HEAT RECOVERY TEST FACILITY

Ian Ball

Air-to-air heat recovery is a means of energy conservation in buildings. The plate type cross flow heat exchangers is predominantly used in the HVAC industry because of their low cost, low pressure drop, and medium to high thermal effectiveness. The two main objectives of the present research are to design, fabricate and commission a new low cost innovative heat recovery test facility, and to utilize the facility to evaluate the thermal performance of cross flow plate type heat exchanger. The heat recovery test facility was designed based on two existing North American standards for testing air-to-air heat recovery devices: ASHRAE Standard 84-1991 and CSA standard C439-00. The test facility uses two independent closed loop ducts that incorporate variable frequency drives to provide precise control of airflow. Thermocouple sensors were embedded in the plate heat exchanger allowing for a determination of the bulk air temperature distribution on both the cold and hot sides of the heat exchanger at a top, middle and bottom planes. The design of the facility was preceded by a pre-test uncertainty analysis based on different sensor bias and operating conditions. The sensitivity results show that airflow measurements have the greatest impact on sensible effectiveness uncertainty. Sensible effectiveness is experimentally determined for both balanced and unbalanced airflow conditions and for varying inlet temperatures. Vertical obstructions of varying widths are placed at the entrance of the plate heat exchanger on both the cold and hot sides. Results of these tests indicate that sensible effectiveness does not decrease, and there is noticeable shrinkage of the cold corner in certain cases.

ACKNOWLEDGMENTS

I wish to extend my sincere thanks and appreciation to my supervisor, Dr. M. Zaheeruddin, for his patience and sage advice.

The installation of the test facility was no small feat, and I am grateful for the efforts of Joe Hrib, a technician for the department of Building, Civil and Environmental Engineering.

The data acquisition, a crucial component of any test facility, was fairly complex in the present research, and demanded, at times, highly creative problem solving. Luc Demers, an electronics and data acquisition technician for the department of Building, Civil and Environmental Engineering, was instrumental in the conception and installation of the data acquisition. He is credited with conceiving, designing, and fabricating a multiplexer that allowed for an enormous expansion in the data acquisition system.

I wish to express my appreciation for the company Circul-Aire Inc., a division of Dectron International, for providing the heat recovery unit for testing.

Mr. Jim Fung, who is one of the pioneering Engineers in air-to-air plate type heat exchangers, provided valuable insight into the design and application of cross flow heat exchangers.

Finally, I especially wish to thank members of my family for their support and patience during the entire process of my M.A.Sc. program. A special thanks for my mother, Mrs. Beryl Ball, a former English teacher, for providing advice on grammatical corrections.

This thesis is dedicated to the memory of the young Indonesian brother of my fiancée Jacklin, Rezka Simauw, who tragically passed away on March 17, 2003, and cannot realize his academic and life goals.

TABLE OF CONTENTS

LIST OF FIGURES

LIST OF TABLES

LIST OF SYMBOLS

α	Thermal diffusivity
a	Width of heat exchanger plate channel
A_{hts}	Heat transfer surface area of plate heat exchanger
A	Open face area of heat exchanger
A_d	Cross-sectional area in the airflow measuring station
b	Height of heat exchanger plate channel
c_{pa}	Thermal heat capacity of air
C_{max}	Maximum heat capacity of cold and hot side of the heat exchanger
C_{min}	Minimum heat capacity of cold and hot side of the heat exchanger
D_h	Hydraulic diameter of flow path within the heat exchanger
ϵ_l	Latent effectiveness
ϵ_s	Sensible effectiveness
$\epsilon_{s,ave}$	Average sensible
ϵ_T	Total effectiveness
h_c	Average heat transfer coefficient on cold side of plate heat exchanger
h_{cal}	Velocity pressure at airflow measuring station on the cold loop side
h_h	Average heat transfer coefficient on hot side of plate heat exchanger
h_{hal}	Velocity pressure at airflow measuring station on the cold loop side
H_d	Height of duct section at airflow measuring station
k_a	Thermal conductivity of air
L_d	Width of duct section at airflow measuring station
$\dot{m}_{cal}$	Mass airflow rate in the cold air loop
$\dot{m}_{hal}$	Mass airflow rate in the hot air loop
$\dot{m}_{min}$	Minimum mass airflow rate between cold and hot air loop side
n	Number of samples in a single test for a particular parameter
Nu	Nusselt number
NTU	Number of transfer units
ρ_{12}	Coefficient of correlation
ρ_{cal}	Air density at the airflow measuring station in the cold air loop side
P	Precision limit
P_b	Barometric pressure
Pr	Prandlt number

p_w	Water vapor pressure
p_{ws}	Saturated water vapor pressure
Q_{cal}	Airflow rate at airflow measuring station in cold air loop
Q_{hal}	Airflow rate at airflow measuring station in hot air loop
RH_{cal}	Relative Humidity at the measuring station in the cold air loop
RH_{cal}	Relative Humidity at the measuring station in the hot air loop
Re	Reynold's number
t	Student-t factor
S	Sample standard deviation
t_{ci}	Cold air inlet temperature at heat exchanger
t_{co}	Cold air outlet temperature at heat exchanger
t_{hi}	Hot air inlet temperature at heat exchanger
t_{ho}	hot air outlet temperature at heat exchanger
t_{cal}	Air temperature at airflow measuring station in cold air loop
t_{hal}	Air temperature at airflow measuring station in hot air loop
U	Overall thermal conductance of plate heat exchanger
U_{Ad}	Airflow measuring station cross sectional area uncertainty
μ_b	Dynamic viscosity of bulk airstream
U_ε	Sensible effectiveness uncertainty
$U_{\varepsilon ave}$	Average sensible effectiveness uncertainty
U_h	Velocity pressure uncertainty
U_L	Length dimension uncertainty
U_{Pb}	Barometric pressure uncertainty
$U_{\rho cal}$	Air density uncertainty at airflow measuring station in cold air loop
U_{pws}	Saturated vapor pressure uncertainty
U_{RH}	Relative humidity uncertainty
μ_s	Dynamic viscosity of the airstream nearest to the plate heat exchanger surface
U_{sp}	Static pressure uncertainty
U_T	Air temperature uncertainty
U_{Wcal}	Humidity ratio uncertainty
U_{Vcal}	Air velocity uncertainty at airflow measuring station in cold air loop
ν	Degrees of freedom in relation to statistics
υ	Dynamic viscosity
V_{cal}	Average air velocity at airflow measuring station in cold air loop

V_{hal} Average air velocity at airflow measuring station in hot air loop

W_{cal} Humidity ratio at airflow measuring station in cold air loop

W_{hal} Humidity ratio at airflow measuring station in hot air loop

1.0 INTRODUCTION

1.1 The Need for Air-to-Air Heat Recovery

The latest spike in crude oil prices in response to the current situation in the Middle East highlights the volatility of the fossil fuel markets and the persistent need for energy conservation. Levine, Price et al., (1996), as part of the World Energy Council (WEC), completed a comprehensive two-year collaborative research project involving participants from 10 countries. In regard to the building sector, the research revealed that approximately 36% of the world's primary energy is consumed by commercial and residential buildings. It also found that energy usage in this sector had been growing by an average annual rate of 2.8% between 1971 and 1992. Even more alarming is the future trends of world energy demand. The WEC forecasts that without any change in current practices, world energy demand in 2020 would be 50-80% higher than levels in 1990. Cox, and Miro (2000) have submitted a report examining Canada's Energy usage. In 1997, the combined building sector was responsible for 31% of the overall energy consumption, as compared with the industrial sector that consumed 39%, and the transportation sector that consumed 27%. Commercial and institutional buildings comprise 13% of the building sector energy demand. Canada, being a cold climate country, realized the largest usage of energy in space heating, 52% of the 13% mentioned above. It was also found that between 1990 and 1997, energy consumption in the commercial and institutional building sector increased by 13.4%. Needless to say, air-to-air energy recovery has the potential to play a major role in reducing energy consumption in buildings. Currently there is only a fraction of existing buildings that incorporates some form of air-to-air energy recovery. The other major issue relating to the need for air-to-air heat recovery is indoor air quality. The current standard in North America for indoor air quality, ASHRAE standard 62-1989, stipulates quantities of outdoor air for different types of occupancy. This need for outdoor air places extra demand on energy usage. However, air-to-air energy recovery allows for a significant reduction of operational costs over the life a building as a result of reduced energy use from boilers, electric heating, chillers, air cooled or water cooled condensers.

1.2 Air-to-Air Heat Recovery

Buildings, either new or retro-fit, that exhaust air, and simultaneously make-up a certain percentage of outdoor air to maintain building pressurization, are potential candidates for applications of air-to-air energy recovery. Energy can be recovered during winter or summer periods. Most energy recovery devices require the proximity of outdoor air and exhaust air ductwork in order to run through the device. Run-around systems are not dependent on the proximity factor (ASHRAE, 2000). The coils for both the supply and exhaust side can be located at a distance and connected by piping. A pump is required to maintain water flow in the system. The other heat recovery devices require that the ductwork for supply and exhaust be routed next to each other to pass through the heat exchanger. There are three generic types of airflow configurations that correspond to the various heat recovery devices. A fourth type has been identified in this present paper to account for hybrid counter flows. The four types are listed as follows:

1. Counter flow
2. Hybrid Counter flow
3. Parallel flow
4. Cross Flow

Types 1., 2., and 4., will be discussed in detail in the following section for plate type heat exchanger. Parallel flow configuration has the lowest effectiveness of the four types and will not be discussed in the present thesis. Heat recovery devices can transfer either sensible or sensible and latent heat. Table 1.1 contains a list of the different types of air-to-air heat recovery devices. This table is based on ASHRAE Systems and Equipment (2000), chapter 42 for heat recovery. The value for cross contamination in the ASHRAE for heat pipes is incorrect since it states 0%. The heat pipes that are supplied by several manufacturers will not be able to maintain 0% cross contamination unless the partition between the two airstreams is completely sealed with epoxy or some other type of sealant material. For any heat recovery device that has a potential for cross contamination, the supply fan should be located on the entering side of the energy recovery

device to produce a positive pressure, and the exhaust fan should be located on the leaving side to produce a negative pressure. Therefore, any cross contamination will flow from the supply side to the exhaust side.

Table 1.1 Comparison of Air-to-Air Energy Recovery Devices (ASHRAE)

	Fixed Plate	Rotary Wheel	Heat Pipe	Run around Coil Loop	Thermosiphon
Airflow arrangements	Counter flow, Cross flow, Parallel flow	Counter flow, Parallel flow	Counter flow, Parallel flow	Counter flow, Parallel flow	Counter flow, Parallel flow
Equipment size, CFM (L/s)	50 (23.6) and up	50 to 70,000 (23.6 to 33,034 L/s)	100 and up (47.2 and up)	100 and up (47.2 and up)	100 and up (47.2 and up)
Types of heat transfer (effectiveness)	Sensible (50 to 80%)	Sensible (50 to 80%), Total (55 to 85%)	Sensible (45 to 65%)	Sensible (55 to 65%)	Sensible (40 to 60%)
Face velocity, fpm (m/s)-common design range	200 to 1000 (1 to 5.0)	500 to 1000 (2.5 to 5.0)	400 to 800 (2.0 to 4.0)	300 to 600 (1.5 to 3.0)	400 to 800 (2.0 to 4.0)
Typical Pressure Drop, in. w.c. (Pa)	0.02 to 1.8 (4.96 to 446)	0.4 to 0.7 (99.2 to 174)	0.4 to 2.0 (99.2 to 496)	0.4 to 2.0 (99.2 to 496)	0.4 to 2.0 (99.2 to 496)
Temperature Range °F (°C)	-70 to 1500°F (-57 to 816°C)	-70 to 1500°F (-57 to 816°C)	-40 to 95 °F (-40 to 35 °C)	-50 to 900 °F (-46 to 482 °C)	-40 to 105 °F (-40 to 40.6 °C)
Unique Advantages	No moving parts, low pressure drop, easily cleaned	Latent transfer, compact large sizes, low pressure drop	No moving parts except tilt	Exhaust airstream can be separated from supply air. Fan location not critical	Exhaust airstream can be separated from supply air. Fan location not critical
Limitations	Latent available in hygroscopic units only	Cold climate may increase service, Cross-air contimination	Effectiveness limited by pressure drop and cost , few suppliers	High effectiveness requires accurate simulation model	Effectiveness limited by pressure drop and cost , few suppliers
Cross Leakage	0 to 5%	1 to 10%	0 to 3%	0%	0%
Heat Rate Control Schemes	Bypass dampers	Wheel speed control over full range	Bypass dampers or tilt upto 10°	Bypass valve or pump speed control	Control valve over full range

1.3 An Overview of Plate Type Air to Air Heat Exchangers

The plate heat exchanger is a passive heat recovery device that contains no moving parts. Plate type heat exchangers consist merely of a stationary, thin, thermally conductive material that separates two moving fluids such as air. Sensible heat is transferred via the thin non-porous barrier by virtue of the temperature difference and the mass flow rates between the two fluids. A detailed discussion of the theory of heat transfer mechanism will be presented in section 2.4. The sensible effectiveness of plate heat exchangers is not as high as enthalpy wheels; however, the main advantages include:

- No moving parts
- Low cross contamination
- Large temperature range
- Relative low cost compared to other heat recovery devices

The materials that are used to fabricate fixed plate heat exchangers include

- Polypropylene
- Aluminum
- Epoxy coated aluminum
- Stainless Steel 304 or 316

Plate heat exchangers are modular in construction thus permitting a large range of CFM (L/s) from 500 CFM (236 L/s) to built up systems on site that have a capacity of 100,000 CFM (47,195 L/s). Some types of plate heat exchangers configurations are more flexible for modular construction than others. The various classifications of heat exchangers will be presented in section 1.3.1.

1.3.1 Plate Heat Exchanger Classification

Plate heat exchangers can be broadly divided into two main categories based on the geometry and airflow patterns through the heat exchanger:

1. Hybrid Counter Flow
2. Cross Flow

Each one of these categories describes how the two air streams flow in relation to each other.

Some manufacturers describe their plate heat exchangers as counter flow. However, upon closer analysis, it is physically impossible to construct an air-to-air plate heat exchanger that is a true counter flow configuration for the full length, L, of the heat exchanger. By definition, a counter flow configuration requires the two air streams to run at 180° to each other across the separating medium during the entire length, L, of the heat exchanger. Figure 1.1 illustrates the ideal flow arrangement for counter flow.

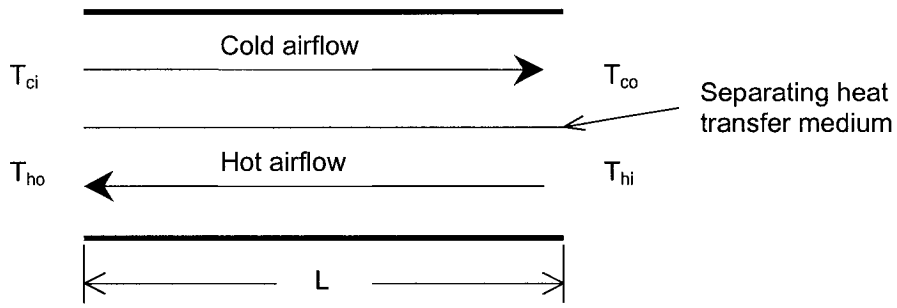

Figure 1.1 Ideal counter flow arrangement

In practice, however, counter flow heat exchangers can only be approximated, as shown in figure 1.2, which illustrates four common hybrid counter flow configurations. In the case of the "U" configuration the air enters the heat exchanger and then makes a sudden 90 ° turn through the main core, then makes another 90° at the exit. The "K" and "L" types have fewer bends and, therefore, a potential higher thermal effectiveness in conjunction with a lower pressure drop in comparison with a "U" type. Within each type of hybrid counter flow heat exchanger, the length d represents a hypothetical distance in which true counter flow heat transfer occurs. The "X" type does not show a d value, because the relative angle between the airflows may never obtain 180°. Depending on the entering air velocities and the degree of diffusion as the air passes through the heat exchanger towards the exit will determine the length of the zone, d, in which the relative angle between airflows will be approximately 180°. Outside of this zone, there is a mix of cross flow and counter flow. Although these heat exchangers are not true counter flow, nevertheless, the thermal effectiveness is generally higher than a cross flow configuration. Cross flow configuration requires that the two air streams flow 90° in relation to each other.

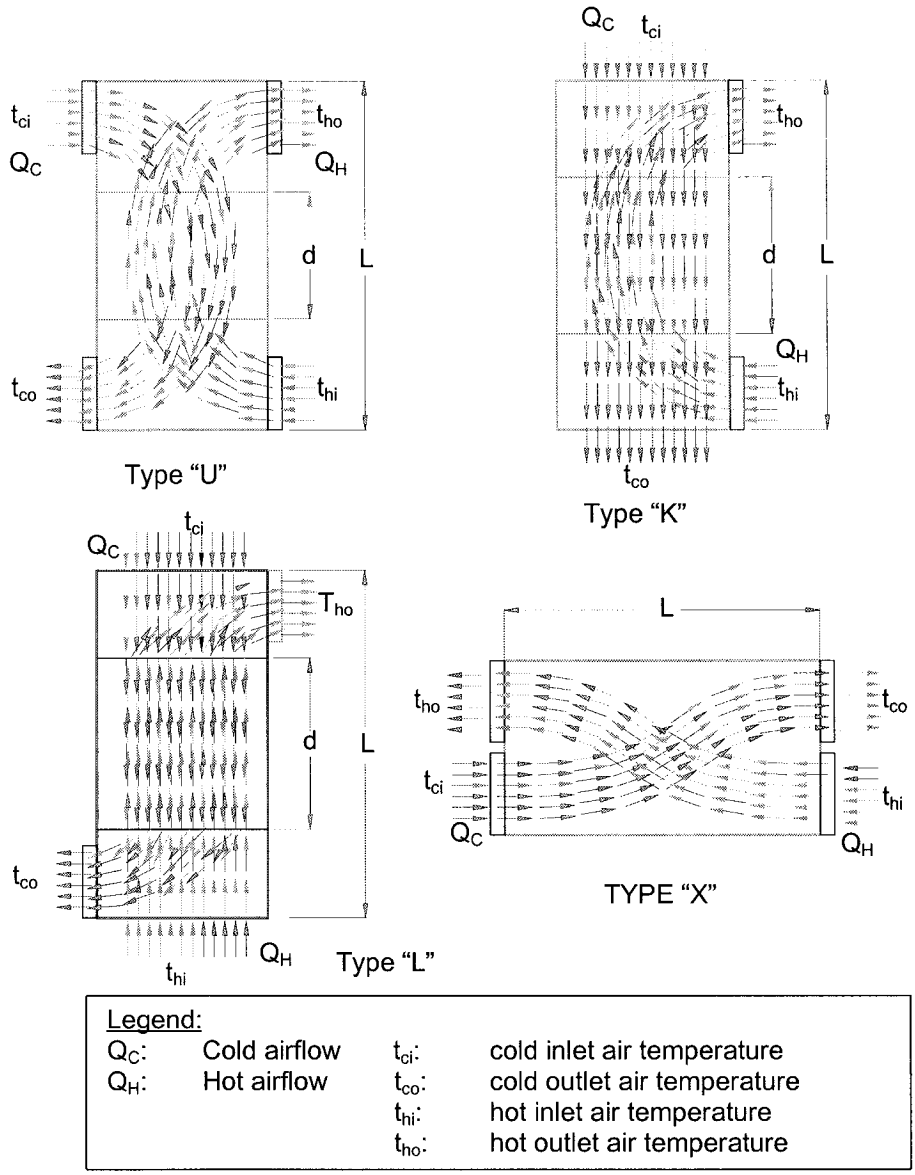

Figure 1.2 Typical hybrid counter flow arrangements for air to air plate type heat exchangers

Cross flow heat exchangers are most often installed in what is described in the industry as a diamond configuration which is a square core rotated 45° to accommodate horizontal ductwork or a package heat recovery air handling unit. As opposed to hybrid counter flow heat exchangers, cross flow heat exchangers are authentic in terms of the consistent angle of 90° between air streams for the entire length, L, of the core. The actual plates of the cross flow heat exchanger

can be either horizontal or vertical. Figure 1.3 can be portrayed as either a plan view or a side elevation view. Cross flow heat exchangers installed horizontally are limited by the weight of the plates pressing down on the bottom most plates. The capacity of horizontal units to support the full or partial weight of the heat exchanger is determined by the strength of the element separating the two plates. For example, dimples or ribbing is used to separate two plates. Depending on the number of dimples per square foot, the capacity of an individual dimple will determine how much weight can be applied on the bottom plates until the dimples collapse. Vertical plates do not have this problem and can be used in very large capacity systems.

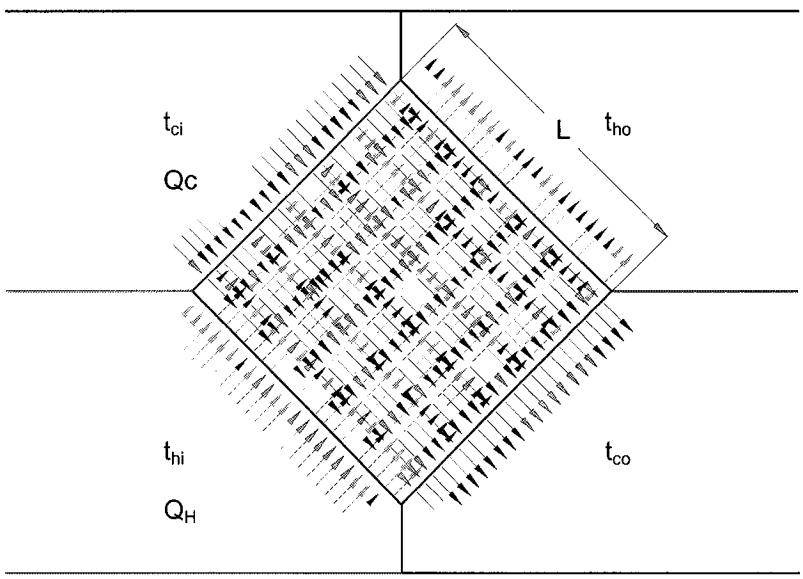

Figure 1.3 Typical cross flow heat exchanger in a diamond shape configuration within ductwork or an air-handling unit

Cross flow heat exchangers are flexible by nature to accommodate large airflows, since the cores are modular and can be built-up to larger cross sections, as shown in figure 1.4. A standard 36" x 36" (914 mm x 914 mm) core can be built-up to a 72" x72" (1829 mm x 1829 mm). As a result the amount of airflow in a 10 ft (3 m) width can now be doubled. For example, a 10' (3 m) wide 36" x 36" (914 mm x 914 mm) core is capable of handling a nominal 15,000 CFM (7079 L/s) at 500 fpm (2.5 m/s) face velocity. If a built-up section is used, i.e., 10' (3 m) wide 72" x 72" (1829 mm x 1829 mm) core, then the capacity of the unit doubles to 30,000 CFM (14,158 L/s), at 500 fpm 2.5 m/s) face velocity. In addition, there is 4 times the amount of surface area for a doubling of the

open face area. The residence time of the air within the core also doubles since the heat exchanger length doubles. Therefore, the effectiveness will increase but so will the pressure drop. Cross flow heat exchangers can also be configured to handle unbalanced airflows.

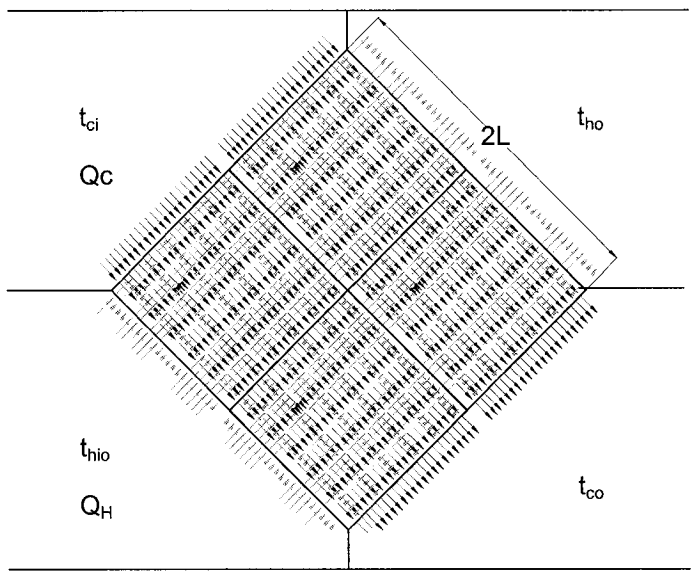

Figure 1.4 Built-up modular cross flow heat exchanger in a diamond shape configuration within ductwork or an air-handling unit

As revealed in figure 1.5, the core face has been doubled in the direction of the cold air stream but remains single in the direction of the hot air stream. However, the residence length of the hot air stream has doubled. The cold airflow rate is now double that of the hot airflow rate, creating an unbalanced system. The advantage of using a type of cross flow as presented in figure 2.5, page 30, permits the reduction of 50% of the surface area that would not significantly contribute to the overall thermal effectiveness. As a result, initial capital cost savings for the heat exchanger and operating costs due to lower pressure drops can be realized. If both sides of the unbalanced heat exchanger are based on a design face velocity of 500 fpm (2.5 m/s), then the pressure drop on the hot air side will be significantly higher since the residence time of the air is double than that of the other side. These types of unbalanced systems are used when one airflow is approximately half of the other. If the airflows do not differ more than 25%, then an unbalanced configuration may not be justified.

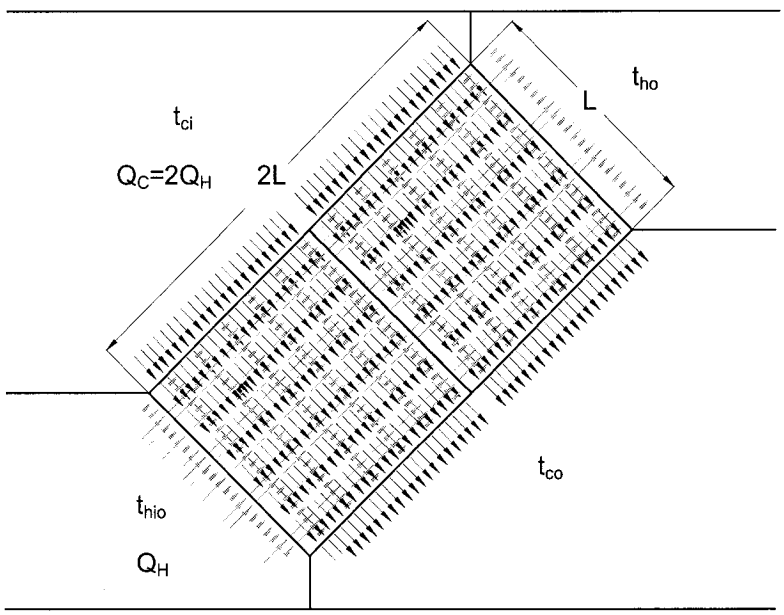

Figure 1.5 Built-up unbalanced modular cross flow heat exchanger

1.3.2 Plate Heat Exchanger Applications

Plate heat exchanger applications refer to the conditions of the air in terms of temperature, contaminant types and concentrations. If the air contains little or no contaminants and the temperature is within an acceptable range with regard to human comfort and safety, then it is defined as a comfort application. Air originating from or being supplied to an industrial or manufacturing process is defined as a process application. Based on these two broad definitions of comfort and process air, plate heat exchanger applications can be grouped into three main categories:

1. Process to Process
2. Process to Comfort
3. Comfort to Comfort

Process to Process

Plate heat exchangers are well suited for process applications due to the nature of their construction and the materials that can be used to build the heat exchanger core. Process to

process applications typically involve the transfer of heat from the exhaust of a process to the incoming air supplying the process. It is not uncommon for an industrial type heat exchanger to handle process air as high as 1600 °F (871 °C). The main considerations in the design of industrial plate heat exchanger include:

1. Corrosive air containing particulate matter or gaseous substances that will easily corrode regular steel or materials. Choice of heat exchanger material is essential to ensuring a long life for the heat exchanger.

2. Condensable liquid produced during the heat transfer process may contain acid of high concentration that must be removed.

3. Filtration can be used to minimize contaminants that reach the heat exchanger. Proper filtration will also reduce the frequency of cleaning.

4. Accessibility is required to clean the heat exchanger core. Drain pans should be placed underneath the entrances and exits of the heat exchange in order to collect water that is used to wash the heat exchanger core. These same drain pans can also serve to collect the condensable liquid during the operation of the unit.

5. The heat exchanger must be constructed in such a way as to account for thermal expansion. Typically stainless steel 316 is the material of preference for high temperature and resistance to a wide variety of gaseous contaminants and corrosive liquids.

Modulation of heat recovery for process to process is generally not necessary since the maximum efficiency is desired. Typical examples include dryers, kilns and ovens.

Process to Comfort

There are many instances in which process heat is wastefully exhausted instead of being recovered to preheat incoming outdoor air supplied to a space occupied by people. This application, process to comfort, can in some cases completely supplement space heating. Typical applications include foundries, strip coating plants, plating operations, molding ovens, paint ovens, and many others. Any process that generates hot gas exhaust is a potential candidate to provide heat recovery to a nearby occupied space. In some cases the amount of exhaust heat available is in excess of the amount required for space heating. There are a few techniques that can be used to regulate the of amount heat required which include:

1. Use of unbalanced air mass flow rates. In other words, the capacity of supply air is a fraction of the capacity of exhaust air. The plate heat exchanger has to be designed to accommodate the unbalanced airflow in terms of heat transfer and pressure drop.

2. A face and bypass damper can be incorporated on the outdoor air/supply air side of the heat exchanger. Air can be bypassed from the heat exchanger from outdoor entering side to the supply side when the air leaving the heat exchanger is too hot. A temperature controller can be used with a sensor located in the mixed air section.

3. A bypass damper can be used to redirect less process air through the heat exchanger. However, the damper has to be constructed to withstand the conditions of the process air.

4. The heat exchanger can be constructed to provide a lower thermal effectiveness.

5. Variable frequency drives can be used on either the supply or exhaust fan motors, or on both to control the respective air mass flow rates.

The feasibility of all these options needs to be assessed at the preliminary design stage. The same considerations discussed in the process to process section are relevant in the process to comfort applications. In addition special attention is required in minimizing cross contamination from the process side to the supply side. Also, the intake and exhaust hoods must be located far enough apart to avoid drawing the contaminated air into the supply air, otherwise described as "short-circuiting". Techniques used to prevent cross contamination include:

1. Adequate sealing of seams that separate the two airstreams.

2. Leak-tight seams on the plate heat exchanger.

3. Fan location on both supply air and process air side.

The ideal fan locations for supply and process air is the push-pull configuration. The resulting pressure differential in the heat exchanger will cause air leakage to flow from the supply side to the process side and not vice versa. A detailed specific example of a process to comfort application involving a molding oven is described below: A heat recovery unit was required to provide preheated air to the offices attached to the molding oven plant. Air at an average temperature of 450 °F (232 °c) was being exhausted from a molding oven process. There were two main considerations in the design of this HRU:

1. The supply air was not to exceed 78 °F (25.6 °C).

2. The exhaust air was not to be cooled below its dewpoint, forming corrosive condensation.

In order to control these two parameters, a face and bypass damper was located on the outdoor air entering side. In addition a face and bypass damper was installed in the process air duct in order to redirect the exhaust air during non-heating periods when the temperature of the exhaust

leaving the heat exchanger was approaching its dewpoint. The designed quantity of outdoor air is 10,000 SCFM (4719 L/s), and the exhaust air is 5000 SCFM (2360 L/s). The heat exchanger was constructed to accommodate an unbalanced airflow. As a result of the high exhaust air temperature, the heat exchanger core was fabricated of stainless steel 316. The unit casing was constructed with galvanized steel in the non-corrosive sections, and stainless steel in the sections exposed to the exhaust air. Extensive thermal breaks were incorporated into the sheet metal design in order to avoid heat transfer to the outer skin of the unit, to reduce heat losses, and for safety reasons. In order to control the supply air temperature, a temperature sensor was located downstream of the heat exchanger on the supply side to sense the mixed air temperature. A face and bypass damper modulated to control the correct supply air temperature. A proportional-integral controller was used. During the spring, summer, and fall seasons when the outdoor air temperature might exceed 55 °F (12.8 ° C), the exhaust air was bypassed through the exhaust stack, and the heat recovery unit fans were shut off. A season changeover thermostat was used.

Comfort to Comfort

The most common air to air heat recovery application is comfort to comfort. Any occupied building that exhausts air while simultaneously providing outdoor air to the space has the potential to utilize heat recovery. Buildings that are retrofitted with heat recovery must account for equipment location and the routing of the ductwork for both supply and exhaust air to accommodate the heat recovery unit. If this task is not feasible for plate heat exchangers, enthalpy wheels, or heat pipes where the air streams require being in close proximity to each other, then a coil runaround loop system may be considered. If a new building is designed with an HVAC system that incorporates heat recovery, then there is greater flexibility in choosing the type of system. Current guidelines for indoor air quality, ANSI/ASHRAE standard 62-1989, provide recommendations for prescribed amounts of outdoor air for various types of building environments. By virtue of this standard, heat recovery has the potential to be used in all buildings. This unit contains a plate type cross heat exchanger.

1.4 Literature Survey

Research and theory specifically on plate type heat exchangers has been covered extensively by Kays and London (1984) for all the possible configurations mentioned in section 1.2. In particular, ε-NTU relationships have been developed for the various cross flow arrangements. Effectiveness, ε, is also defined in ASHRAE 2000, HVAC Systems and *Equipment Handbook*, chapter 44 based on laboratory measurements. Gawley, H.N., and Fisher, D.R., (1975) elaborates on the proper usage of the ratio of supply air mass flow rate to the minimum air mass flow rate, i.e. $\frac{\dot{m}_s}{\dot{m}_{\min}}$ in the ASHRAE definition of ε. The theoretical effects of non-uniform mass flow rate on thermal performance of cross flow heat exchangers have been studied by a couple of researchers.

Chiou (1978) presents a sophisticated mathematical model to determine effectiveness in a cross flow heat exchanger due to two-dimensional non-uniform fluid flow distribution. In his paper, he develops a flow non-uniformity factor to quantify the degree of thermal performance degradation. The basis of his theoretical analysis is for cases where the core frontal area is larger than the inlet duct or where the exchanger is placed close to the exit or inlet of the fluid-moving device. This is particularly relevant for compact heat recovery units that incorporate a plate heat exchanger or for abrupt transitions to heat recovery devices installed in ductwork.

Shah (1981) has developed a mathematical model to evaluate the effectiveness reduction due to non-uniform airflow using a two parallel path method. However, examples are not presented in his paper that would show the degree of effectiveness reduction as a result of various permutations of airflow path areas and air velocities. Presently, in view of the literature dealing with non-uniformity flow in air-to-air cross flow plate heat exchangers, there are no tables or charts containing the thermal performance reduction factors. To date, there are no experimental studies dealing with the effect of non-uniform airflow on thermal effectiveness reduction in cross flow plate heat exchangers.

In contrast, there are several studies that involve the experimental study of various air-to-air heat recovery devices. The preponderance of the experimental research is focused on rotary air-to-air heat exchangers. As early as 1974, Fisher, D.R., performs an experimental study on an air-to-air rotary heat exchanger, also known as enthalpy wheels. Gudac, G.J., et al, (1981) observed that in 1975, ASHRAE RP-173 was initiated to determine the applicability of the test method, ASHRAE RP-133 for testing air-to-air rotary exchangers, to other types of air-to-air energy recovery systems. More recently, Ciepliski , D. L. (1997) has performed an experimental study on enthalpy wheels. Simonson, C.J. (1998) has published papers on the experimental study of enthalpy wheels, including part load operation. Heat pipes have also been the subject of research by McFarland, J.K., (1996) and Guo, P., (1997).

There are far fewer research papers on air-to-air plate type heat exchangers. Bantle, R.L., (1987) has studied frost formation on plate type heat exchangers. Savadkouhian (1981) experimentally evaluated the thermal performance of a counter flow fixed plate air-to-air heat exchanger. There is a definite void of research with specific regard to air-to-air cross flow plate type heat exchangers. Research carried out on heat recovery devices is typically based on ASHRAE Standard 84-1991, Method of Testing Air-to-Air Heat Exchangers. CSA Standard C439-00, 2000, Standard Laboratory Methods of Test for Rating the Performance of Heat/Energy-Recovery Ventilators, is more specifically used to assess the thermal performance of small packaged energy recovery units containing cross flow plate heat exchangers. Ciepliski, Besant, and Simonson (1998) recommend that uncertainty analysis should be included in testing air-to-air heat recovery devices to evaluate the accuracy of the results. They provide recommendations for improvements to the ASHRAE Standard, 84-1991. They also discuss the method of pre-test uncertainty analysis as required by ASME PTC 30-1991 to ensure that the predicted uncertainty remains within ± 5% based on the choice of instrumentation and operating conditions for laboratory measurements. Coleman, H.W., and Steel, W.G, (1989) present a detailed method for carrying out a pre-test uncertainty analysis.

The sensitivity analysis could provide valuable insight into which sensors or operating conditions have the greatest impact on effectiveness uncertainty. Besides effectiveness, the

phenomenon of the cold corner in cross flow plate heat exchangers is a subject that has not been widely studied. There is no published research to date that experimentally examines the temperature distribution in air-to-air cross flow heat exchangers. Bantle, R.L., (1987) measures the temperature of a counter flow heat exchanger core on the supply side only. Only five measurements are taken manually with a hand held Type T Thermocouple Thermometer. The sensors were installed after the heat exchanger was fabricated, thus are placed closer to the exterior edges of the core. This system of measurement cannot provide detailed information regarding the distribution of temperatures within the heat exchanger. Several other papers dealing with certain specific aspects of heat recovery systems are referenced in the following chapters throughout the thesis.

1.5 General Objectives

The literature survey reveals that there is a considerable lack of research with regard to air-to-air cross flow plate heat exchangers. Furthermore, experimental studies of the temperature distributions within air-to-air cross flow plate heat exchangers could not be found. Cross flow plate heat exchangers are among the most common type of air-to-air heat recovery device that are used in HVAC applications due to their low cost, low pressure drop, and reasonably high effectiveness. There is a definite need for research pertaining to the performance of cross flow plate heat exchangers. In order to accurately study the sensible effectiveness of cross flow plate type heat exchangers, a complete test facility for heat recovery devices needs to be designed, fabricated, installed and commissioned. ASHRAE standard 84-1991 is the main guide in North America for testing air-to-air heat recovery devices. However, the layout of the test facility in the standard strongly favors counter flow heat recovery devices such as enthalpy wheels and heat pipes. This issue will be elaborated in chapter 4. CSA Standard C439-00, 2000 is more geared towards cross flow plate heat exchangers within packaged heat recovery ventilators. The current standards for testing heat recovery devices have scant guidelines regarding uncertainty analysis. As a result of the highly competitive nature of the HVAC market, manufacturers design very compact heat recovery packaged units in which fans, filters or coils are installed very near to the entrance or exit of the plate heat exchanger thus creating non-uniform airflow conditions. In

many instances these types of compact designs result in the complete obstruction of a portion of a plate type heat exchanger. The impact of these obstructions on the performance of the heat recovery device is completely ignored. Similarly, plate type heat exchangers installed as stand-alone devices in ductwork may contain sudden transitions or bends that also create non-uniform airflow conditions. Further to the above, the following are some of the specific objectives in this thesis.

1. Expand an existing mathematical model from Shah (1981) for non-uniform airflow through a cross flow plate heat exchanger to allow for a more realistic analysis of thermal performance reduction. Several permutations of non-uniform airflow conditions will be used to evaluate the effect of thermal performance reduction.
2. Perform a pre-test uncertainty analysis to study the effects of instrumentation accuracy (Bias) and operating conditions on sensible effectiveness uncertainty. Graphical curves will be generated to illustrate the sensitivity of instrument accuracy and operating conditions that will provide a basis for selecting the measurement systems and the establish the operating range of a heat recovery test facility.
3. Design, and fabricate a new, low cost, innovative, flexible heat recovery test facility that can provide accurate measurements for all heat recovery devices, in particular cross flow plate heat exchangers.
4. Use the new heat recovery test facility to evaluate the sensible effectiveness of a cross flow plate heat exchanger for both balanced and unbalanced airflow conditions for a range of entering cold air temperatures.
5. Simulate obstructions at the entrance of the heat exchanger on both the cold and hot side in the heat recovery test facility, and evaluate the impact on sensible effectiveness.
6. Study the temperature distributions inside the heat exchanger on both the cold and hot side for balanced and unbalanced airflow, and for the tests involving the simulated obstructions.

The above contributions will provide insight into the performance of air-to-air cross flow plate heat exchangers and in particular the temperature distributions that can occur. This is particularly

relevant with regard to the phenomenon of the "cold corner" effect in cross flow heat exchangers. Although frost growth inside the heat exchanger will not be studied in the present work, the temperature distributions will shed light on the extent of the cold corner for a variety of operating conditions.

1.6 Thesis Structure and Main Contributions

The thesis is organized in a manner that presents the theoretical efforts followed by the substantial experimental work and results. In particular, the various mathematical models for sensible effectiveness are presented in chapter 2 to provide a conceptual framework for the experimental set-up. In addition, a mathematical contribution is provided in reference to sensible effectiveness reduction as a result of non-uniform airflow. A significant portion of the thesis deals with the design of a new air-to-air heat recovery test facility and the corresponding measurement system including the data acquisition. In order to ensure that the test facility is designed to provide accurate measurements, an in-depth pre-test uncertainty analysis is presented in chapter 3. The sensitivity curves developed in terms of the effect of sensor accuracy and operating conditions on the uncertainty sensible effectiveness are a major contribution. A full description of the mechanical and electrical systems of the heat recovery test facility is elaborated in chapter 4. The measurement system and data acquisition warranted a complete chapter by themselves considering the innovations relative to the existing standards and other test facilities described in the literature. Contributions in reference to measurement techniques are also presented in chapter 5. A detailed description of the type of tests conducted in the new heat recovery test facility is full described in chapter 6. In addition, experimental results are presented in graphical form. Chapter 7 provides a summary of the most significant results for all the tests, conclusions, and recommendations for future work that stem from the present research. The appendices provide supplementary information.

1.7 Units of Measure

The units of measure that are predominantly used in the HVAC industry in North America are still imperial units, as a result of the influence of the dominant U.S.A. market. Canada uses both S.I. and imperial units. In some cases, specifications and schedules prepared by Canadian consulting Engineers consist of the dual units. In this thesis, dual units will be presented. The typical imperial and S.I. units that will be used are listed as follows:

Temperature:	Degree Fahrenheit (°F) ; Degree Celsius (°C)
Air Flow:	Cubic Feet per Minute (CFM); Liters per second (L/s)
Static air pressure:	inches of water column (in. w.c).; Pascals (Pa)
Barometric pressure:	inches of mercury (in. Hg); millimeters of mercury (mm of Hg)
Length:	inches (n or "); millimeter mm

The imperial units will be placed first, followed by the S.I. units in brackets, since all of the test data were collected and subsequent calculations were made in imperial units.

2.0 THERMAL PERFORMANCE THEORY FOR CROSS FLOW PLATE HEAT EXCHANGERS

The mathematical techniques used to evaluate the thermal performance of air to air heat recovery devices has been extensively covered, notably by Kays and London (1984). The main parameter that is used to designate the thermal capacity for heat recovery devices is effectiveness, ε.

Effectiveness can be classified as either sensible (ε_s), latent (ε_l), or total (ε_t). In this paper, only ε_s , will be used, since plate heat exchangers are essentially sensible heat recovery devices. The term efficiency is sometimes used instead effectiveness with regard to air to air heat recovery devices. In reference to ASHRAE fundamentals, chapter 44, dealing with air-to-air heat recovery devices, the term effectiveness is used which is defined as follows.

Effectiveness, ε = (Actual Energy transfer) ÷ (Maximum Available Energy transfer)

Air-to-air heat recovery devices effectiveness is not fixed for a particular heat exchanger, but is a function of the ratio of heat capacities of the two air streams, the amount of heat transfer surface area, and the overall heat transfer coefficient. The effectiveness of a particular heat recovery device is dependent on the operating conditions. The graphs for the $\varepsilon - NTU$ relationships presented below will illustrate the range of effectiveness that can be achieved for cross flow configuration. Effectiveness will be the term used in the current thesis. The two principal methods in determining ε for a particular heat recovery device include the following:

1. Experimental methods utilizing existing test guidelines such as ASHRAE Standard 84-1991 within acceptable uncertainty boundaries.
2. Analytical or mathematical models utilizing well known formulations.

In section 2.1 the expression for effectiveness for laboratory measurements as defined in ASHRAE Standard 84-1991 will be presented. In addition, a formulation for effectiveness incorporating the average of supply and exhaust effectiveness as developed by Simonson et al. (1997) will be included. The focus of the current research is with respect to cross flow plate type heat exchangers. In this context, the well-established formulations for ε developed by Kays and London (1984) will be reviewed for cross flow configurations. Non-uniform airflow conditions are known to adversely affect the thermal performance of heat exchangers in cross flow

configuration. A mathematical model developed by R. K. Shah, (1980), provides a means to evaluate the effectiveness degradation by considering two parallel airflow paths through the unmixed side of the heat exchanger. This model will be presented and studied for various permutations of non-uniform airflow and unequal areas for the two paths. As one of the principal contributions to the present work, the two path model will be expanded to incorporate three parallel paths with equal and non-equal flow areas. A series of graphs will be presented to illustrate the effects of non-uniform airflow on ε.

2.1 Effectiveness Evaluation Using Laboratory Measurements

Laboratory measurements are often used to evaluate the effectiveness of air-to-air heat exchangers. ASHRAE Standard 84-1991is the principal standard in North America for testing air-to-air heat exchangers. ARI standard 1060, which is based on ASHRAE Standard 84-1991, uses the same relation to evaluate effectiveness. The equation is defined as follows:

$$\varepsilon = \frac{\dot{m}_s(X_2 - X_1)}{\dot{m}_{\min}(X_3 - X_1)} \tag{2.1}$$

where:

ε	Total, latent or sensible effectiveness of a heat exchanger
X_1, X_2 and X_3	Enthalpy, humidity or air temperature at heat exchanger supply inlet/exit, and exhaust inlet respectively
$\dot{m}_s$	Supply air mass flow rate
$\dot{m}_{\min}$	Minimum air mass flow rate between supply and exhaust

In the present paper only sensible effectiveness, which is a function of dry bulb temperatures, will be considered. Therefore, equation 2.1 can be restated in terms of air temperatures.

$$\varepsilon = \frac{\dot{m}_s(t_2 - t_1)}{\dot{m}_{\min}(t_3 - t_1)} \tag{2.2}$$

Where:

t_1, t_2 and t_3 is the air temperature at heat exchanger supply inlet/exit, and exhaust inlet respectively.

$\dot{m}_s$ is the supply air mass flow rate

$\dot{m}_{\min}$ is the minimum air mass flow rate of $\dot{m}_s$ and $\dot{m}_e$.

$\dot{m}_e$ is the exhaust air mass flow rate

Equation 2.2 can also written in terms of the exhaust air mass flow rate and air temperatures:

$$\varepsilon = \frac{\dot{m}_e(t_3 - t_4)}{\dot{m}_{\min}(t_3 - t_1)} \tag{2.3}$$

Another conventional method for representing the air temperatures is as follows:

$t_{ci} = t_1$ cold inlet supply air temperature

$t_{co} = t_2$ cold outlet supply air temperature

$t_{hi} = t_3$ hot inlet exhaust air temperature

$t_{hi} = t_4$ hot outlet exhaust air temperature

This subscript convention will be used for the remainder of this paper. Figure 2.1 (a) shows the scheme of airflow for air-to-air heat exchangers from ASHRAE Standard 84-1991 in a counter flow arrangement. It is worth mentioning that ASHRAE Standard 84-1991 was originally developed for enthalpy wheels and heat pipes that are counter flow heat exchangers. Therefore, there is a stronger emphasis on counter flow arrangements as opposed to cross flow arrangements. Figure 2.1 (b) shows an airflow scheme for cross flow.

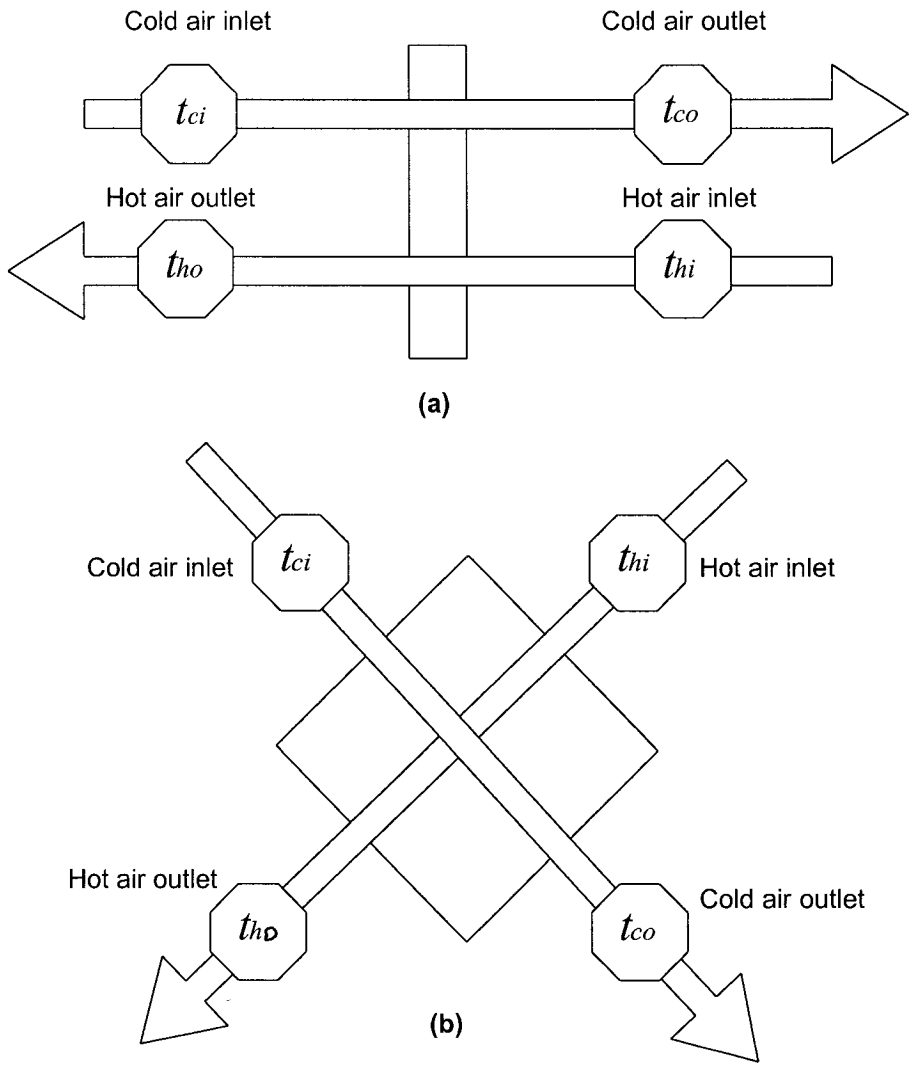

Figure 2.1 Scheme of airflow for air-to-air heat exchangers (a) ASHRAE Standard 84-1991 counter flow (b) Cross flow

The original concept of the effectiveness relation in equation 2.2 is based on the idea of a counter flow heat exchanger having infinite surface area in which ε = 1.0. In this case, the difference in air temperature between the cold inlet, t_{ci}, and cold outlet, t_{co}, is equal to the maximum possible temperature difference between the cold inlet, t_{ci} and the hot inlet, t_{hi}, i.e., $t_{co} - t_{ci} = t_{hi} - t_{ci}$. In addition, $\dot{m}_s = \dot{m}_{\min}$, and therefore, for the perfect counter flow heat exchanger,

$$\varepsilon = \frac{\dot{m}_s(t_{co} - t_{ci})}{\dot{m}_{\min}(t_{hi} - t_{ci})} = 1.0$$

An earlier paper by Gawley and Fisher (1975) provides a clear explanation on the proper usage of the ratio of supply air mass flow rate to the minimum air mass flow rate, i.e. $\frac{\dot{m}_s}{\dot{m}_{\min}}$. This explanation also applies to the ratio of the exhaust air mass flow rate to the minimum air mass flow rate, i.e., $\frac{\dot{m}_e}{\dot{m}_{\min}}$. In this paper, Gawley and Fisher reveal that $\dot{m}_{\min}$ (or $W_{\min}$ as he uses instead of $\dot{m}_{\min}$) must be used instead of $\dot{m}_e$, otherwise the numerator would be larger than the denominator. Thus $\varepsilon > 1.0$, and the heat transfer would exceed that of a perfect heat exchanger, which is impossible. Therefore it can be stated that maximum available energy for heat recovery, $q_{\max}$, is the product of the maximum temperature difference on the heat exchanger and the airflow with the minimum heat capacity: $q_{\max} = \dot{m}_{\min} \times (t_{hi} - t_{ci})$. It can be observed that the heat capacity term, c_p, has not been included in equation 2.1, 2.2, and 2.3 since it is assumed to be constant for the range of temperatures encountered in regular HVAC applications. As we have seen ε can be expressed in terms of the heat transfer on either the supply or exhaust side. However, Simonson et al. (1997a, 1997b) present laboratory measurements using the average of the supply and exhaust side effectiveness expressed as

$$\varepsilon_{s,\,ave} = \frac{\dot{m}_s(t_{co} - t_{ci}) + \dot{m}_e(t_{hi} - t_{ho})}{2\dot{m}_{\min}(t_{hi} - t_{ci})} \qquad \textbf{(2.4)}$$

This expression is known to provide the lowest uncertainty in calculated effectiveness as will be revealed in detail in chapter 3. Equations 2.1 to 2.4 are convenient for laboratory measurements. However, when effectiveness is required to be assessed at the design stage, it may not be practical nor feasible to fabricate a heat exchanger and then have it tested in a laboratory. In this case, ε can be evaluated using mathematical methods. The next section will delve into the theoretical formulations for effectiveness particularly for cross flow plate heat exchangers.

2.2 ε-NTU Relationships for Cross Flow Plate Heat Exchangers

The well established analytical formulations developed by Kays and London (1984) for plate type heat exchangers can be evaluated using the equations in which effectiveness, ε, is a

function of the Number of Transfer Units, NTU, and the ratio of minimum heat capacity to maximum heat capacity of the two airstreams, $C = C_{\min}/C_{\max}$.

$$\varepsilon = f(NTU, C) \tag{2.5}$$

It is noted that temperatures are not directly involved in the evaluation of effectiveness. A review of the $\varepsilon - NTU$ relationships for single pass cross flow heat exchangers will be reviewed in this section. Single pass refers to the air passing through the heat exchanger once only. NTU is a dimensionless variable that is used to quantify and compare the thermal capacity for different heat exchangers. It is defined as follows:

$$NTU = \frac{UA_{hts}}{C_{\min}} \tag{2.6}$$

This expression provides a ratio between the heat transfer potential of the heat exchanger to the minimum heat capacity of the two air streams. The heat transfer potential of a heat exchanger is evaluated based on the overall thermal heat transfer coefficient, U, and the heat transfer surface area shared between the two air streams, A_{hts}. U is calculated as follows:

$$U = \frac{1}{\frac{1}{h_c} + \frac{t}{k_{hx}} + \frac{1}{h_h} + R_f} \tag{2.7}$$

The thermal resistance of the heat exchanger plate material, $R_{hx} = \frac{t}{k_{hx}}$, is sufficiently small to be neglected since thickness of the material, t, is very thin, and the corresponding thermal conductivity, k_{hx}, is much higher than air. It will be assumed that the air is clean and does not cause fouling of the heat exchanger surface. Thus, thermal resistance as a result of fouling, R_f, will also be neglected. The equation for U is restated as follows:

$$U = \frac{1}{\frac{1}{h_c} + \frac{1}{h_h}} \tag{2.8}$$

The remaining terms in the above expressions consist of the heat transfer coefficient for the cold and hot sides of the heat exchanger surface and are evaluated using known empirical

formulations. The heat transfer coefficients are derived in terms of the Nusselt no., Nu, thermal conductance of air, k_a, and the hydraulic diameter of the flow path, D_h.

$$h_c = \frac{D_h \times k_a}{Nu_c} \tag{2.9}$$

It will be assumed that the thermal conductance of air, k_a, will be constant for the range of temperatures that will be considered on both the cold and hot sides of the heat exchanger, (k_a = 0.0145 Btu/hr ft °F). The hydraulic diameter, D_h, is a constant value for both sides of the heat exchanger that consist of identical geometrical configurations. The hydraulic diameter, D_h, represents an equivalent diameter for the particular non-circular cross sectional area of the heat exchanger. The hydraulic diameter, D_h, for rectangular cross sectional areas, which represents the geometry for plate type heat exchangers, is defined as follows:

$$D_h = \frac{4 \times Cross\ Sectional\ Area}{Wetted\ Perimeter} = \frac{4ab}{(2a+2b)} = \frac{2ab}{(a+b)} \tag{2.10}$$

The dimensions a and b represent the width and plate spacing of a single a channel, as illustrated in figure 2.2. The term that is the most difficult to assess is the Nusselt number, Nu. There are myriad empirical relationships that are used to evaluate Nu. As accurately observed by K.J. Bell (1980), there are very few published data on specific channel characteristics. Somerton, Genik et al (1998) has developed a classification system for Nusselt number correlations. They identify five separate classes used to choose the relevant Nu correlation. Four factors that have been identified in relation to plate type heat exchangers include:

1. Flow driving mechanism: Forced convection
2. Flow domain: Internal flow
3. Surface geometry: Flat surface with embossing
4. Flow direction: Normal to axis for each flow

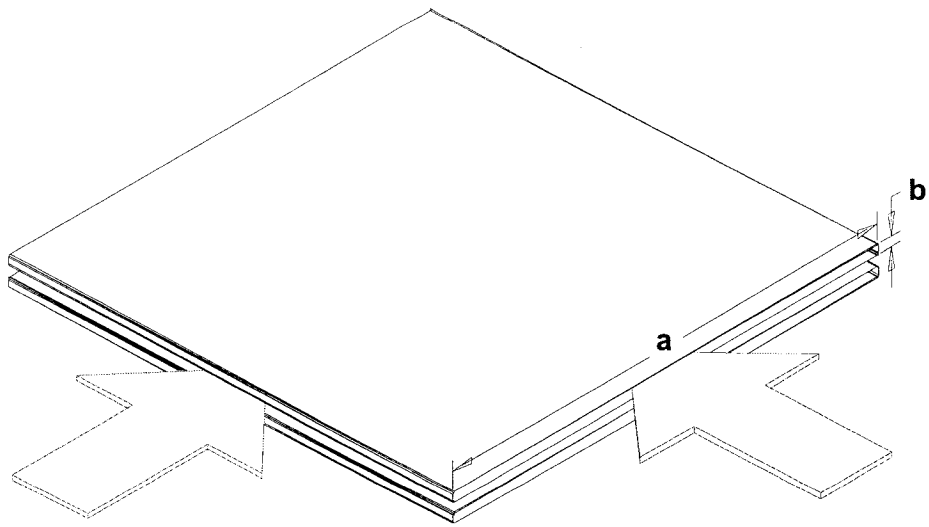

Figure 2.2 Dimensions "a" and "b" of plate heat exchanger channel for calculating the hydraulic diameter.

The fifth factor relates to surface orientation with regard to natural convection, which is not applicable in the current case. The dimensionless variables that are used to calculate Nu include Reynold's number, Re, and Prandlt number, Pr. Ranges of Reynold's number and Prandlt number are used to define the suitability for a particular empirical formulation for Nu. The empirical formula that was found to be the most relevant for narrow channels with a short length, as in the case for plate type heat exchangers, is defined as follows:

$$\overline{Nu} = 3.66 + \frac{\left(0.0668 \times \left(\frac{L}{D_h}\right) \times \mathrm{Re} \times \mathrm{Pr}\right)}{\left(1 + 0.04 \times \left(\frac{L}{D_h}\right) \times \mathrm{Re} \times \mathrm{Pr}\right)} \left(\frac{\mu_b}{\mu_s}\right)^{0.14} \qquad \textbf{(2.11)}$$

This correlation is typically used in evaluating the average Nusselt number for laminar flow in short tubes and ducts with uniform wall temperature. The plate heat exchanger temperature will be highly non-uniform. However, the variation of dynamic viscosity between the plate, μ_s ,and the bulk airstream, μ_b , is negligible, and can be assumed to be constant throughout the heat exchanger length. Therefore, the term $\left(\frac{\mu_b}{\mu_s}\right)^{0.14}$ can be removed from equation 2.11 when

applied to the current study of plate type heat exchangers. Recall that Re is defined as the ratio of air velocity inertia to viscosity:

$$\mathrm{Re} = \frac{\rho_a \times v_{ave} \times D_h}{\upsilon} \tag{2.12}$$

Where ρ_a is the air density, v_{ave} is the average air velocity passing into and through the heat exchanger, and υ is the dynamic viscosity. In calculating Re, it is assumed that ρ_a, and υ are constant throughout the flow path. Recall that Pr is defined as the ratio of kinematic viscosity, ν to the thermal diffusivity, α, i.e., $\mathrm{Pr} = \frac{\nu}{\alpha}$. The Prandtl number for air is constant for a large range of temperatures, i.e., $\mathrm{Pr} = 0.71$. The heat capacity of the cold and hot airflow is defined in terms of the mass flow rate, $\dot{m}$ and the specific heat capacity of air, c_{pa}.

Cold airflow heat capacity: $C_c = \dot{m}_c \times c_{pa} = \rho_a \times \dot{Q}_c \times c_{pa}$

Hot airflow heat capacity: $C_h = \dot{m}_h \times c_{pa} = \rho_a \times \dot{Q}_h \times c_{pa}$

$\dot{Q}_c$ and $\dot{Q}_h$ are the cold and hot volume air flow rates for the cold and hot sides respectively. The minimum heat capacity, $C_{\min}$, is chosen as the smaller of C_c and C_h. The variable C is defined as the ratio $\frac{C_{\min}}{C_{\max}}$. All the variables required for determining the Number of Transfer Units, NTU, have been identified. In considering a cross flow configuration, there are four equations that can be used to calculate ε. The equations, by Kays and London (1984) are chosen based on the following combination of conditions of the airflow through the heat exchanger:

1. $C_{\min}$ is mixed, and $C_{\max}$ is mixed:

$$\varepsilon = NTU \times \left[\frac{NTU}{1 - e^{-NTU}} + \frac{(NTU)(C)}{1 - e^{(-NTU)(C)}} \right] \tag{2.13}$$

2. $C_{\min}$ is unmixed, and $C_{\max}$ is unmixed:

$$\varepsilon = 1 - e^{\left[\frac{1}{C\eta} \times \left(e^{(-NTU)(C)(\eta)_{-1}}\right)\right]} \tag{2.14}$$

The variable η is defined in as a function of NTU, i.e., $\eta = NTU^{-0.22}$

3. $C_{\min}$ is unmixed and $C_{\max}$ is mixed:

$$\varepsilon = \frac{1}{C} \times \left(1 - e^{(-C)\left(1 - e^{(-NTU)}\right)}\right) \tag{2.15}$$

4. $C_{\min}$ is mixed and $C_{\max}$ is unmixed:

$$\varepsilon = 1 - e^{\left(\frac{1}{-C}\right)\left(1 - e^{(-NTU)(C)}\right)} \tag{2.16}$$

The meaning of mixed and unmixed refers to the degree in which the streamline flows cross over and mix with adjacent streamlines through the length of the heat exchanger. Some plate heat exchangers are constructed of fluted or corrugate channels that do not permit air to mix with other adjacent channels. Other plate heat exchangers are constructed of a dimpled embossed pattern that allows more lateral movement of the air, thus encouraging mixing between streamlines.

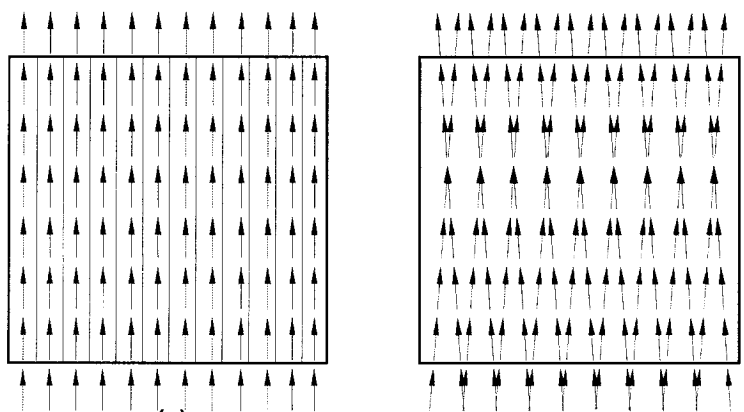

Figure 2.3 Plate type heat exchanger flow paths (a) unmixed, (b) mixed

Figure 2.3 illustrates examples of an unmixed and a mixed flow path. The four sets of equations for cross flow effectiveness have been evaluated for a range of NTU from 0.25 to 9.75 at increments of 0.25. Figure 2.4 presents the curves for C_{min}/C_{max}=1 for all four cases of cross flow and includes the curve for counter flow for comparative purposes. The heat exchanger design characteristics that have been used to develop these curves are based on the following:

1. The overall cross flow plate heat exchanger dimensions are 36"x36"x18" (914 mm x 914 mm x 457 mm).

2. The plate spacing is chosen to be 3/8" (9.5 mm). The corresponding hydraulic diameter, D_h, is 0.061 ft (18.5 mm).

3. The number of plates within the heat exchanger is 41. The overall heat transfer area, A_{hts}, is 940 sqft (86.3 m^2).

4. The range of volume airflow rates corresponding to the above mentioned range of NTU is from 750 CFM (354 L/s) to 27,900 CFM (13,167 L/s). The extremely high airflow rate is used to illustrate the variation of ε as NTU becomes very small.

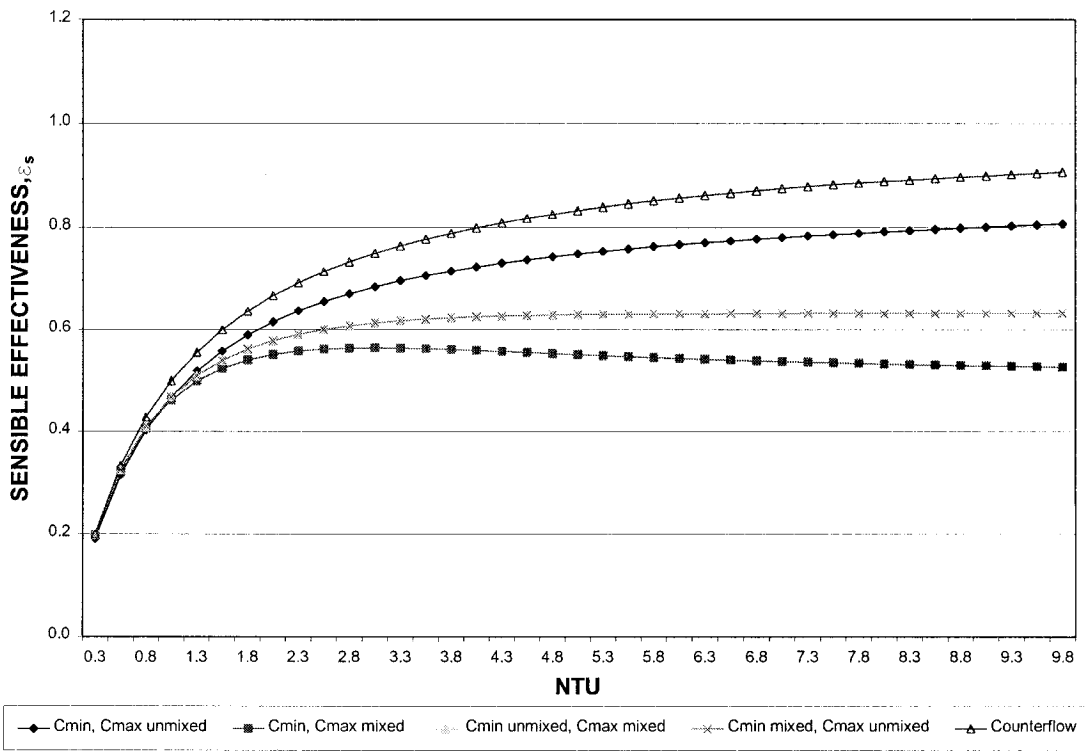

Figure 2.4 Theoretical Sensible effectiveness versus NTU for all cases of cross flow and counter flow when C_{min}/C_{max}=1.0

The counter flow arrangement possesses the highest theoretical effectiveness values for a given NTU, followed by the cross flow case when both C_{min} and C_{max} is unmixed. The effectiveness for counter flow and unmixed cross flow asymptotically approaches 1.0 for increasing NTU. It is interesting to note that counter flow obtains a value of ε =0.99 at NTU =100, and unmixed cross flow obtains a value of ε =0.99 for NTU =1000. In reality, it would not be economical or practical to construct heat exchangers with such high values of NTU, as the heat exchanger surface area A_{hts} would require being enormous relative to C_{min}. The two cases when one of the airflows is mixed and the other unmixed asymptotically approaches ε =0.6321. It is observed that ε rapidly levels off at NTU = 3.0, which implies that any increase in UA_{hts} relative to C_{min} for $NTU > 2.5$ will not contribute to greater effectiveness when one of the airflows is mixed and the other is unmixed. The case for both C_{min} and C_{max} mixed produces the lowest values ε in comparison with the other cross flow cases. It can be observed that ε obtains a maximum value of 0.5645 at NTU =3.0, and then decreases to ε =0.5 as NTU approaches infinity.

2.3 *Effectiveness Reduction due to Two Non-Uniform Parallel Airflow Paths on the Unmixed Side and Uniform Airflow on the Mixed side.*

The effectiveness equations 2.13 to 2.16 are based on the assumption of uniform airflow from the entrance passing through the entire length of the heat exchanger. In real installations, non-uniform airflow may occur due to installation constraints, connecting ductwork, fabrication flaws in the heat exchanger, and poor transitions to filters or coils. Thermal performance degradation may occur as a result of non-uniform airflow within the heat exchanger. A mathematical model developed by Shaw (1981) provides a method to calculate the reduced effectiveness based on two paths containing different air velocities on one side of the exchanger while the airflow on the other side remains uniform. In order to set up the model, figure 2.5 illustrates the two parallel paths that each has a uniform airflow velocity of v_1 and v_2 flowing through A_1 and A_2 respectively on the hot air side. The individual heat capacity of the two airstreams is obtained by multiplying the air velocity with the corresponding area and the specific

heat capacity of the air, i.e. $C_{h,1} = C_{\min,1} = c_{pa} \times v_1 \times A_1$ and $C_{h,2} = C_{\min,2} = c_{pa} \times v_2 \times A_2$. The airflow on the cold side is mixed and uniform.

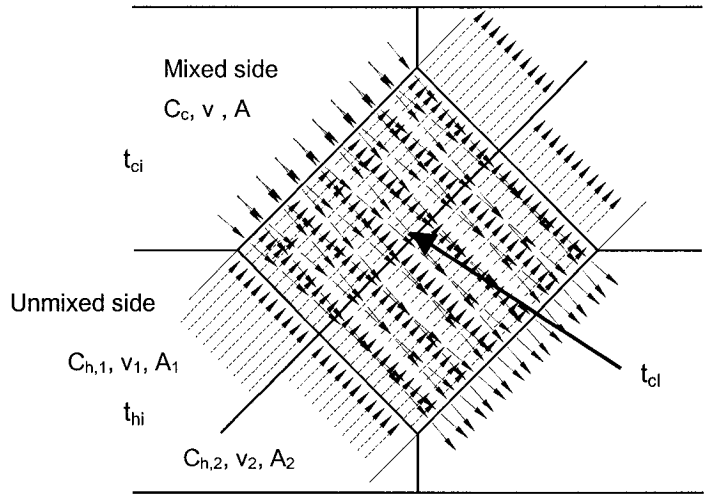

Figure 2.5 Idealized flow non-uniformity on the unmixed side for two parallel paths of a mixed-unmixed cross flow plate heat exchanger

Note that the airflow is unmixed in the two parallel paths on the hot side. Therefore, the $\varepsilon - NTU$ relationship that will be used will be for the case $C_{\min}$ unmixed and $C_{\max}$ mixed which corresponds to equation 2.15. The derivation of the effectiveness, ε_h, for the simple case of two parallel paths containing different air velocity is commenced by considering the energy balancing for both paths:

$$q_1 = \varepsilon_{h,1} \times C_{h,1} \times (t_{hi} - t_{ci}) = C_c \times (t_{c,i} - t_{c,I}) \tag{2.17}$$

Solving for the unknown entering cold temperature, $t_{c,I}$, entering the second path on the hot side:

$$t_{c,I} = t_{c,i} + \left(\frac{\varepsilon_{h,1} \times C_{h,1}}{C_c} \right) (t_{h,i} - t_{c,i}) \tag{2.18}$$

The energy balance on the second path, q_2 is as follows:

$$q_2 = \varepsilon_{h,2} \times C_{h,2} \times (t_{hi} - t_{c,I}) \tag{2.19}$$

Substituting (2.18) into (2.19) gives:

$$q_2 = \varepsilon_{h,2} \times C_{h,2} \times \left(1 - \frac{\varepsilon_{h,1} \times C_{h,1}}{C_c}\right)\left(t_{hi} - t_{c,1}\right) \tag{2.20}$$

The total heat transfer on the hot side is the sum of the two paths:

$$q = q_1 + q_2 = \varepsilon_h C_h \left(t_{ci} - t_{hi}\right) \tag{2.21}$$

The resulting effectiveness, ε_h, can be derived from equations (2.17) to (2.21) and is presented as follows:

$$\varepsilon_h = \frac{1}{C_h}\left[\varepsilon_{h,1} C_{h,1} + \varepsilon_{h,2} C_{h,2}\left(1 - \frac{\varepsilon_{h,1} \times C_{h,1}}{C_c}\right)\right] \tag{2.22}$$

The percent effectiveness reduction can now be evaluated based on the following ratio:

$$\Delta\varepsilon = \left(\frac{\varepsilon_{h,o} - \varepsilon_h}{\varepsilon_{h,o}}\right) \times 100 \tag{2.23}$$

$\varepsilon_{h,o}$ is the effectiveness if there is uniform airflow on the hot side. $\varepsilon_{h,1}$ and $\varepsilon_{h,2}$ are calculated by substituting $C_1 = \frac{C_{h,1}}{C_c}$, $NTU_1 = \frac{U_1 A_1}{C_{h,1}}$ and $C_2 = \frac{C_{h,2}}{C_c}$, $NTU_2 = \frac{U_2 A_2}{C_{h,2}}$ into equation 2.15 respectively. Although this model has been presented in the literature, examples to illustrate the scale of effectiveness reduction for air-to-air plate type heat recovery devices have not been published hitherto. It is of practical interest to discover the combination of areas and velocities that will cause the greatest reduction in effectiveness. This type of information could aid designers in assessing effectiveness correction factors at the design stage, and trouble shooting heat exchangers that are not performing in-situ according to original design calculations. Various permutations of area flow paths and air velocities have been selected to generate curves of effectiveness degradation. The corresponding airflow rates for each path have been calculated based on the permutations of air velocity and path face area. Conservation of mass airflow rate is respected in each case. The permutations have been divided into four different path area couples. For each path area couple there are seven combinations of non-uniform air velocities. The mass airflow rates for each path are calculated to ensure conservation of mass. Table 2.1 presents all 28 permutations. The Area A, represents the full open area with a single path instead of two parallel paths on the hot side. The area, A_1 and A_2 individual paths in the two path system

is calculated as a specific fraction of the full frontal area, A. For example, the first case involves dividing the full area in half, i.e., $A_1 = A_2 = 0.5A$. The other three cases involve increasing asymmetric areas for the two paths. For each permutation, the velocities, v_1 and v_2, are depicted in terms of a factor of the average air velocity, $v_{h,ave}$, in the hot air side if there is one uniform path. The velocity of the airflow in path 1, v_1, varies from $0.875v_{h,ave}$ to $0.125\ v_{h,ave}$ in increments of 0.125. The velocity in the second path will depend on the mass airflow rate balance for the two paths. In order to simplify calculations, the air density will be assumed to be constant for the range of conditions. Therefore, the airflow rate will be used instead of the mass airflow rate. The velocity for $v_{h,ave}$, v1, and v2 is assumed to be constant upon entrance and throughout the heat exchanger. For each path velocity and area there is a corresponding hot side airflow rate, Q_{h1} and $Q_{h1,}$ that is presented in terms of percentage of the total airflow rate on the hot side, Q_h. The preceding sample calculation is used to illustrate how the values in table 2.1 are obtained. As an example consider the overall airflow rate of 1500 CFM (708 L/s) on the hot side flowing through $A_1 = 0.25A$ and $A_2 = 0.75A$ for a non-uniform air velocity of $v_1 = 0.375v_{h,ave}$. The calculations are as follows:

Total face area:	$A = 3.53\ ft^2\ (0.324\ m^2)$
Average air velocity on the hot side:	$v_{h,ave} = 1500\ ft^3/min \div 3.53\ ft^2 = 425\ ft/min$ $v_{h,ave} = (708\ L/s \div 0.324\ m^2) * 1/1000\ m^3/L = 2.19\ m/s$
Air velocity in path 1:	$v_1 = 0.375 \times v_{h,ave} = 0.375 \times 425 = 159\ ft/min$ $v_1 = 0.375 \times v_{h,ave} = 0.375 \times 2.19 = 0.82\ m/s$
Air flow rate in path 1:	$Q_1 = v_1 \times A_1 = 159\ ft/min \times 0.25 \times 3.53\ ft^2 = 140\ CFM$ $Q_1 = v_1 \times A_1 = 0.82\ m/s \times 0.25 \times 0.324\ m^2 \times 1000 = 66.4\ L/s$
Air flow rate percentage in path 1:	$\%Q_1 = (140/1500) \times 100\% = (66.4/708) \times 100\% = 9.3\%$
Air flow rate in path 2:	$Q_2 = Q - Q_1 = 1500 - 140 = 1360\ CFM$ $Q_2 = Q - Q_1 = 708 - 66.4 = 642\ L/s$
Air flow rate percentage in path 2:	$\%Q_1 = (1360/1500) \times 100\% = (642/708) \times 100\% = 90.7\%$
Air velocity in path 2:	$v_2 = Q_2 / A_2 = Q_2 / 0.75A = 1360/(0.75 \times 3.53) = 514\ ft/min$ $v_2 = Q_2 / A_2 = Q_2 / 0.75A = 642/(0.75 \times 0.324 \times 1000) = 2.64\ m/s$
Air velocity factor in path 2:	$v_{2\ factor} = v_2 / v_{h,ave} = 514/425 \cong 2.64/2.19 \cong 1.208$

Table 2.1 Area and Air Velocity Permutations for Calculating Effectiveness Reduction due to Two Path Non-Uniform Airflow

		AIR VELOCITY FACTORS OF THE AVERAGE FOR PATHS 1 AND 2													
		PERCENT MASS AIRFLOW RATES IN PATHS 1 AND 2													
CASES		1		2		3		4		5		6		7	
PATH AREAS		v_1	v_2	v_1	v_2	v_1	v_2	v_1	v_2	v_1	v_2	v_1	v_2	v_1	v_2
A_1	A_2	Q_1	Q_2	Q_1	Q_2	Q_1	Q_2	Q_1	Q_2	Q_1	Q_2	Q_1	Q_2	Q_1	Q_2
0.5A	0.5A	0.875	1.125	0.750	1.250	0.625	1.375	0.500	1.500	0.375	1.625	0.250	1.750	0.125	1.875
		44%	56%	33%	67%	31%	69%	25%	75%	19%	81%	13%	88%	6%	94%
0.375A	0.625A	0.875	1.075	0.750	1.150	0.625	1.225	0.500	1.300	0.375	1.375	0.250	1.450	0.125	1.525
		33%	67%	28%	72%	23%	77%	19%	81%	14%	86%	9%	91%	5%	95%
0.25A	0.75A	0.875	1.042	0.750	1.083	0.625	1.125	0.500	1.167	0.375	1.208	0.250	1.250	0.125	1.292
		22%	78%	19%	81%	16%	84%	13%	88%	9%	91%	6%	94%	3%	97%
0.125A	0.875A	0.875	1.018	0.750	1.035	0.625	1.054	0.500	1.071	0.375	1.089	0.250	1.107	0.125	1.125
		11%	89%	9%	91%	92%	8%	6%	94%	5%	92%	3%	97%	2%	98%

Four graphs containing seven individual curves per graph for $\Delta\varepsilon$ versus average air velocity on the hot side are presented in figures 2.6 to 2.9. The range of volume airflow rates is from 706 CFM (333 L/s) to 2740 CFM (1293 L/s), which corresponds to approximately $\mathrm{Re} = 1100$ to $\mathrm{Re} = 5027$. The same heat exchanger characteristics used to develop the curves for figure 2.4 are used in figures 2.6 to 2.9. The first principal observation is that $\Delta\varepsilon$ increases for increasing air velocity. It is also observed that the rate of change of effectiveness reduction with respect to the average air velocity, i.e, $\frac{d\Delta\varepsilon}{dv}$, increases as the difference between v_1 and v_2 increases. The largest $\Delta\varepsilon$ for figures 2.6 to 2.9 is 11.1% which occurs in figure 2.6 for $A_1 = A_2 = 0.5A$, $v_1 = 1.875v$ and $v_2 = 0.125v$. This non-uniformity represents 6.25% of the airflow rate flowing through 50% of the heat exchanger area, while the remaining 93.75% of the mass flow rate flows through the other 50%.

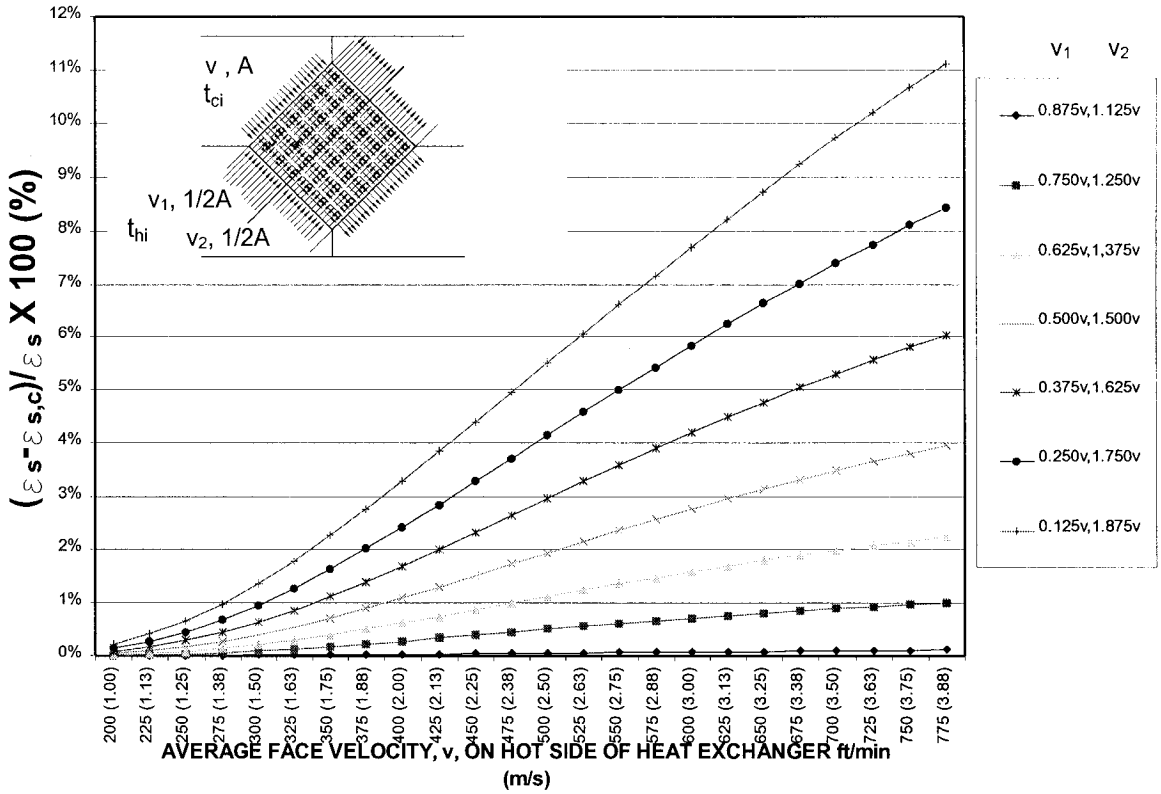

Figure 2.6 Effectiveness reduction $\Delta\varepsilon$ versus average face velocity on the hot side of the heat exchanger for two path non-uniform air velocities and A_1=0.5A; A_2=0.5A

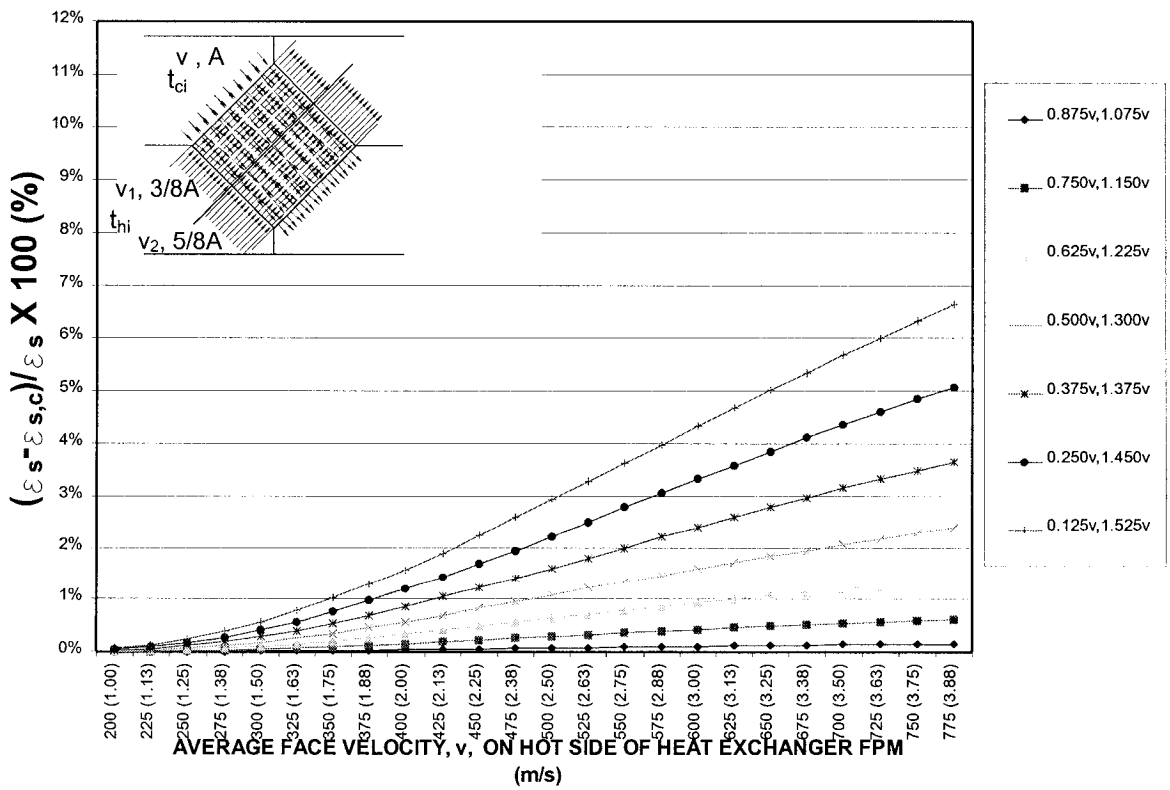

Figure 2.7 Effectiveness reduction $\Delta\varepsilon$ versus average face velocity on the hot side of the heat exchanger for two path non-uniform air velocities and A_1=0.625A; A_2=0.375A

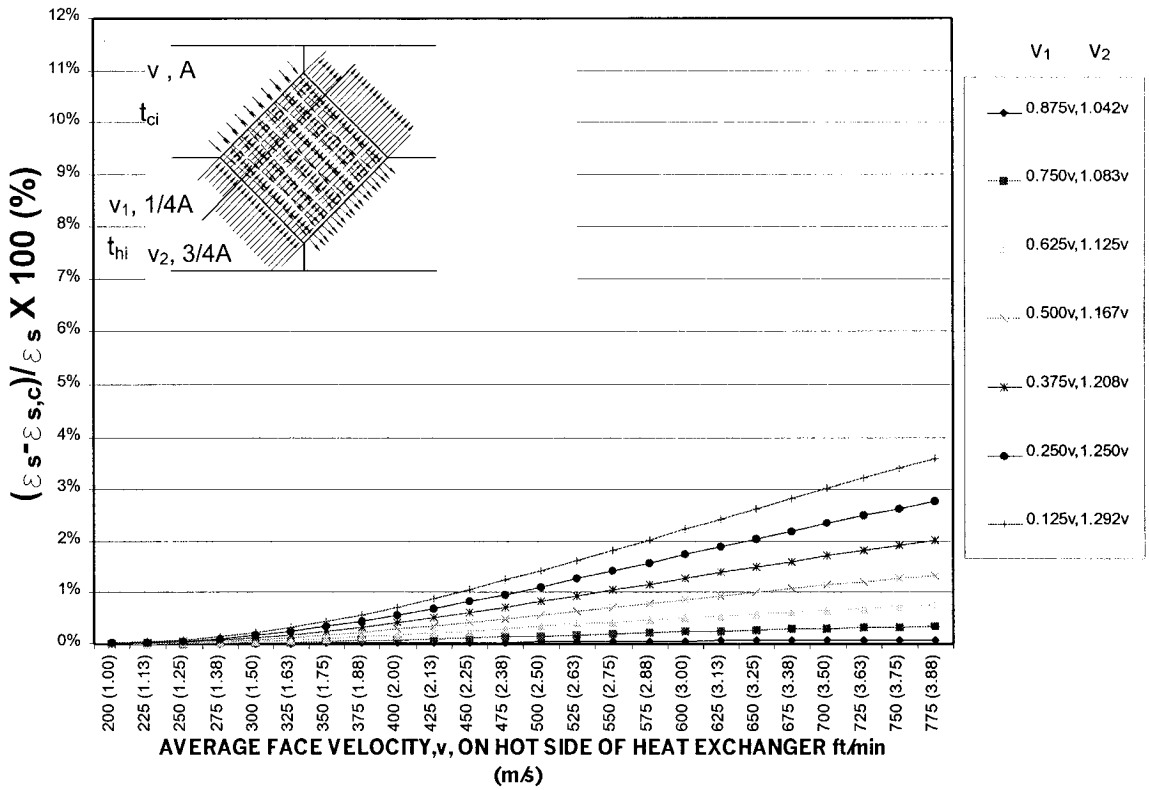

Figure 2.8 Effectiveness reduction $\Delta\varepsilon$ versus average face velocity on the hot side of the heat exchanger for two path non-uniform air velocities and A_1=0.25A; A_2=0.75A

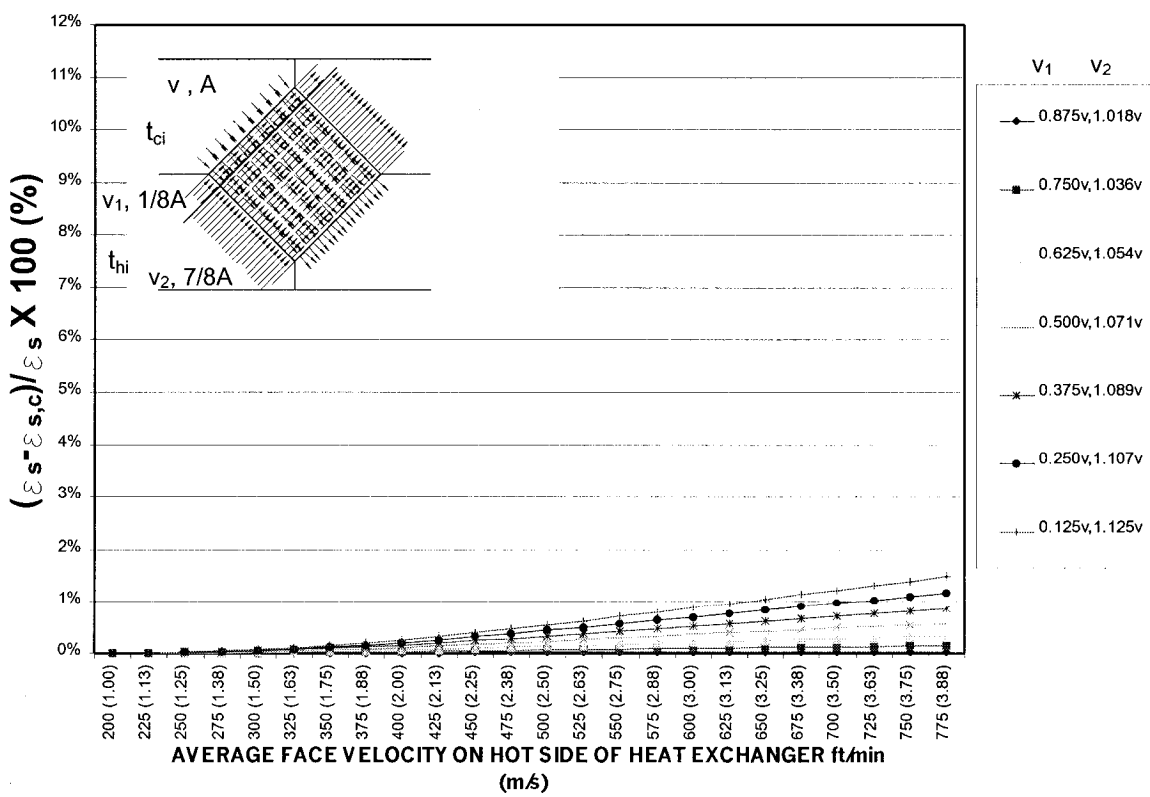

Figure 2.9 Effectiveness reduction $\Delta\varepsilon$ versus average face velocity on the hot side of the heat exchanger for two path non-uniform air velocities and A_1=0.125A; A_2=0.875A

the heat exchanger area. This result is expected intuitively, since it represents the largest non-uniformity over the largest area. The seven curves of the series gradually reduce in magnitude as the asymmetry of the path areas becomes more pronounced. The smallest $\Delta\varepsilon$ occurs for the largest asymmetric path areas (A_1=7/8A , A_2=1/8A) in combination with the smallest difference between v_1 and v_2. The largest air velocity difference between the two paths has only a marginal impact on $\Delta\varepsilon$ as seen figure 2.9. Therefore, the above curves suggest that maximum non-uniformity air velocity occurring over equal areas has the greatest effect on $\Delta\varepsilon$, whereas the maximum non-uniformity over the largest highly asymmetric path areas has a marginal impact. The above curves are based on a reasonable assumption that the smaller airflow rate flows through the corresponding smaller path area. However, in the case in which the opposite is considered, i.e., the maximum airflow flowing through the smaller path area, the effectiveness reduction increases tremendously. In order to illustrate this example, the path areas for figure 2.8 have been reversed but with the same fixed velocities, v_1, for the first path. As a result of the airflow rate balance, notice how v_2 substantially increases. When v1=0.125v, v2 is 3.625 times the average velocity, v. Table 2.2 presents the air velocities and mass airflow rate percentages for the revised path areas, A_1=0.75A and A_2=0.25

Table 2.2 Reversed Path Area and Corresponding Air Velocity Permutations for Calculating Effectiveness Reduction due to Two Path Non-Uniform Airflow.

		AIR VELOCITY FACTORS OF THE AVERAGE FOR PATHS 1 AND 2													
		PERCENT MASS AIRFLOW RATES IN PATHS 1 AND 2													
CASES		1		2		3		4		5		6		7	
PATH AREAS		v_1	v_2	v_1	v_2	v_1	v_2	v_1	v_2	v_1	v_2	v_1	v_2	v_1	v_2
A_1	A_2	Q_1	Q_2	Q_1	Q_2	Q_1	Q_2	Q_1	Q_2	Q_1	Q_2	Q_1	Q_2	Q_1	Q_2
0.75A	0.25A	0.875	1.375	0.750	1.750	0.625	2.125	0.500	2.500	0.375	2.875	0.250	3.250	0.125	3.625
		66%	34%	56%	44%	47%	53%	38%	62%	29%	71%	19%	81%	9%	91%

The series of curves corresponding to table 2.2 is presented in figure 2.10. Notice the significant increase in $\Delta\varepsilon$ for all velocity combinations.

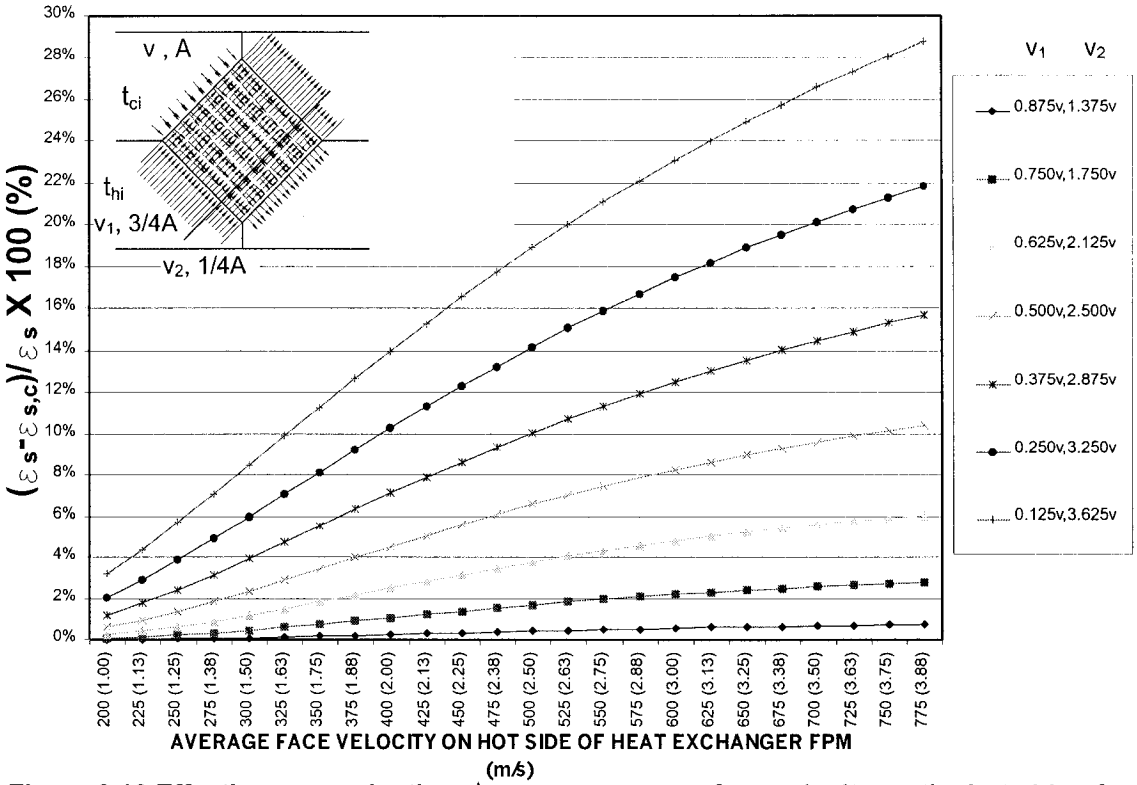

Figure 2.10 Effectiveness reduction $\Delta\varepsilon$ versus average face velocity on the hot side of the heat exchanger for two path non-uniform air velocities and A_1=0.75A; A_2=0.25A

$\Delta\varepsilon$ increases to 28.8% when 9% of the airflow flows through 75% of the overall area, and 91% of the airflow flows through 25% of the overall area. It should be noted that this flow arrangement is highly improbable in real systems.

The principal limitation of this method of evaluating effectiveness reduction due to non-uniform airflow is the assumption of only two paths. In practice there may be several paths of non-uniform airflow. In the next section, the model for effectiveness will be expanded to three parallel paths to provide a more realistic solution to the problem of effectiveness reduction due to non-uniform airflow.

2.4 Effectiveness Reduction due to Three Non-Uniform Parallel Airflow Paths on the Unmixed Side and Uniform Airflow on the Mixed side.

The consideration of a three parallel path model is a new development with respect to the reviewed literature since it has not been hitherto published. The model will be developed similarly to the two path method. Figure 2.11 illustrates the three paths, and the corresponding uniform airflow velocities of v_1, v_2, and v_3 flowing through areas A_1, A_2, and A_3 respectively on the hot

air side. The added complexity of the three path method involves solving for two unknown air temperatures, t_I and t_J, located on the cold side of the heat exchanger on the boundary plane between the first and second, and the second and third paths. These two unknown temperatures are solved by first considering an energy balance for each of the three parallel paths.

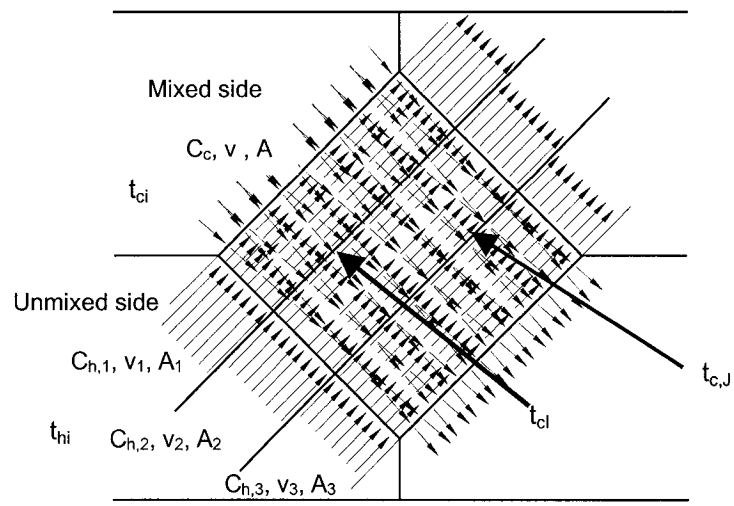

Figure 2.11 Idealized flow non-uniformity on the unmixed side for three parallel paths of a mixed-unmixed cross flow plate heat exchanger

The energy balance for q_1 presented in equation 2.17 does not change from the two path model. Similarly, $t_{c,I}$ is solved according to equation 2.18. Equations for q_2, $t_{c,J}$ and q_3 are derived as follows:

$$q_2 = C_{h,2} \times \varepsilon_{h,2} \times \left(t_{h,i} - t_{c,I}\right) = C_c \times \left(t_{c,J} - t_{c,I}\right) \quad \textbf{(2.24)}$$

$t_{c,J}$ is derived from equation (2.24):

$$t_{c,J} = t_{c,I} + \frac{C_{h,2}}{C_c} \times \varepsilon_{h,2} \times \left(t_{h,i} - t_{c,I}\right) \quad \textbf{(2.25)}$$

Equation 2.18 can be substituted into equation (2.25) to complete the derivation of $t_{c,J}$. q_3 is derived as follows:

$$q_3 = C_{h,3} \times \varepsilon_{h,3} \times \left(t_{h,i} - t_{c,J}\right) \quad \textbf{(2.26)}$$

The effectiveness for the three separate paths, $\varepsilon_{h,1}$, $\varepsilon_{h,2}$ and $\varepsilon_{h,3}$ is solved from equation (2.15).

The total heat transfer can now be solved:

$$q = q_1 + q_2 + q_3 = \varepsilon_h \times C_h \times (t_{h,i} - t_{c,i}) \qquad \textbf{(2.27)}$$

The reduced effectiveness, ε_h, is derived from equations (2.17), (2.18), and (2.24) to (2.27):

$$\varepsilon_h = \frac{1}{C_h}\left[C_{h,1}\varepsilon_{h,1} + C_{h,2}\varepsilon_{h,2}\left(1 - \frac{C_{h,1}\varepsilon_{h1}}{C_c}\right) + C_{h,3}\varepsilon_{h,3}\left(1 - \frac{C_{h,1}\varepsilon_{h,1}}{C_c} - \frac{C_{h,2}\varepsilon_{h,2}}{C_c}\left(1 - \frac{C_{h,1}\varepsilon_{h,1}}{C_c}\right)\right)\right] \qquad \textbf{(2.28)}$$

The percent effectiveness reduction can now be evaluated based on equation (2.23). The number of permutations of path areas and air velocities is too numerous to present in the present work. Three different area combinations have been used in conjunction with the same air velocities for the first path, v_1, as in table 2.2. The permutations for the three path cases are presented in table 2.3.

Table 2.3 Area and Velocity Permutations for Calculating Effectiveness Reduction due to Three Path Non-Uniform Airflow

		AIR VELOCITY FACTORS OF THE AVERAGE FOR PATHS 1, 2 AND 3																				
		PERCENT MASS AIRFLOW RATES IN PATHS 1, 2 AND 3																				
CASES		1			2			3			4			5			6			7		
PATH AREAS		v_1	v_2	v_3	v_1	v_2	v_3	v_1	v_2	v_3	v_1	v_2	v_3	v_1	v_2	v_3	v_1	v_2	v_3	v_1	v_2	v_3
A_1	A_2 & A_3	Q_1	Q_2	Q_3	Q_1	Q_2	Q_3	Q_1	Q_2	Q_3	Q_1	Q_2	Q_3	Q_1	Q_2	Q_3	Q_1	Q_2	Q_3	Q_1	Q_2	Q_3
0.33A	0.33A	1.125	1.000	0.875	1.250	1.000	0.750	1.375	1.000	0.625	1.500	1.000	0.500	1.625	1.000	0.375	1.750	1.000	0.250	1.875	1.000	0.125
		38%	33%	29%	42%	33%	25%	46%	33%	21%	50%	33%	17%	54%	33%	13%	58%	33%	9%	63%	33%	4%
0.4A	0.3A	1.125	0.958	0.875	1.250	0.918	0.750	1.375	0.985	0.625	1.500	0.833	0.500	1.625	0.792	0.375	1.750	0.750	0.250	1.875	0.708	0.125
		45%	29%	26%	50%	28%	22%	55%	26%	19%	60%	25%	15%	65%	24%	11%	70%	22%	8%	75%	21%	4%
0.5A	0.25A	1.125	1.000	0.750	1.250	0.875	0.625	1.375	0.750	0.500	1.500	0.625	0.375	1.625	0.500	0.250	1.750	0.375	0.125	1.875	0.188	0.063
		56%	25%	29%	62%	22%	16%	69%	19%	12%	75%	16%	19%	81%	13%	6%	88%	9%	3%	93%	5%	2%

The corresponding curves for table 2.3 are shown in figures 2.12 to 2.14. The same trend for effectiveness reduction is observed for the three path model. The largest effectiveness reduction of $\Delta\varepsilon$ = 11.2% occurs in figure 2.14 for A_1=0.5A, A_2=A_3=0.25A, v_1=1.875v, v_2=0.19v, and

v_3=0.06v. This represents the largest airflow non-uniformity flowing through the largest difference in areas, i.e., 93% of the mass airflow rate flows through the ½ of the area, while the remaining 7% flows through the other two flow paths. In section 2.1, the equations for the laboratory measurements were presented. The focus of the present work is experimental, and therefore accuracy and precision of measurements and the subject of pre-test uncertainty analysis will precede the presentation of a description of the test facility and the results.

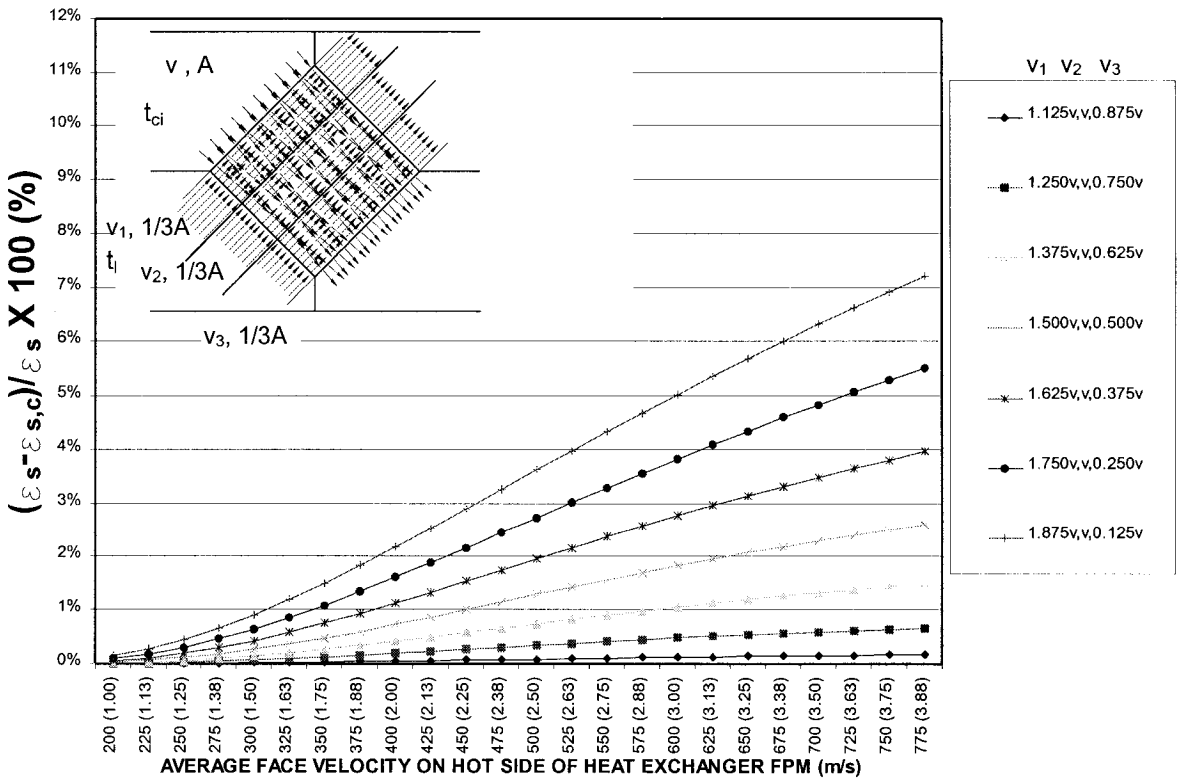

Figure 2.12 Effectiveness reduction $\Delta\varepsilon$ versus average face velocity on the hot side of the heat exchanger for three path non-uniform air velocities and A_1=0.333A; A_2=0.333A; A_3=0.333A

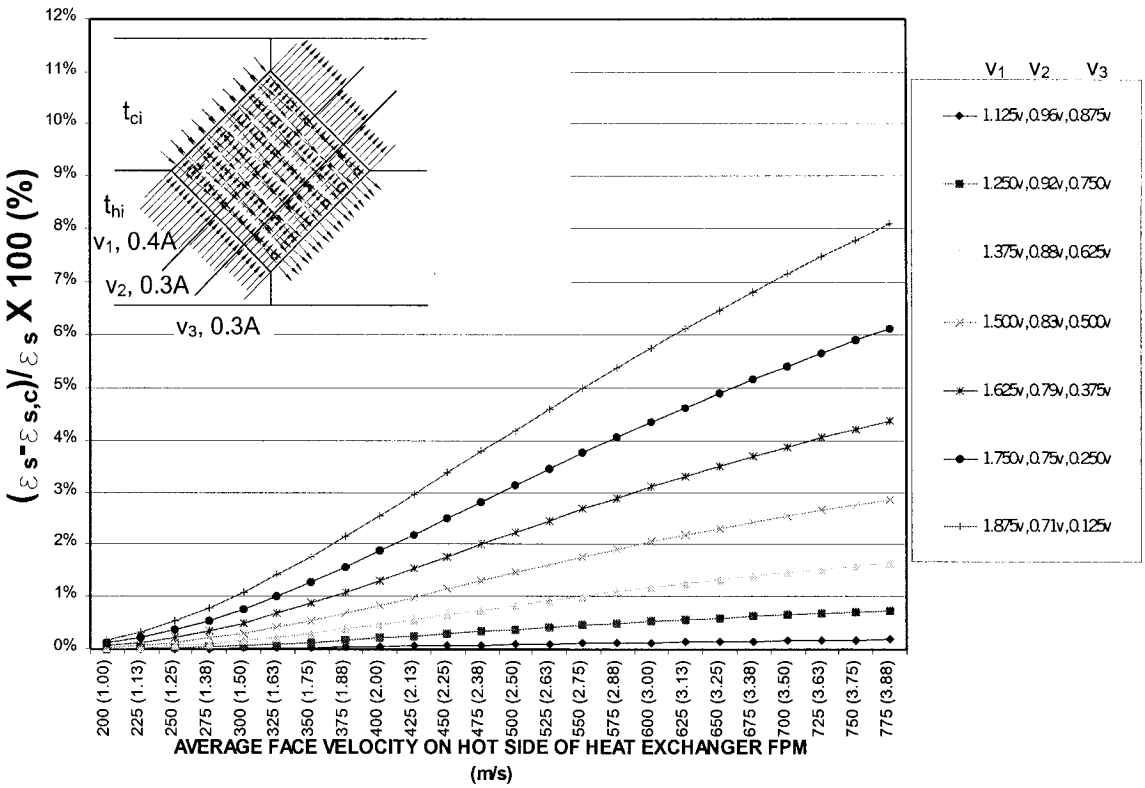

Figure 2.13 Effectiveness reduction $\Delta\varepsilon$ versus average face velocity on the hot side of the heat exchanger for three path non-uniform air velocities and A_1=0.4A; A_2=0.3A; A_3=0.3A

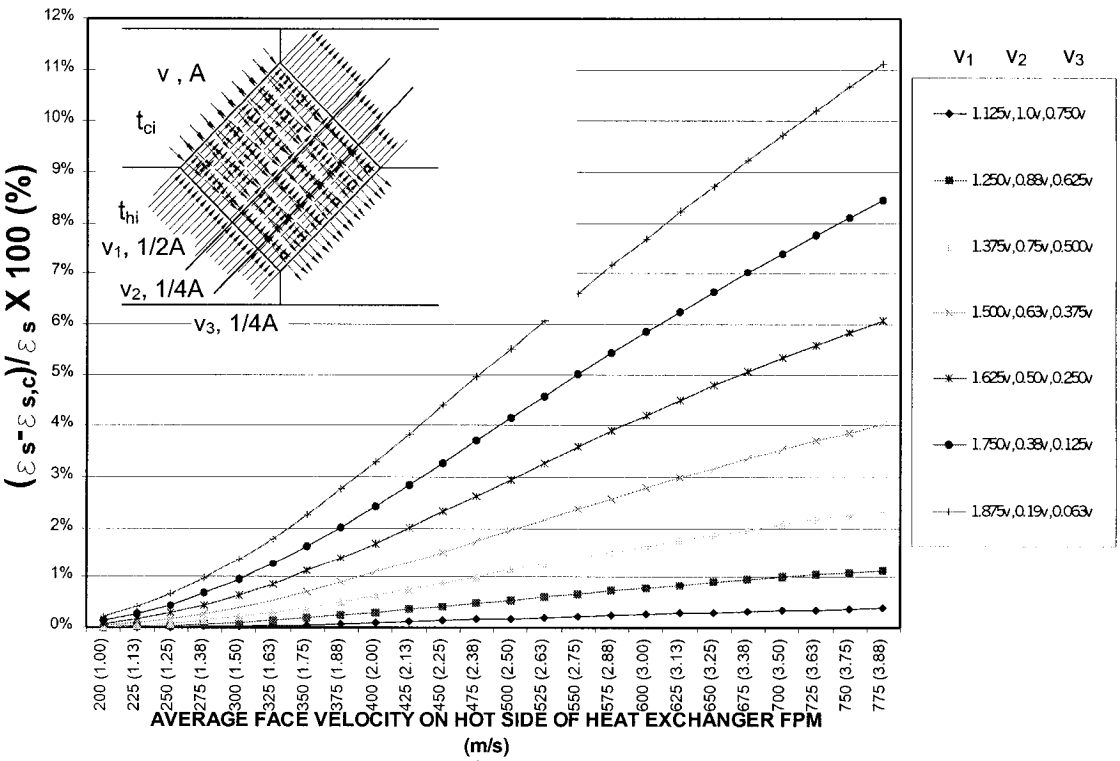

Figure 2.14 Effectiveness reduction $\Delta\varepsilon$ versus average face velocity on the hot side of the heat exchanger for three path non-uniform air velocities and A_1=0.5A; A_2=0.25A; A_3=0.25A

3.0 PRE-TEST UNCERTAINTY ANALYSIS

Ultimately laboratory experiments of any type can be judged based on the level of accuracy of the measuring instruments used and the precision of the measurements. Utilizing the combination of both accuracy and precision in assessing the validity of an experiment is commonly known as uncertainty analysis. The following quote from NIST TH 1297 sums up the importance of uncertainty analysis:

"A measurement result is complete only when accompanied by a quantitative statement of its uncertainty."

Coleman and Steele (1989) reinforce this idea by stating that data collection is a small portion of the entire experimental process. Ciepliski and Besant (1998) recommend that uncertainty analysis be the prime criteria for accurately testing air-to-air heat recovery devices. In their paper they describe pre-test selection procedures that minimize uncertainty associated with operating conditions. In the following sections, a detailed analysis of the effect of both measurement uncertainty and operation conditions on sensible effectiveness uncertainty will be presented. ASHRAE Guideline 2-1986 (RA 96) suggests that all measurements should include three parts:

- Best value
- ±Confidence limits or uncertainty interval
- The associated probability, typically 0.95 or 95% confidence for N ≥ 30

Uncertainty consists of systematic, fixed or constant error, also known as bias errors, β, and random error also known as precision, P. The total error, δ, can be calculated for one measurement as the sum of these two uncertainty components.

$$\delta = \beta + P \qquad \textbf{(3.1)}$$

An important distinction must be made between the concept of error and uncertainty. NIST TN 1297 makes the distinction by explaining that the output of a measurement after correction can be very close to the unknown value of the result, and therefore have insignificant error even though it might have a large uncertainty. Figure 3.1 illustrates the combinations of good and poor accuracy

and precision. $\overline{X}'$ represents the true value of the quantity being measured. The best estimate of the true value is the average of the measurements, $\overline{X}$ defined as follows:

$$\overline{X} = \frac{1}{n} \times \sum_{i=1}^{n} X_i \tag{3.2}$$

In order to quantify how the data scatter around the average value, the standard deviation of a population, σ, is defined as follows:

$$\sigma = \left[\frac{1}{n} \times \sum_{i=1}^{n} \left(X_i - \overline{X}' \right)^2 \right]^{1/2} \tag{3.3}$$

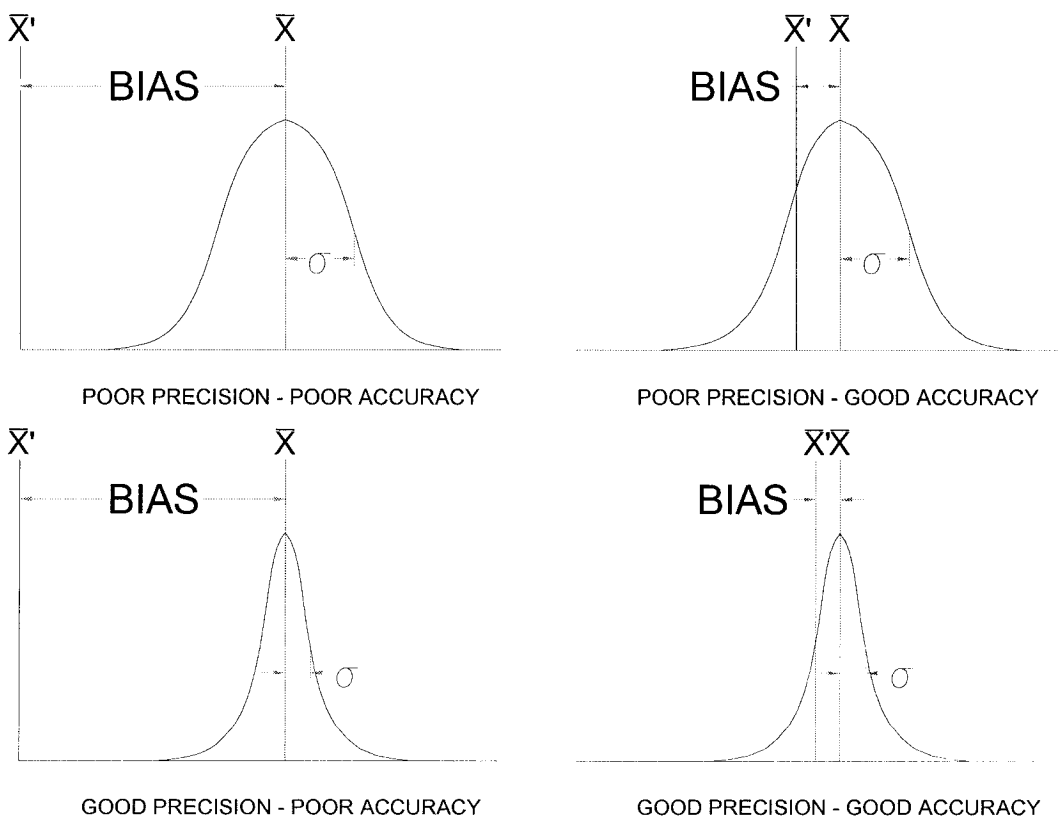

Figure 3.1 Four combinations of accuracy and precision (Benedict and Wyler (1979))

Uncertainty analysis is not only the final step of an experiment as part of the data analysis section but also an essential tool at the planning stage of an experiment to determine if the available instrumentation has adequate accuracy to produce results within acceptable uncertainty limits. The concept of a pre-test uncertainty analysis is not new and was proposed by Rousseau (1974), in reference to estimating the precision in heat rate testing. He does not consider errors related to setup, calibration and response, but only those due to data scatter. Furthermore, he presents a table of measurement effects on heat rate. Based on this table it is possible to identify the parameter that is most sensitive in terms of its effect on heat rate. In the following sections relating to pre-test analysis a curve for each measured parameter will be presented to illustrate in a graphical form the sensitivity of the individual measurement uncertainty and operating conditions on the overall effectiveness uncertainty. Coleman and Steele (1989) suggest that during the planning stage of an experiment only the overall uncertainty be considered. At the planning stage instrumentation might not have been chosen yet, and, therefore, any bias is likely to be either positive or negative. Both the bias and precision errors will be combined into one value for estimation purposes. It is essential to properly assign the values of uncertainty for the individual measuring instruments, otherwise the results of a pre-test uncertainty analysis will be meaningless.

Ciepliski (1997) makes recommendations to include pre-test and post-test methods of uncertainty analysis in the stated results of heat recovery test standards. Lassahn (1985) makes a case that, although Uncertainty analysis is becoming more frequently used, there still appears to be a lack of standard definitions and, therefore, a resulting lack of meaning for uncertainty. Standards have now been established, such as ANSI/ASME PTC 19.1-1985 and NIST TN 1297. However, there does not appear to be a universal standard method for uncertainty analysis. Both of the aforementioned standards for uncertainty analysis offer somewhat different approaches and definitions. As will be seen further in this section, it will be possible to identify which measured parameters have greater effect on the result. In other words, a sensitivity analysis can be performed with regard to the effect of the individual measured variables on the final result.

Benedict and Wyler (1979) demonstrate a sensitivity analysis on heat rate of a steam turbine. They perform a sensitivity analysis by changing each individual variable one at a time and observing the effect on the confidence interval of the result. This sensitivity analysis will allow the experimenter to identify the variables that require greater accuracy as compared to variables that require lesser accuracy. This opportunity allows greater flexibility and potential cost savings in selecting the instrumentation and sensors. The primary motivation in presenting this material is to illustrate the sensitivity of both measurement and operating conditions on the uncertainty of sensible effectiveness. Moffat (1985) makes a succinct observation regarding the cost savings as a result of an uncertainty analysis at the planning phase of an experiment:

"The important point to remember is that desk-time is cheaper than test-time."

Moffat (1985) elaborates extensively on the use of uncertainty in the planning stage of an experiment. In his proposed method of pre-test uncertainty analysis, the individual estimates account for both reading uncertainties (precision) and calibration uncertainties (bias). He uses an Nth order replication in his pre-test uncertainty analysis. The intention of his method is to produce an uncertainty interval for the result such that any person in any laboratory using any set of measuring instruments can produce results that agree with his predictions. One of the primary objectives of this section is to produce a pre-test uncertainty analysis for testing sensible heat recovery devices that can be practically used by any person in any laboratory. Replication is a fundamental concept in the field of statistics, but it is often not feasible to realize a higher order replication to validate an experimental result. Replication and repetition are synonymous, but within the context of uncertainty analysis and statistics the two terms need to be distinguished from each other. Repetition, as the name implies, refers to an event such as an experiment that is repeated as a function of time. Repetition can be thought as a part of a two-dimensional process in which a variable is measured at a particular time rate, i.e., sample per second/minute/hour etc... Repetition involves changing one parameter at a time. Replication can involve changing several experimental parameters at one time and therefore can be two dimensions or higher. Three main orders or levels of replication in reference to uncertainty analysis can be defined as follows:

Zeroth order replication-

A steady state parameter is measured once using a measuring instrument that has a known Bias. Since the parameter is only measured one time, precision or random error is eliminated from the measurement uncertainty. The only uncertainty arises when different observers interpret the data differently. Typically, the uncertainty at this level is assigned one half the least division of the measuring instrument. Zeroth order replication is often used in pre-test uncertainty analysis to assist in selecting instrumentation.

First Order Replication-

As replication approaches higher orders, the experiment can be viewed with greater degrees of freedom. In a first order replication, measurements are taken as a function of time, thereby introducing precision or random errors associated with the unsteadiness of the measured process. The standard statistical tools such as mean and standard deviation can be applied to assess the precision of the sample of measurements. Naturally, more readings will result in a more confident estimation. A first order replication allows for the discovery of systematic errors in instrumentation and other factors that affect the steadiness of the measured variable.

N^{th} Order Replication-

In the hypothetical scenario in which measuring instrumentation, and the actual laboratory changes for each experiment, in addition to time, then an N^{th} order level of uncertainty is required. At this level of replication, Bias is no longer fixed but is dependant on the individual measuring instrument for each experiment. In general, the uncertainty for an Nth order replication experiment will be higher than for a first order replication experiment. In the present research, different instrumentation will not be used and the location of the measurements will remain constant, because of the costly nature of this extra research.

One of the objectives of this work is to highlight the lack of guidelines for pre-test, during test, and post-test uncertainty analysis in the present standards for testing air-to-air heat recovery devices. The basic equations for uncertainty will be presented in addition to the way they are applied in the case of determining sensible effectiveness uncertainty. The most significant

contribution of this section will be the presentation of graphs depicting the sensitivity of both the individual measurement uncertainty and operating conditions on the sensible effectiveness uncertainty. The graphs will shed light on how to maximize the information obtained during a pre-test uncertainty analysis.

3.1 Uncertainty analysis in Relation to Testing Standards for Heat Recovery

The existing standards on testing air-to-air heat recovery devices currently provide no guidelines on performing uncertainty analysis at any stage of the experiment including planning, during, and post-testing. In most cases, such as ASHRAE std 84-1991 and CSA C439-00 (supersedes CSA C439-1988), only precision and accuracy uncertainty limits are specified for each measurement. Both of these standards provide no guidelines on performance uncertainty analysis. Guidelines can be found in ASHRAE Guideline 2-1986 (RA 96), Engineering Analysis of Experimental Data, which was a standard prior to 1986. The guideline does not offer specific levels of bias and precision uncertainties for heat recovery test standards, but it does present a methodology and equations in performing both a pre-test and post-test uncertainty analysis. In section 4.2 of the guideline, called Generalized Experimental Procedure, a series of steps are identified to assess the measurement technique that provides the best choice between a low uncertainty and high cost. It suggests that critical measurements must be identified and reduced. The most comprehensive standard for uncertainty analysis is ASME PTC 30-1985, which requires that both the pre-test and post-test uncertainty analysis not exceed $\pm$ 5 % or the test is deemed unacceptable. Table 3.1 compares the accuracy and precision of various measuring instruments for the different standards. If uncertainty guidelines are provided, then this encompasses both accuracy and precision, as in the case of ASME PTC 30-1985. Mueller, Howell et al (1981) present a paper on the early development of a standard test facility for air-to-air energy recovery systems for ASHRAE STD 84-78, the predecessor of the current std 84-1991. In the appendix of their paper they discuss uncertainty analysis of test data and the influence of the selected instrumentation on the heat exchanger effectiveness. The equations for uncertainty developed in Mueller and Howell's paper was not adopted by the ASHRAE standards.

Table 3.1 Comparison of Accuracy and Precision for the different standards

1985	ASHRAE std 84-1991 ARI std 1060-1997		CSA C439-00		ENV std 308-1996		ASME PTC 19.1-
Measurement Parameter	Accuracy	Precision	Accuracy	Precision	Accuracy	Precision	U_{RSS}(95%)
Temperature, DB	±0.1 °C	±0.05 °C	±0.5 °C	N/A	±0.2 K	N/A	±0.2 °F
Temperature, WB	±0.1 °C	±0.05 °C	±0.5 °C	N/A	±0.3 °F	N/A	±0.1 °F
Temperature, Dp	±0.2 °C	±0.1 °C	±0.4 °C	N/A	N/A	N/A	N/A
Relative Humidity	±2%	±1%	N/A	N/A	N/A	N/A	N/A
Pressure	±1%*	±0.5%	±1%*	N/A	±3%	N/A	N/A
Tracer Gas	±0.1%	±0.05%	±0.1%**	N/A	±10%	N/A	N/A
Length or Diameter***	±0.2%	N/A	±0.2%	N/A	N/A	N/A	N/A

* ± 1% refers to the maximum observed reading or ± 0.005 in. w.c. (±1.25 Pa), whichever is larger

** Both standards, ASHRAE 84-1991 and CSA C439-00 describe the accuracy of the tracer gas as the injection rate that will be sufficient so that a carryover of 0.1% into airstream no. 4 is within the measuring capability of the device being used.

*** This accuracy specification originates from ASHRAE Std 51-85, Laboratory Methods of Testing Fans for Rating. It specifies that diameters will be within the ±0.2% of the mean at each plane in reference to a nozzle.

The CSA C439-00 does not specify the required level of precision for measurements. In addition, the standard also requires that other parameters relating to power consumption of the heat recovery ventilator are to be measured, including all electrical components such as motors, heaters, and damper actuators. Heat losses through the unit casing and air leakage are factored into the overall heat recovery efficiency as defined in section 9.33 of CSA C439-00. The complexity of the sensible heat recovery equation for this standard is illustrated as follows:

$$\varepsilon_{shr} = \frac{\left(\sum_{i=1}^{n} \dot{m}_{s,i} \times c_p \times \left(T_{5,i} - T_{1,i}\right) \times \Delta\theta\right) - Q_{SF} - Q_{SH} - Q_C - Q_D - Q_L}{\left(\sum_{i=1}^{n} \dot{m}_{\max,i} \times c_p \times \left(T_{3,i} - T_{1,i}\right) \times \Delta\theta\right) + Q_{EF} + Q_{EH}} \qquad \textbf{(3.4)}$$

where:

ε_{shr} : Sensible heat recovery efficiency

n : The number of times that data is recorded

i : i^{th} time that data is recorded

$\dot{m}_s$: Mass flowrate of outdoor air. $\dot{m}_s = \dot{m}_2 \times (1 - R)$ where:
$\dot{m}_2$: mass flow rate at station 2, kg/s and
R : Exhaust-air-contamination ratio

c_p : Specific heat of air

T_1, T_3 : Dry-bulb temperature in heat recovery ventilator on the entering supply side, and entering exhaust side respectively

T_5 : Dry-bulb temperature for net outdoor air that accounts for the exhaust-air-transfer ratio, R ; the difference in enthalpy between leaving supply side and exhaust entering side of the heat recovery ventilator; and the humidity ratio difference between leaving supply side and exhaust entering side of the heat recovery ventilator.

$\dot{m}_{max}$: Maximum mass flow rate of $\dot{m}_s$ or $\dot{m}_e$.

$\Delta\theta$: Time between airflow measurements

Q_{SF} : Energy input into supply airstream attributed to fan/motor

Q_{EF} : Energy input into exhaust airstream attributed to fan/motor

Q_{SH} : Energy used by heater in supply airstream, and energy use attributed to compressor

Q_{EH} : Energy used by heater in exhaust airstream

Q_C : Casing heat transfer, where: $Qc = \sum_{i=1}^{n} UA_i \times (T_{case,i} - T_{air}) \times \theta_t$

Q_D : Defrost energy use

Q_L : Heat loss due to casing leakage

Uncertainty would have to be estimated for all the variables listed above and for their corresponding nested variables. There is no mention on the accuracy or precision required for measuring the energy losses and gains. Based on the complexity of the above equation for heat recovery effectiveness, and the number of variables involved, the task of performing a pre-test or post-test uncertainty would be time consuming. That exercise will be left for a future work on uncertainty analysis relating to air-to-air heat recovery.

None of the above mentioned standards have uniform and consistent styles for presenting accuracy and precision. Even within a standard there is no consistency in presenting the accuracy and precision. There are three main forms in presenting manufacturer listed accuracy:

1. Percentage of reading, ± P %
2. Percentage of full-scale measurement range, ± P %
3. Constant value for the given measurement range, ± R

Where P is the percentage and R is a value. As an example for pressure readings, ASHRAE std 84-1991 states: "±1% of the maximum observed reading or ±0.0005 in. w.c. (±1.25 Pa) whichever is larger.". In this case, there are two forms of accuracy presentation for one parameter, pressure. It is preferred to present a reasonable range of constant value accuracy, ± R, for a particular parameter. The ± 1% of maximum observed reading in combination with accuracy of other instruments might cause the propagated error to exceed the specified final uncertainty for the result. Furthermore, the maximum observed reading would not be known until the testing has been performed. Therefore, this presents a dilemma for the experimenter in regard to selecting an instrument prior to testing. All of the listed instrument accuracy's should provide a range of values that provide flexibility for the experimenter to find a balance between cost and the final uncertainty of the result. In presenting a reasonable range of constant value accuracy, the experimenter can convert the constant value to a ± P % of full scale for a particular sensor and determine if it is within the specified accuracy range.

Typically, pressure transducer accuracy is described in terms of ±% of full scale (FS). Scale is an important consideration in relation to accuracy. For example a pressure transducer that has a range from 0 to 1" in. w.c. (0 to 248 Pa) with a ±1% FS (±0.01" in. w.c. or ± 2.5 Pa) accuracy will be more accurate than a pressure transducer with a range from 0 to 5" in. w.c. (0 to 1240 Pa) with the same level of accuracy (±0.05" in. w.c. or ±12.4 Pa). The first pressure transducer is 5 times more accurate than the second one.

Another important consideration in the selection of a sensor and other measuring instruments is that the manufacturer specified accuracy is usually listed as constant over its

measuring range. The accuracy of relative humidity is described in ± P%, since the assumption is that the accuracy is constant over the 0 to 100 % range. However, not all humidity transmitters have a constant accuracy over the entire range of measurement. There are humidity transmitters on the market that specify that the accuracy (2% or 3%) is only between 10 to 90%. For example, one manufacturer's humidity transmitter specifies ± 2% between 0% RH and 90% RH, and ± 3% RH between 90% RH and 100% RH. It is important to be aware of this fact when selecting the humidity transmitter for testing purposes, in particular when the conditions might require measurement of either very humid or very dry air. The humidity transmitters that are used in the present research have an accuracy of ± %2 RH for 0% RH to 100% RH. Price and Suby (2000) present a salient example of the selection of different chilled water flow meters based on the manufacturer listed accuracy. In their example the accuracy for some of the flow meters is range specific. In other words, the accuracy for the low end of the meter is specified in addition to the accuracy for the remaining range. They observe from their example that false conclusions can be drawn from measured data if the uncertainty in the measurement is not considered correctly.

The level of accuracy described for the tracer gas is ambiguous in all standards. For example, ASHRAE std 84-1991 requires an accuracy of ±0.1% for crossover by tracer gas. Does the ±0.1% refer to the measured concentration of tracer gas? The standard CSA C439-00 does not explicitly state the required accuracy but gives the following guideline: "section 8.2.2 An inert gas will be injected into the airstream before fan No. 2. The injection rate will be sufficient that a carry-over of 0.1% into airstream no. 2 is within the measuring capability of the device being used." Therefore no specific accuracy is specified.

None of the standards provide any guidelines in presenting the accuracy of the results. Section 8 in ASHRAE STD 84-1991 gives a brief description of which parameters and results should be presented including the family of curves indicating face velocity versus effectiveness for a range of mass flow rations, $\dot{m}_{min}/\dot{m}_{max}$, from 0.5 to 1.0. In section 3.3, it will be demonstrated on how the effectiveness uncertainty is profoundly influenced by the operating

conditions. CSA C439-00 provides a more detailed example of a report sheet on the performance of a Heat Recovery Ventilator (HRV) but does not include any section on the accuracy of the results. ARI std 1060-1997 is principally based on ASHRAE std 84-1991, except for a few additional requirements. There is no more information on the accuracy of the measurements, but there is a mention on testing tolerances. Throughout the duration of the test, the section 4 of the standard stipulates that the airflow will remain within a tolerance of ± 1.5% or ± 5 scfm (±2.36 L/s), whichever is greater. The stability of the airflow in the system will depend upon the type of fan, the fan performance curve for the range of operating conditions, the connecting ductwork, the location of the airflow station, and the type of airflow station. The standard also specifies that the measured pressure differentials across the heat exchanger will remain within a specified tolerance of ± 0.05 in. of H_2O [± 12.5 Pa] for the duration of the test. ARI std 1060-1997 differs from ASHRAE std 84-1991 in that it specifies the specific range and increments of air flow rates that the heat recovery devices require to be tested. The ranges and increments are specified as follows:

Q < 250 scfm (118 L/s)	→ Q_{incr}=10 scfm (4.72 L/s)
250 scfm (118 L/s)≤ Q < 500 scfm (236 L/s)	→ Q_{incr}=25 scfm (11.8 L/s)
500 scfm (236 L/s)≤ Q < 1000 scfm (472 L/s)	→ Q_{incr}=50 scfm (23.6 L/s)
Q ⩾ 1000 scfm (472 L/s)	→ Q_{incr}=100 scfm (47 L/s)

It is important to highlight that if uncertainty analysis is included in a test that covers a range of airflow rates it might change based on the operating conditions. The operating conditions in some cases might govern the uncertainty of the effectiveness, in particular when the measured parameter is small relative to the scale of the measuring instrument. This will be demonstrated clearly in section 3.4. The other operating condition that should be assessed is the maximum temperature difference in the heat exchanger, i.e., the cold loop entering, t_{ci} versus the hot loop entering, t_{hi} (supply and exhaust entering). ARI std 1060-1997 specifies a temperature difference of 35°F (19.3°C) in heating mode, and of 20°F (11.1°C) in cooling mode. ASHRAE std 84-1991 specifies a temperature difference of 54°F (30°C) in heating mode and of 25°F (14°C) in cooling mode.

Ciepliski, Besant, and Simonson (1998) present several proposed revisions for ASHRAE STD 84-1991. 9 out of the 13 proposed revisions involve uncertainty. Proposal number 10 presents limits for the level of uncertainty to satisfy the test standard:

Sensible Effectiveness Uncertainty: $U_{\varepsilon s} < \pm 5\%$

Latent Effectiveness Uncertainty: $U_{\varepsilon l} < \pm 7\%$

Total Effectiveness Uncertainty: $U_{\varepsilon t} < \pm \dfrac{|\varepsilon_t - \varepsilon_l|5\% + |\varepsilon_t - \varepsilon_s|7\%}{|\varepsilon_t - \varepsilon_s|}$ or $\pm 5\% > U_{\varepsilon t} < \pm 7\%$

The proposed revisions also included an increase of 2 ½ % increase in uncertainty for field testing.

3.2 Theory of Pre-test Uncertainty analysis

A pre-test uncertainty analysis will be conducted based on the NIST TN1297, and ASME PTC 30-1985. The TN 1297 recognizes two categories of uncertainty analysis: Type A and type B. Type A is based on a statistical approach when sufficient amount of data is available from tests. Standard statistical tools such as calculation of sample standard deviation is defined as follows:

$$S = \sqrt{\frac{\sum_{i=1}^{n} \left(\bar{X} - X_i\right)^2}{(n-1)}} \qquad \textbf{(3.5)}$$

Other techniques that can be used include the method of least squares to fit a curve to data in order to estimate the standard deviations, and to carry out an analysis of variance to identify and quantify random effects that can occur in certain types of measurements. It also important to mention that the number of readings per instrument has a significant impact on determining the confidence interval based on a two-tailed student-t distribution. Typically, a minimum of 30 readings is required in order to obtain the t factor of 2. The precision limit can then be estimated based on the following formulation:

$$P = tS \qquad \textbf{(3.6)}$$

Where S is known as either the sample standard deviation or the precision index. t can be obtained from established tables for student-t distributions for different sample sizes. If the sample size is n, then the number of degrees of freedom, ν, is defined as $n-1$. The sample standard deviation, S, looses one degree of freedom from the population standard deviation, σ. Type B uses other means for determining the uncertainty, such as the following (TN 1297):

- Previous measurement data,
- Experience with or general knowledge of the behavior and property of relevant materials and instruments,
- Manufacturer published specifications indicating accuracy of measuring instrument,
- Data provided in calibration and other reports, and
- Uncertainties assigned to reference data taken from handbooks.

For a pre-test Uncertainty analysis, since data has not be obtained at this stage, typically, a type B evaluation will be used. The main guide for the Uncertainty analysis in this thesis will be based on ASME PTC 19.1-1991. Some terminology from TN 1297 will also be used. Uncertainty consists of two components: Bias error, B, and the random or precision error, P. Bias error represents the fixed or constant error from one measurement to the next and is known more commonly as accuracy. Bias error usually results from calibration errors, scale reading errors, errors due to Analogue to Digital conversion, and other errors associated with the data acquisition. Bias errors can be either positive or negative.

Typically, the desired result cannot be measured directly and is calculated using more basic measured parameters. Since more than one variable is involved in calculating the experimental result, the uncertainties of the individual parameters must be accounted for and combined to establish the overall uncertainty. This is also known as propagation of uncertainty. Coleman and Steele (1989) define the pre-test uncertainty analysis as a general uncertainty analysis. At the planning stage, it is difficult to estimate the precision error, or the random error due to repeated measurements. Furthermore, the instrumentation might not have been selected, thus allowing flexibility to choose the type of sensors that will not allow the overall uncertainty to exceed the required level. Therefore, bias and precision uncertainties are not considered

separately, but instead the overall measurement uncertainties are considered. The general equation that describes the overall uncertainty for a particular result, r, is as follows:

$$U(y) = \left[\left(\frac{\partial f}{\partial X_1} U_{X1} \right)^2 + \left(\frac{\partial f}{\partial X_2} U_{X2} \right)^2 + \ldots + \left(\frac{\partial f}{\partial X_J} U_{XJ} \right)^2 \right]^{1/2} \quad \textbf{(3.7)}$$

Where $y = f(X_1, X_2, \ldots, X_J)$ is the result of the experiment as a function of the J variables of X_i, and U_{Xi} is the corresponding uncertainty for each variable. It should be observed that the partial derivatives are taken of the result with respect to each individual variable. Therefore, all of the other variables are held constant. The partial derivative, $\frac{\partial f}{\partial X_i}$, is also denoted as the absolute sensitivity coefficient, ϑ_i, according to Coleman and Steele (1989).

$$\vartheta_i = \frac{\partial f}{\partial X_i} \quad \textbf{(3.8)}$$

Equation 3.7 is often called the law of propagation of uncertainty or the root-sum-of-squares method (RSS method). Equation 3.7 is used when the variables are independent in reference to each other. When there are variables that are dependent on each other, an extra term is added for co-variance. Co-variance refers to two variables that will be measured by the same sensor. In the following equation 3.9, the term for co-variance has been added to the equation for general uncertainty for two variables, (X_1, X_2), that are co-variant:

$$U(y) = \left[\left(\frac{\partial f}{\partial X_1} U_{X1} \right)^2 + \left(\frac{\partial f}{\partial X_2} U_{X2} \right)^2 + \ldots + \left(\frac{\partial f}{\partial X_J} U_{XJ} \right)^2 + 2 \left(\frac{\partial f}{\partial X_1} \frac{\partial f}{\partial X_2} \rho_{12} U_{X1} U_{X2} \right) \right]^{1/2} \quad \textbf{(3.9)}$$

The term ρ_{12} is the coefficient of correlation. It is defined as follows:

$$\rho_{12} = \frac{U_{X1X2}}{U_{X1} \times U_{X2}} \quad \textbf{(3.10)}$$

The coefficient of correlation is between 1 and –1. In the following section the application of the pre-test uncertainty analysis in reference to the sensible effectiveness uncertainty of a plate type heat exchanger will be presented.

3.3 *Application of Pre-test Uncertainty analysis*

The first step in this analysis is to identify the resulting parameter of the experiment that combines the uncertainty of the individual measurements. This can be established through the data reduction equations for each variable. In the case of thermal performance of an air-to-air energy recovery device, the main defining result of the experiment is sensible, latent or total effectiveness. Sensible effectiveness and average sensible effectiveness were defined in chapter 2. However, we need to further breakdown the main formulation in order to extract the measured parameters as shown in figure 3.2. The measured parameters have been identified from the main and nested equations for sensible effectiveness. They include:

t_{ci}: Dry bulb temperature at heat exchanger inlet on the cold loop side.

t_{co}: Dry bulb temperature at heat exchanger outlet on the cold loop side.

t_{hi}: Dry bulb temperature at heat exchanger inlet on the hot loop side.

t_{ho}: Dry bulb temperature at heat exchanger outlet on the hot loop side.

t_{cal}: Dry bulb temperature at the cold air loop airflow station.

t_{hal}: Dry bulb temperature at the hot air loop airflow station.

P_b: Barometric pressure.

φ_{cal}: Relative humidity at the airflow station in the cold air loop.

φ_{hal}: Relative humidity at the airflow station in the hot air loop.

h_{cal}: Average velocity pressure at the airflow station in the cold air loop.

h_{hal}: Average velocity pressure at the airflow station in the hot air loop.

W_d, H_d: Width and height of duct

During the expirements a possible way to reduce the number of pressure transducers by utilizing a scani-valve that allows multiple measurements of pressure for one pressure transducer was discovered. This method will be described in detail in chapter 5. The same pressure transducer using a scani-valve

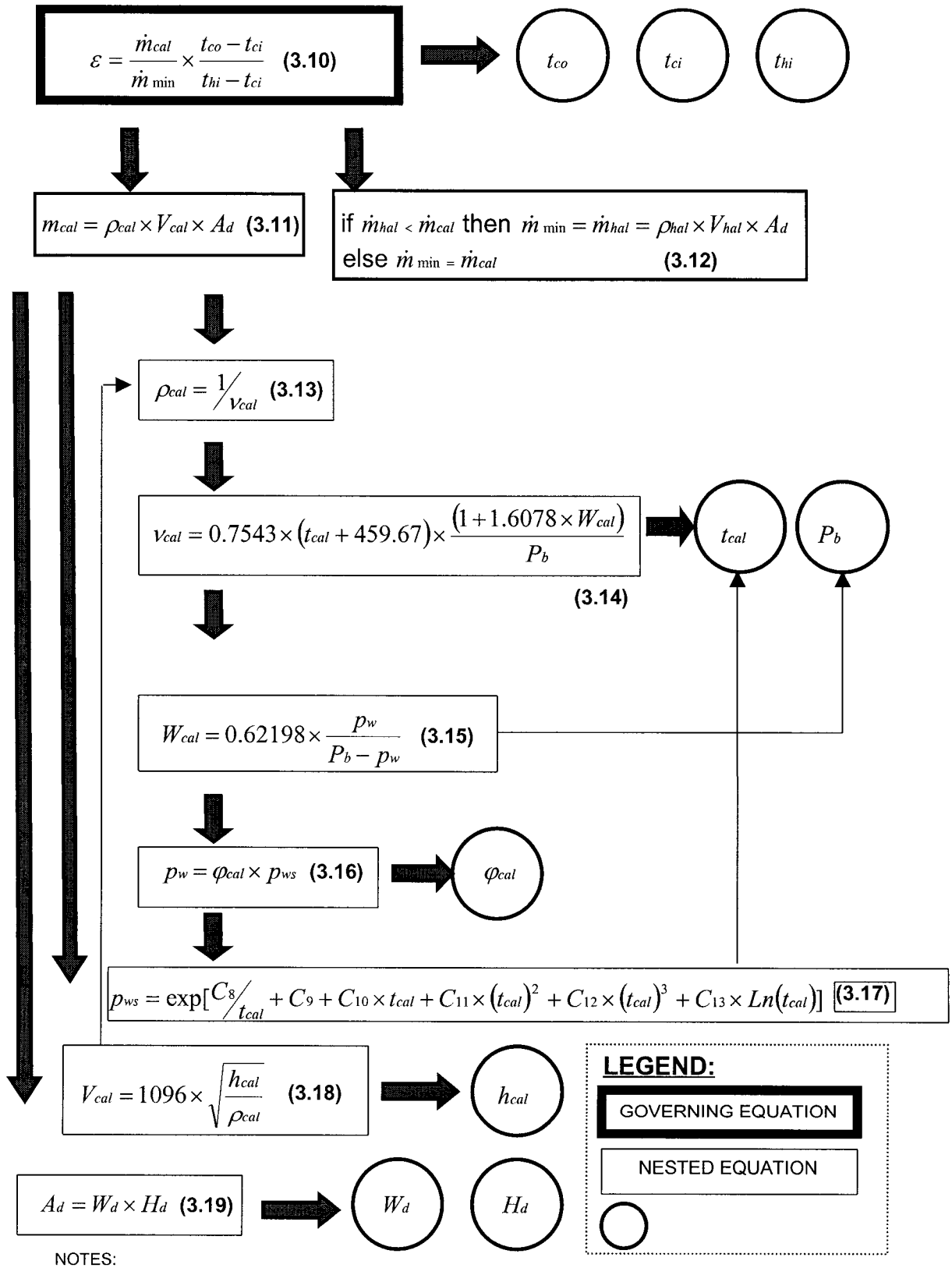

NOTES:
(1) THE COEFFICIENTS CAN BE FOUND IN ASHRAE FUNDAMENTALS 2001, P 6.2

Figure 3.2 Analytical Breakdown of the Governing Equation for Thermal Effectiveness

can measure both the cold and hot air loop velocity pressures. In view of this, the uncertainty analysis will include the case of co-variance between these two variables.

The pre-test uncertainty for the sensible effectiveness uncertainty, U_ε, and average sensible effectiveness, $U_{\varepsilon_{ave}}$, for the case of independent variables will be calculated based on the following equations:

$$U_\varepsilon = \left(\left(\frac{\partial \varepsilon}{\partial \dot{m}_{cal}} U_{\dot{m}_{cal}} \right)^2 + \left(\frac{\partial \varepsilon}{\partial \dot{m}_{\min}} U_{\dot{m}_{\min}} \right)^2 + \left(\frac{\partial \varepsilon}{\partial T_{ci}} U_{tci} \right)^2 + \left(\frac{\partial \varepsilon}{\partial T_{co}} U_{tco} \right)^2 + \left(\frac{\partial \varepsilon}{\partial T_{hi}} U_{thi} \right)^2 \right)^{1/2} \quad \textbf{(3.20)}$$

$$U_{\varepsilon ave} = \left(\left(\frac{\partial \varepsilon_{ave}}{\partial \dot{m}_{cal}} U_{\dot{m}_{cal}} \right)^2 + \left(\frac{\partial \varepsilon_{ave}}{\partial \dot{m}_{\min}} U_{\dot{m}_{hal}} \right)^2 + \left(\frac{\partial \varepsilon_{ave}}{\partial T_{ci}} U_{tci} \right)^2 + \left(\frac{\partial \varepsilon_{ave}}{\partial T_{co}} U_{tco} \right)^2 + \left(\frac{\partial \varepsilon_{ave}}{\partial T_{hi}} U_{thi} \right)^2 + \left(\frac{\partial \varepsilon_{ave}}{\partial T_{hi}} U_{thi} \right)^2 \right)^{1/2} \quad \textbf{(3.21)}$$

The partial derivatives of the effectiveness equation are taken with respect to the individual variables. t_{ci}, t_{co}, t_{hi}, and t_{ho} can be measured directly, and the uncertainty can be estimated. The remaining variables, i.e., the mass flow rates, need to be further reduced to the data reduction equation that contains the measured parameters. The uncertainty for the mass flow rates is as follows:

$$U_{\dot{m}_{cal}} = \left(\left(\frac{\partial \dot{m}_{cal}}{\partial \rho_{cal}} U_{\rho cal} \right)^2 + \left(\frac{\partial \dot{m}_{cal}}{\partial V_{cal}} U_{Vcal} \right)^2 + \left(\frac{\partial \dot{m}_{cal}}{\partial A_d} U_{Ad} \right)^2 \right)^{1/2} \quad \textbf{(3.22)}$$

The corresponding uncertainties for the air density, $U_{\rho cal}$, the air velocity, U_{Vcal}, and the cross sectional area of the duct, U_{Ad}, are as follows:

$$U_{\rho cal} = \left(\left(\frac{\partial \rho_{cal}}{\partial T_{cal}} U_{Tcal} \right)^2 + \left(\frac{\partial \rho_{cal}}{\partial W_{cal}} U_{Wcal} \right)^2 + \left(\frac{\partial \rho_{cal}}{\partial P_b} U_{Pb} \right)^2 \right)^{1/2} \quad \textbf{(3.23)}$$

$$U_{Vcal} = \left(\left(\frac{\partial V_{cal}}{\partial h_{cal}} U_{hcal} \right)^2 + \left(\frac{\partial V_{cal}}{\partial \rho_{cal}} U_{\rho cal} \right)^2 \right)^{1/2} \quad \textbf{(3.24)}$$

$$U_{Ad} = \left(\left(\frac{\partial A_d}{\partial L_d} U_{Ld} \right)^2 + \left(\frac{\partial A_d}{\partial H_d} U_{Hd} \right)^2 \right)^{1/2} \quad \textbf{(3.25)}$$

The humidity ratio uncertainty, $U_{W_{cal}}$, requires to be further reduced to the following equation:

$$U_{W_{cal}} = \left(\left(\frac{\partial U_{W_{cal}}}{\partial \phi_{cal}} U_{\phi_{cal}} \right)^2 + \left(\frac{\partial U_{W_{cal}}}{\partial p_{ws}} U_{p_{ws}} \right)^2 + \left(\frac{\partial U_{W_{cal}}}{\partial P_b} U_{P_b} \right)^2 \right)^{1/2} \quad \textbf{(3.26)}$$

Finally, the saturated vapor pressure uncertainty, $U_{p_{ws}}$, is the last of the nested equations:

$$U_{p_{ws}} = \frac{\partial p_{ws}}{\partial t_{cal}} U_{t_{cal}} \quad \textbf{(3.27)}$$

In regard to co-variance between h_{cal} and h_{hal}, the following additional terms would be added to equation 3.9:

Co-variance term for $U_{\varepsilon} = 2 \times \left(\frac{\partial \varepsilon}{\partial h_{cal}} \times \frac{\partial \varepsilon}{\partial h_{\min}} \times \rho_{h_{cal}, h_{\min}} \times U_{h_{cal}} \times U_{h_{\min}} \right)$ **(3.28)**

Co-variance term for $U_{\varepsilon_{ave}} = 2 \times \left(\frac{\partial \varepsilon}{\partial h_{cal}} \times \frac{\partial \varepsilon}{\partial h_{hal}} \times \rho_{h_{cal}, h_{hal}} \times U_{h_{cal}} \times U_{h_{hal}} \right)$ **(3.29)**

As mentioned earlier, the coefficients of correlation, $\rho_{h_{cal}, h_{\min}}$, $\rho_{h_{cal}, h_{hal}}$, will be assumed to be 1. It is possible that either one of the partial derivatives creates a negative sign for the value. The absolute value taken for the co-variance term in order to ensure the resulting uncertainty is positive.

In the process of estimating the uncertainties for the individual measurements, it might seem natural to overestimate some of the values. In fact, by over estimating the uncertainties it is likely the real faults in the experiment might be concealed. Moffat (1982) discusses this phenomenon and suggests that uncertainties be conservatively chosen. The estimated uncertainties for all the measured parameters are provided in Table 3.2.

Table 3.2 Estimated Uncertainties for the Measured Parameters

Measured Parameter	Estimated Uncertainty
Temperature	U_T = ± 0.5 °F (±0.24 °C)
Barometric Pressure	U_{Pb} = ± 0.01 in. Hg (± 34 Pa)
Relative Humidity	$U_\varphi = U_{RH}$ = ± 2% RH for 0 to 100 %RH
Velocity Pressure	U_h = ± 0.002 in. w.c. (± 0.5 Pa)
Static Pressure	U_{sp} =± 0.05 in. w.c. (± 12 Pa)
Length or Width of Duct	U_L = ± 1/32 inches (± 0.8 mm)

The above uncertainties are represented as both positive and negative based on the assumption of a normal or Gaussian distribution, in honor of Karl Friedrich Gauss (1777-1855), who derived the curve from a study of errors in repeated measurements of the same quantity. One of the principle characteristics of a Gaussian distribution is that the data scatter is symmetrically distributed around the population mean in the shape of a bell shaped curve. The uncertainties in table 3.2, which were based on manufacturer's specified accuracy, will be used in the following section to derive sensitivity curves for uncertainty effectiveness as a function of both measurement uncertainty and operating conditions.

3.4 Sensitivity Analysis of Effectiveness Uncertainties

One of the primary objectives of a pre-test uncertainty analysis is to understand and quantify the level of sensitivity that individual variables have on the resultant uncertainty for a range of values. The two main classifications of variables that affect the resultant uncertainty are the uncertainties of the individual measurements and the operating conditions. The estimated uncertainties for the different variables are listed in Table 3.2. The main equation and the nested equation for sensible effectiveness were defined in figure 3.2. The average sensible

effectiveness is derived in a similar manner. A baseline of values for the typical operating conditions of the heat recovery test facility is defined as follows:

T_{ci} =15 °F (-9.4 °C) T_{co} =45 °F (7.2 °C) ϕ_{cal} =30% ϕ_{hal} =70%

T_{hi} =72 °F (22.2 °C) T_{ho} =42 °F (5.6 °C) P_b =29.921in. Hg (101.3 Kpa)

A_d =1.361 ft^2 (0.125 m^2) $Q_{cal} = Q_{hal}$ = 1515 CFM (715 L/s)

The software MathCad version 6.0 was used to program the equations for determining sensible effectiveness uncertainty as shown in Appendix A. MathCad greatly facilitates the use of complex mathematical functions, such as partial derivatives, that are used extensively in this particular program. MathCad requires that the equations be written in a particular order. The most basic equations for the vapor pressure of moist air in both the hot and cold loop air flow stations is derived first followed by variables that incorporate vapor pressure of moist air, i.e., the density of the air. The density of air is required in order to calculate the air velocity. The air velocity is used to calculate the airflow, which is used finally to calculate the sensible effectiveness. At each stage, the uncertainty is calculated for the individual variables. The final equations of the MathCad program are those for the sensible effectiveness uncertainty, average sensible effectiveness uncertainty, and their corresponding uncertainties incorporating co-variance. The baseline case for the operating condition was chosen to represent the typical operating condition in the test facility. The range of conditions in the test facility need to be defined in order to study its effect on the sensible effectiveness uncertainty. The range of conditions include the range of air flows, temperatures, and relative humidity that the test facility will be able to accommodate with respect to the size of the fans, motors, plate heat exchanger, cooling coils, heating coils, and humidifier. The initial measuring instrumentation selected must also account for the range of conditions. The range of operating conditions and the limiting factors in the test facility are defined in Table 3.3. As Table 3.3 illustrates, the limiting factors for the operating conditions can be either a function of a physical constraint of a particular component such as a fan motor or the accuracy of the selected instrumentation. It should be noted that barometric pressure was not included in the list of variables since it obviously cannot be controlled and is dependent on the ambient conditions during the period of the test.

Table 3.3 Operating Range for Different Variables

Variable	Operating range	Limiting factor(s)
Temperature	10 to 90°F	Cooling and Heating coils
Relative Humidity	10 to 80 %RH	Humidifier/ambient conditions
Air Flow range	750 to 2800 CFM	Accuracy of Pressure transducer at low end of
	(354 to 1321 L/s)	Motor Horse power at the high end of range

The MathCad program can run for only one particular set of conditions at one time. Therefore, the program was run for each case, and the resulting values were transferred to an excel spreadsheet. Once a complete range of either parameter uncertainties or operation conditions was entered into a spreadsheet, a graph was easily constructed in excel. Each graph contains four separate curves representing the normalized effectiveness for the following:

1. Normalized Sensible Effectiveness Uncertainty, $\frac{U_\varepsilon}{\varepsilon}$, non-covariance

2. Normalized Sensible Effectiveness Uncertainty, $\frac{U_\varepsilon}{\varepsilon}$, covariance

3. Normalized Average Sensible Effectiveness Uncertainty, $\frac{U_{\varepsilon ave}}{\varepsilon ave}$, non-covariance

4. Normalized Average Sensible Effectiveness Uncertainty, $\frac{U_{\varepsilon ave}}{\varepsilon ave}$, covariance

The two variables that are covariant are the velocity pressures for the cold and the hot air loop air flow stations in the case when they share the same pressure transducer through the scani-valve. The pre-test uncertainty analysis involving the covariance of the velocity pressure will allow a comparison with the case of non-covariance. The first series of graphs (figures 3.3 to 3.7) illustrates the sensitivity of the sensible effectiveness uncertainty as a function of the basic parameter uncertainties for temperature, velocity pressure, relative humidity, barometric pressure, and duct dimension H x W. The next group of graphs (figures 3.8 to 3.10) illustrate the sensitivity

of the effectiveness uncertainty as a function of the operating conditions. There are several general observations that can be made regarding all the graphs:

1. The average sensible effectiveness uncertainty, $U_{\varepsilon ave}$, with non-covariant variables produces the lowest uncertainty as a function of each variable and the operating conditions.
2. The sensible effectiveness uncertainty, U_{ε}, with covariant variables produces the highest uncertainty as function of each variable and the operating conditions.
3. The sensible effectiveness uncertainty is higher when applying the covariant variables.
4. The difference between the effectiveness uncertainty for covariant and non-covariant variables increases with decreasing accuracy except for temperature uncertainty.

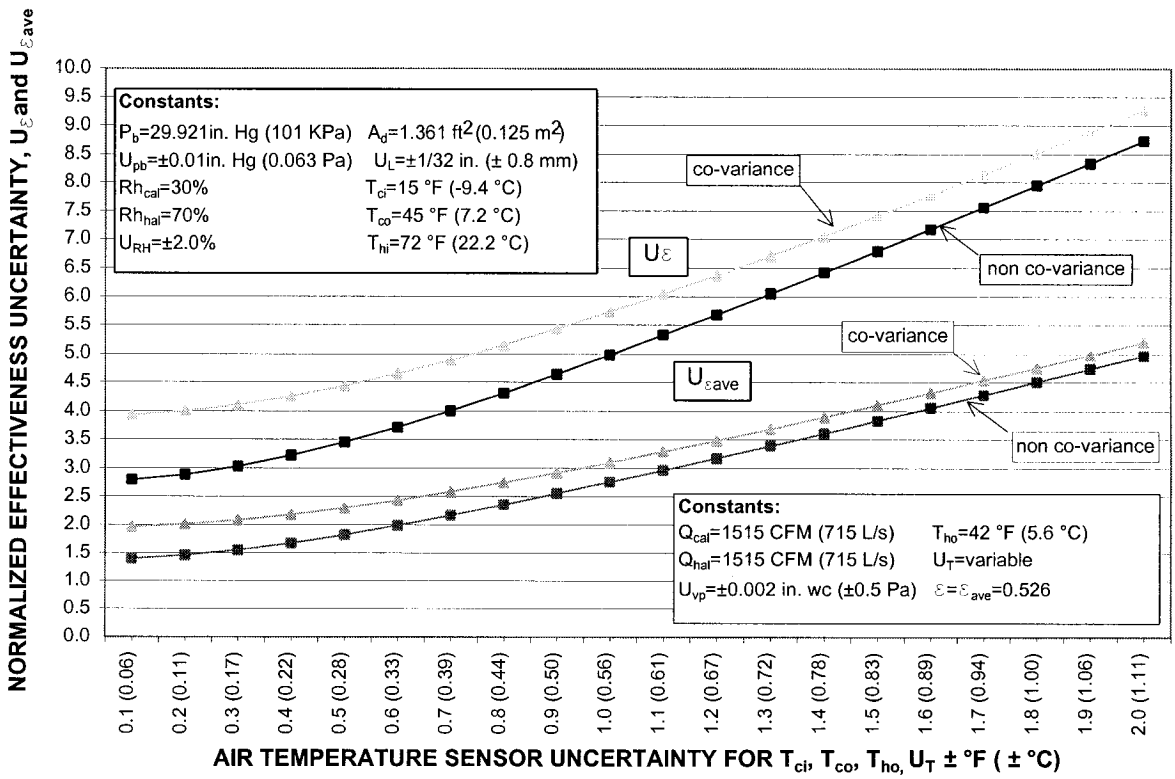

Figure 3.3 The effect of temperature sensor uncertainty on normalized effectiveness uncertainty

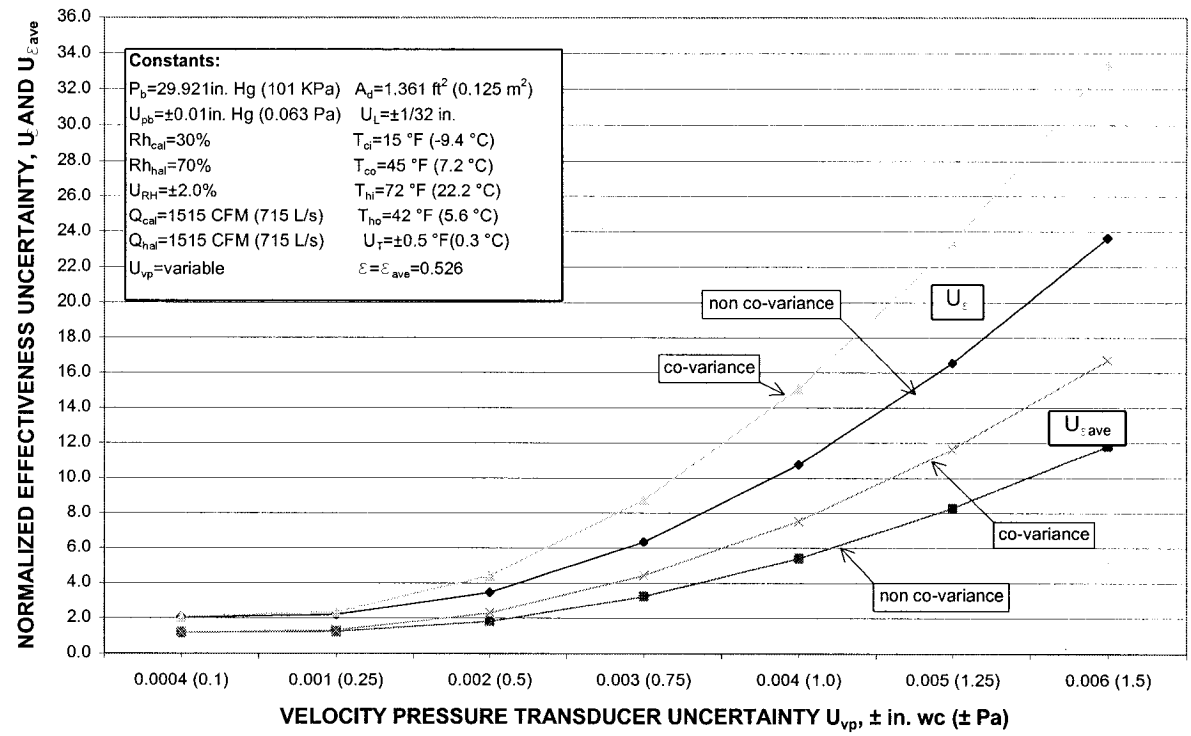

Figure 3.4 The effect of velocity pressure transducer uncertainty on normalized effectiveness uncertainty

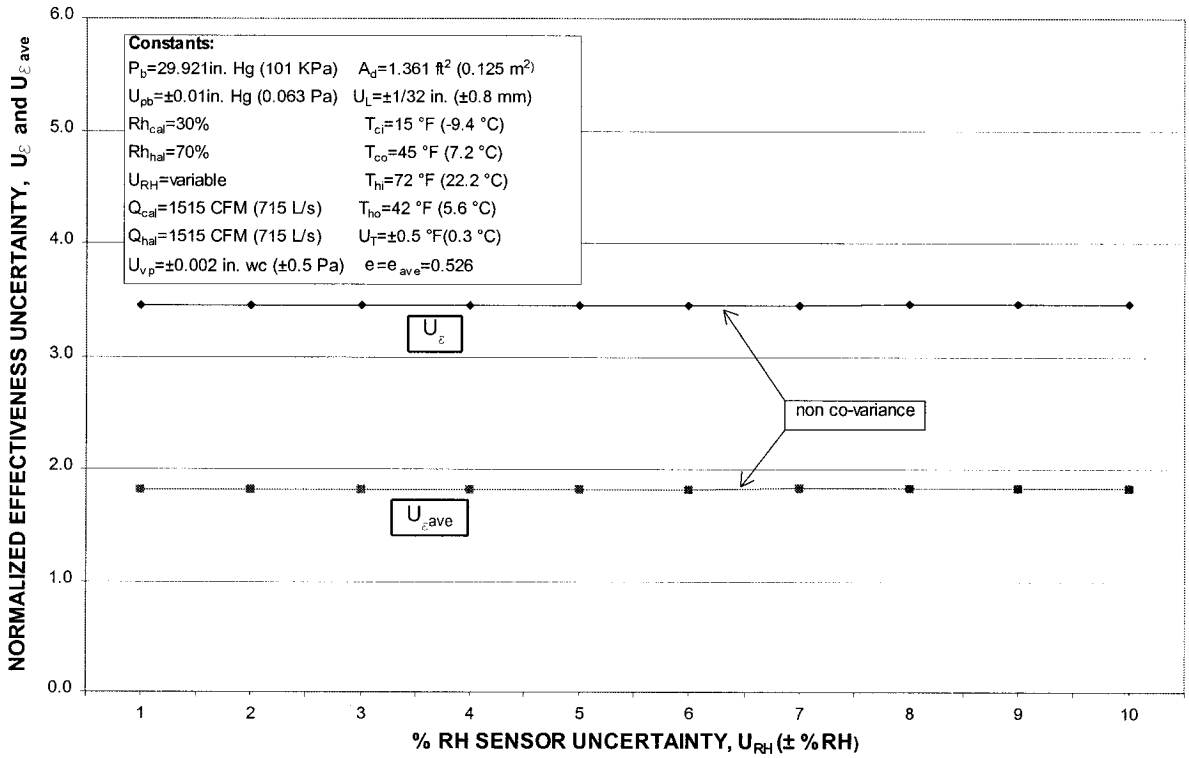

Figure 3.5 The effect of relative humidity uncertainty on normalized effectiveness uncertainty

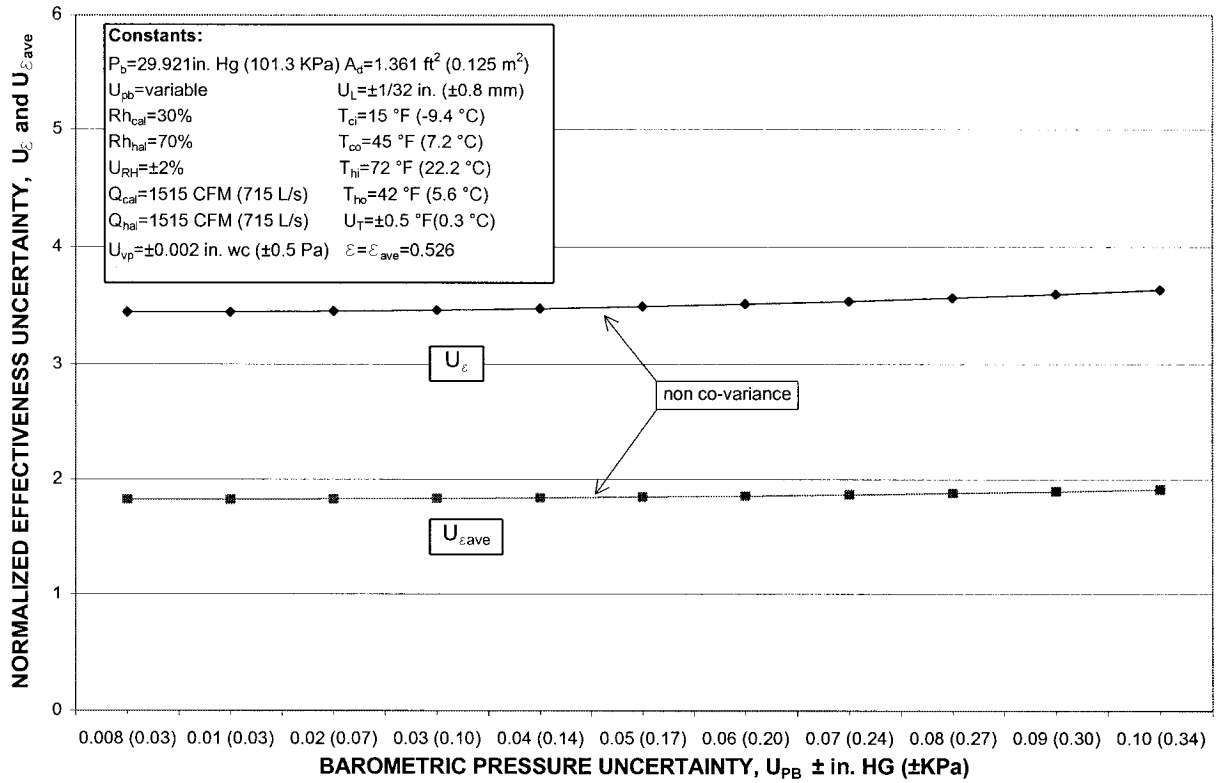

Figure 3.6 The effect of barometric pressure uncertainty on normalized effectiveness uncertainty

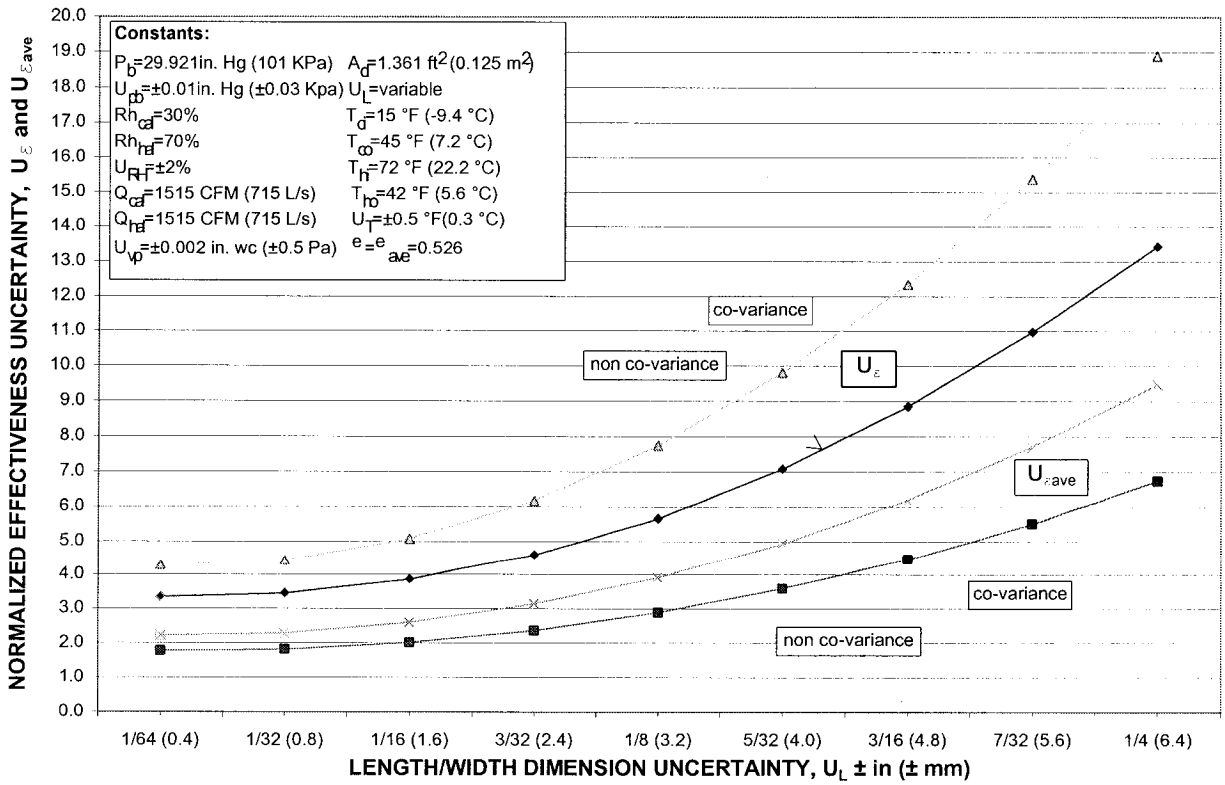

Figure 3.7 The effect of length/width dimension uncertainty on normalized effectiveness uncertainty

It can be observed that velocity pressure uncertainty has the greatest impact on the effectiveness uncertainty for the type of airflow station that is proposed for the test facility. The air flow station will consist of a grid of tubes that will measure the total pressure at various points across the duct and the static pressure at one point. The difference between the total pressure and static pressure is the velocity pressure. The design and calibration of the airflow station will be described in detail in chapter 5. This type of airflow station typically has lower velocities than nozzles, and, therefore, will experience greater uncertainty if the accuracy of the transducer is not adequate. The curves in figure 3.4 rise rapidly with increasing lower velocity pressure accuracy. Therefore, the selection of the pressure transducer is the most critical aspect in minimizing the uncertainty in the sensible effectiveness. The curves begin almost flat for the highest accuracy for all four cases, i.e., sensible and average sensible effectiveness uncertainty for non-covariance and covariance. The affect of covariance has a drastic impact on the effectiveness uncertainty. The two other variables that have a significant impact on the effectiveness uncertainty include temperature and the measuring tape used to measure the dimensions H x W of the duct at the location of the air flow station. The temperature uncertainty affects the sensible effectiveness in a more linear fashion as compared to the velocity pressure as shown in figure 3.4 and 3.3. The reason for this is the result of the first partial derivative for both the temperature and velocity pressure. The relative humidity and barometric pressure uncertainties have a negligible affect on the sensible effectiveness uncertainties as observed in figures 3.5 and 3.6. This result is expected since there is no transfer of latent energy between the two airstreams, and the latent effects relating to condensation are not considered in this analysis. Therefore, the relative humidity sensor does not require a high accuracy, because it does not significantly influence the sensible effectiveness uncertainty. ASHRAE STD 84-1991 specifies a accuracy of 2% for the relative humidity sensor. In light of the present analysis for sensible effectiveness, a humidity sensor of less accuracy, i.e. 3%, can be used. In the case of enthalpy wheels Ciepliski (1997) observes that latent and total effectiveness are very sensitive to relative humidity measurements. The difference in cost between a relative humidity sensor with accuracy of 2% and 3% for one supplier is 200.00 CAN$. In previous studies on uncertainty analysis relating to heat recovery

effectiveness there is no mention of the effect of the area measurement for the calculation of the mass flow rate. Furthermore, as discussed in section 3.1 and seen in table 3.1, the standards do not emphasize the area measurement accuracy. Figure 3.8 illustrates the effect of the measurement uncertainty relating to the dimension measurement of the cross sectional area of the duct at the airflow station. A standard tape measure can measure to the nearest 1/16 inch (1.6 mm). However, observer error can also be significant. For an accuracy of ± 3/16 inch (4.8 mm) the normalized sensible effectiveness uncertainty for non covariant variables is 4.5. This result indicates that the dimensions of the duct must be measured carefully with an accurate tape measure.

The effect of the operating conditions is quite revealing except for the relative humidity and the barometric conditions that did not have any effect on the sensible effectiveness uncertainty. The effect of the temperature difference between the cold and hot loop air entering the heat exchanger has a significant impact on the sensible effectiveness uncertainty. The data was obtained by varying the temperature of the cold loop entering air temperature. The hot air entering temperature, 72 °F (22.2 °C), was held constant. The leaving temperature from the heat exchanger for the cold and the hot air loop had to be adjusted to maintain a constant effectiveness. For the baseline case, when the cold loop entering air temperature was set at 15 °F (-9.4 °C), the cold air leaving temperature was adjusted to 45 °F (7.2 °C) and the hot air leaving temperature was adjusted to 42 °F (5.6 °C) to achieve an effectiveness, $\varepsilon = \varepsilon_{ave} = 0.526$. When the cold loop entering air temperature was set at 20 °F (-6.7 °C), then the corresponding cold air leaving temperature was adjusted to 47°F (8.3 °C), and the hot loop leaving air temperature was set to 44.65 °F (7.0 °C) to maintain $\varepsilon = \varepsilon_{ave} = 0.526$. Figure 3.9 demonstrates that as the temperature difference increases between the entering cold and hot air loops, the sensible effectiveness uncertainty decreases in a parabolic manner. The sensible effectiveness with covariant variables is particularly sensitive to the temperature. For a temperature difference of only 12 °F (6.7 °C) the normalized sensible effectiveness uncertainty is 10.5. In comparison to the average sensible effectiveness with non-covariant variables the normalized sensible effectiveness uncertainty is almost half, i.e. 5.78. It is also observed that the

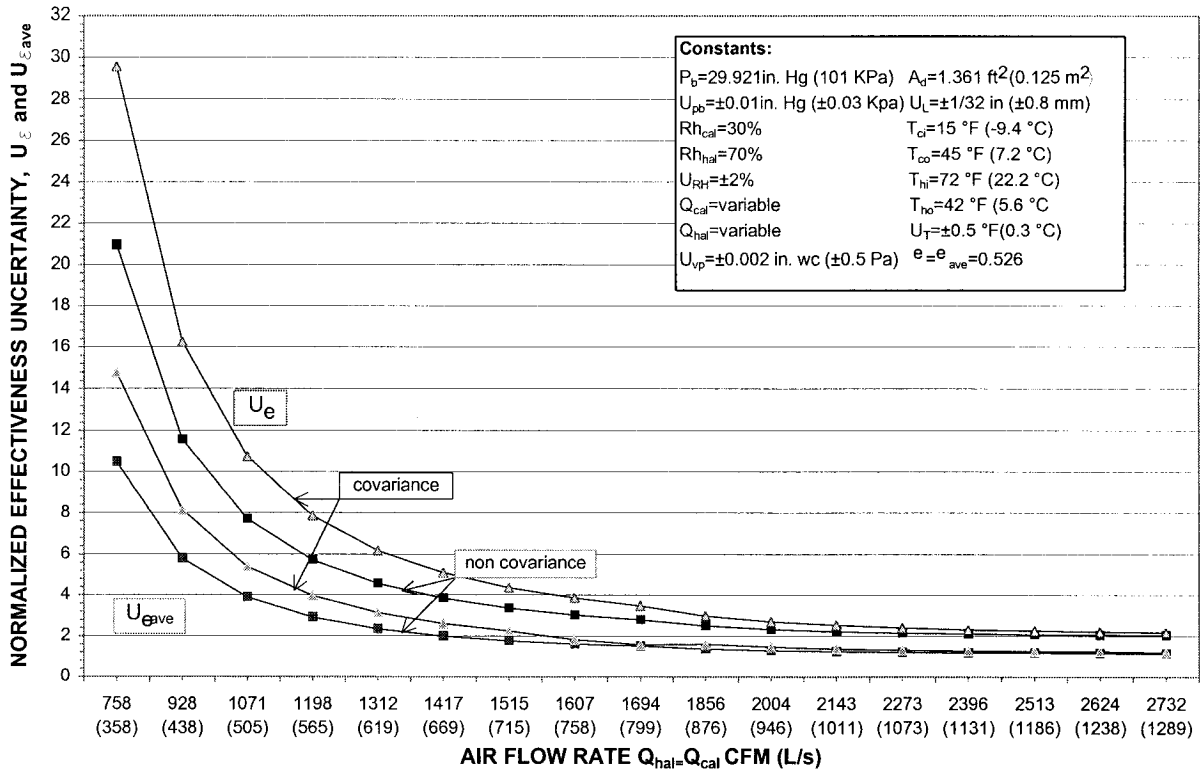

Figure 3.10 The effect of airflow rate on normalized effectiveness uncertainty

covariant and non-covariant variables converge for the smaller temperature differences as the sensible and average sensible effectiveness uncertainty increases.

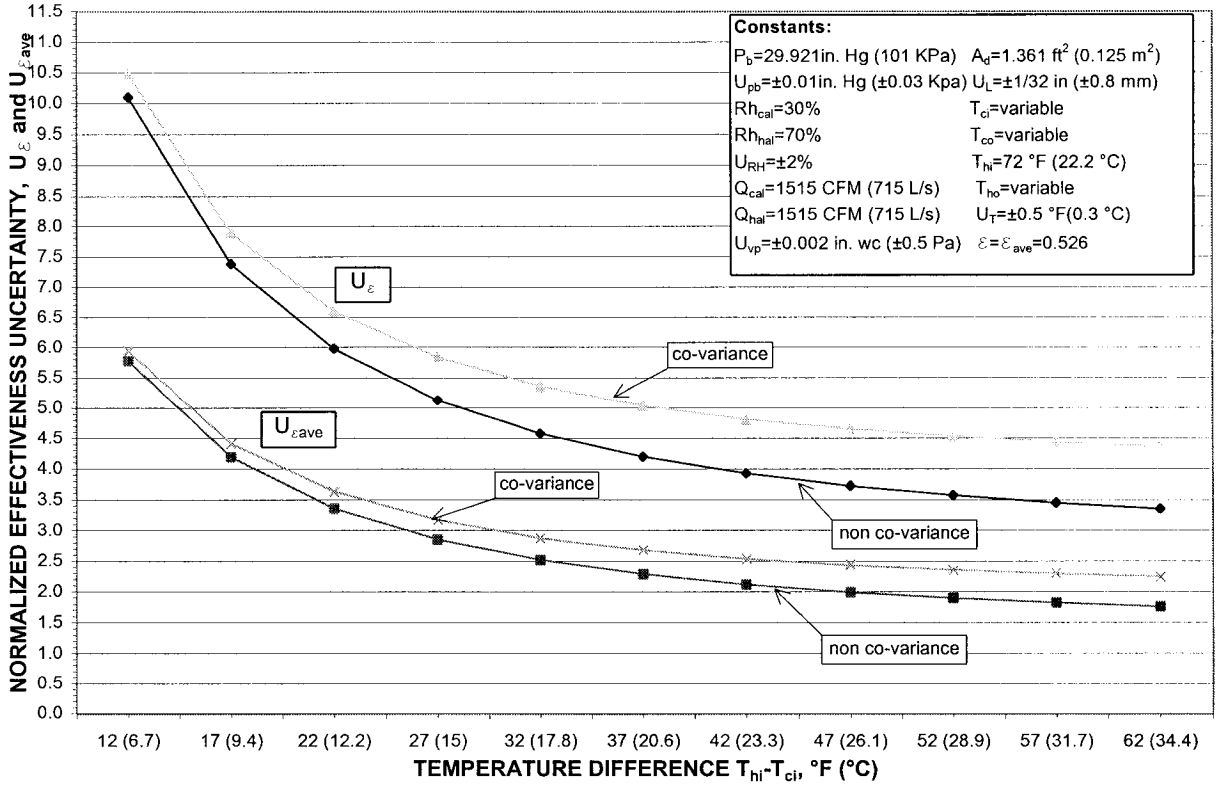

Figure 3.8 The effect of temperature difference, $T_{hi} - T_{ci}$, on normalized effectiveness uncertainty

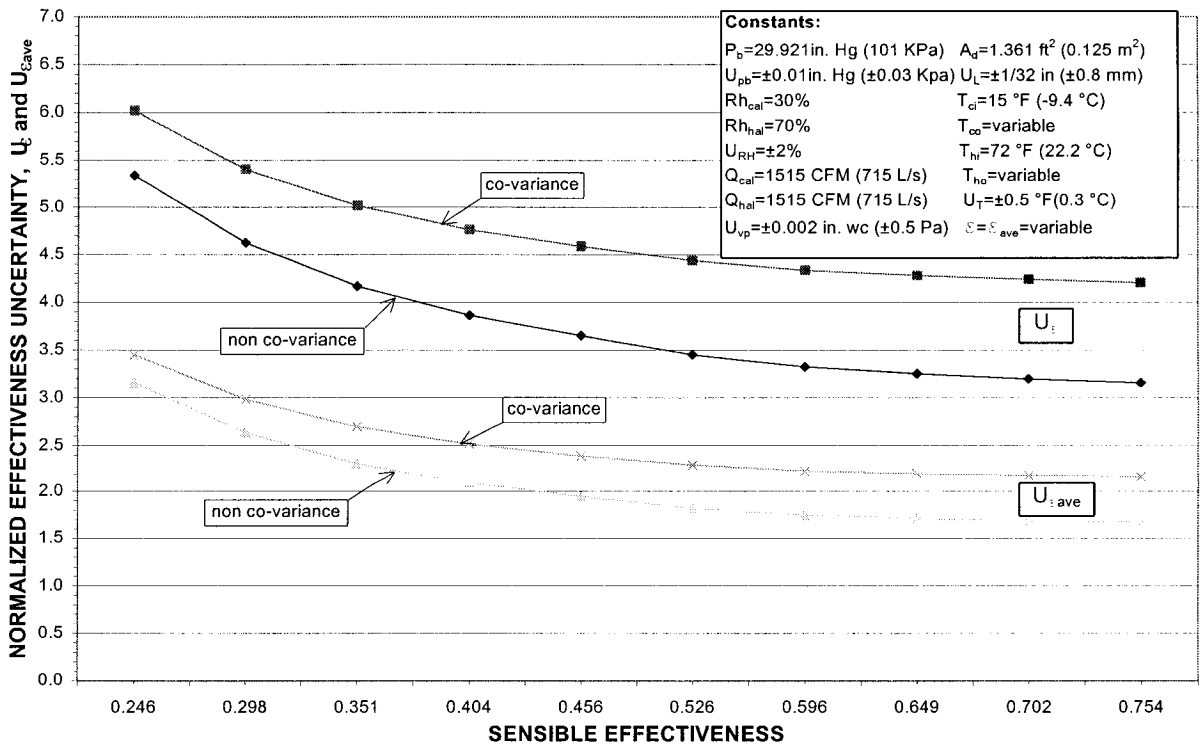

Figure 3.9 The effect of sensible effectiveness on normalized effectiveness uncertainty

4.0 DESIGN OF NEW EXPERIMENTAL TEST FACILITY FOR CROSS FLOW PLATE HEAT EXCHANGER

The initial basis for the overall design of the experimental set-up was derived from both ASHRAE standard 84-1991 and CSA standard C439-00. Both standards provide guidelines to assist the industry and public by establishing a uniform method of testing and rating air–to-air heat recovery devices. Since the guidelines are geared more towards industry and the public, it does not provide more rigorous guidelines that would allow for more comprehensive testing of heat recovery devices in terms of temperature and airflow distributions entering and exiting the heat recovery device or within the core itself. The existing standards can be considered adequate for simple thermal performance evaluation under ideal laboratory conditions. However the actual thermal performance of the heat exchanger can vary widely based on the installation and surrounding components such as ductwork, fans, heating and cooling coils. CSA C439-00 does consider the thermal performance of a heat exchanger installed in a packaged energy recovery unit. Furthermore this standard also provides guidelines to account for heat gains and losses through the casing, casing air leakage, fans, fan motors, heating coils, and defrost energy. The distribution of the airflow and temperature is not considered in either standard. One of the main objectives of this present research is to study the thermal performance and temperature distribution for a cross flow plate heat exchanger. The heat exchanger is installed in a test facility that simulates the physical layout of a package air-handling unit. However, the instrumentation requirements respect or exceed the heat recovery test standards. As elaborated in chapter three, the predicted uncertainty of the sensible effectiveness can be less than ± 5% for this test facility. Field studies of heat recovery devices for the most part do not allow for the same level of uncertainty as laboratory experiments. In the paper by Johnson, Simonson and Besant (1998), in-situ testing of a heat pipe and energy wheel revealed uncertainties in the range of ± 7% to ± 12%. The principal cause for the higher uncertainties was attributed to non-uniform temperature distributions in the ducts prior to entering the heat recovery device. Shah (1981) also observes that non-uniform airflow at the inlet of a heat exchanger can reduce the effectiveness. Chiou (1978) presented a mathematical method for determining thermal performance deterioration in

cross flow heat exchangers due to flow non-uniformity. Measuring airflow in ducts is another significant source of uncertainty. The connecting ductwork is the responsibility of the mechanical contractor, and there is rarely any coordination with the heat recovery manufacturer at the design, fabrication, and installing stage of the project. When the heat recovery device is incorporated in a packaged unit, the manufacturer can ensure that at least the non-uniform conditions within the unit are minimized through thoughtful design. Therefore the portion of the test facility containing the plate heat exchanger is designed as a typical air-handling unit. The remaining facility, including the ductwork and instrumentation, is designed using the existing test standards as a guide. The heating and cooling components are located in the ductwork connecting to the heat recovery unit. The size of the test facility is limited by the available space in the laboratory. A double tunnel closed loop concept is chosen for the facility. A distinction will be made between the concept of a single tunnel open loop system and a double tunnel closed loop system. The various advantages and disadvantages of both systems will be elaborated in section 4.1. It was decided to include a section dealing with the progressive stages of development of the research facility tracing the history of the project from preliminary design to final commissioning. This section can serve as an example for other researchers who intend to develop a test facility for testing heat recovery devices. The other main sections in this chapter will include a detailed description of all the mechanical and electrical components.

4.1 General Characteristics of the Test Facility

Prior to a detailed description of the facility, the general characteristics of the test facility will be presented and compared with the existing standards.

4.1.1 Overall Arrangement and Comparison with standards

The initial concept to design a test facility that can accommodate a plate type heat exchangers with cross flow configuration evolved after an extensive review of ASHRAE std 84-1991 for testing heat recovery devices. The original standard, that stemmed from the ASHRAE committee TC 5.5 in collaboration with the University of Manitoba, was developed originally for

enthalpy wheels and heat pipes, coil run-around systems, and plate heat exchangers in counter flow configuration. The test facility can be adapted to accommodate a cross flow heat exchanger, but it is not evident at first glance. Figure 4.1 (a) illustrates the schematic of the test facility as presented in ASHRAE std 84-1991 with a cross flow plate heat exchanger superimposed over the layout.

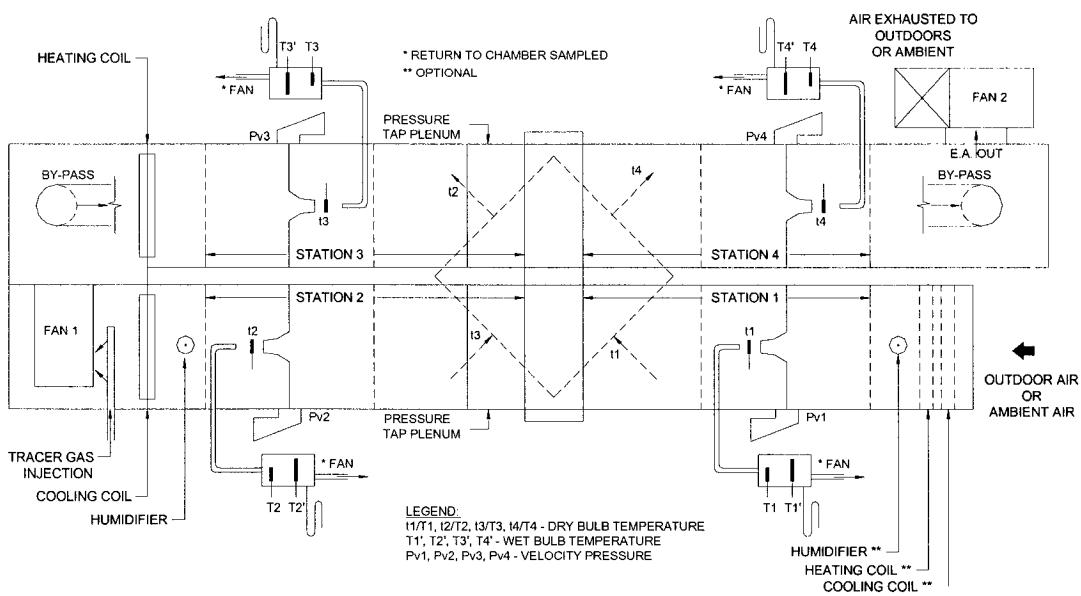

(a)

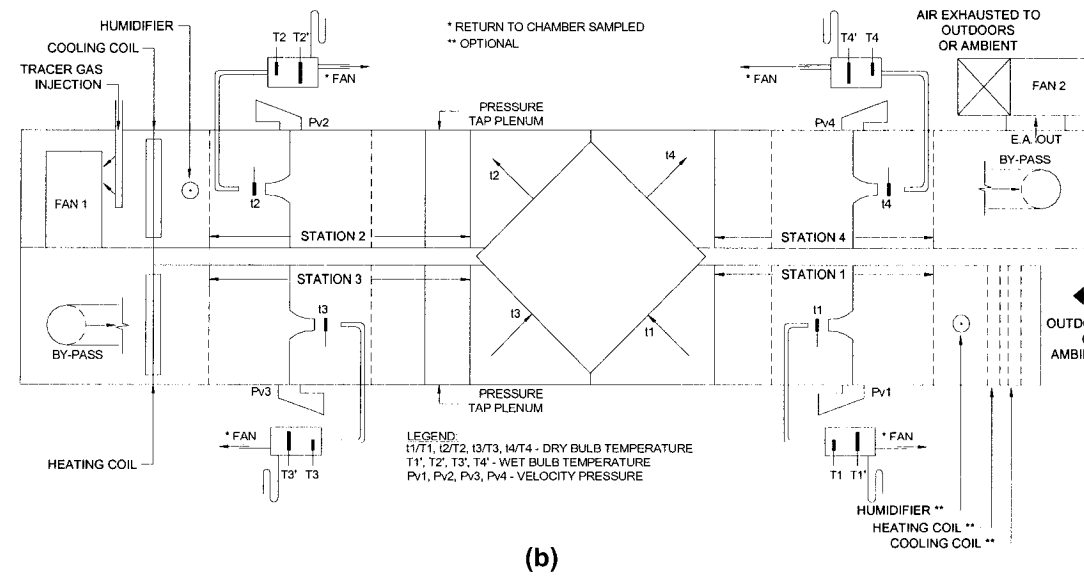

(b)

Figure 4.1 Schematic diagram of typical air-to-air heat exchanger test equipment with a cross flow plate heat exchanger (a) superimposed on the plan view layout (b) integrated into facility

A re-arrangement of the measuring stations 2 and 3 is needed to accommodate the cross flow plate heat exchanger as shown in figure 4.1 (b). However, the length of the facility will increase by minimum of 4 feet, since the diamond shape nature of the cross flow plate heat exchanger takes up more space than a heat pipe or enthalpy wheel. The layout shown in figure 4.1 (b) is not used for two principal reasons:

1. The overall length of the ASHRAE std 84-1991 arrangement needed more space than was available in the existing lab.
2. An entirely closed circuit system was required.

The heat recovery test facility layout in CSA standard C439-00 as shown in figure 4.2 provides a more suitable arrangement for the present research. In particular it is potentially more compact in terms of length since the ductwork loops over the top of the heat recovery unit. It is specifically arranged to suit cross flow plate heat exchangers. The schematic in figure 4.2 suggests that the heat exchanger is in a vertical position. The present facility will incorporate a plate heat exchanger in a horizontal position. In this way the facility will be able to accommodate other types of heat recovery devices in the future.

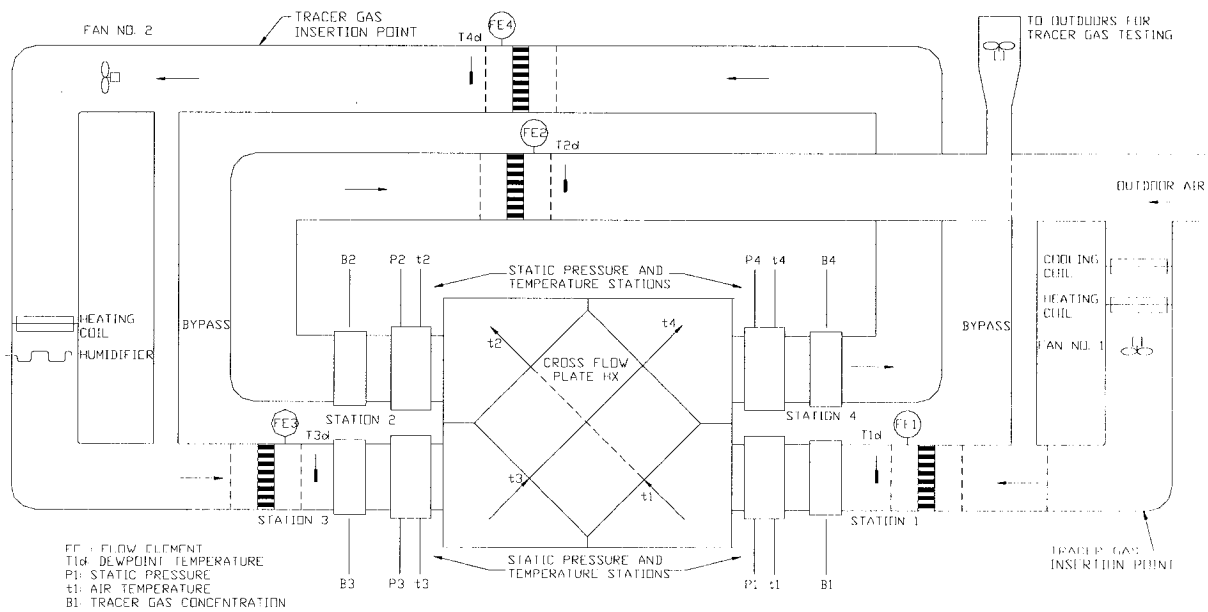

Figure 4.2 Schematic of Test Facility for Heat/Energy-Recovery Ventilators for CSA standard C439-00

One of the differences between ASHRAE 84-1991, C439-00 and the present test facility is the location of the airflow stations. The airflow stations in reference to ASHRAE 84-1991 are located

within the measuring stations containing the static pressure taps and dry bulb/wet bulb temperature sensors. The airflow measuring stations in reference to C439-00 are located separately from the temperature/pressure measuring stations. In accordance with ASHRAE STD 51-1985, Laboratory Methods of Testing Fans for Rating, the air flow measuring stations require at least 8.5 duct diameters from the fan. Therefore, the airflow measuring stations are located in the ductwork where there is a long straight section to minimize non-uniform airflow. One of the principal differences of the present test facility is the reduced number of airflow stations. Two airflow stations are used instead of four for the following reasons:

1. The amount of space available did not permit long lengths of duct to support the extra two airflow measuring stations.
2. As a result of the reduced length of duct, and hence less potential duct leakage, it was deemed acceptable to install one airflow measuring station per side.
3. The reduced number of airflow stations allowed for cost savings on extra pressure transducers and labor time to install the extra stations.

The location of the airflow measuring stations had a significant effect upon the layout of the test facility. The airflow measuring stations are located in approximately the middle of the overhead duct sections in both the cold and hot air loop. Figure 4.3 shows 3-dimensional drawing of the new heat recovery test facility. The choice of using overhead ductwork to save on horizontal space allowed for a more compact installation. This was one of the key features of the design. Figure 4.4 illustrates the space available in the existing laboratory with the new heat recovery test facility. Space is required around the entire test facility to allow for access to mechanical, electrical, and instrumentation components. In addition, space is required to permit replacing the heat exchanger core. The laboratory contained other test facilities in addition to the heat recovery test bench.

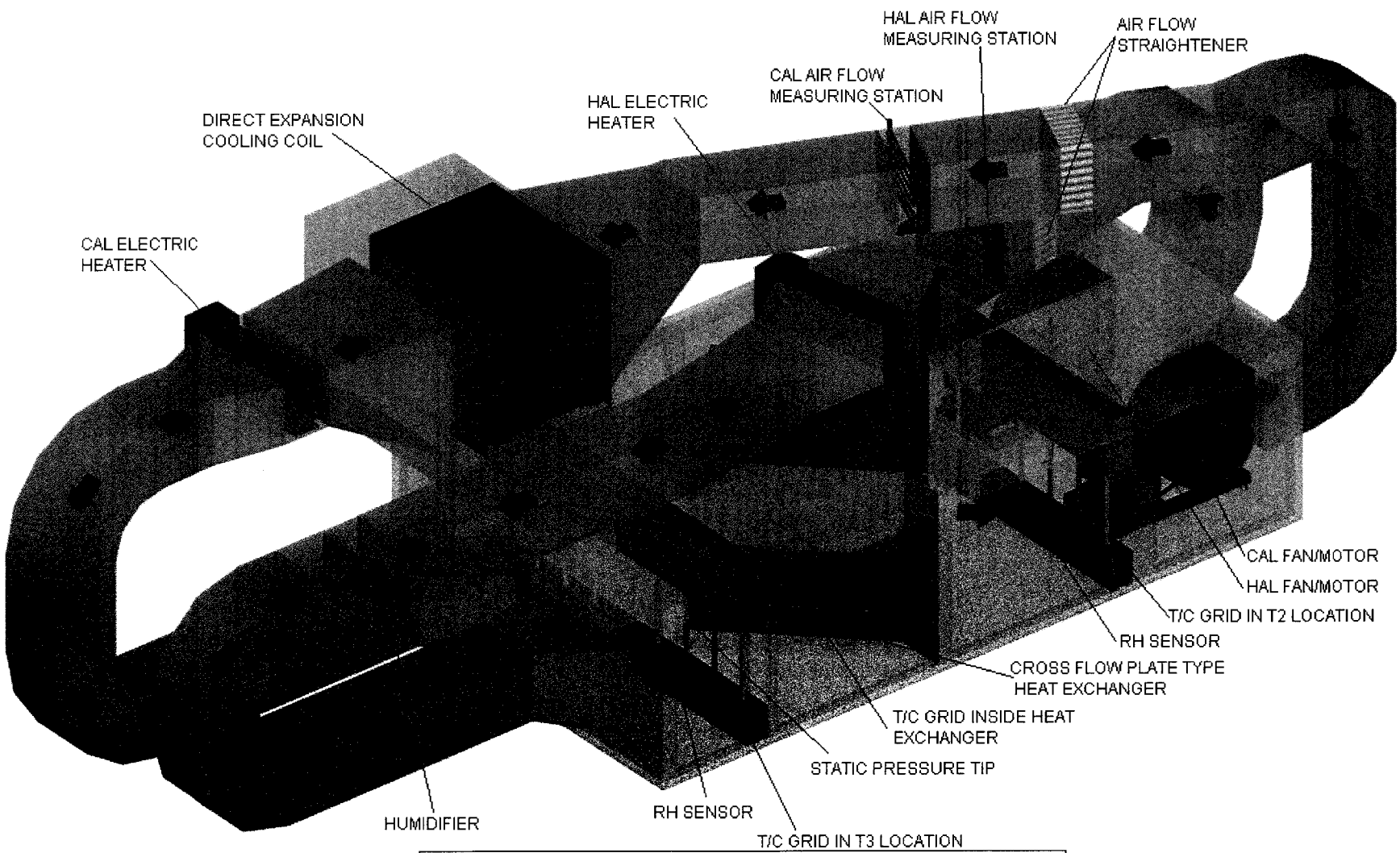

Figure 4.3 3-Dimensional Layout of Heat Recovery Test Facility

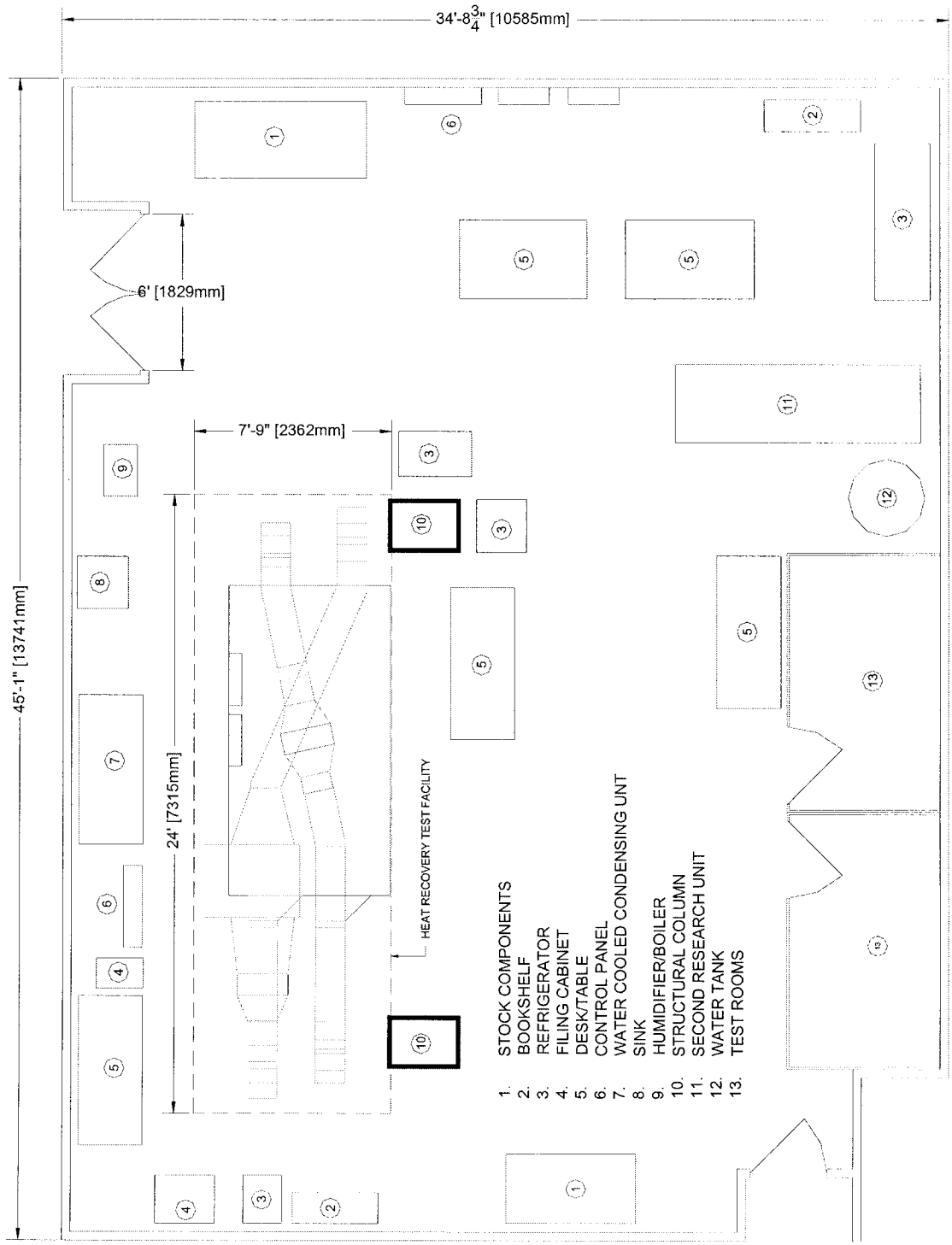

Figure 4.4 Layout of Heat Recovery Test Facility in the Existing Laboratory

4.1.2 Capacity of the Test Facility

The size and capacity of the facility is dependent on three main criteria:

1. Available space in existing laboratory
2. Existing compressor/condenser capacity
3. Available electrical power for fan motors and heaters
4. Standard capacity used in the industry

The criteria that set the limit for the maximum capacity of the system is the available electrical power. If the available electrical power were sufficient to allow for a larger system, it would not be necessary to exceed 3000 CFM (1416 L/s), which represents a standard size of heat recovery unit used in a typical building. The maximum airflow capacity of the system was designed for 3000 CFM. The average nominal capacity of the system for balanced airflow is 1500 CFM (708 L/s). The minimum airflow rate, 750 CFM (354 L/s), is limited by the accuracy of the pressure transducers as revealed in chapter 3. All of the components are sized and designed based on the maximum and minimum airflow requirements. ASHRAE std 84-1991 requires a minimum temperature difference between the two entering air sides of 54 °F (12.2 °C) for establishing the thermal performance of a heat recovery device subject to winter conditions. Assuming the air temperature in the hot air loop side entering the heat exchanger can be maintained at 75 °F (24 °C), then the minimum temperature entering the heat exchanger on the cold air loop side is 21 °F (-6.1 °C). In anticipation of future studies of frost control techniques using the new test facility, it is desired to have the capacity to reduce the temperature well below freezing, i.e., -10 °F (-23.3 °C). Based on the average nominal airflow rate and the lowest temperature required, the capacity of the cooling coil is determined. It is important to evaluate the available compressor capacity at very low refrigeration suction pressures in order to determine if it is possible to reduce the air temperature to the desired level. The full description of the refrigeration system will be presented in section 4.3. The existing electric heaters have ample capacity to obtain temperatures above 100 °F (37.8 °C). The maximum temperature is set at 120 °F (48.9 °C) in order to avoid any undesired effects related to high temperature. In summary, the full range capacity of the heat recovery test facility is as follows:

AIRFLOW RANGE: 750 CFM (354 L/s) to 3000 CFM (1416 L/s)

TEMPERATURE RANGE: -10 °F (-23.3 °C) to 120 °F (48.9 °C)

4.1.3 Double Tunnel-Closed Loop System

The ductwork of the present test facility more closely resembles the arrangement in CSA C439-00 rather than ASHRAE std 84-1991. The ductwork in ASHRAE std 84-1991 can be described as a single tunnel open loop system. Observing the layout in figure 4.1, air is drawn from either the outdoors or ambient into the test facility ductwork. Depending on the temperature and humidity of the outdoor or ambient air, further conditioning can be provided to meet the specified conditions entering the heat exchanger. The same air leaving the heat exchanger on the first stage is supplied to the second stage. This air can be heated or heated and humidified prior to entering the heat exchanger for the second stage. In the final stage of the process the air leaving the second stage is exhausted to either the outside or ambient air. The same air passes through the two sides of the heat recovery device, and, therefore, is considered a single tunnel system. The air is continually drawn and exhausted from either the outdoors or ambient, and thus can be described as an open loop system. This arrangement uses two fans to overcome the static resistance across the heat recovery device. However the airflow can only be increased on one side. Ciepliski (1997) uses four fans instead of two in an open loop arrangement. The two extra fans are used to maintain the pressure in the heat recovery device near standard atmospheric pressure to minimize carryover and cross leakage through enthalpy wheels. The conditions that exist in real energy recovery units are less ideal than this arrangement. When air is drawn from the outdoors or ambient, there is potentially more conditioning required for obtaining the desired conditions entering the heat exchanger. This implies that the heating and cooling plant must be sized to account for the worst case conditions unless the tests are performed at the time of year that is suitable for the entering conditions.

The present test facility is a double tunnel closed loop system as shown in figure 4.3. Each side of the heat exchanger is completely independent of the other side. In addition both tunnels re-circulate the same air rather than drawing from the ambient or outdoor air. This

system was conceived to provide superior flexibility in controlling the conditions independently on both sides. The two loops are called the cold air loop and hot air loop. As the name implies, the cold air loop will simulate the winter conditions, and the hot air loop will simulate air returning from an occupied space. In addition the mass airflow rates of either loop can be controlled completely independently of each other. The proposed set-up in ASHRAE std 84-1991 allows only the second stage of the heat exchanger to have a larger airflow relative to the first stage by virtue of the single tunnel dual fan arrangement. The present test facility offers total flexibility in providing the airflow rates that can be larger in either the cold or hot loop. The primary limiting factors are the fan performance, and the capacity of the fan motor horsepower. As the airflow rate is increased, the static pressure increases as a function of the air velocity across the various components in the system. An increased static pressure will subsequently increase the fan brake horsepower as a function of the fan laws. The fan motor full load amps is subsequently reached as the airflow rate is increased. Any further increase will cause the thermal overload to trip resulting in the motor shutting down.

Another advantage of the double tunnel, closed loop system is the reduced heating and cooling loads. In reference to open loop systems, the ambient air during the summer can be hot and humid and thus requires significant cooling to reduce the temperature. The advantage of the closed loop system is that the air is gradually brought down to a low temperature with less cooling capacity. The only energy added to the air through the system is through the plate heat exchanger, fan/motor, and gains through the unit casing and ductwork. During each pass through the direct expansion coil the air is dehumidified until only sensible cooling is occurring. Essentially the moisture is wrung out of the air through consecutive passes through the cooling coil. Once the latent energy has been removed from the air the temperature will drop much faster. If the air is already dry, then the cooling load is almost completely sensible. This phenomenon was observed during the commissioning stage of the test facility. The outdoor air can vary even during the period of a test if a sudden rainstorm occurs, or temperature swings as a result of varying solar radiation. During the winter season an option can be provided to utilize outdoor air in order to minimize the operating costs of using the compressors to cool the air.

4.2 Identify/Define Research Objectives

The origin of the initial idea to develop a heat recovery test facility is motivated by a need to understand the thermal performance and temperature distribution specifically within cross flow plate heat exchangers installed in energy recovery units. The current test standards are based on ideal laboratory conditions. Therefore it was conceived to design a test facility that could simulate to a certain extent a real air-handling unit in terms of its physical layout. However, the instrumentation and sensor accuracy would equal or exceed the existing standards. Furthermore, the test facility would serve for future research with regard to innovative frost control techniques for cross flow plate heat exchangers. The actual time spent on conceiving the research objectives is very short compared to the overall timeline of the complete development of the test facility. A literature review of other heat recovery test facilities provided a significant direction for the development of the existing test facility.

4.2.1 Preliminary Conceptual Design

The first crucial decision was to establish the capacity range of the test facility in terms of airflow rates and temperature ranges. An iterative process was required to evaluate the required cooling capacity and verify that it did not exceed the capacity of the existing compressor/condenser. For example during the first iteration the minimum air temperature was chosen to be –25 °F (-32 °C). The calculated cooling exceeded the capacity of the existing system. The final minimum air temperature was calculated to be –10 °F (-23.3 °C). At this early stage of the project four principle factors governed the preliminary design of the facility:

1. Allowable space for the facility in the existing laboratory.
2. Available power, i.e. voltage and amperage.
3. Existing instrumentation and data acquisition.
4. Available condensor/compressor capacity.

4.2.2 Detailed Design

The detailed design stage is where the specific dimensions of the unit are determined, mechanical and electrical components are sized and selected, and the layout inside the laboratory is established. Accessibility and flexibility are key characteristics to the design. All the components in the system need to be accessible for installation purposes during fabrication and for servicing after the unit is installed. The unit is designed to allow for replacing the plate heat exchanger with another one of the same or different size. Space was allotted on both sides of the unit in the laboratory for allowing access to the heat exchanger. Another significant factor in the detailed design stage that cannot be overlooked is the size of the unit with regard to the size of the openings to pass the unit into the building, along the hallway, and through the double doorway into the laboratory. The governing door opening size determines the largest allowable section size of the unit. The unit is designed in three sections, as shown in figure 4.5.

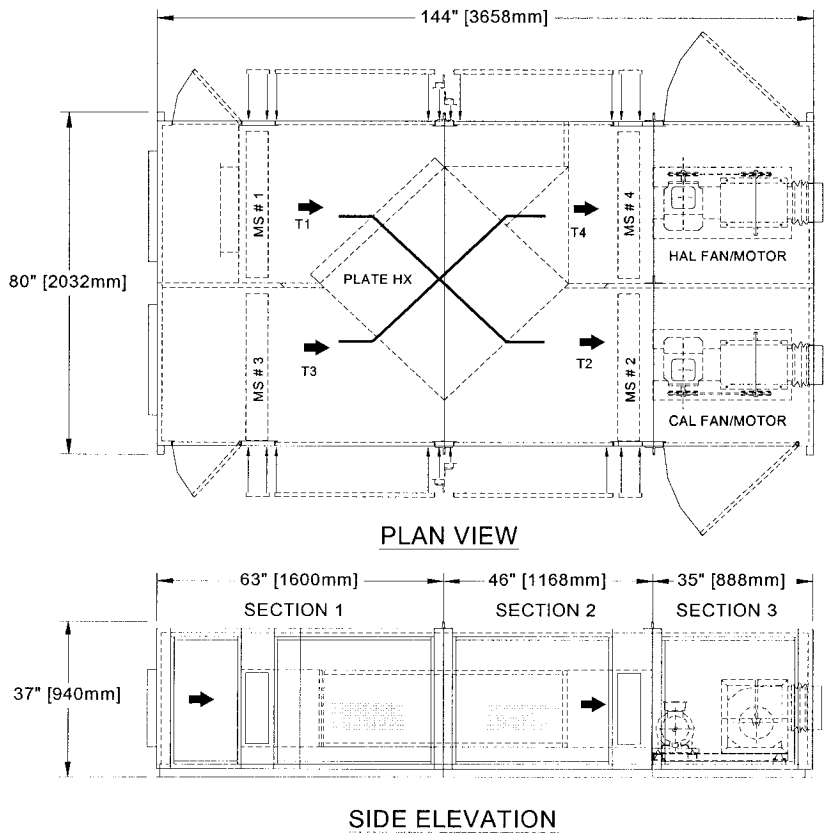

Figure 4.5 Heat recovery unit designed in three sections

4.2.3 Mechanical and Electrical Installation in the Laboratory

The three sections of the unit were shipped unassembled to the laboratory in order to pass through the doors. The sections were placed on an adjustable base that was built specifically for the heat recovery test facility to control the level of the unit. The three sections were bolted together. The joints between the sections contain neoprene gasket and silicone caulking to ensure air tightness. The plate heat exchanger was installed into the unit and sealed around the perimeter joints with silicone caulking. The control panels were installed on support brackets above the roof of the unit. The power and control wiring were installed between the unit and the control panels.

4.2.4 Ductwork Assembly

The ductwork was designed during the detailed design stage. The ductwork was subcontracted to a company specializing in ductwork fabrication. The ductwork was fabricated in sections and installed onto the fully assembled heat recovery unit. Each adjoining section of ductwork is provided with silicone caulking to ensure a leak tight duct. Access panels are provided at locations where sensors and airflow measuring stations are installed. The access panels contained neoprene gaskets around the perimeter edge of the door jam to be compressed when the panel is screwed onto the section of ductwork. Transition sections were fabricated for the cooling coil and electric duct heaters. The refrigeration work included piping the evaporator to the existing compressor/condensor packaged and charging the system with refrigerant.

4.2.5 Sensor/Instrumentation Installation

This stage of the project involved the following tasks:

- Preparation of thermocouple wires for temperature grids within the unit. Preparation included establishing lengths of the thermocouple wire from point of measurement to the multiplexer, and from the multiplexer to the data acquisition terminal blocks. The thermocouple wire is cut, and one end of the wire is soldered in conformance with the proper techniques for creating the hot junction. Thermocouple wires were methodically identified with wire numbers at both ends.

- Installation of thermocouple wires from the measurement point to the multiplexer and data acquisition. Small holes were drilled through the unit floor to allow a bundle of thermocouple wires to pass through them. Once the wires are in place, silicon sealant is used to fill the hole around the wires to prevent air leaks.
- The output signals from the humidity transmitters are wired to the data acquisition.
- Velocity pressure transducers were installed on special brackets near the airflow measuring stations and wired to the data acquisition. Static pressure transducers were installed on brackets and also connected to the data acquisition. Plastic tubing was installed from the pressure transducers to the point of measurement.
- Installation of airflow measuring station.
- Programming the data acquisition with Labview Software.
- Calibration of individual sensors not including the airflow measuring stations.

The longest task was the programming due to the complexity of the program in conjunction with the external multiplexer and the number of measurement points. Once the program was fully functional the heat recovery test facility could be commissioned with respect to instrumentation systems.

4.2.6 Commissioning and Calibration

The mechanical systems of the unit were checked prior to the completion of the sensor/ instrumentation installation. For example fans, heaters, and the cooling coil were verified for proper functioning prior to the completion of the sensor installation and the programming of the data acquisition. Once the airflow stations were installed, they were calibrated using a hot wire anemometer. The calibration covered the entire capacity range of the fan/motor using the variable frequency drives. All of the sensors in the heat recovery test facility were verified through the data acquisition.

4.2.7 Commencement of Testing

The testing commenced following the full commissioning of the test facility. Each test is preceded with a verification of all the measurement points in the system.

4.3 Description of Heat Recovery Test Facility

The components of the heat recovery test facility can be divided into three main categories that include mechanical, electrical, and instrumentation. Instrumentation will be covered extensively in chapter 5.

4.3.1 Unit construction

The heat recovery unit casing consists of a double wall construction with a 16 gauge satin coated steel on the exterior and 20 gauge satin coated steel on the interior panels. The unit is fabricated in three sections. Each section has a 4 " (102 mm) structural "C" channel base. 2 "x 2 " (51 mm x 51 mm) angles are welded on the ends of the unit that bolt together. ¼ " (6.4 mm) thick neoprene gasket and silicone sealant is used to seal the adjoining sections of the unit to provided a leak tight joint. The interior of the unit including the floor is insulated with 1" (25.4mm) thick, 3 lbs/cuft (0.0368 Kg/m^3) density insulation. All seams exterior and interior of the unit are sealed with silicone caulking. Access panels contain full-length piano hinges and quick release latches. Neoprene gasket coated with petroleum jelly is applied on all doorjambs. The door contains a knife-edge that compresses into the neoprene gasket providing a tight seal.

4.3.2 Plate type heat exchanger

The heat exchanger used for the heat recovery test is fabricated from 0.008" (0.2 mm) thick aluminum sheets. The plates are passed through a press die in which a specific pattern of truncated conical dimples and ribbing is formed into the sheet. Figure 4.6 illustrates the formed pattern for a sample section of the plate heat exchanger. The dimples are used to create the spacing between adjacent plates when they are lined up. The dimples are both raised or sunk on the surface of aluminum to allow for dimple spacing on both sides. The pressure of the die press controls the dimple spacing. Heavier pressure will cause a deeper dimple, therefore allowing for larger plate spacing. Larger plate spacing contains less heat transfer surface area per unit volume of the heat exchanger than smaller plate spacing. Both the dimples and the long

diagonal ribbing is used to give strength to the aluminum sheet it will not collapse under its own weight or the pressure from air passing through the heat exchanger. The heat exchanger is rated for a maximum of 10 " w.c. (2480 Pa) static pressure and operating temperatures less than 150 °F (65.6 °C). Normal operating pressures for typical heat recovery units will rarely exceed 4 " w.c. (992 Pa). The small edge ribs provide rigidity to the edges of the aluminum sheet. The dimples and ribbing increase turbulence within the heat exchanger to enhance the overall heat transfer coefficient. The dimples and ribs

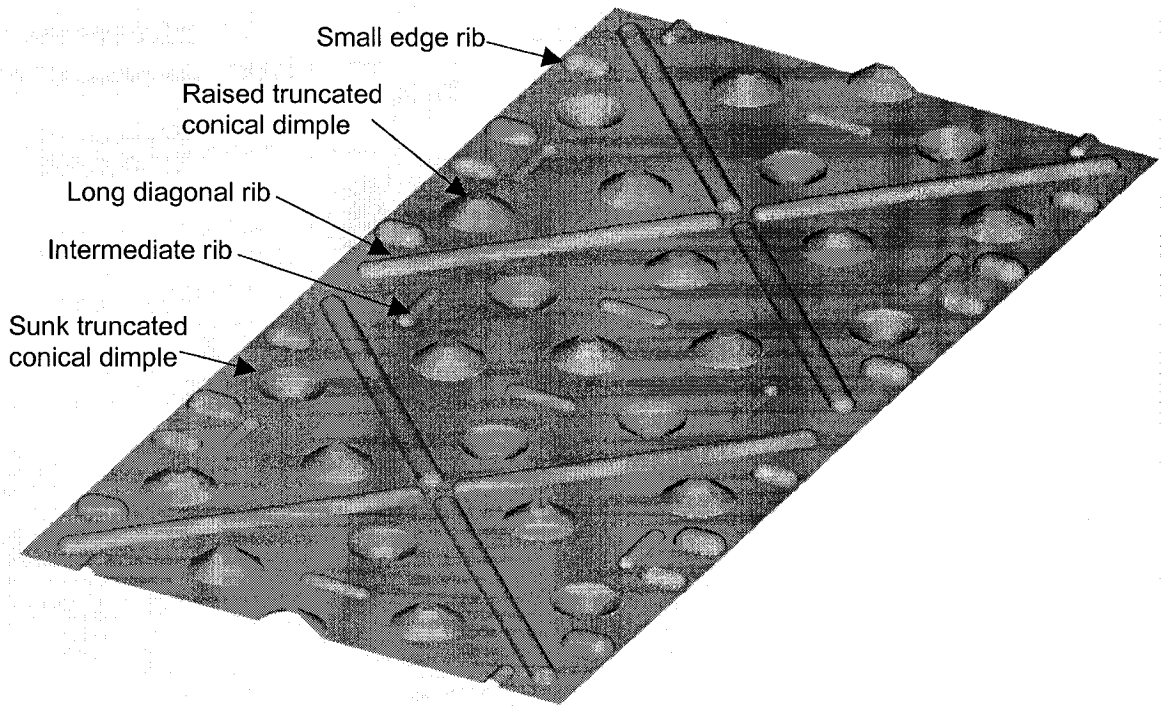

Figure 4.6 Sample area topography of plate type heat exchanger

result in increased surface area. One of the variables that determine the effectiveness of the heat exchanger, as elaborated in chapter 2, is the quantity of heat transfer surface area. The increase of surface area for a 3/8" (9.5 mm) plate spacing is calculated by adding up the individual surface areas of the individual dimples and ribs, and subtracting the original projection of these 3-dimensional shapes on the flat sheet of aluminum. Figure 4.7 visually depicts the calculation of the increased surface area due to the dimples and ribs. In comparison with a flat sheet of

aluminum, the dimples and ribs increase the surface area by 27.5% for 3/8" (9.5 mm) plate spacing.

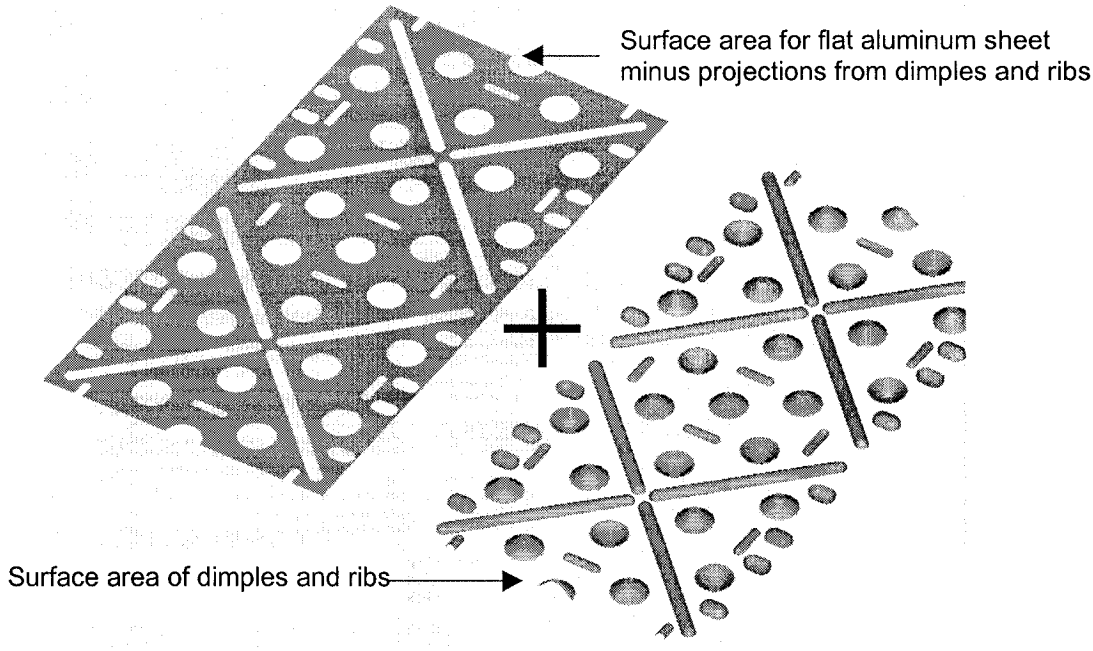

Figure 4.7 Extended surface area of aluminum sheet with dimples and ribs

The cross flow plate heat exchanger is fabricated in a manner that allows the two airstreams to be isolated, thus preventing cross contamination. The fabrication of the heat exchanger involves several steps:

1. The aluminum plate is supplied in rolls of standard widths of 24" (610 mm), 36" (914 mm) and 48" (1219 mm).

2. A decoiler machine is used to unroll the aluminum sheet.

3. The aluminum sheet is passed through a series of rollers to remove protrusions, kinks or bends.

4. The sheet is passed through a pressing machine that forms the specific topography on the surface of the aluminum. Position switches that move the sheet 6 " (152 mm) at one time control the die press. The die press itself is 6 " (152 mm) wide. Therefore the length of the sheets is always increments of 6 " (152 mm).

5. A shearing machine automatically cuts the formed sheet at a predetermined length. The lengths of the sheet depend on the size of the plate heat exchanger.

6. The current heat exchanger consists of a 36" (914 mm)x 36" (914 mm) folded sheets. In order to obtain the correct length, a 72" (1829 mm) sheet is formed, cut, and then folded in half. The dimples are lined up when the sheet is folded to ensure that the spacing between the sheets is maintained.

7. The open end of the folded sheet is sealed with a 1-1/4 " (32 mm) "V" strip. The "V" strip consists of 0.012 in. thick aluminum that is supplied by the aluminum supplier in 1-1/4 " (32 mm) wide strips. The strips are cut to length, and then formed in a "V" shape. A 1/8 " (3.2 mm) thick bead of silicone is applied to the inside portion of the "V". The "V" strip is placed on the open ends of the folded sheet, and crimped with a hydraulic crimping tool along the entire length. As the pressure is applied by the crimping tool to the strip, the silicone is spread inside the strip to ensure a leak-tight seal.

8. The next step in the process involves connecting the individual folded sheets together to form the heat exchanger core. The same process described to install the "V" strip is used to connect adjacent folded sheets. This step is crucial in creating two distinct channels for a cross flow configuration.

9. Once all the folded sheets are connected together, the core is placed within the supporting frame and is correctly squared.

10. End plates are placed at each end of the heat exchanger core. End plates are constructed of 16 gauge galvanized steel.

11. Supporting angles that cover the edges of the plate connects the end plates. Support angles are constructed of 16 gauge galvanized steel.

12. Silicone is applied abundantly along the supporting angles to ensure a leak-tight seal.

The size of the cross flow plate heat exchanger that will be used in the heat recovery test facility is presented in figure 4.8. The Heat exchanger consists of the following characteristics:

- Manufacturer: Circul-Aire Inc. Division of Dectron International
- Model: PMW-36X-18
- Type: Cross flow
- Plate spacing: 3/8 inches ((9.5 mm)
- Quantity of plates: 41
- Heat transfer surface area: 940 Sqft (86 m^2), including 1.275 factor for dimples and ribs.

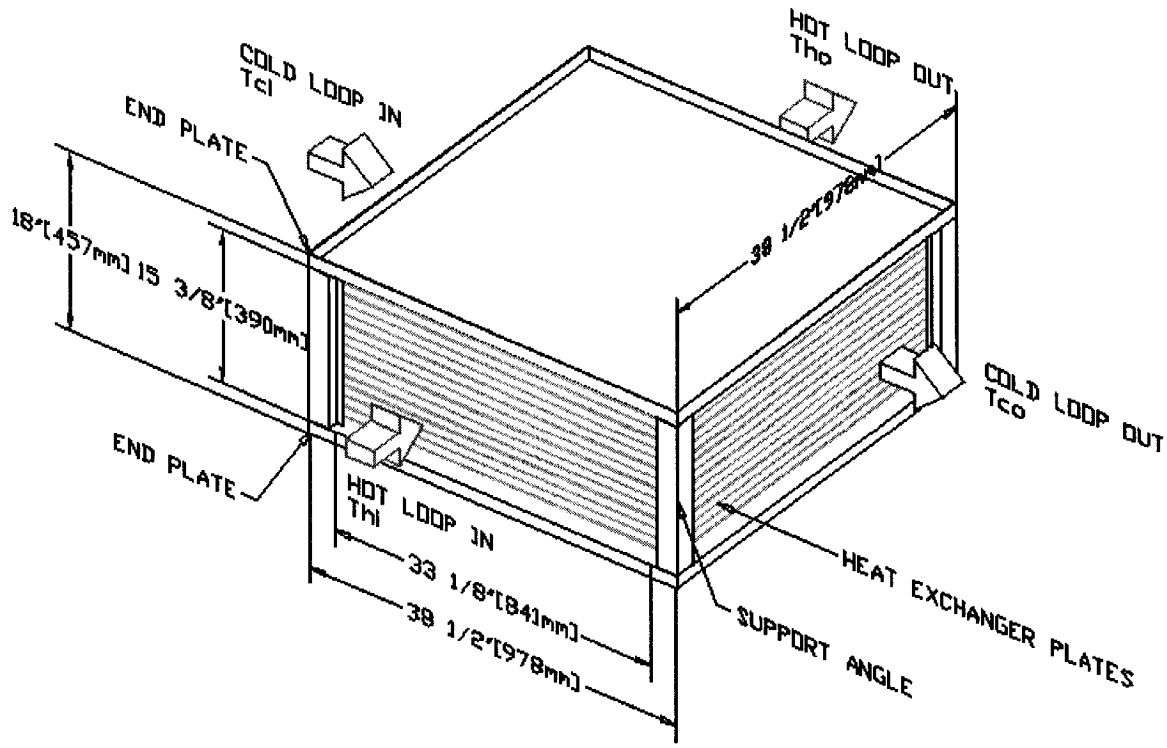

Figure 4.8 The cross flow plate heat exchanger, model PMW-36X-18, used in the heat recovery test facility

4.3.3 Cold and Hot loop fans

The fans used in both the cold and hot loops are forward curve blowers, Delhi model 910-8 as shown in figure 4.9. The blower is selected based on the maximum airflow rate and static pressure of the test facility. The forward curve blower is deemed as the best choice of fan for the range of airflows and static pressures within the heat recovery test facility. As mentioned above, the maximum airflow for the heat recovery test facility is 3000 CFM (1416 L/s). The static pressure for each component in both the cold and hot loop is determined at its maximum face velocity corresponding to the maximum airflow. The sum of the static pressures provides the total static pressure that is used in calculating the fan performance for the selected fan. Table 4.1 provides a summary of the static pressures and the total static pressure for both the cold and hot loops. Since the cold loop contains a direct expansion coil, the total static pressure is higher than

the hot loop. The fan performance curves for both the hot and cold loop is provided in figure 4.10 and 4.11 respectively.

Table 4.1 Total static pressure calculation for the hot and cold loops

COLD LOOP COMPONENTS	STATIC PRESSURE in. w.c. (Pa)	HOT LOOP COMPONENTS	STATIC PRESSURE in. w.c. (Pa)
Airflow straightener	0.2 (50)	Airflow straightener	0.2 (50)
Airflow measuring station	0.1 (25)	Airflow measuring station	0.1(25)
Direct expansion coil	1.5 (372)	Electric Heater	0.25 (62)
Electric Heater	0.25 (62)	Plate heat exchanger	1.7 (421)
Plate heat exchanger	1.7 (421)	Ductwork	0.5 (124)
Ductwork	0.5 (124)	-	-
TOTAL STATIC PRESURE	4.25 (1054)	TOTAL STATIC PRESURE	2.75 (682)

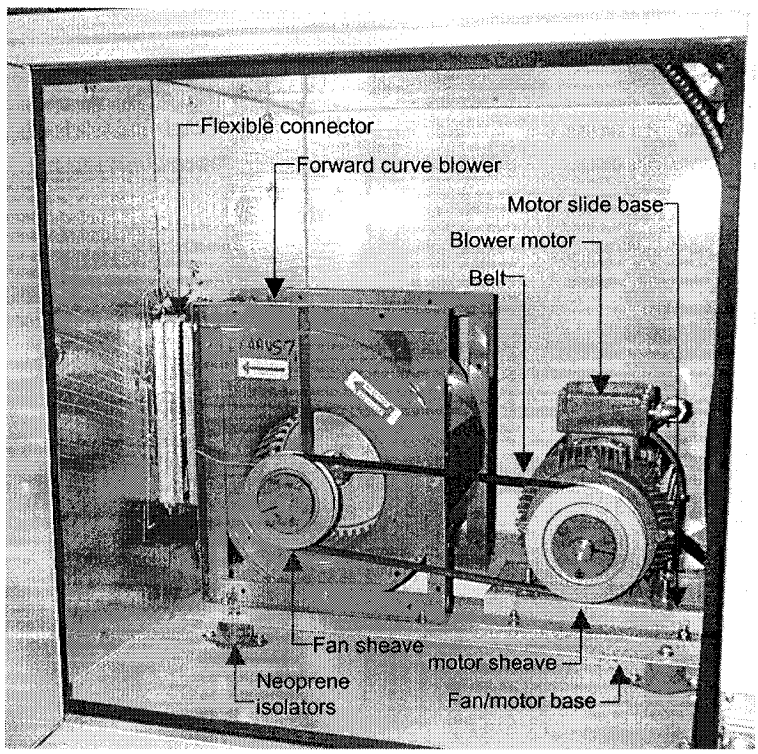

Figure 4.9 Forward curve blower, motor and accessories for both hot and cold loops in heat recovery test facility

A software program supplied by the blower manufacture, Delhi, is used to calculate the fan performance. Although the fans are selected for the maximum airflow and static pressure, the entire range of airflows is considered in the selection of the fan. The motor horsepower is sized based on 110% of fan brake horsepower. The blower is belt drive as opposed to direct drive. A fan and motor sheave is provided with a 1:1 ratio. In other words, at 60 hz, the motor operates at 1750 RPM, the blower will rotate at the same RPM. A variable frequency drive is used to control the fan motor RPM, which in turn will control the airflow rate. The blower and motor are installed on an integral base that is isolated from the unit floor and casing by neoprene isolators and flexible connectors. The motors operate on a voltage of 208 Vac, 3 phase, and 60 hz. The cold air loop blower motor is selected to be 5 hp (3.75 KW), since the blower brake horsepower from figure 4.11 is 3.96 bhp. In reference to the blower performance curve for the hot loop, the motor is selected to be 3 hp (2.2 KW) since the bhp is below 3, and the system will not be running exclusively at the highest airflow rates. The decision to use the 3 hp (2.2 KW) is also based on lower cost of the motor and variable frequency drive.

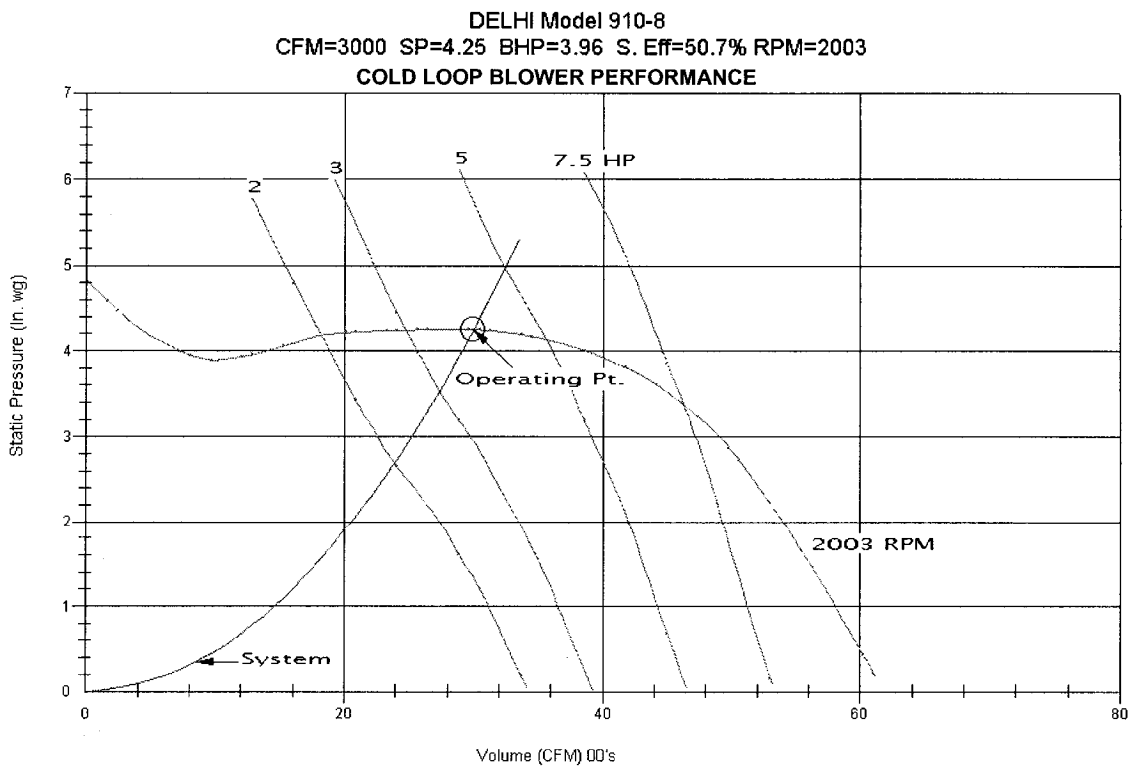

Figure 4.10 Blower performance curve for the cold loop

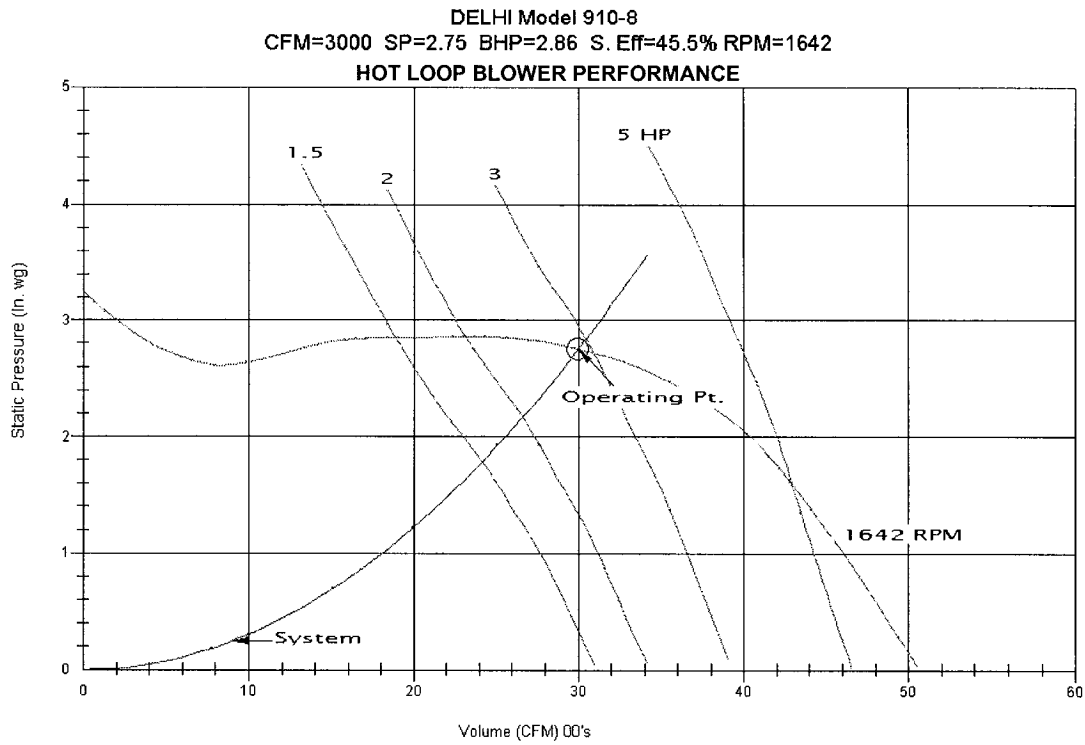

Figure 4.11 Blower performance curve for the hot loop

Most of the heat recovery tests will be run at well below the maximum airflow rate of 3000 CFM (1416 L/s). The variable frequency drives used to control the fan motor rpm are adjustable from 0 to 120 hz, allowing for a large range of airflow rates. In addition precise control of the airflow is possible as the frequency is adjustable to the second decimal place, i.e., 60.00 hz. The frequency can be input either manually from the variable frequency drive keypad, or automatically from a 0-10 Vdc signal from the data acquisition system.

4.3.4 Ductwork

The ductwork is constructed from 20 gauge galvanized steel. The geometry of the ductwork, and the fact that it loops over the top of the heat recovery unit, requires it to be built in a variety of sections. Rectangular elbows are used to loop the ductwork over the top of the unit. Transitions are used to mate different areas from components to the ductwork and from the ductwork to the heat recovery unit. All ductwork sections are joined using transverse standing drive slip joints. Longitudinal joints consist of a Pittsburgh lock seam. The ends of the ducts that

connect to heating or cooling components consist of a perimeter flange. All joints are sealed with silicone sealant within the duct. Access panels are provided at strategic locations to allow for the installation and maintenance of sensors. All access panels contain a neoprene gasket that is tightly compressed onto the duct by sash lock latches. Access panels are located upstream and downstream from the direct expansion coil. Insulation is installed only on the cold loop side since heat gains on the hot loop side is desirable. The insulation consists of two layers of 2" (50 mm) thick rigid board. The insulation is held in place by plastic straps. Aluminum duct tape is used to seal between adjacent pieces of insulation.

4.3.5 Direct expansion cooling coil

The cold loop contains a direct expansion refrigeration coil that is used to simulate cold climate air temperature entering the plate heat exchanger. The coil was especially designed for the application of a closed loop circuit and a very low air temperature. The coil has 28 rows and 4 fins per inch. The low fin spacing allows for frost build-up on the coil without significantly affecting the pressure drop and airflow. Since it is a closed loop system, any latent load in the air will be removed during the first few passes through the coil. Once the latent load is removed from the circulating air, then only sensible load will be removed. Therefore, frost on the coil is not expected to build-up. The coil consists of ½" (12.7 mm) copper tubes and aluminum plate fins. An enclosure was built to contain the coil and drain pan. The enclosure is suspended above the unit with an access door on the side. Two layers of 2" (50 mm) thick rigid board insulation are applied over the entire surface of the enclosure. Figure 4.12 contains a photo of the enclosure containing the coil. The coil is connected to an existing refrigeration system consisting of a 7.5 ton reciprocating semi-hermetic compressor at –20 °F (-28.9 °C) suction and 100 °F (37.8 °C) condensing. The compressor will deliver approximately 28.3 tons at 40 °F (4.4 °C) evaporating temperature based on R-22. The refrigerant is replaced with R-408, which has slightly better capacity at the lower suction temperatures. The condenser is a water cooled system, utilizing a shell and tube heat exchanger, with a maximum heat removal capacity of 35 tons per hour at a condensing temperature of 100 °F (37.8 °C). The condenser is designed to use city water. The

unit is constructed in accordance to ASME standards, with the design working pressure of 125 psig (861 KPa) on the water side and 400 psig (2756 KPa) on the refrigerant side. The condenser is equipped with a modulating water regulating valve, refrigerant liquid line shut-off valve 5/8" (16 mm) size, filter driers, moisture indicators, suction line liquid accumulator 1 3/8" (35 mm) and a liquid line solenoid valve operating on 120 volts. A propeller type fan is installed over the

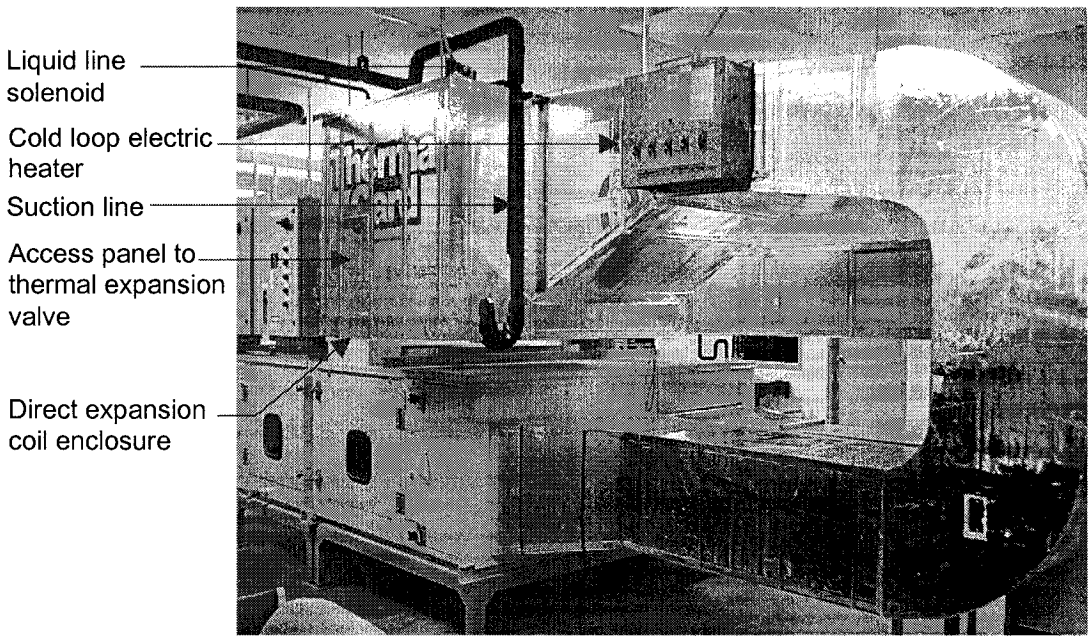

Figure 4.12 Direct expansion coil enclosure and cold loop electric heater

area of the compressor's motor housing to provide sufficient ventilation while it is running. The semi-hermetic compressor contains capacity control from 100% down to 33% that is accomplished by closing off suction gas into three cylinder inlet cavities. Control piston assemblies in the head using main lubricating oil as a power source and controlled by solenoid valves provide 5 stages of cooling, 100%, 83%, 66%, 50%, or 33%. Two position switches located on the main control console manually energize the stages. The compressor motor is 40 hp (29.3 kW) operating on 575 volts, 3 phase, and 60 Hz. The compressor allows for suction

gas cooling of the motor windings. Furthermore, thermistors are implanted into each phase winding that continually monitor temperature for added motor protection. High and low pressure safety cut-out switches are provided. The low-pressure switch is used as a pump down when the liquid solenoid is shut down. In this case the compressor will cut-out at the low pressure in order to isolate the refrigerant within the condenser and receiver. This reduces chances of refrigerant leakage when the system is idle. During compressor off periods an insert type crankcase heater maintains the oil dilution. The pump down cycle also forces the oil to return to the compressor where the crankcase heaters will heat it. A pilot light on the control console indicates that the crankcase heater is energized when the compressor is shut down. Pressure gauges for suction and condensing temperature and pressure is provided on the control console. In addition, entering and leaving water temperature gauges from the water-cooled condenser are also provided. The compressor, water-cooled condenser and the control console are shown in figure 4.13.

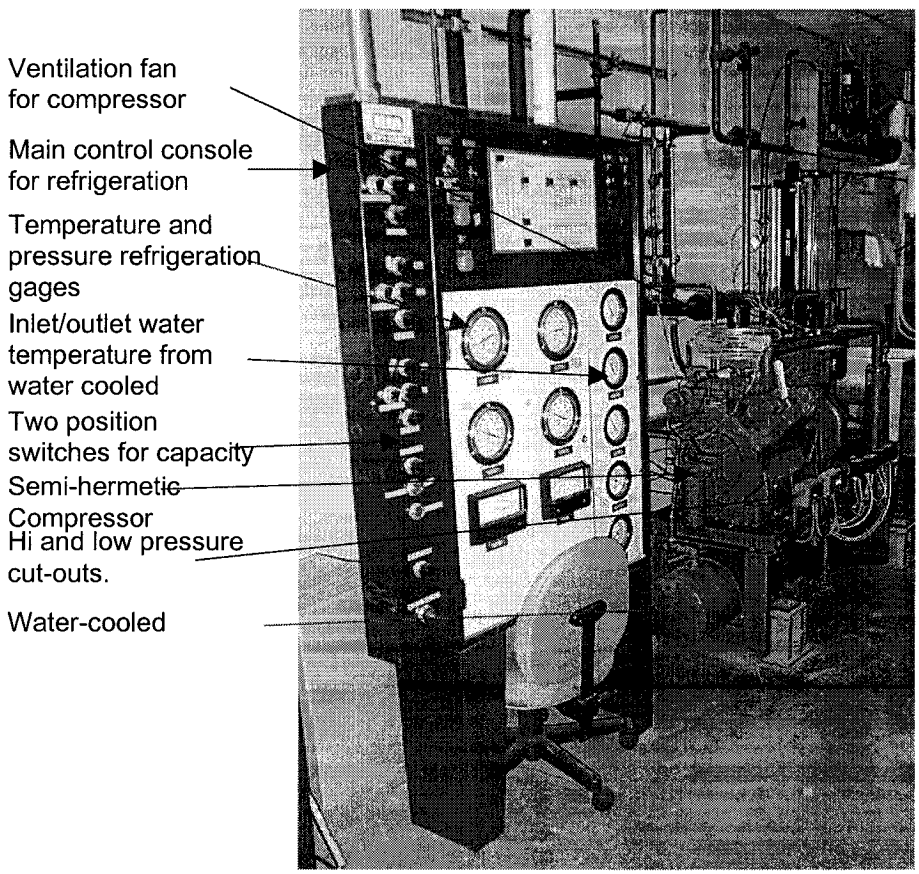

Figure 4.13 Compressor, water-cooled condenser and control console for heat recovery test facility

4.3.6 Electric heaters

Each of the cold and hot air loops contain an electric heater operating on 600 volt, 3 phase, and 60 Hz. The heaters contain nickel-chromium open coil elements that are supported by non-rotating zircon-ceramic bushings. The bushings are contained within a galvanized steel frame and have a high resistance to thermal shock and mechanical impact. The terminals of the elements consist of stainless steel lugs. Thermal cut-outs are provided to safeguard the elements from overheating. An air-proving switch is interlocked with the heater to ensure it is off when there is no airflow. Each heater is fully controlled via a SCR (Silicone Controlled Rectifier). The electric heater on the cold loop, which has a capacity of 26 Kw, is located just downstream from the direct expansion cooling coil. It is shown in figure 4.12. The cooling coil does not have precise control of the air temperature. Therefore, the principal function of this heater is to provide fine tune control of the air temperature entering the cold loop side of the plate type heat exchanger. Based on the maximum airflow rate, 3000 CFM (1416 L/s) and the nominal design airflow, 1500 CFM (708 L/s), the corresponding maximum temperature rises is based on the following equations:

$$q_{htg,\,cal} = \frac{1.08 \times Q_{cal} \times (\Delta T)}{3413}\ \text{, KW} \qquad \textbf{(4.1)}$$

Re-arranging the variables to obtain ΔT,

$$\Delta T = \frac{3413 \times (q_{htg,\,cal})}{1.08 \times Q_{cal}}\ \text{, °F} \qquad \textbf{(4.2)}$$

For $q_{htg,\,cal} = 26\ KW$ and $Q_{cal} = 3000$ CFM (1416 L/s) : $\Delta T = 27$ °F (15 °C)

For $q_{htg,\,cal} = 26\ KW$ and $Q_{cal} = 1500$ CFM : $\Delta T = 55$ °F (30.6 °C)

During actual tests, the required maximum temperature rise may rarely exceed $\Delta T = 10$ °F (5.6 °C). For example if a 15 °F (8.3 °C) air temperature is required at the cold loop entering side of the heat exchanger, the cooling coil may bring the temperature down to approximately 10 °F (5.6 °C), and the heater is used to obtain 5 °F (2.8 °C) temperature rise. The electric heater on the hot loop, which has a capacity of 52 Kw, is located just downstream from the airflow station as

illustrated in figure 4.3. This heater has a significant role to maintain the air temperature entering the heat exchanger on the hot loop side between 65 °F (18.3 °C) and 75 °F (23.9 °C). In most cases, the tests will be performed with a 70°F entering temperature to simulate actual return air conditions from a building space in a cold climate. The temperature rise needed is much higher than the cold loop since the average air temperature leaving the hot loop side of the heat exchanger will be near freezing, i.e., 32 °F (0 °C).

For $q_{htg,cal} = 52\ KW$ and $Q_{cal} = 3000$ CFM (1416 L/s): $\Delta T = 55$ °F (30.6 °C)

For $q_{htg,cal} = 52\ KW$ and $Q_{cal} = 1500$ CFM (708 L/s) : $\Delta T = 110$ °F (61.1 °C)

The above temperature rises are more than adequate to achieve the required air temperature.

4.3.7 Humidifier

A steam humidifier is incorporated into the hot loop to allow for humidity control for future tests. In the present work humidity is not a factor. The humidity is generated from a 60 KW Sussman electric steam boiler operating on 600 volt, 3 phase, and 60 Hz. The boiler has a capacity to generate a maximum of 175 lbs/hr (79.4 Kg/hr) of steam at 212°F (100 °C). The design range is from 68°F (20 °C) 20% RH, and 20.3 grains (0.0029 lb_w/lb_a) to 68°F (20 °C), 80% RH, and 81.9 grains (0.0117 lb_w/lb_a). The calculations used to determine the maximum humidity required for future testing is as follows:

$Q_{hal,\max} = 3000$ CFM (1416 L/s), 68°F (20 °C), 80% RH, and 81.9 grains (0.0117 lb_w/lb_a)

Moisture rate: $$\dot{W} = Q_{hal,\max} \times 4.5 \times (w_2 - w_1),\ \text{Lbs/hr} \qquad \textbf{(4.3)}$$

Substituting the values into equation 4.3 gives

$$\dot{W} = 3000 \times 4.5 \times (0.0117 - 0.0029)$$

$$\dot{W} = 118.8\ \text{Lbs/hr (53.9 Kg/hr)}$$

Therefore, the steam boiler has adequate capacity. The boiler is equipped with an automatic water level control and a low water cut off that shuts the boiler down when the water supply in the boiler drops below a safe operating level. The heating elements are 0.42" (10.7 mm) in diameter and constructed of stainless steel. The boiler vessel is constructed in accordance with section I

of ASME Boiler and Pressure Vessels codes. A water level sight glass is provided. Several safety features are included such as a steam safety valve that opens on rise of pressure when excessive steam pressure builds up; steam pressure gauge; and a manual reset pressure control for high pressure cut-out. The piping was extended to reach the location of the manifold that was located downstream from the heater in the hot air loop ductwork as shown in figure 4.14. A modulating steam valve, Belimo G213/NM24-SR, with 0-10 Vdc signal is provided to control the level of humidity.

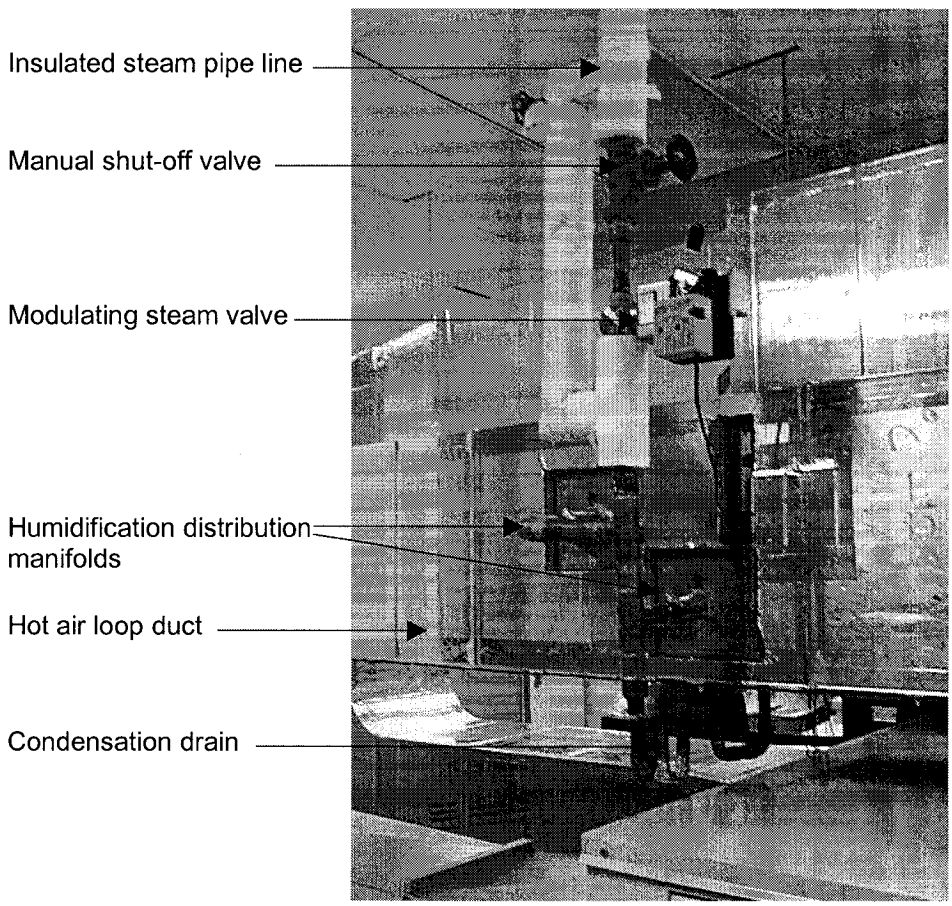

Figure 4.14 Humidification distribution manifolds in hot air loop ductwork

4.4 *Description of Electrical and Control Systems*

Two electrical control panels are supplied for the heat recovery test facility to accommodate the two primary supply voltages, 575 V/3 ph/60 Hz, and 208 V/3 ph/ 60 Hz. The fan motors are selected to operate on 208 V, because the variable frequency drives are much less expensive than those available for 575 V. The other high voltage components, such as the heater, compressor, and steam humidifier all operate on 575 V. The control panels are designed to contain all of the required temperature controllers and variable frequency drives, contactors, transformers, and fusing. Figure 4.15 shows the external layout of the two control panels. The electrical schematics for the heat recovery test facility are located in Appendix B.

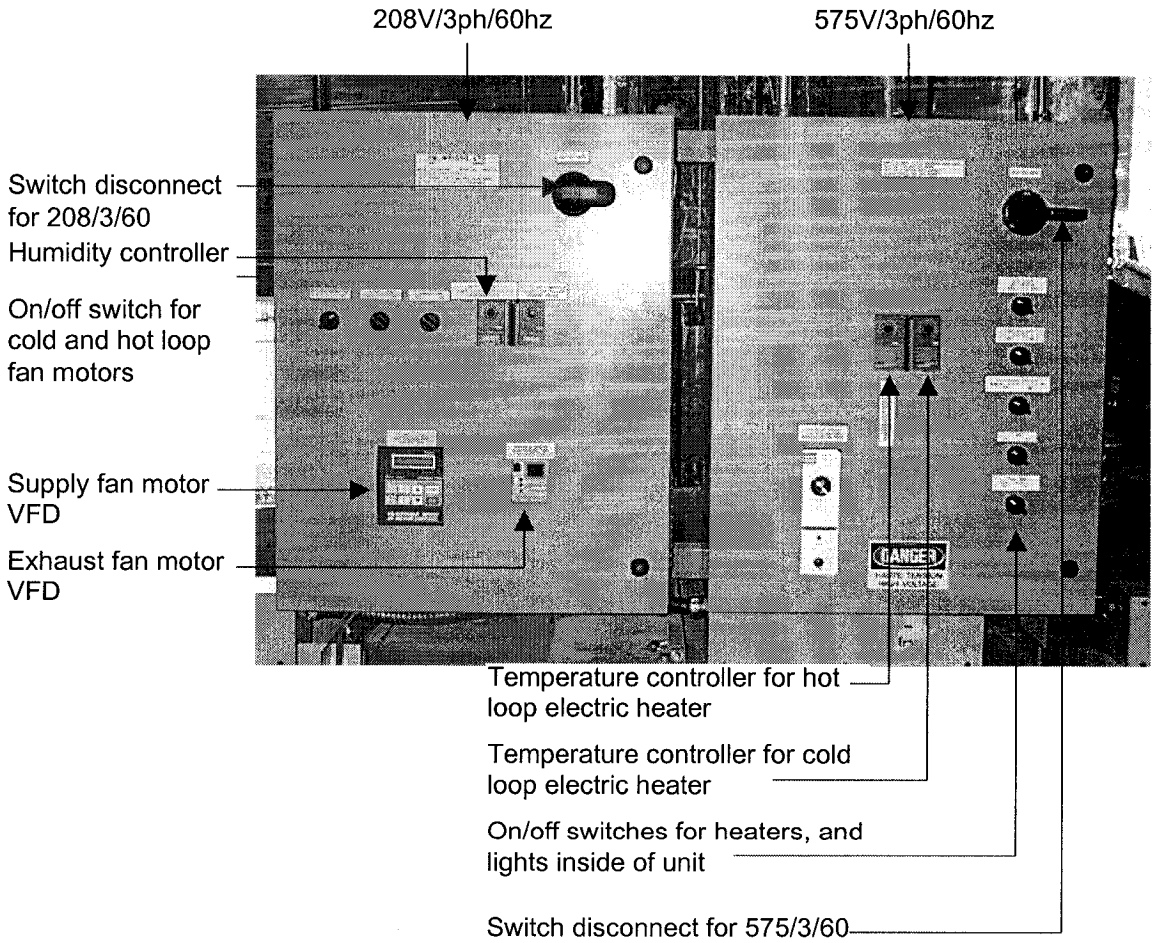

Figure 4.15 Control panels for heat recovery test facility

5.0 INSTRUMENTATION AND DATA ACQUISITION

The pre-test uncertainty analysis presented in chapter 3 in conjunction with ASHRAE STD 84-1991 formed the basis for the selection of the instrumentation and data acquisition. The sensitivity analysis allowed an optimization of the selection of sensors with respect to cost and accuracy. The sensitivity analysis also revealed the effect of the operating conditions on the normalized sensible effectiveness uncertainty. This chapter will deal with the specific instrumentation, data acquisition, and software program that were used for the tests. Among the topics that will be covered are: a detailed description of all the sensors and their operating principles; the accuracy of the sensors; an explanation of the calibration method; and the physical location within the test facility. Once the sensors were installed in their designated positions and correctly tagged, readings were taken and compared with a reference value to ensure that the wiring and installation was correct. In light of the large number of measured points, a system of tagging was developed to facilitate tracking and identifying them. Each sensor is identified with a unique tag at the measured point and at the other end where the wires terminate in the data acquisition. In total there are 128 measured points in the test facility. Table 5.1 provides a summary of all the measured points. ASHRAE STD 84-1991 provides a guide for the selection and location of the sensors, but there are several differences that will be revealed in this chapter.

One of the unique features of this heat recovery test facility is the use of the thermocouple grids to measure the bulk air temperature at different points and planes within the plate heat exchanger on both the cold air loop and hot air loop side. The literature review revealed that there are no previous studies that use such an extensive grid of thermocouples to study the temperature distribution in a full scale cross flow plate heat exchanger. Cross flow configuration produces larger non-uniform temperature distributions than both counter flow and parallel flow. In particular, the phenomenon of cold corner can be studied more closely using this technique. A detailed description of this novel measuring technique will be presented in section 5.4.

Table 5.1 Summary table of measurement points for heat recovery test facility

MEASURED PARAMETER	VARIABLE DESIGNATION	QTY OF POINTS	TYPE OF SENSOR	UNIT	OUTPUT SIGNAL	DAQ AUTOMATED	ACCURACY
BULK AIR TEMPERATURE WITHIN CHANNELS OF THE HEAT EXCHANGER	REFER TO TABLE	68	TYPE 'K' THERMOCOUPLE	°F (°C)	-5.97 to 50.66 mV	YES	±1.5°F
COLD AIR LOOP TEMPERATURE ENTERING HEAT EXCHANGER	REFER TO TABLE	12	TYPE 'T' THERMOCOUPLE	°F (°C)	-5.6 TO 17.82 mV	YES	±0.5°F
COLD AIR LOOP TEMPERATURE LEAVING HEAT EXCHANGER	REFER TO TABLE	12	TYPE 'T' THERMOCOUPLE	°F (°C)	-5.6 TO 17.82 mV	YES	±0.5°F
HOT AIR LOOP TEMPERATURE ENTERING HEAT EXCHANGER	REFER TO TABLE	12	TYPE 'T' THERMOCOUPLE	°F (°C)	-5.6 TO 17.82 mV	YES	±0.5°F
HOT AIR LOOP TEMPERATURE LEAVING HEAT EXCHANGER	REFER TO TABLE	12	TYPE 'T' THERMOCOUPLE	°F (°C)	-5.6 TO 17.82 mV	YES	±0.5°F
COLD LOOP AIR FLOW STATION TEMPERATURE	T_{cal}	1	TYPE 'T' THERMOCOUPLE	°F (°C)	-5.6 TO 17.82 mV	YES	±0.5°F
HOT LOOP AIR FLOW STATION TEMPERATURE	T_{hal}	1	TYPE 'T' THERMOCOUPLE	°F (°C)	-5.6 TO 17.82 mV	YES	±0.5°F
COLD AIR LOOP RELATIVE HUMIDITY LEAVING HEAT EXCHANGER	ϕ_{hco}	1	POLYMER CAPACITANCE SENSOR	% RH	0 - 10 Vdc	YES	±2%
HOT AIR LOOP RELATIVE HUMIDITY ENTERING HEAT EXCHANGER	ϕ_{hhi}	1	SOLID STATE HUMIDITY SENSOR	% RH	0 - 10 Vdc	YES	±2%
HOT AIR LOOP RELATIVE HUMIDITY LEAVING HEAT EXCHANGER	ϕ_{hho}	1	POLYMER CAPACITANCE SENSOR	% RH	0 - 10 Vdc	YES	±2%
COLD AIR LOOP AIR FLOW STATION RELATIVE HUMIDITY	ϕ_{hcal}	1	SOLID STATE HUMIDITY SENSOR	% RH	0 - 10 Vdc	YES	±2%
HOT AIR LOOP AIR FLOW STATION RELATIVE HUMIDITY	ϕ_{htal}	1	POLYMER CAPACITANCE SENSOR	% RH	0 - 10 Vdc	YES	±2%
STATIC PRESSURE ACROSS HEAT EXCHANGER ON COLD AIR LOOP SIDE	$P_{s,ci}$	1	PRESSURE TRANSDUCER	INCHES W.C.	4 - 20 mA	YES	±0.05 in. W.C.
STATIC PRESSURE ACROSS HEAT EXCHANGER ON HOT AIR LOOP SIDE	$P_{s,co}$	1	PRESSURE TRANSDUCER	INCHES W.C.	4 - 20 mA	YES	±0.05 in. W.C.
STATIC PRESSURE ACROSS HEAT EXCHANGER ON COLD AIR LOOP SIDE	$P_{s,hi}$	1	PRESSURE TRANSDUCER	INCHES W.C.	4 - 20 mA	YES	±0.05 in. W.C.
STATIC PRESSURE ACROSS HEAT EXCHANGER ON HOT AIR LOOP SIDE	$P_{s,ho}$	1	PRESSURE TRANSDUCER	INCHES W.C.	4 - 20 mA	YES	±0.05 in. W.C.
VELOCITY PRESSURE IN COLD AIR LOOP TO OBTAIN FLOW RATE	$P_{v,cal}$	1	PRESSURE TRANSDUCER	INCHES W.C.	4 - 20 mA	YES	±0.002 in. W.C.
VELOCITY PRESSURE IN HOT AIR LOOP TO OBTAIN FLOW RATE	$P_{v,hal}$	1	PRESSURE TRANSDUCER	INCHES W.C.	4 - 20 mA	YES	±0.002 in. W.C.
AIR VELOCITY	V	40	HOT WIRE ANEMOTER	fpm OR m/s	N/A	NO	±0.015 m/s OR 3 fpm
BAROMETRIC PRESSURE	P_B	1	MERCURY COLUMN	INCHES Hg	N/A	NO	
TOTAL NO. OF AUTOMATED MEASURED POINTS		129					
TOTAL NO. OF MANUALLY MEASURED POINTS		41					

The number of measured points was initially limited to 48 universal inputs based on the existing data acquisition (designated as DAQ hereinafter) system from National Instruments. This number of points fell significantly short of the desired number of points required to establish meaningful results within the context of the experimental goals of this research. This limitation was successfully overcome through the development of a multiplexer external to the DAQ but controlled by digital inputs stemming from the DAQ. The multiplexer allowed the 48 points to be expanded to 128 points. In light of the large number of measured points, it was necessary to develop a program compatible with the hardware that would allow for the automation of the DAQ. The program was developed using the software called Labview and was adapted to account for the multiplexer. After several versions and much debugging, the program was finally successfully operational for the test facility. A detailed description of the DAQ hardware, the multiplexer, and the software program will be presented in section 5.4

5.1 Description of Measurement Systems

The principle measuring systems include the airflow stations, temperature entering and exiting the plate heat exchanger, relative humidity at three locations only, and static pressure at the four measuring stations

5.1.1 Air Flow Measuring Stations - Cold and Hot loop

There is one airflow measuring station in each the cold and the hot air loop. The location of the airflow stations in the test facility are indicated in figure 4.3.. In view of the limited space available in the laboratory for the test facility, the ductwork that loops over the top of the plate heat exchanger was used to install the airflow station. The longest straight lengths of duct are installed over the top of the plate heat exchanger to accommodate the airflow measuring stations. The stations are installed at least 5 duct diameters downstream from any transitions or elbows. Airflow straighteners are installed approximately 2 ½ duct diameters downstream from the stations. The airflow straighteners consist of a bundle of ½ " (12.7 mm) diameter plastic straws, 3 " (76.2 mm) long. The airflow measuring stations consist of the following components:

1. The total and static pressure measuring grid.
2. Pressure transducers.
3. The plastic tubing between the pressure transducer and measuring grid.
4. Scani-valve.
5. Thermo-couple thermopile.
6. A series of tapped holes on the duct corresponding to each row of total pressure measuring tubes. The holes are plugged when not in use to prevent air leakage from the system.

The main measuring grids for the cold and hot air loops were fabricated specifically for the test facility, the size of duct, and the range of airflows to be used for the tests. The grid consists of ¼" (6.4 mm) outside diameter copper tubing. The grid was fabricated with 4 interconnected vertical tubes spaced 3" (76.2 mm) center to center. Each tube has 5 holes spaced at a distance of 2 ½" (63.5 mm) center to center with ½" (12.7 mm) copper tubes extending from the vertical tubes. The reason these copper tube extensions were installed is to reduce the effect of eddies and turbulence as the air flows around the main vertical tubes. The copper tube extensions are orientated parallel and facing the airflow direction. The grid was carefully installed to ensure that the tube extensions do not deviate from the direction of the airflow. Each point measures the local total pressure. A total of 20 points are included on the grid. The local total pressure consists of the following equation:

$$P_{TP,i} = P_{VP,i} + P_{SP} \quad \textbf{(5.1)}$$

Where

$P_{TP,i}$: Local total air pressure at point i.

$P_{VP,i}$: Local velocity pressure at point i.

P_{SP} : Static pressure that is assumed to be constant in the plane of the measuring grid in all directions.

The copper tubes for the local total pressure are interconnected to each other. A barbed fitting extending from the measuring grid to outside of the duct provides the external connection to either the scani-valve or directly to the high side of a pressure transducer via a 1/8" (3.2 mm) O.D. plastic tube. The tubes are tightly fitted onto the barbed connections to eliminate leakage.

The reading measured at the barbed fitting represents the average total pressure of the 20 measuring points, represented by the following equation:

$$\overline{P}_{TP} = \frac{\sum_{i=1}^{n=20} P_{TPi}}{20} \quad \textbf{(5.2)}$$

Where

$\overline{P}_{TP}$: Average total pressure at the air flow station

By substituting equation 5.1 into 5.2 results in the following equation:

$$\overline{P}_{TP} = \frac{\sum_{i=1}^{n=20} \left(P_{VPi} + P_{SP}\right)}{20} \quad \textbf{(5.3)}$$

Equation 5.3 can be reduced as follows:

$$\overline{P}_{TP} = P_{SP} + \frac{\sum_{i=1}^{n=20} \left(P_{VPi}\right)}{20} \quad \textbf{(5.4)}$$

$$\overline{P}_{TP} = P_{SP} + \overline{P}_{VP} \quad \textbf{(5.5)}$$

The static pressure is measured at one point on the grid, perpendicular to the air stream, which represents the static pressure in the plane of the air flow station. It is important to ensure that the static pressure tip is perpendicular to the airflow direction in order to eliminate the effect of velocity pressure. A barbed fitting protrudes from the duct for the static pressure measurement. A 1/8" (3.2 mm) O.D. plastic tube runs from the barbed connection to either the scani –valve or the low side of the pressure transducer. The length of tubing was kept to a minimum of 6 ft (1.8 m) from the barbed connection to the scani-valve or pressure transducer. The smaller tube diameter was chosen to allow for a faster response time in measuring velocity pressure. The two parameters that are measured as pressure differential are the average total pressure, $\overline{P}_{TP}$, and the average velocity pressure, $\overline{P}_{VP}$. Re-arranging equation 5.5 allows the resulting average velocity pressure to be measured.

$$\overline{P}_{VP} = \overline{P}_{TP} - P_{SP} \quad \textbf{(5.6)}$$

There were two methods of measuring the velocity pressure based on the number of pressure transducers available. Initially, there was only one pressure transducer with the desired accuracy available for measuring the velocity pressure. An innovative technique was conceived utilizing a scani-valve to measure multiple points of pressure. The scani-valve was also used to transfer static pressure to a pressure transducer. Each port scani-valve can receive as many as 48 points. In the case of this test facility, only a maximum of 6 points would be required: 2 points for the velocity pressure for the cold and hot air loops, and 4 points for the static pressures. However, two separate ports were required to measure the differential pressure between the average total pressure and the static pressure. An available scani-valve was used in the present research. This permitted cost savings on the pressure transducers, in particular for the higher accuracy velocity pressure transducers that have an 0.4% accuracy for a 0 – 0.25 inch w.c.. There are three main drawbacks in using the scani-valve. The first disadvantage was revealed in chapter 3 in reference to the increased uncertainty of the sensible effectiveness as a result of the co-variance between the cold and hot air loop velocity pressure. This could be partially offset by using the formulation for the average sensible effectiveness, and using airflow rates higher than 1200 CFM (566 L/s). This produced a normalized uncertainty of approximately 4%. The second disadvantage involved the settling time of the pressure transducer required between the two velocity pressure channels. When the scani-valve switched channels the pressure changed on the same pressure transducer. In the case of unbalanced airflow between the cold and the hot air loops, the difference in velocity pressure was significant. The change in pressure caused a significant delay in the pressure transducer to produce stable readings for the next channel. In some cases the delay is 15 seconds or more between channels. This caused an overall delay on the sample period for all the points in the system. When the system is studied in steady state, this time delay will not impact the results. However in the case of transient analysis, the scale of the delay will cause an overly low sampling rate and thus increase the aliased effect. The third disadvantage also relates to the sampling period time. After the scani-valve switches to the last channel, it receives a digital signal that controls the return to its initial or zero position. The

transition from the last channel to zero position causes a delay in the overall sampling period. The same impact for the settling time of the pressure transducer also applies to this case. The scani-valve requires two digital signals: one signal causes a switching to the next channel; the second signal returns the scani-valve to the zero channel. Figure 5.1 shows a picture of the scani-valve set-up with the pressure transducers. Figure 5.2 shows the airflow measuring station and the barbed connections that extend from the duct.

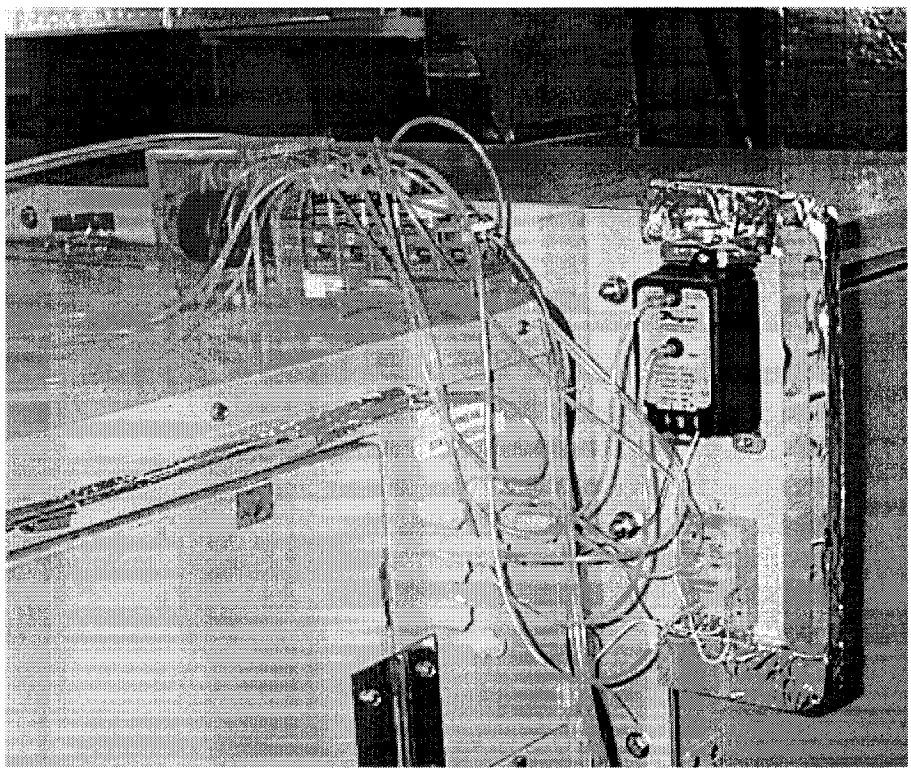

Figure 5.1 Scani-valve set-up in conjunction with pressure transducer

In the future, more velocity pressure transducers would be installed, and thus the scani-valve would no longer be needed. Presently each airflow measuring station has an independent velocity pressure transducer. All the variables are independent and the sampling period can be significantly shortened.

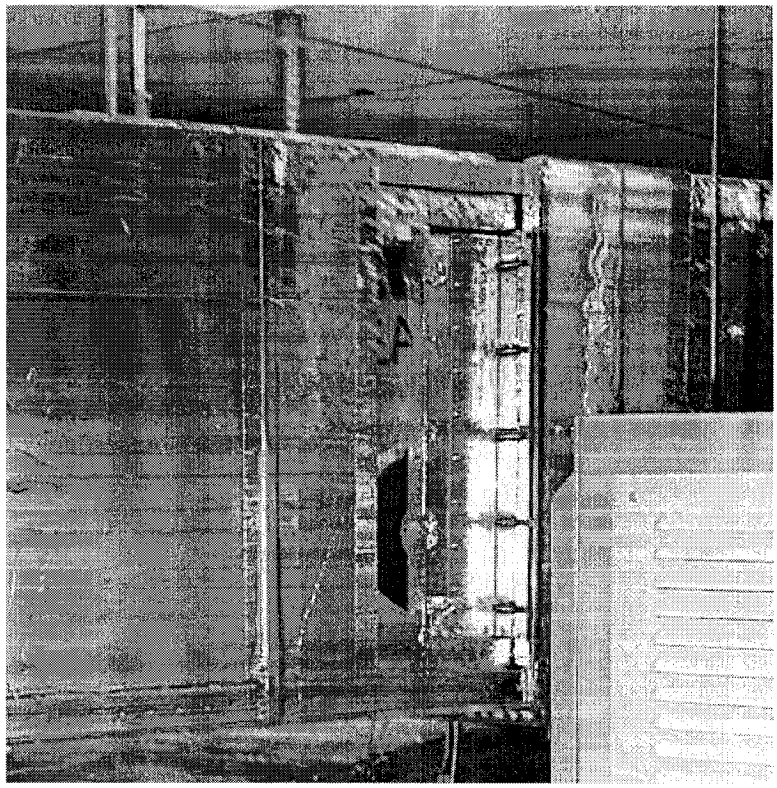

Figure 5.2 Air flow measuring station in cold air loop

The pressure transducers used for measuring velocity pressure consist of a Dywer series 677 that has a range of 0 to 0.5 inches w.c., 0.4% accuracy full scale or ± 0.002 inches w.c.. The transducers have an output signal of 4 to 20 milliamps. A 500 Ohm resistor is used to convert the 4 to 20 milliamp signal to a 2 to 10 Vdc signal. The transducer is rated for 250 milliseconds response time. The specification indicates that the pressure transducers were factory calibrated. In addition they were calibrated in the laboratory using a Dwyer Microtector electronic Hook Gage Manometer. The Microtector has a specified accuracy and repeatability of ± 0.00025 inches w.c., and complies with the USA Federal Specification GGG-C-105A . It is also traceable to a master at the National Bureau of Standards.

A thermopile consisting of type "T" thermocouples with twisted pairs at each of the measuring points on the airflow grid is used to measure the average dry bulb air temperature. The relative humidity is measured at the measuring stations prior to the fan. Since there was no moisture added or removed in the system during the testing of the heat exchanger, the relative humidity could be calculated at the airflow measuring station, knowing the dry bulb air temperature and relative humidity prior to the fan intake. Figure 5.3 contains an example of the psychometric process in determining the relative humidity at the airflow station.

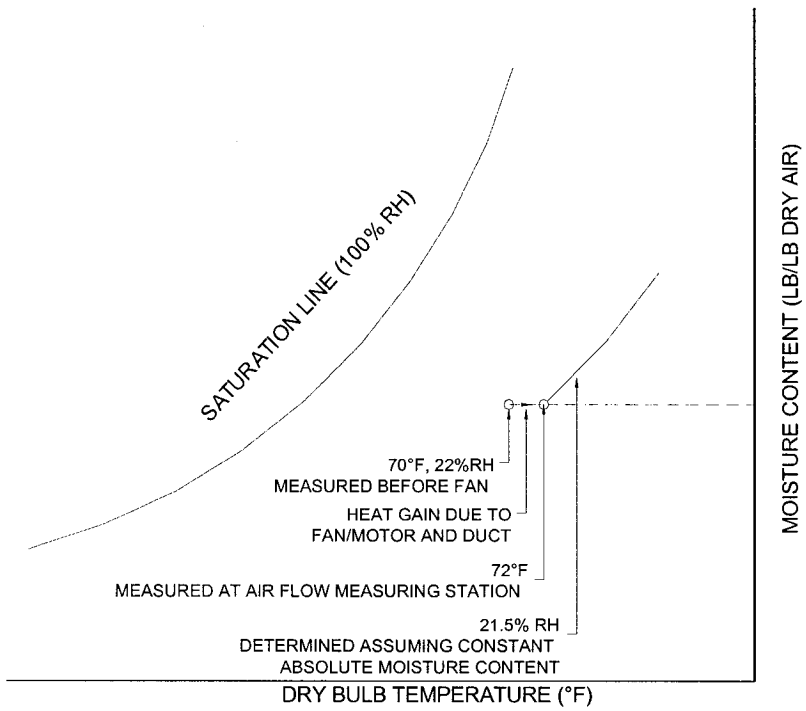

Figure 5.3 Method for determining relative humidity at the airflow measuring station

The sensitivity analysis of the effectiveness uncertainty in chapter 3 revealed that the velocity pressure had the most significant effect. Based on this information, it was necessary to calibrate not only the pressure transducers but also the entire airflow measuring station. The calibration consists of making a comparison between another measuring system that has a known and low accuracy. The method chosen involved measuring air velocity with a hot wire anemometer at each of the points on the airflow grid. Holes are drilled into the side of the duct. The locations of

the holes correspond with the rows of measurement points for total pressure. The hot wire anemometer contains a telescoping probe with an imperial scale engraved on its surface indicating distance from the tip of the probe in units of inches. Since the distance between the points horizontally across the duct is known, the air velocity can be measured at the same points. The method for measuring the air velocity involved the following process:

1. Unplug one of the holes in the side of the duct.
2. Insert the telescoping probe to the desired point.
3. Wait for several seconds to allow the velocity reading to settle to the local velocity.
4. There is a certain amount of fluctuation at all the points. The hot wire anemometer contains a function that averages the readings for an adjustable period of time. The sampling period was selected for 20 seconds.
5. The average value is recorded.
6. The process is repeated for the next point.
7. All the average velocities are entered into an excel spreadsheet.
8. The average of the 20 points is calculated.
9. The area of the duct cross section is known. Therefore, the airflow rate can be calculated using:

$$Q_{cal} = \overline{V}_{cal} \times A_d \text{ and } Q_{hal} = \overline{V}_{hal} \times A_d$$

Where the above variables are defined as follows:

Q_{cal}, Q_{hal}: The airflow rate at the measuring station in the cold and hot air loop.

$$\overline{V}_{cal} = \frac{\sum_{i=1}^{n=20} V_{cal,i}}{20} \text{ and } \overline{V}_{hal} = \frac{\sum_{i=1}^{n=20} V_{hal,i}}{20}$$

$\overline{V}_{cal}$, $\overline{V}_{hal}$: The average air velocity at the measuring station in the cold and hot air loop.

$V_{cal,i}$, $V_{hal,i}$: The air velocity at a measuring point on the measuring station grid in the cold and hot air loop.

A_d: The cross sectional area of the duct in the plane of the airflow measuring station.

Next, the velocity pressure, dry bulb air temperature, and the relative humidity located near the fan intake is recorded for both the cold and hot air loop through the DAQ. A program specifically

for calibration of the airflow measuring station was developed using Labview software program. This data is automatically entered in an excel spreadsheet via the program. The velocity is calculated using equations 3.15 to 3.20 in figure 3.2. This entire process is repeated for the complete airflow rate range of the test facility at increments of approximately 100 CFM (47.2 L/s). The airflow rate is controlled by the variable frequency drive for each fan motor. The frequency was incremented by 2 Hz over the range of airflow rate. The process of calibrating the airflow measuring stations is depicted in figures 5.4 as a flowchart. The setup procedure involved stabilizing the temperature and airflow in both the cold and hot air loops until a steady state condition was achieved. A temperature of 70 °F (21.1 °C) was maintained in both loops for the range of airflow rates. The cold air loop system was energized first in order to cool the air temperature several degrees below 70 °F (21.1 °C). If both systems were started at the same time, then it would take longer to stabilize the temperature to the desired level since the fan motor in both systems added heat. The direct expansion coil offset this heat gain. The flowchart in figure 5.5 depicts the actual airflow calibration procedure.

The calibration curves for both the cold and the hot air loop airflow measuring stations for both air velocity and airflow rate are presented in figure 5.6. It can be seen from these curves that there is excellent agreement between the hot wire anemometer and the velocity pressure method for almost the entire range of air velocities. The curve begins to deviate for the low air velocity that corresponds with a low velocity air pressure. This curve demonstrates the sensitivity of the velocity pressure transducer at lower air velocity. This confirms the results of the sensitivity analysis in relation to the velocity pressure transducer uncertainty and the sensible effectiveness uncertainty.

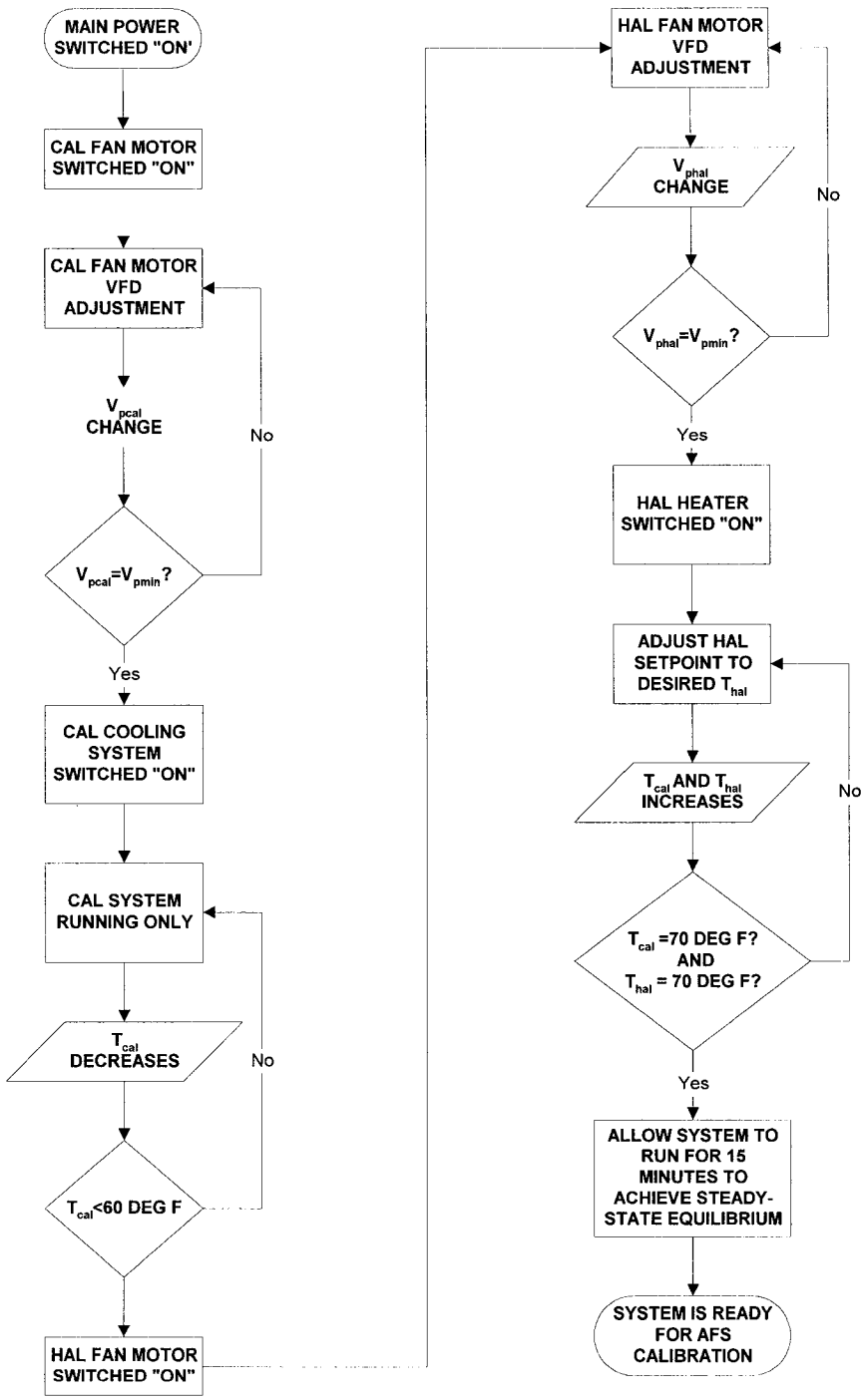

Figure 5.4 Set-up procedure for airflow measuring station calibration

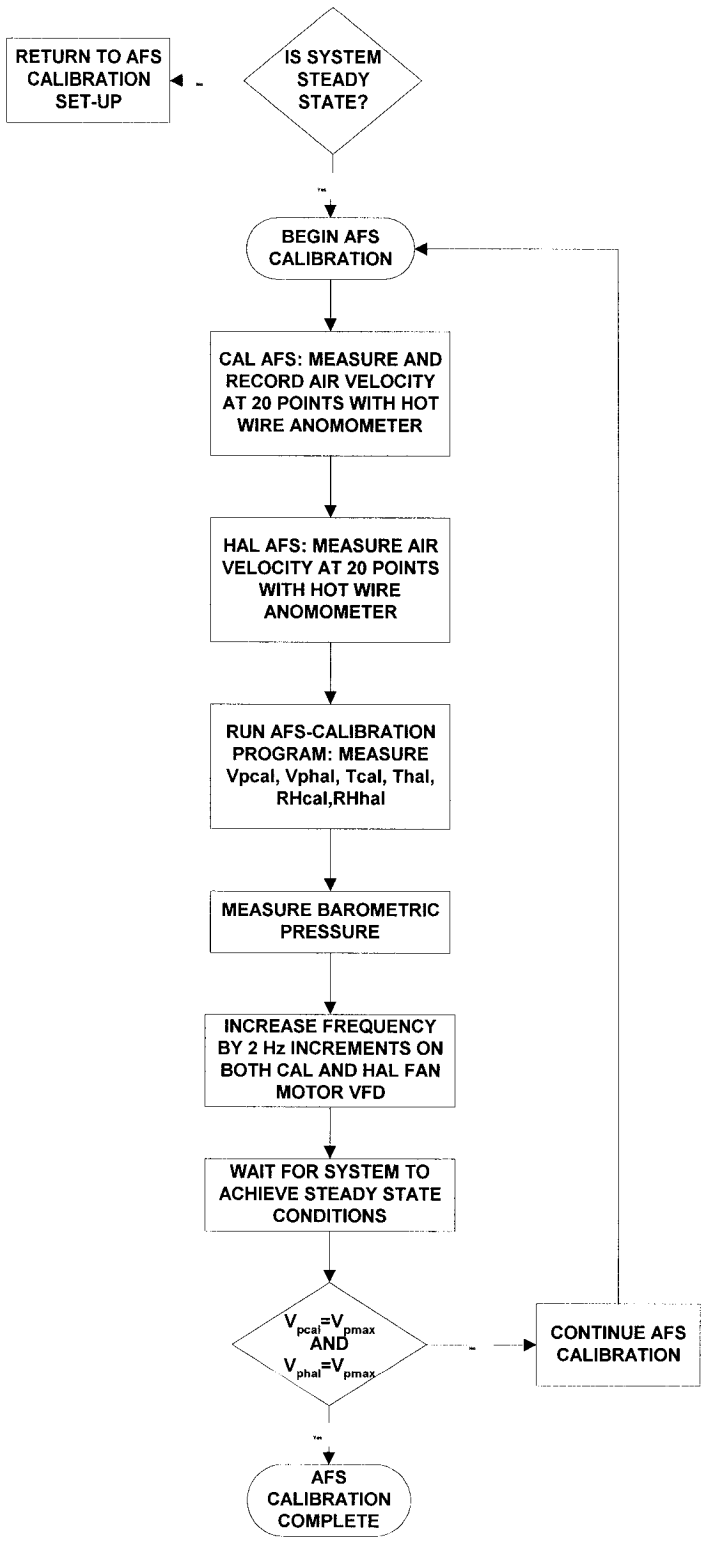

Figure 5.5 Procedure for airflow measuring station calibration

a)

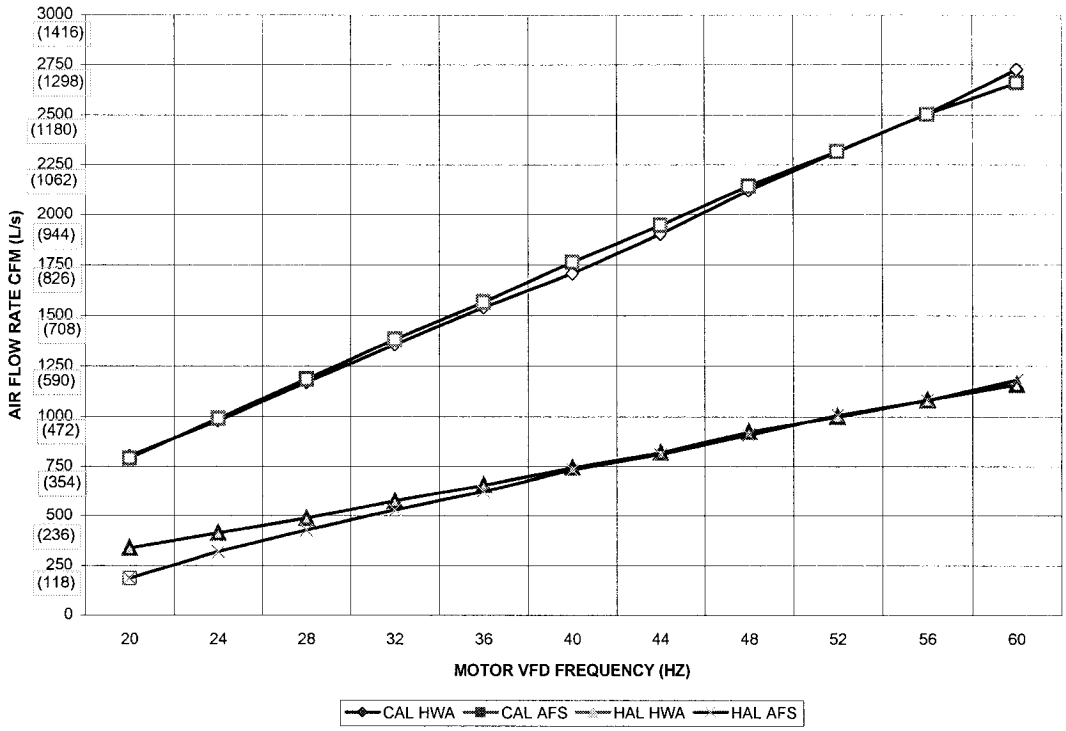

b)

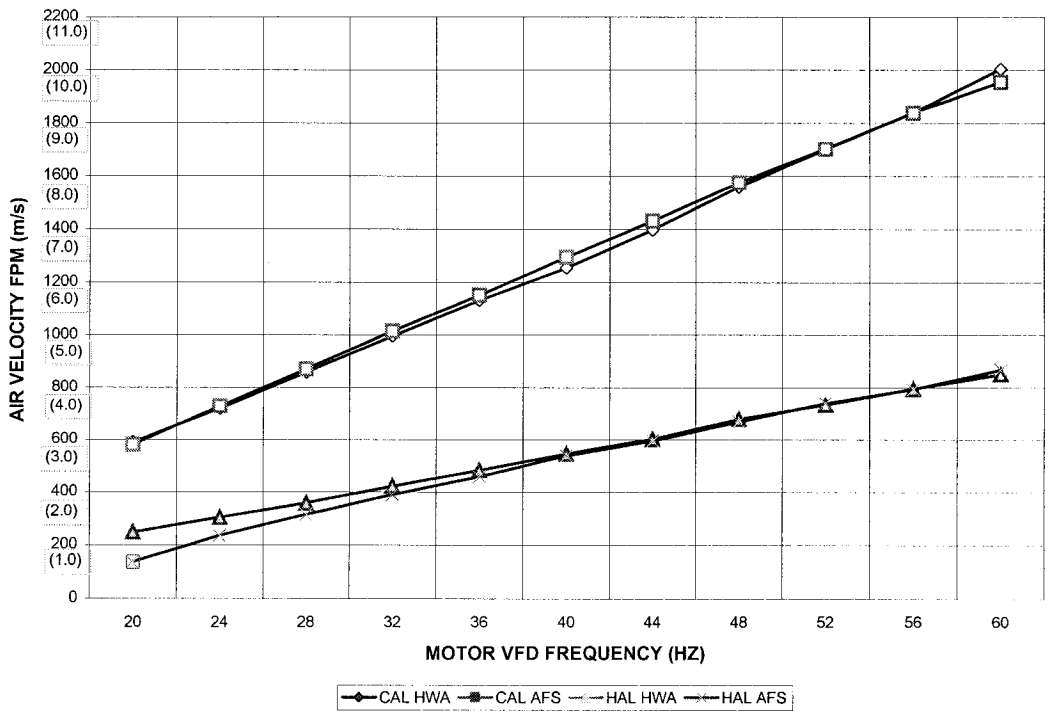

Figure 5.6 Calibration curves for the cold and hot airflow measuring stations: a) Airflow rate versus fan motor vfd frequency and b) Air velocity versus vfd frequency.
CAL= Cold Air Loop; HAL= Hot Air Loop; HWA= Hot Wire Anemometer ; AFS= AirFlow Station

5.1.2 Temperature Measurement

Air temperature is measured at several locations inside the test facility. The air temperature at the airflow measuring station was discussed in the previous section. The temperature measurements inside the plate heat exchanger will be covered in section 5.3. The main focus of this section is the measurement of the temperature at the four measurement stations surrounding the plate heat exchanger. These measurement stations are modeled after the guidelines in ASHRAE STD 84-1991. T-type thermocouples are used to construct the measurement grids because of the expected temperature range during testing, the low accuracy, and low cost. Another reason why a thermocouple temperature sensor was chosen is because of its faster response as compared to a RTD (Resistance Temperature Detector) and thermistors. Each of the four measurement stations consists of 12 individual points located at the center of the equal size squares that form the rectangular grid. Figure 5.7 shows the four grids, and the tags

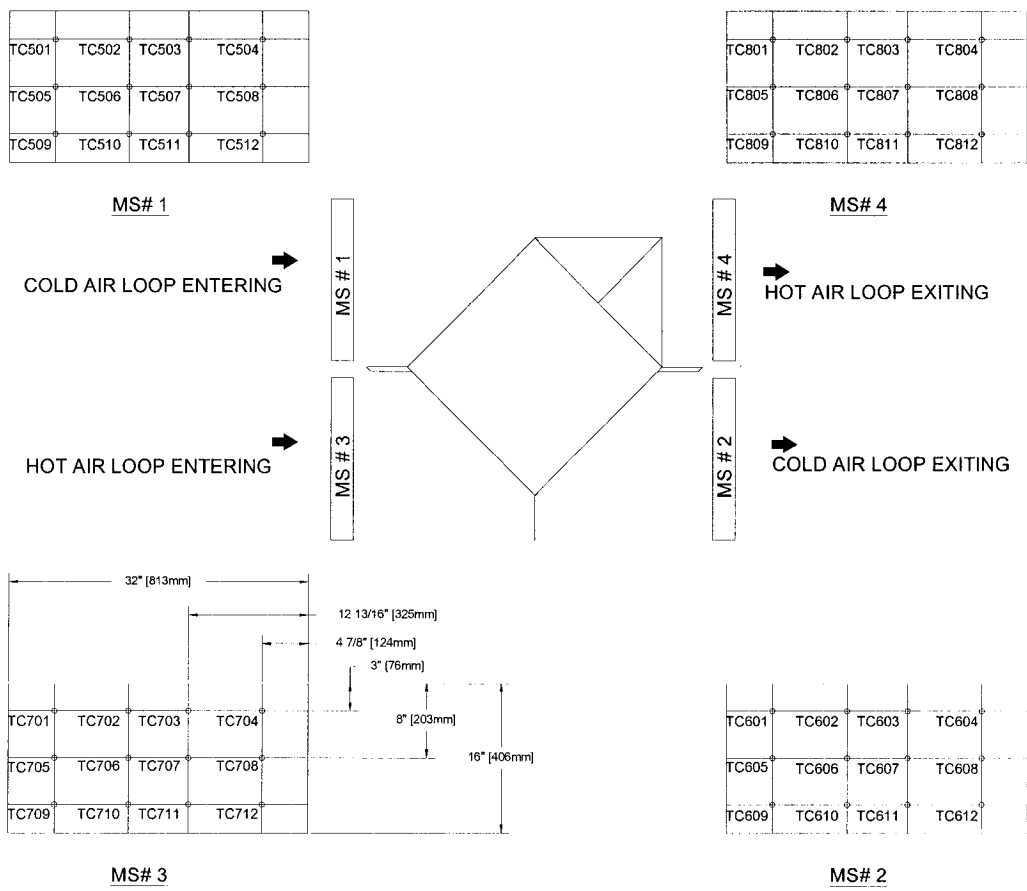

Figure 5.7 Type "T" Thermocouple grid at the four measuring stations entering and exiting the heat exchanger in cold and hot air loop

Figure 5.8 shows a picture of the temperature grid. Thin galvanized strips were used to support the thermocouple wire to minimize disturbance of the airflow.

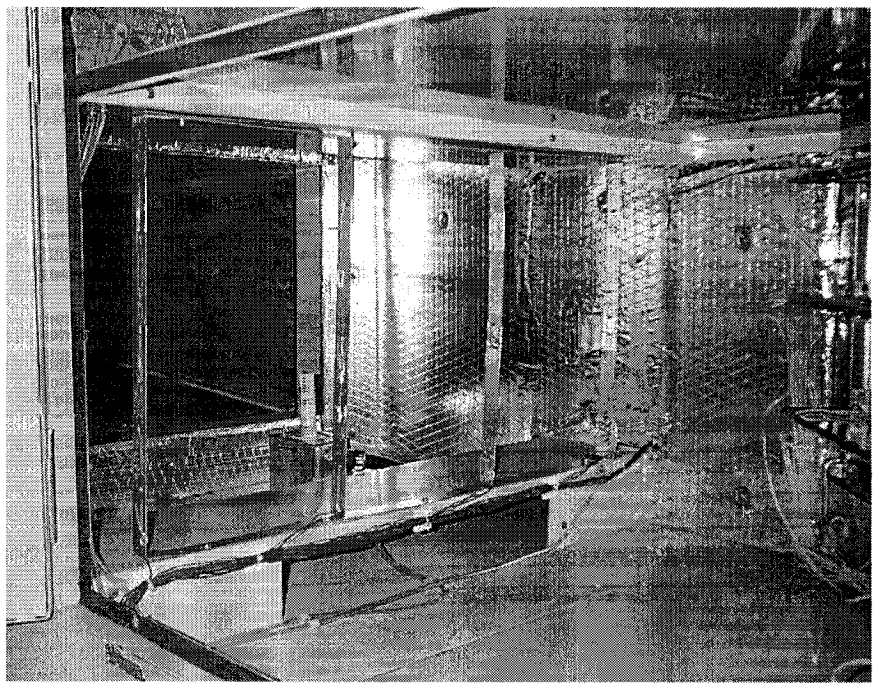

Figure 5.8 Thermocouple grid located at measuring station in hot air entering side of heat exchanger

Diamond shape configurations are more common for cross flow plate heat exchangers, particularly for packaged energy recovery air handling units. It is of practical interest to study the temperature distribution entering and leaving a cross flow plate heat exchanger with regard to the effect on thermal performance. Although temperature distribution will be presented, the effect on thermal performance will be left for future experimental studies. The thermocouple wire is connected to the terminal blocks on the multiplexer which is connected to the DAQ terminal block. The DAQ contains a built-in cold junction compensation. Prior to any test each point on the temperature grid is compared with a reference temperature at the grid using a hand held digital temperature meter.

5.1.3 Relative Humidity Measurement

Relative humidity measurements are required only to calculate the air density that is used to calculate the air velocity. As observed in chapter 3, the relative humidity has a negligible effect on the sensible effectiveness uncertainty. Nonetheless, accurate humidity transmitters were purchased for possible future testing that will account for latent effects including condensation. ASHRAE STD 84-1991 specifies that each of the four measuring stations requires either a wet bulb air temperature or relative humidity sensor. In a test facility that is used to study sensible effectiveness exclusively, the changes in absolute moisture content in the air stream in either the cold or hot air stream is negligible. In particular, on the cold air loop side where the air is heated, there is no addition of moisture across the heat exchanger, assuming that the cross contamination is insignificant, i.e. less than 0.1%. In view of this assumption rather than installing a humidity sensor at both the heat exchanger entering and leaving measuring stations, only one is installed at the leaving side. Once the relative humidity is established on the leaving side, then it can be extrapolated on the entering side from the psychometric process depicted in figure 5.3. On the hot air loop, a relative humidity sensor is installed on both the entering and leaving side of the heat exchanger. Future studies will involve an examination of frost effects in cross flow plate heat exchangers and thus will require accurate relative humidity measurements on both entering and leaving side. The present research will not include testing that involves frost formation on the heat exchanger. In total, 3 relative humidity sensors are used in the test facility. The location of the relative humidity sensor corresponds with the measurement stations at either the entering or leaving side of the heat exchanger.

There were two types of relative humidity transmitters used in the test facility. One type is used for temperatures below and the other for above freezing temperatures, i.e. 32 °F (0 °C). The temperature of the air entering on the hot loop is typically well above freezing conditions. The reason that these two types of relative humidity sensors were chosen was based on cost. The sensors for below freezing were typically double the cost for the regular sensors. In any case, both types of transmitters have manufacturer's specified accuracy of $\pm$ 2% RH. The transmitter

used for the below freezing application is a MAMAC model HU-224-2-VDC. The sensing element uses a bulk polymer capacitance technology. The manufacturer states that the hysteresis is less ± 1%. The accuracy of ± 2% RH is applied through 0 to 100 % RH, according to the manufacturer specification. The sensor is factory calibrated using NIST traceable standards. Both types of sensors were also calibrated in the laboratory. The rated temperature range for relative humidity measurements is from -30 °F (-35 °C) to 130 °F (55 °C). The temperature in the coldest section of the test facility is not expected to drop below –20 °F (-28 °C). The relative humidity sensor used for the above freezing application is a Viconics model H71 and has an accuracy of ± 2 %RH for 0 to 100 %RH. The sensor is specified to be used within a range of temperatures from 41 °F to 122 °F (5 °C to 50 °C). All sensors required 24 Volts ac power to generate its respective 0 to 10 Volts dc output signal. The 24 Volts ac is taken from the unit control panel that contained a transformer with 24 Volts ac on the secondary side.

The relative humidity sensors were calibrated using an Omega Relative Humidity Generator, model RHCL-1, and an Omega Relative Humidity Monitor, model RHB-2. The Relative Humidity Generator functions by pumping in ambient air and dividing the flow into two separate paths. The first path is a desiccant to remove the moisture from the air. The other path passes the air through a saturator to obtain 100% humidity. Next the two airstreams are rejoined in a specific controlled proportion in a mixing chamber to obtain the desired relative humidity. The air then passes into the captive or test chamber where the relative humidity sensor is installed. 800 ml of distilled water is used in the saturator chamber bath. An increment/decrement switch is used to control the generated relative humidity. Each time a new relative humidity level is set, the captive chamber requires at least 5 minutes to settle to its new equilibrium. The Relative Humidity Generator is used in conjunction with the Relative Humidity Monitor that uses an optical condensation hygrometry technology. This technology is extremely accurate and produces no hysteresis. The RHB-2 is calibrated against standards that are traceable to NIST. The specified accuracy is ± 0.5 to 40 %RH and ± 1.25 to 95 %RH. The dewpoint accuracy is ± 0.2 °C. The chilled mirror sensor consists of a metallic mirror surface cooled by a thermoelectric heat pump unit it reaches a temperature at which condensation forms.

The moisture on the mirror is optically detected by virtue of scattering losses. The mirror temperature is measured with a platinum resistance thermometer. The thermoelectric heat pump utilizes the Peletier effect whereby when a voltage is passed through two dissimilar electric semi-conductors a temperature differential is created. One of the conductors acts as the heat sink while the other acts as the heat rejecter. In comparison to a refrigeration system, the heat sink represents a cooling coil such as direct expansion; the heat rejecter represents the condenser; the voltage represents the power or compressor of the system. All three relative humidity sensors were calibrated.

5.1.4 Static Pressure Measurement

Static pressure is measured at all four measuring stations. The difference between the entering and leaving side static pressure represents the static pressure drop across the plate heat exchanger. Two methods for measuring the static pressure were compared. The first method is based on ASHRAE Std 84-1991, section 5.2.3.5, in which four taps are located on each interior side of the duct connected to a manifold. The taps are centered on the vertical sides and the horizontal sides of the ducts. A five-connection manifold can be used to connect the four connections and the output to the pressure transducer. The taps are smooth, free from surface irregularities, and flush with the interior surface of the duct. The diameter of the taps is 1/8 " (3.2 mm). A barb fitting is provided on the outside of the unit to connect plastic tubing. It is located in the approximately in the center of the measuring station. The tip is parallel with the direction of the airflow. Holes perpendicular to the airflow are provided on the side of the tip. Static pressure was measured using both methods for a variety of pressures, and a difference of less than 1% was observed. The static pressure tips were used instead of the 4-tap method for the reason of a simplified installation procedure. The plastic tube connecting from the static pressure tip to the pressure transducer consisted of ¼ " (6.4 mm) diameter. The distance from the furthest static pressure tip was approximately 15 ft (4.5 m). Each pressure transducer used for measuring static pressure consists of a Dywer model 668-5 that has a range of 0 to 5 inches w.c., 1.0 % accuracy full scale or ± 0.05 inches w.c.. The transducer has an output signal of 4 to 20 milliamps. The

specification indicates that the pressure transducers are factory calibrated. They are also calibrated in the laboratory using a Dwyer Microtector electronic Hook Gage Manometer.

5.1.5 Barometric Pressure

Barometric pressure is measured with a mercury column utilizing a vernier scale providing an accuracy of $\pm$ 0.01 inch of Hg. The barometric pressure was monitored at the beginning and the end of a test. The barometric pressure change during the period of a test was expected to be negligible.

5.2 Thermocouple Temperature Grid inside Plate Heat Exchanger

The literature review revealed only one paper on air-to-air plate type heat exchangers that incorporated an experimental study of the internal temperatures of the cores in a full-scale test. Bantle (1987) includes core temperature measurements in a counter-flow plate heat exchanger. He installed a total of 11 temperature sensors inside the core. Five of the sensors were used to study the core temperature distribution. However the sensors were installed after the heat exchanger was fabricated, and, therefore, the placement could only be near the exterior edges of the core. This prevented a more detailed study of the actual core temperature distribution.

Cross flow plate heat exchangers exhibit a 2-dimension non-uniform temperature distribution within the plates from the entering to the leaving edge. The cold corner phenomenon for cross flow plate heat exchangers is a direct result of this non-uniform temperature distribution. Figure 5.9 illustrates the approximate location of the cold corner inside a cross-flow plate heat exchanger. The size of the area in the cold corner containing the lowest temperatures inside the heat exchanger will

depend on the several variables listed as follows:

1. Temperatures entering the heat exchanger on supply and exhaust sides.
2. Supply and Exhaust airflow rate.
3. Reynold's number, and overall local heat transfer coefficient, U
4. Surface characteristics, such as raised dimples and ribbing

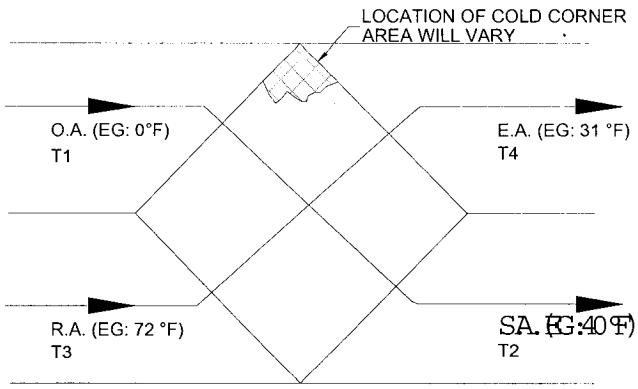

Figure 5.9 Location of cold corner in a cross-flow plate type heat exchanger

Cold corner is a concern particularly during frost conditions. This research will not cover the effects of frost on the thermal performance of the plate heat exchanger. However, the temperature distribution inside the channels will be recorded and analyzed under regular, non-frosting conditions on three distinct elevations inside the heat exchanger core. The three elevations correspond to the top, middle and bottom sections of the plate heat exchanger. The objective is to compare the temperature distribution between the three elevations and to observe any variation. At each elevation, a temperature grid is installed on both the cold and the hot air sides. Therefore a total of 6 temperature grids are installed in the heat exchanger. The top and bottom grids contain 3 rows and 3 columns, adding to a total of 9 points. The middle grid contains 4 rows, and 4 columns, adding to a total of 16 points. With respect to all the temperature grids inside the heat exchanger, a total of 68 thermocouple sensors are installed. The thermocouple temperature grids are installed at the fabrication stage of the plate heat exchanger. In the present research the bulk air temperature within the heat exchanger channel is measured as opposed to the aluminum core temperature.

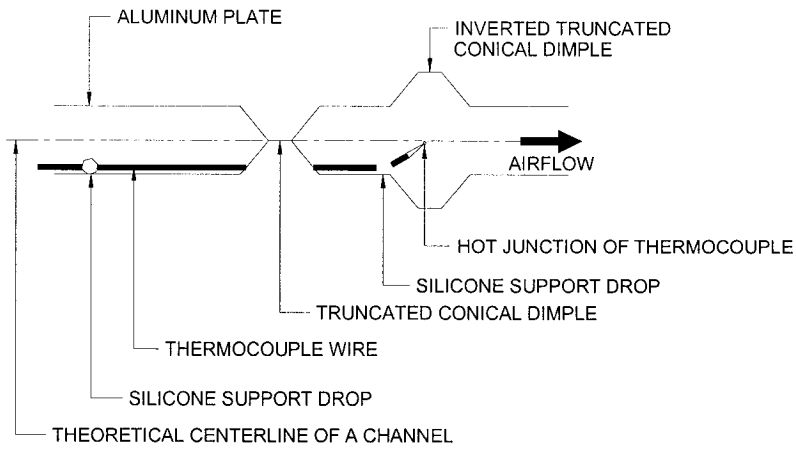

Figure 5.10 Ideal arrangement for hot junction of thermocouple between to heat exchanger plates

The hot junction of the thermocouple is installed so that it is suspended approximately in the middle of the upper and lower of the channel to sense the bulk air temperature. The hot junction is held in place with silicone just at the point where the wire exits from the thermocouple insulation to ensure that the tip does not touch the aluminum surface. Figure 5.10 illustrates the ideal arrangement of the hot junction of the thermocouple. If the thermocouple wire touches the aluminum surface, the aluminum acts as a second ground thus distorting the temperature. There is only one ground at the cold junction side of the thermocouple. One of the technical challenges was the choice of a non-intrusive method of fastening the thermocouple wire to the aluminum plate. The term non-intrusive refers to both disturbances to the airflow and to the heat transfer to the aluminum plate. The author decided to uses drops of silicone sealant to hold the thermocouple wire into place. The wire is first taped to the surface to hold it temporarily while the silicone drops hardened over a period of several hours. The thermocouple wire is installed parallel to the airflow direction. In order to reduce costs, the lengths of the thermocouple wire from each sensor point to the terminal blocks inside the unit are calculated. Figure 5.11 shows a picture of the bottom, middle and top elevation thermocouple grids being installed at the fabrication stage of the plate heat exchanger. Figure 5.12 shows the plate heat exchanger with the thermocouple wire installed in the test facility.

a)

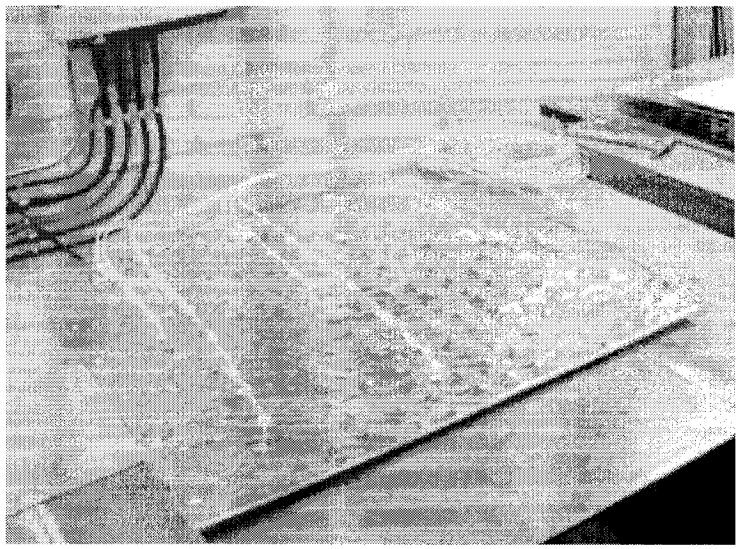

b)

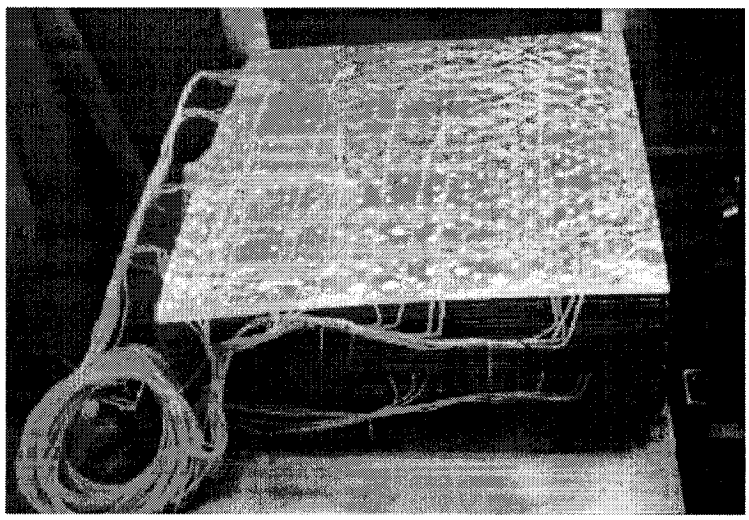

c)

Figure 5.11 Installation of thermocouple grids at the (a) bottom, (b) middle and (c) top elevation of plate heat exchanger

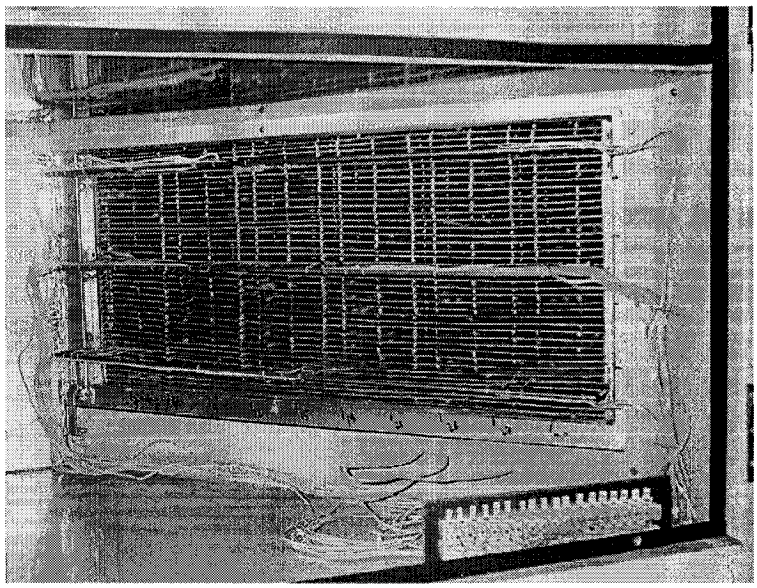

Figure 5.12 Plate heat exchanger containing the thermocouple grid installed in the test facility

Thermocouple connectors are used to extend the thermocouple wire from within the unit to the multiplexer terminal blocks outside of the unit. The large number of measurement points required a methodical tagging system. At the fabrication stage, as the thermocouple wire was installed, each wire at the edge of the core received a specific tag identifying its unique location. In light of the large number of measurement points to be collected, a comprehensive data acquisition system was developed to automate the data collection.

5.3 Data Acquisition System

The available data acquisition systems did not have the capacity to accommodate the 128 measurement points. The available National Instruments data acquisition has the potential to increase to the required number of points, but the cost to expand the system would run into the thousands of dollars. A decision was made to fabricate an external multiplexer system in-house at a minimal cost. The multiplexer will be discussed in detail in section 5.4.2. The software program Labview was used to develop a comprehensive data acquisition program that allowed the data collection to be automated.

5.3.1 Hardware

The existing National instrument data acquisition consists of four main components:

1. The terminal blocks for the connection of input and output signals to the signal conditioning modules.
2. The signal conditioning modules.
3. The main Chassis to contain and to power the signal conditioning modules. It also routes the conditioned signals to the data acquisition card.
4. The data acquisition card installed in the computer that acquires the conditioned signals and controls the signal conditioning modules.

The process of selecting a data acquisition requires a thorough knowledge of the type of signals produced from the sensors and the type of conditioning they may need. For example, thermocouples typically produce signals less than 50 mV and thus are subject to distortion from electrical noise, particularly in the range of 50 or 60 Hz picked up from power lines. Typically, a lowpass filter 2 or 4 Hz cutoff bandwidth is used to eliminate the electrical noise. Thermocouple signals may change only 7 to 40 μs for every 1 °C change. Therefore the low voltage signals need to be amplified to a level that improves the resolution and sensitivity from the analogue to digital conversion. The signal conditioning modules from National Instruments are called Signal Conditioning Extensions for Instrumentation or SCXI modules and include the following:

- A 32 channel Analogue input module that contains a sensor for cold junction compensation for the thermocouple measurements. This module is used exclusively for the thermocouples and pressure transducers. Cold junction compensation corrects for voltages that form at the connection of the thermocouple leads to the dissimilar metals of the measurement device. The model of the module is SCXI-1102. The corresponding terminal block used in conjunction with this model is SCXI-1300. This terminal block has no pre-wired ground reference, and therefore, each thermocouple connection is needed to be separately wired to a ground reference. The module can receive thermocouple signals, millivolt, and current amps. The low pass filter is fixed for each channel at 2 Hz. The maximum sampling rate is 333 Ks/s (3 μs per channel). This sampling rate far exceeds the desired range of sampling rates for this test facility.

- A 16 channel Analogue input module that internally multiplexes the signals from all the channels to a single isolated instrument amplifier and lowpass filter. The model of the module is SCXI-1122. The corresponding terminal block used in conjunction with this model is a SCXI-1320 that also contains an on-board temperature sensor for cold junction compensation. This module has a range of lowpass cutoff filter ranging from 4 hz to 4 Khz that can be set for the type of analogue signal. In addition, the module can be configured for a variety of amplifier gains depending on the range of the input signals. The gains range from 0.01 for ± 250 Vrms to 2000 for ± 2.5 mV. This module was used to receive the 0 to 10 Vdc signals from the relative humidity sensors. The module was configured for a 0.5 gain. The maximum sampling rate of this module is 100 Ks/s as a result of the multiplexing to a single amplifier and lowpass filter. Regardless, the maximum sampling rate is not required.
- A 6 independent and isolated channel analogue output module. This module is used to generate the 5-Volt digital inputs used to control the external multiplexer. The model of this module is a SCXI-1124, and the corresponding terminal block is SCXI-1325.

The SCXI modules are contained in a chassis that can accommodate a maximum of 12 modules. A total of 8 chassis could theoretical be daisy-chain connected amounting to a potential of 3072 measurement channels. The Chassis contains a SCXIbus that acts as a conduit for routing signals to the data acquisition card, transferring data, and passing timing signals. The data acquisition card used contains 12 bit resolution and can receive 16 single-ended analogue inputs. The model used is a PCI-MIO-16E-4.

5.3.2 External Multiplexer

The thermocouple sensors take up the largest portion of the measurement points. The total number of thermocouple points as per table 5.1 is 118. The static pressure and velocity pressure signals were used to fill in the remaining multiplexer channels. The total number of points that are multiplexed is 125. The multiplexer consists of terminal blocks, switching relays, isolating relays, and optoisolators all soldered to a circuit board. Each channel on the multiplexer board consists of 3 relays that switch between 4 terminal blocks. There are a total of 32 output

channels connecting to 128 input channels. Therefore there are 128 channels available. A digital 5 V signal is sent from the data acquisition to two main isolating relays. The signals from the data acquisition pass through optoisolator coupling relays that provide a ground break isolation between the multiplexer board and the data acquisition. The two main relays rout an external 5 Vdc source to the individual relays that control the switching between the 4 individual channels. The logic of the switching from a two-relay system to a three-relay system is depicted in table 5.2.

Table 5.2 Multiplexer Switching Logic

Two Isolating Relays	Three Switching Relays	Four Input Channels
0,0 (0 V, 0 V from daq)	0,0,0	1,0,0,0 (Channel 1)
0,1 (0 V, 5 V from daq)	0,0,1	0,1,0,0 (Channel 2)
1,0 (5 V, 0 V from daq)	1,0,0	0,0,1,0 (Channel 3)
1,1 (5 V, 5 V from daq)	1,1,0	0,0,0,1 (Channel 4)

Figure 5.13 illustrates the sequence of operation for the switching action of the multiplexer for the 4 channels.

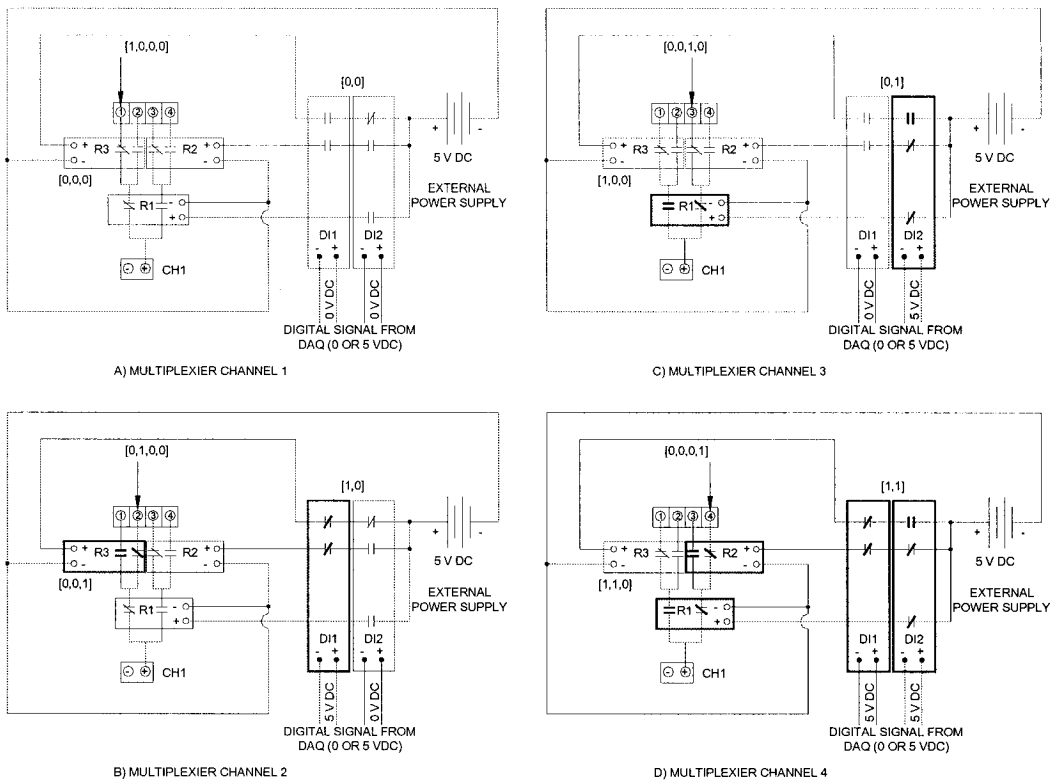

Figure 5.13 Multiplexer sequence of operation for switching logic

For each of the set of four input channels, a common terminal block is provided. Therefore, each of the four channels must have the same type of sensor connected to it. The first 17 sets of 4 channels are used for the type K thermocouples from the heat exchanger. The next 12 sets of 4 channels are used for the type T thermocouples at the measuring stations at the entrance and exit of the heat exchanger. The remaining sets of 4 channels are used for the type T thermocouple in the airflow stations and the pressure transducers. The entire set-up of the daq and instrumentation is schematically illustrated in figure 5.14

5.3.3 Data Acquisition Software

The software used to configure and program the data acquisition is Labview from National Instruments. Labview has a built-in program for configuring the SCXI modules. This program allows the user to add new modules to the list and to configure them accordingly. The configuration allows the user to set certain parameters such as the gain and the low-pass cut-off frequency for the whole module. None of the modules used permitted a channel by channel

adjustment of the gain and filtering options. Once the entire modules were added and configured, the individual channels on each module were configured. Each channel could be configured for the type and range of signal for the particular sensor. The Analogue Input modules, SCXI-1102 and SCXI-1124, allowed the choice of a specific thermocouple. In addition, the configuration allowed the choice of using a built-in or an external sensor for the cold junction compensation. In the present research, the built-in sensor was used. This temperature sensor was verified using an accurate hand-held digital temperature meter. The configuration also allowed the introduction of customized mathematical formulations for describing the relationship between the measured signal and the physical value. The configuration allowed for linear relationships only. Therefore only sensors that have linear responses throughout their full-scale ranges could be programmed into Labview. Labview has pre-programmed formulas for various thermocouples. The velocity pressure transducers produced a 4 to 20 mA signal that was transformed using a 500 Ω resistor to 2 to 10 Vdc signal. The full scale range of the velocity pressure transducer is from 0 to 0.5 inches w.c.. The generic equation used the following simple linear relationship:

$$Y = mx + b$$

$$m = slope = \frac{(0.5-0)in.\ w.c.}{(10-2)Vdc} = 0.0625\ \ in.\ w.c./Vdc$$

$x = 2$ to 10 Vdc and b can be solved when $x = 2$ Vdc since $Y = 0$ in. w.c.:

$0 = 0.0625 \times 2 + b \rightarrow b = -0.125$

The following formulation for velocity pressure is programmed into the particular channel.

$$Y = 0.0625x - 0.125\ in.\ w.c.$$

Formulations for static pressure and relative humidity were also developed and applied to the relevant channel. Each channel was uniquely tagged. In regard to the channels receiving 4 signals from the external multiplexer, the tag included the name of the four individual sensors. For example, the four thermocouple sensors TC10, TC28, TC400, TC51, the SCXI-1102 channel number 1 is tagged TC-10-28-400-51 in order to keep track of the large number of points. Once all the channels

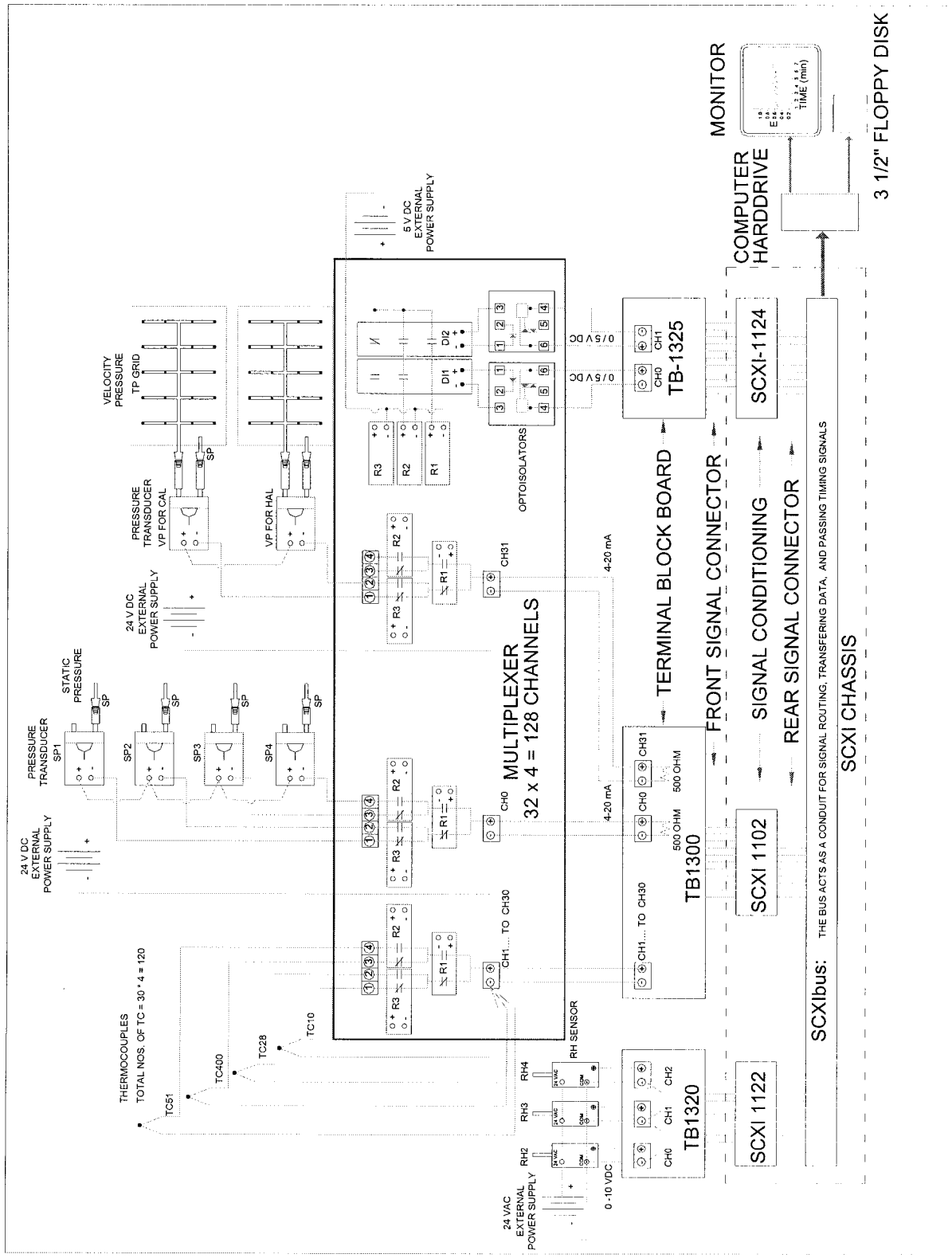

Figure 5.14 General schematic layout of instrumentation and data acquisition

had been configured and tagged, the next step involved developing the actual program to control the collection of data. Labview is a graphically based programming language. Graphical blocks in the program represent all the functions for data acquisition, timing, and logical operations. The blocks are dragged onto the programming page and connected to other relevant blocks. Each block contains a series of terminals that are virtually wired to other blocks. Labview contains graphical representations for If/then, For/Next, While/do, and a sequence structure. The For/Next structure was used to switch between the four channels on the multiplexer. The 0 V and 5 V digital output function was pasted in each of the four For/Next pages to control the switching. The sampling rate was determined from estimating the longest governing response time in the system. The system components that are considered as contributors to the overall response of the system include the sensors, data acquisition, external multiplexer, the time for air to complete one complete circuit inside the system, direct expansion coil, and the heater. The response time for anyone of the sensors was less than 1 second. The data acquisition alone could produce sampling rates much faster than the response time of any component. The multiplexer is limited by the time it takes for the relays to switch from "on" to "off' and vice versa. Prior to the measurement and data collection, the system is brought to a steady state. Thus the changes due to the direct expansion coil and heater are negligible. Initially when the scani-valve was used to route the signals for the velocity and static pressure, a considerable time delay in the system was discovered. Each time the scani-valve completes the fourth channel, a normally closed signal is sent to the scani-valve controller causing it to automatically return to the zero/home position. The time it takes for the scani-valve to return to its home position was roughly measured as 12 to 15 seconds, a long time in relation to transient changes in the system. In addition, it was discovered that as the scani-valve switched from one channel to the next, the same pressure transducer required several seconds to settle to the new signal. In particular, when either the cold or the hot air loop velocity pressure is significantly different, the time required for the transducer to settle to the new signal iss on the order of 15 to 20 seconds. Since this change occurred twice in one measurement period, i.e., switching from the cold to the hot and back to the cold air loop airflow station, the sampling period required a minimum of double the settling time. The sampling time

was set at a minimum of 40 seconds. This sampling period is acceptable in the case of a steady state analysis. However, in the case of future work involving the study of frost control mechanism, the system will require a transient analysis, and the sampling period needs to be less than half the smallest change in the system according to the Nyquist theorem. Once individual pressure transducers replaced the scani-valve, the sampling period was reduced to 4 seconds. This time period is limited to the switching of the external multiplexer relays. In other words, all 129 data points can be collected within a 4 second period. In reference to other research on heat recovery devices, the sampling period in some cases is on the scale of minutes.

6.0 THERMAL PERFORMANCE TESTING AND TEMPERATURE DISTRIBUTIONS

Several types of experiments on the cross flow plate type heat exchanger have been achieved utilizing the newly developed heat recovery test facility. Each test is preceded by a thorough check of all the measurement points using the Labview's channel viewer program in conjunction with the data acquisition. This program lists all of the configured channels and allows each point to be checked for sensor error. The multiplexer is manually incremented using the channel viewer program for each of the 4 channels as described in section 5.3.2. Once all the points are verified the variable frequency drives for both the supply and exhaust fan motors are adjusted to the desired air flow rates. The airflow rates could be monitored on the computer display. The direct expansion cooling coil is operated prior to any heating coils in order to allow the air temperature in the cold air loop to descend below the desired value entering the plate heat exchanger. Next, the heater in the hot air loop is energized. The setpoint of the temperature controller is adjusted to the desired value. The cold air loop heater located downstream from the direct expansion cooling coil is energized, if necessary, to provide more refined control of the air temperature. Occasionally the airflow rates require further adjustment as the temperature changes within the loops. The system is allowed to run until a steady-state condition is achieved. In reality, 100% steady state is impossible to obtain. An acceptable amount of sensor fluctuation is tolerated. Steady state conditions refers to maintaining the airflow rates of both the cold and hot air loops and the temperatures entering and exiting the heat exchanger within a certain $\pm$ range. The pre-test uncertainty analysis revealed in chapter 3.0 that airflow rates and airflow rate uncertainties significantly influence effectiveness uncertainty. In the case of the airflow rates, a $\pm$ 1.5 % of the desired airflow rate was deemed acceptable. As an example, if the target airflow rate is 1500 CFM (708 L/s), then the level of acceptable fluctuation is not to exceed 1500x($\pm$ 0.015) = $\pm$ 22.5 CFM ($\pm$ 10.6 L/s). Typically the fluctuations become more pronounced for higher airflow rates due to possible turbulence effects at the airflow measuring station. The acceptable level of fluctuation for air temperature is set at $\pm$ 5.0 %, since the resulting temperature displayed on the monitor represents an average temperature of 12 points. The

fluctuation of the individual thermocouple points is usually less than $\pm 1\%$ of the reading. Following each test the resulting data is statistically checked to verify that the test was conducted under the defined steady state conditions. The precision part of the 95% uncertainty bounds will reflect whether or not significant fluctuations occurred during measurement. A post test uncertainty analysis will be presented in section 6.6. Due to the enormous amount of data collected during one test, a visual basic program in Microsoft Excel was developed to sort and process the data. This program is elucidated in section 6.1.

The first type of tests on the plate heat exchanger involved evaluating the average sensible effectiveness for a range of airflow rates and temperature differences between $T1_{ave}$ and $T3_{ave}$. These effectiveness curves will be presented in section 6.2. The purpose of the next set of tests involved revealing the sensible effectiveness of the heat exchanger under unbalanced airflow conditions. The single graph that was generated in section 6.3 illustrates the effect of varying the ratio of Q_{cal}/Q_{hal} from 0.5 to 2.0.

Often in real air handling units, the various components such as filters or coils are contained in a very compact space that causes an abrupt transition upstream or downstream from the plate heat exchanger. A series of tests is performed to evaluate the effect of symmetric and asymmetric blank off plates located on the air entering side of the heat exchanger. The methods for testing and results are presented in section 6.4.

In all heat recovery tests, the distribution of temperature within the heat exchanger core is measured and graphically displayed to allow comparison and analysis. Section 6.5 deals with the temperature distributions.

6.1 Data Processing

In this section, the flow of data will be traced from the measurement point to the final graphical figure. The total number of data points collected in one sample period as defined in chapter 5 is 129. These include air temperature, air temperatures within the heat exchanger, relative humidity measurements, velocity pressures. During the data acquisition, four separate files are used to store the data of the 129 points. The reason that four files are created is

because of the nature of the data acquisition program in conjunction with the switching between four channels on the multiplexer. The average length of the tests is approximately 20 minutes. This time period is deemed long enough to provide a large sample population of data, n>>30 points. The data acquisition sampling rate is set at one sample of 129 points every 10 seconds. Governed by the relay switching on the multiplexer, the approximate time to collect the 129 points through the four channels is approximately 4 seconds. The total number of sample periods in 20 minutes is 20 min x 60 s/10 s = 120. Therefore the total number of data points in one test is 120 sample periods x 129 samples/sample periods = 15, 480. The largest portion of the data is the thermocouple temperature measurements within the plate heat exchanger. The data flow from point of measurement to the data file is illustrated in figure 6.1. The data is automatically sent from the four channels to a Microsoft Excel™ file. The four separate files are then manually amalgamated into a single data file. The time that would be required to manually sort the enormous amount of data into a desired format and perform calculations would be unacceptably long. It was necessary to develop a program to sort the data and perform calculations automatically. The program was developed using visual basic in Microsoft Excel™ and is listed in Appendix C. The post-test flow of data is illustrated in figure 6.2. The amalgamated data file contains four separate sheets for the raw data from the original four channels. Another sheet contains the general summary of the data, excluding the temperature distributions which are on a separate sheet. The visual basic program performs calculations for sensible effectiveness, and the statistical treatment of the results including 95% and 99% uncertainties. This information is summarized on another sheet for the result summary. The largest portion of the raw data originated from the thermocouple temperature measurements from the grid inside the plate heat exchanger. As discussed in section 5.2, there are a total of 6 temperature grids within the heat exchanger. The data processing task was to extract the data from the four raw data sheets and format it in a rectangular table that reflects the orientation of the actual grid. The grids in the top and bottom section of the heat exchanger contain 9 data points, and the middle grid contains 16 data points. The temperature grid tables are used to develop temperature distribution surface charts.

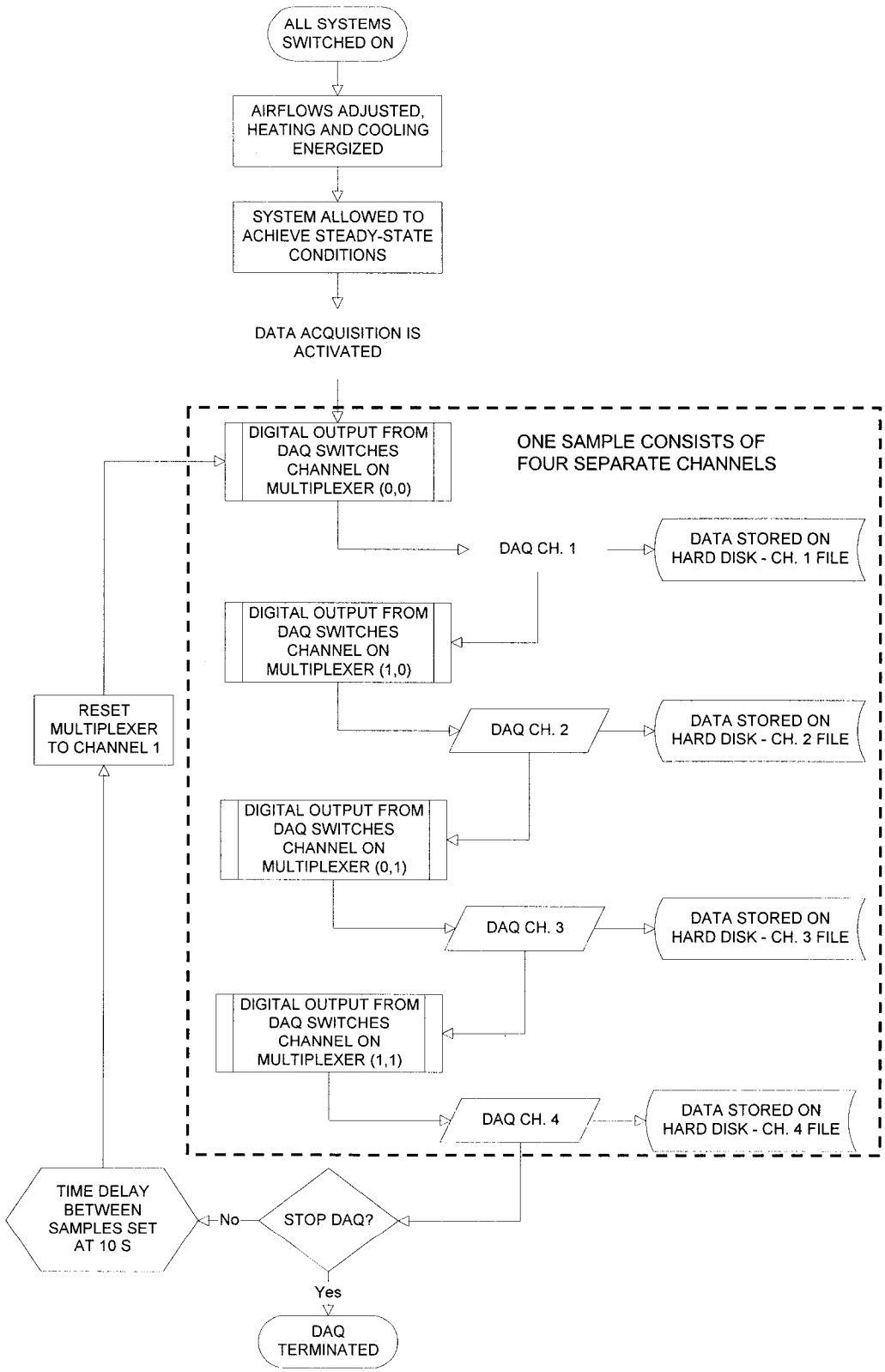

Figure 6.1 Flow of data during testing

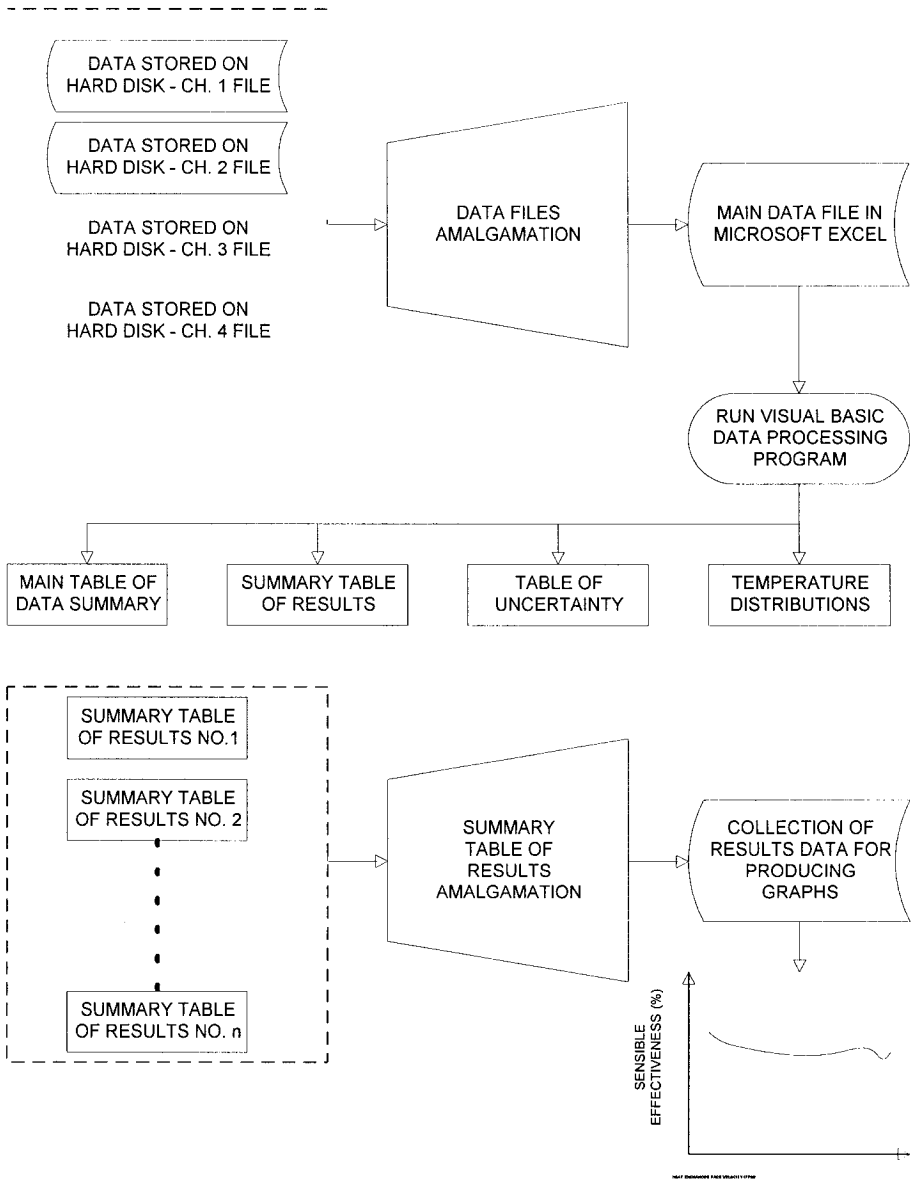

Figure 6.2 Post-test data processing

6.2 Sensible Effectiveness for Balanced Airflows

The first series of tests involved evaluating the sensible effectiveness of the heat exchanger for balanced airflows, i.e., $Q_{cal}/Q_{hal} \approx 1.0$. Since the two air loops are independent with separate fans, it was difficult to obtain 100% balanced airflows. However it was possible to maintain not more than 1.5 % difference between the hot and cold loop airflows. Typically, the largest difference occurred for either the smallest or largest airflow rates. In most tests the two airflows did not vary more than 0.5 %. The tests were carried out for a range of airflow rates and temperature difference between $T1_{ave}$ and $T3_{ave}$. These two temperatures are located at the entrance of the heat exchanger on the cold and hot air loop sides respectively. $T3_{ave}$ did not vary significantly, whereas $T1_{ave}$ was varied from 10 °F (-12 °C) to 40 °F (4.4 °C) at increments of 10 °F (-12 °C). The airflow rate range is 750 CFM (354 L/s) to 1850 CFM (873 L/s) at approximately 50 CFM (23.6 L/S) increments. The average sensible effectiveness is calculated in all tests since it produces the lowest uncertainty according to the pre-test uncertainty analysis in chapter 3.

Test proceedure:

Commencement of test-

1. The cold air loop fan is energized.
2. The data acquisition is activated and the program initiated.
3. The cold loop airflow is verified from the computer monitor. The variable frequency drive is adjusted to obtain the correct airflow.
4. The compressor is energized. All four solenoids are switched on. Full cooling is engaged.
5. The cold loop is allowed to run without the hot loop to allow the air in the cold loop to drop more rapidly to the desired temperature entering the heat exchanger.
6. The hot air loop fans are energized. The variable frequency drive is adjusted to obtain the desired airflow rate within ± 1.5% of the cold air loop airflow.
7. The electric heater on the hot air loop is energized. The setpoint on the temperature controller is set to the desired temperature.
8. The airflows for both loops are checked and final adjustments are made on their respective variable frequency drives.
9. The system is allowed to run until a steady state condition is achieved.
10. The data collection program is started. The four files are given specific names.

11. The test is allowed to run for a minimum of twenty minutes.

12. During the test, the values of airflow, temperature, and sensible effectiveness are monitored in real time to ensure no anomalies during the test.

13. The test is terminated once the data acquisition is halted.

(a)

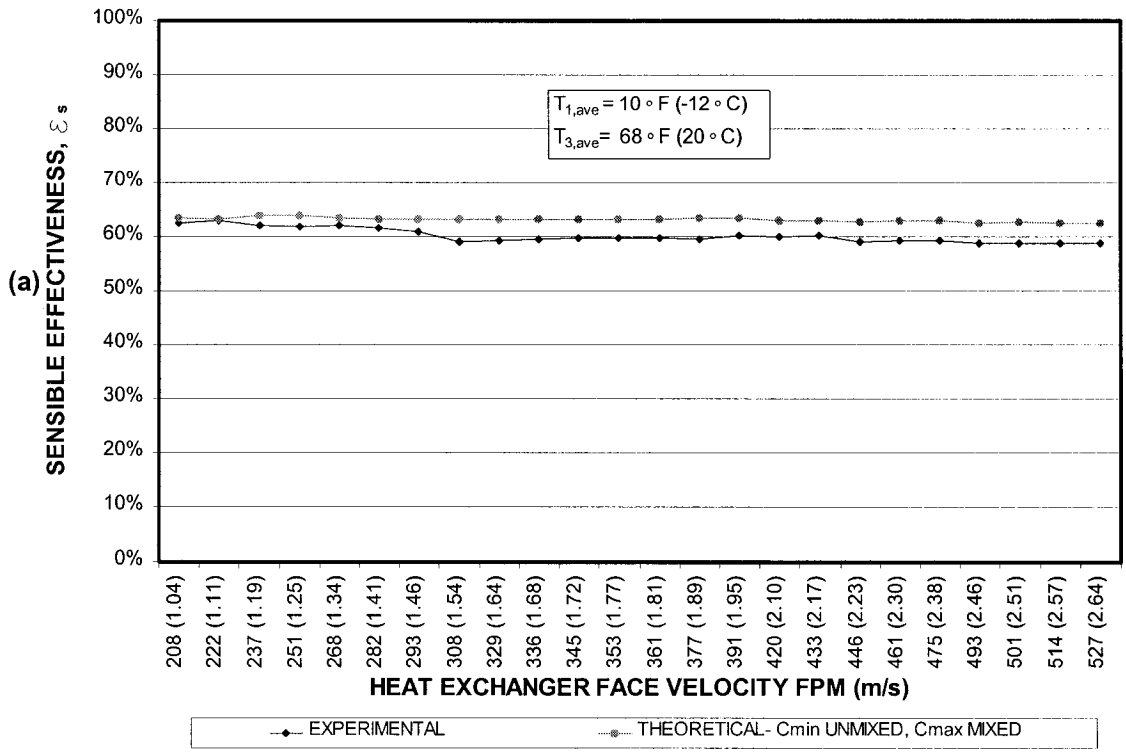

(b)

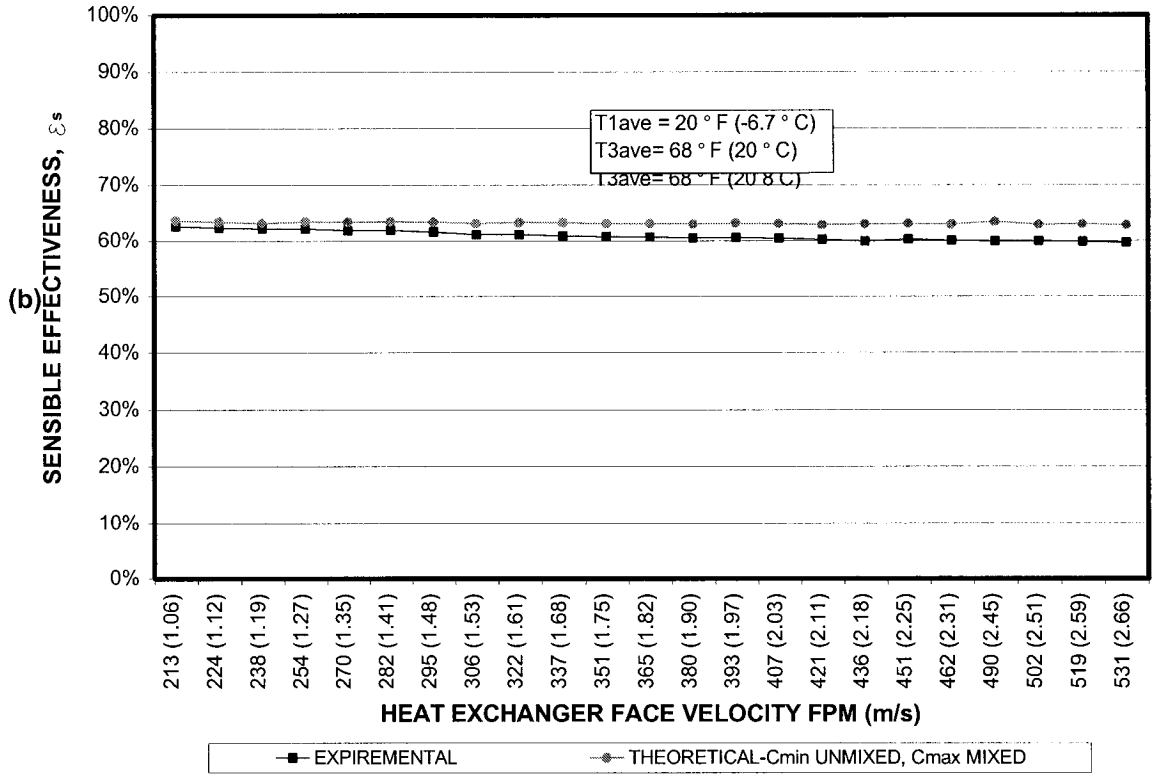
100%
90%
80%
70%
60%
50%
40%
30%
20%
10%
0%
SENSIBLE EFFECTIVENESS, ε_s
T1ave = 20 ° F (-6.7 ° C)
T3ave= 68 ° F (20 ° C)
213 (1.06)
224 (1.12)
238 (1.19)
254 (1.27)
270 (1.35)
282 (1.41)
295 (1.48)
306 (1.53)
322 (1.61)
337 (1.68)
351 (1.75)
365 (1.82)
380 (1.90)
393 (1.97)
407 (2.03)
421 (2.11)
436 (2.18)
451 (2.25)
462 (2.31)
490 (2.45)
502 (2.51)
519 (2.59)
531 (2.66)
HEAT EXCHANGER FACE VELOCITY FPM (m/s)
EXPIREMENTAL
THEORETICAL-Cmin UNMIXED, Cmax MIXED

(c)

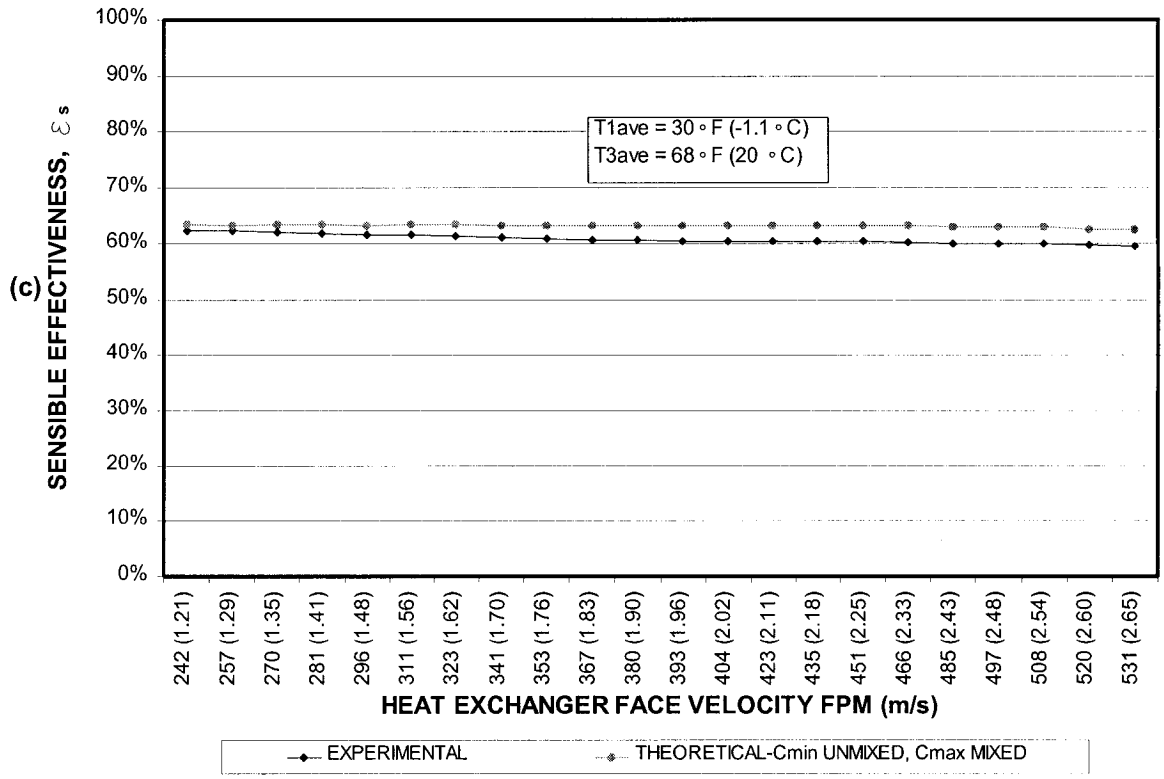
100%
90%
80%
70%
60%
50%
40%
30%
20%
10%
0%
SENSIBLE EFFECTIVENESS, ε_s
T1ave = 30 ◦ F (-1.1 ◦ C)
T3ave = 68 ◦ F (20 ◦ C)
242 (1.21)
257 (1.29)
270 (1.35)
281 (1.41)
296 (1.48)
311 (1.56)
323 (1.62)
341 (1.70)
353 (1.76)
367 (1.83)
380 (1.90)
393 (1.96)
404 (2.02)
423 (2.11)
435 (2.18)
451 (2.25)
466 (2.33)
485 (2.43)
497 (2.48)
508 (2.54)
520 (2.60)
531 (2.65)
HEAT EXCHANGER FACE VELOCITY FPM (m/s)
EXPERIMENTAL
THEORETICAL-Cmin UNMIXED, Cmax MIXED

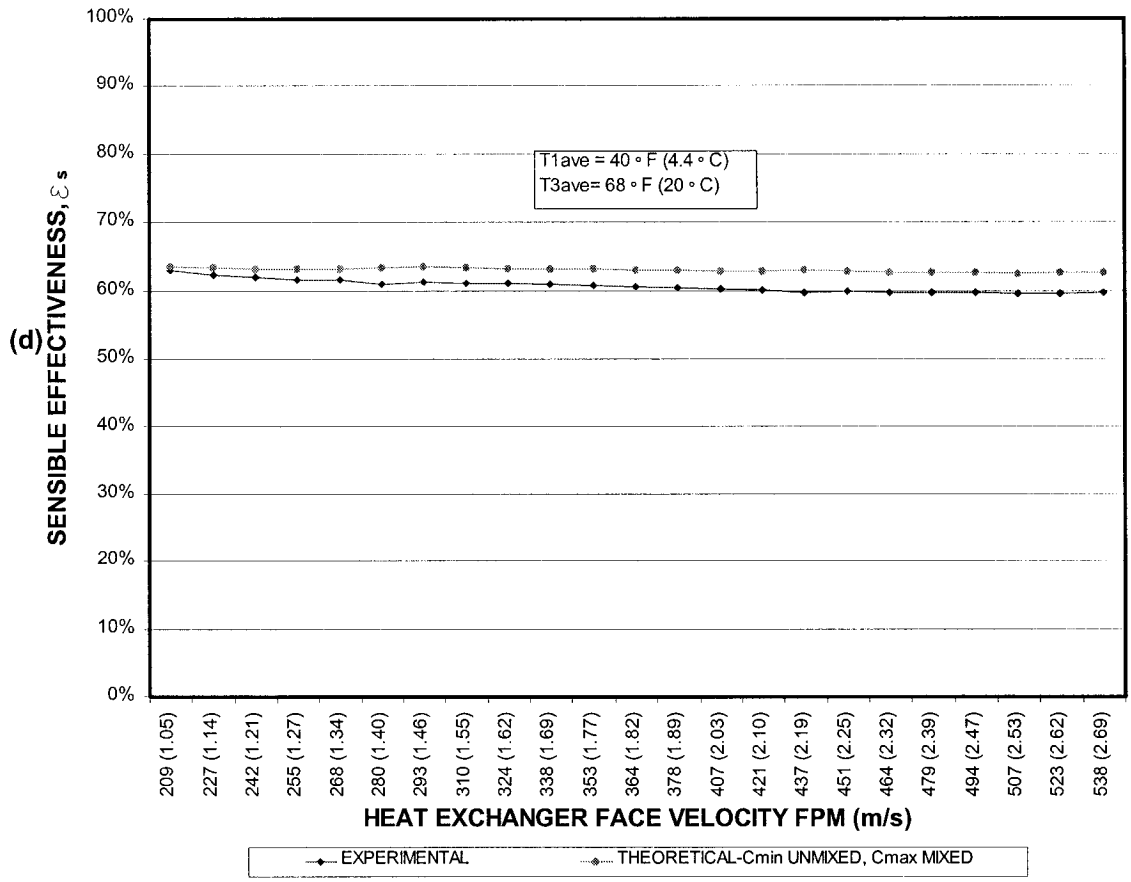

Figure 6.3 Average sensible effectiveness (experimental and theoretical) versus heat exchanger face velocity for (a) T_{1ave} = 10 °F (–12.2 °C), (b) T_{1ave} = 20 °F (-6.7 °C), (c) T_{1ave} = 30 °F (-1.1 °C), (d) T_{1ave} = 40 °F (4.4 °C)

Figure 6.3 presents both the experimental and the theoretical average sensible effectiveness for different heat exchanger face velocities ranging from 205 fpm (1.03 m/s) to approximately 538 fpm (2.69 m/s) for four different $T1_{ave}$. The measured airflows along with the surface area of the heat exchanger are used to calculate the NTU and theoretical sensible effectiveness, $\varepsilon_{s,th}$. For the given heat exchanger the face velocity range corresponds to a range of NTU from approximately 3.8 to 9.6, and a range of Reynold's number from 1381 to 3365. The experimental variation of ε_s for all of the above graphs does not vary more than 63.1% to 58.7% for the entire range of heat exchanger face velocities. This represents a percentage difference of 7.2% between the highest and lowest ε_s. The theoretical formulation for cross flow heat exchanger that best matches the experimental results is the case in which one airflow is mixed and the other

airflow is unmixed. This corresponds to either equation 2.15 or 2.16. The largest theoretical variation for the entire range of face velocities for all tests is 5.4% percent difference from lowest to highest $\varepsilon_{s,th}$. The theoretical curve appears to be converging to its asymptotic value as predicted previous illustrated in figure 2.4. There is good agreement between theoretical and experimental sensible effectiveness. The experimental sensible effectiveness does not vary more than a maximum of 6% of the theoretical sensible effectiveness at the highest face velocities. The decrease in experimental sensible effectiveness for the higher face velocities may be the result of greater airflow non-uniformity and increased measurement precision uncertainty, predominantly with airflow. It appears that the variation of temperature difference between $T1_{ave}$ and $T3_{ave}$ does not affect the sensible effectiveness for the range of airflows considered.

6.3 Sensible Effectiveness for Unbalanced Airflows

In most cases the supply and exhaust airflows passing through an air-to-air heat exchanger are not equal. The reason for the unbalanced airflow is usually related to maintaining the interior of building under either negative or positive pressure. The sensible effectiveness for unbalanced airflows will depend upon the ratio of the heat capacities of the two air streams, C_{min}/C_{max} , the heat exchanger surface area, and NTU. The tests conducted involved maintaining the hot air loop airflow constant at approximately 1500 CFM (708 L/s) and varying the cold air loop from 750 CFM (354 L/s) to 3000 CFM 1416 (L/s). This corresponds to a ratio of Q_{cal}/Q_{hal} from 0.5 to 2.0. The base case for this test is a ratio of Q_{cal}/Q_{hal}=1.0. As seen in the tests for the balanced airflow, the average sensible effectiveness hovers around 0.6. This will be the expected minimum value of a parabolic curve for the unbalanced airflow. Figure 6.4 presents both the experimental and predicted curves for the sensible effectiveness subjected to unbalanced airflow. The maximum sensible effectiveness occurs at both extremes, Q_{cal}/Q_{hal}=0.5 and Q_{cal}/Q_{hal}=2.0, ε_s= 0.769 and ε_s= 0.784 respectively.

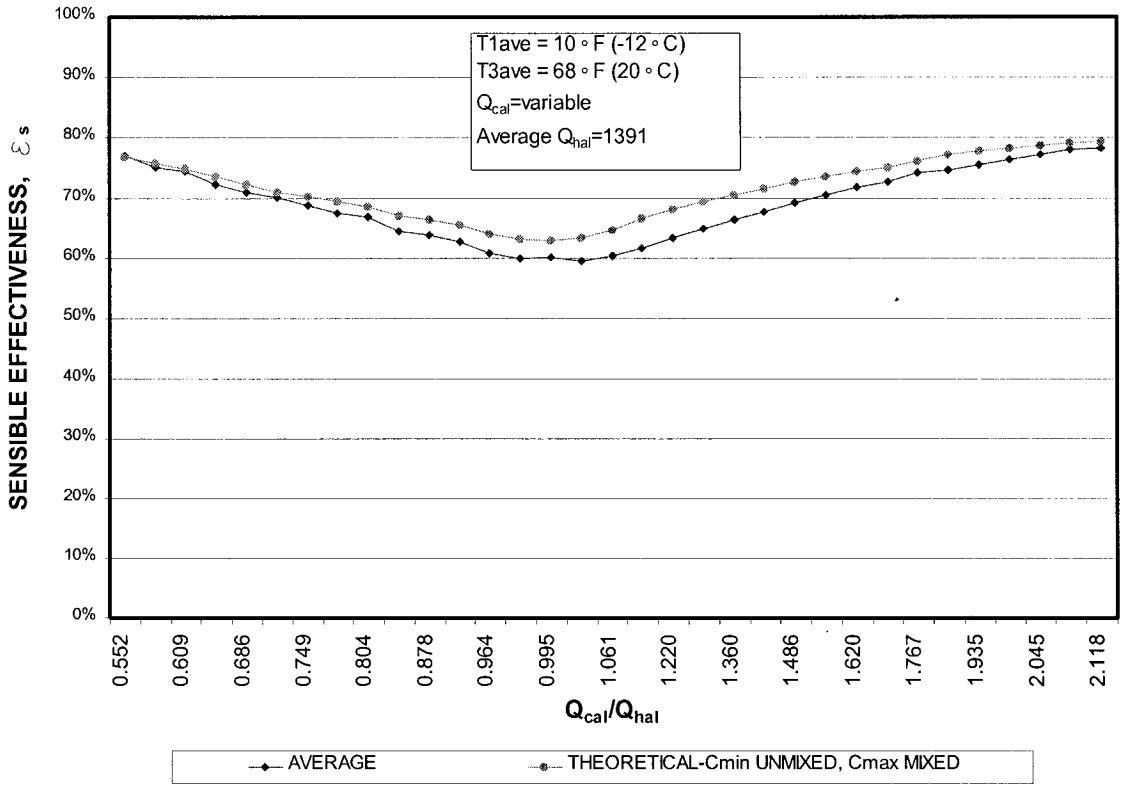

Figure 6.4 Average sensible effectiveness (experimental and theoretical) versus ratio of Q_{cal}/Q_{hal}

6.4 The Effect of Obstructions on Sensible Effectiveness

Plate heat exchangers are often installed downstream from components that contain smaller cross sectional areas. These components may, in some cases, obstruct and cause an uneven airflow at the entrance of the heat exchanger. The effects of uneven airflow on thermal performance are rarely considered in the design of packaged energy recovery units. Filters, fans, coils, and duct openings are often located in very close proximity to the entrance or exit of the heat exchanger. The blank-off walls supporting these components can be considered as obstructions to the airflow through the heat exchanger. It is within this context that a series of tests were conceived to study the effect of obstructions on the sensible effectiveness of a cross flow plate heat exchanger. The obstructions consist of pieces of rigid board insulation that completely block a vertical section of the heat exchanger on the entrance side. The obstructions

were placed on both the cold loop and the hot loop entering side of the plate heat exchanger. Figure 6.5 illustrates an example of a 24" (610 mm) obstruction located on the cold loop side near the exterior wall. Asymmetric and symmetric obstruction configurations were used. The asymmetric obstructions are located in four locations within the heat recovery unit: near the exterior wall on the cold air loop side; near the center wall on the cold air loop side; near the exterior wall on the hot air loop side; and near the center wall on the hot air loops side. In the case of the asymmetric obstructions, three sizes were used across the heat exchanger: 8" (203 mm), 16" (406 mm) and 24" (610 mm).

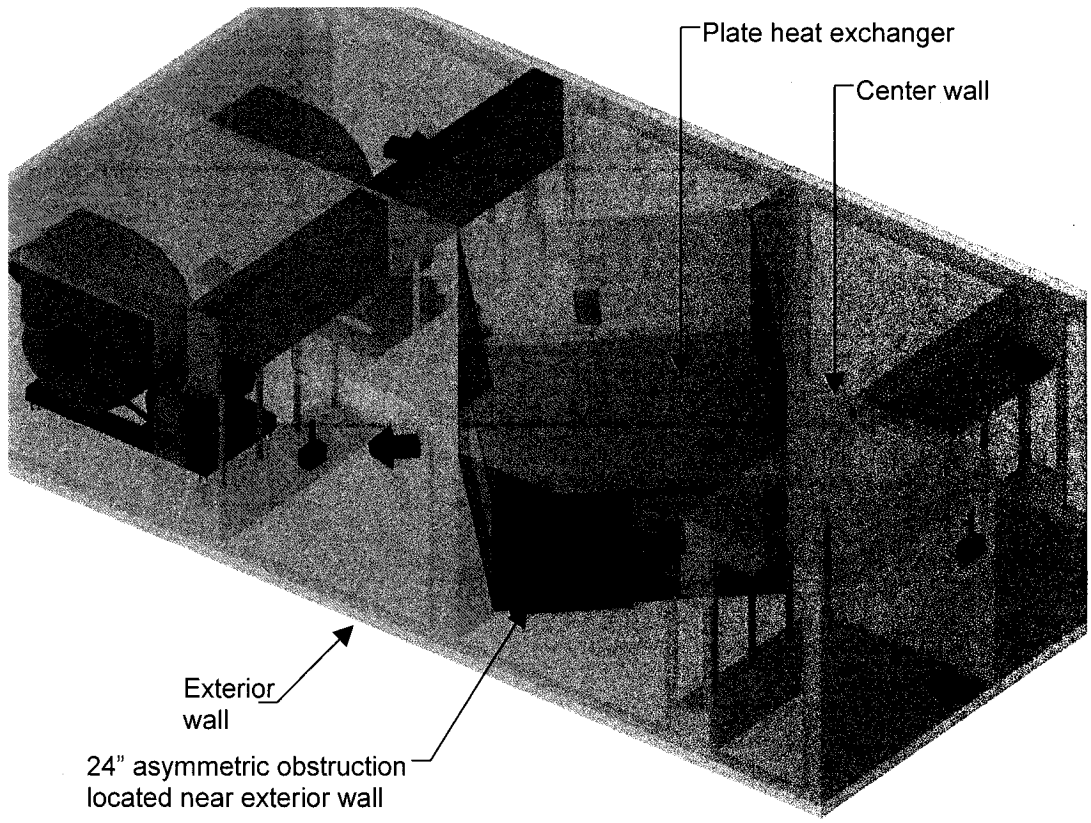

Figure 6.5 Example of 24" (610 mm) obstruction located on cold loop side near exterior wall

The overall heat exchanger width opening is 33 1/8" (841 mm). Therefore, the largest of the asymmetric obstructions represents a blockage of 72.4% of the open area. The symmetric obstructions consisted of two pieces of identical size rigid board insulation placed at both sides of

the plate heat exchanger opening, thus forcing the air through the center. In the final test, symmetrical obstructions are placed on both the cold loop and hot loop side simultaneously. The test with the largest area blocked consists of a quantity of two 14" (356 mm) wide vertical obstructions, totaling 28" (711 mm) out of the width of 33 1/8" (841 mm). This represents a blockage of 84.5% of the open area. The seams between the obstruction boards and the unit wall or adjacent boards were covered with aluminum duct tape to ensure a leak-tight obstruction. The tests were conducted at two different airflow rates, 1870 CFM (882 L/s) and 1500 CFM (708 L/s). Both $T1_{ave}$ and $T3_{ave}$ were held relatively constant for all tests. Figure 6.6-6.8 presents bar charts of the sensible effectiveness for both airflow rates and for all cases of obstructions. In an overview of all the obstruction tests, it can be observed that the sensible effectiveness does not decrease significantly below the base case for zero obstruction.

Asymmetric Obstructions:

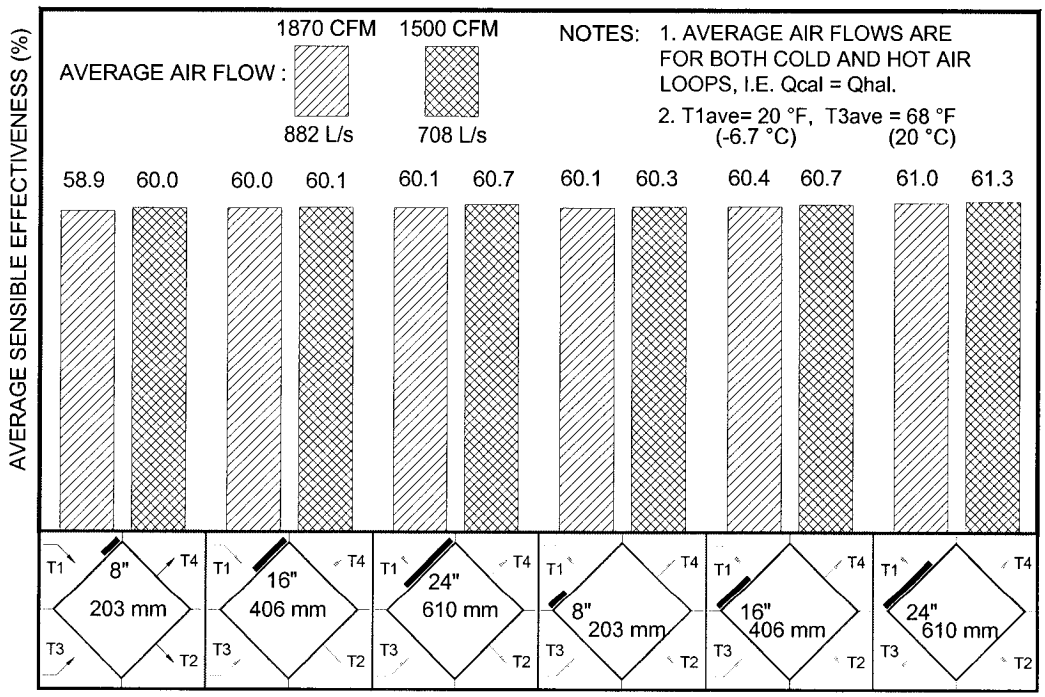

SINGLE ASYMMETRIC BLANK-OFF LOCATED ON COLD AIR ENTERING HEAT EXCHANGER

Figure 6.6 Sensible effectiveness for single asymmetric blank-off located on the cold air entering side of the heat exchanger

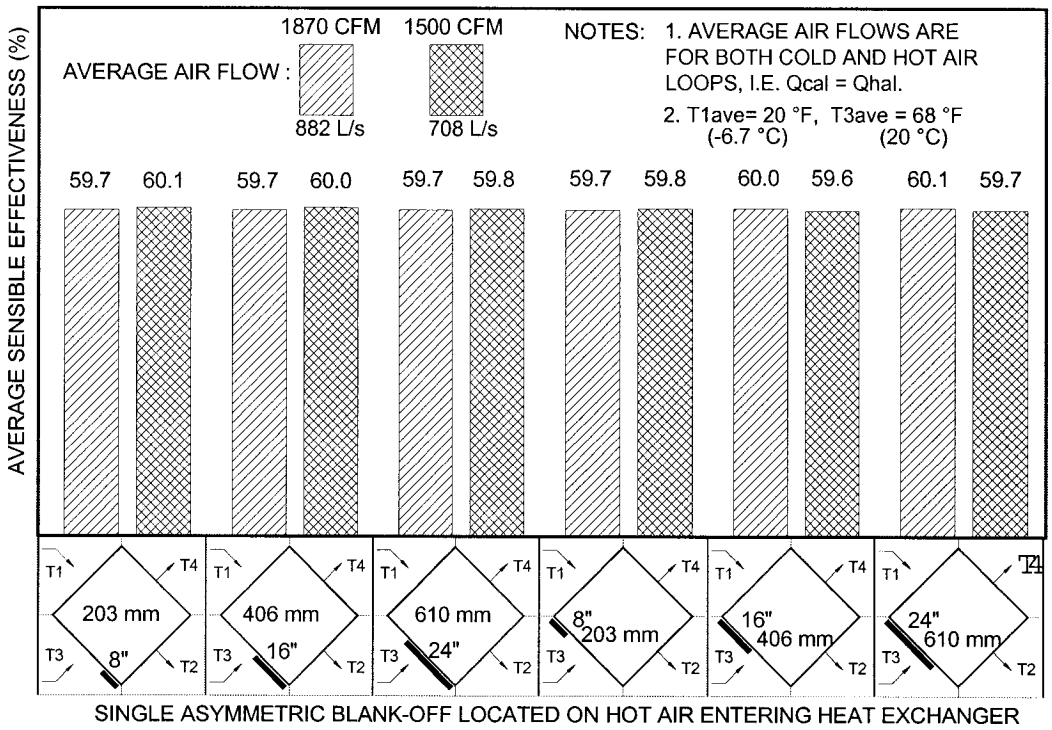

Figure 6.7 Average sensible effectiveness for single asymmetric blank-off plates located on the hot air entering side of the heat exchanger

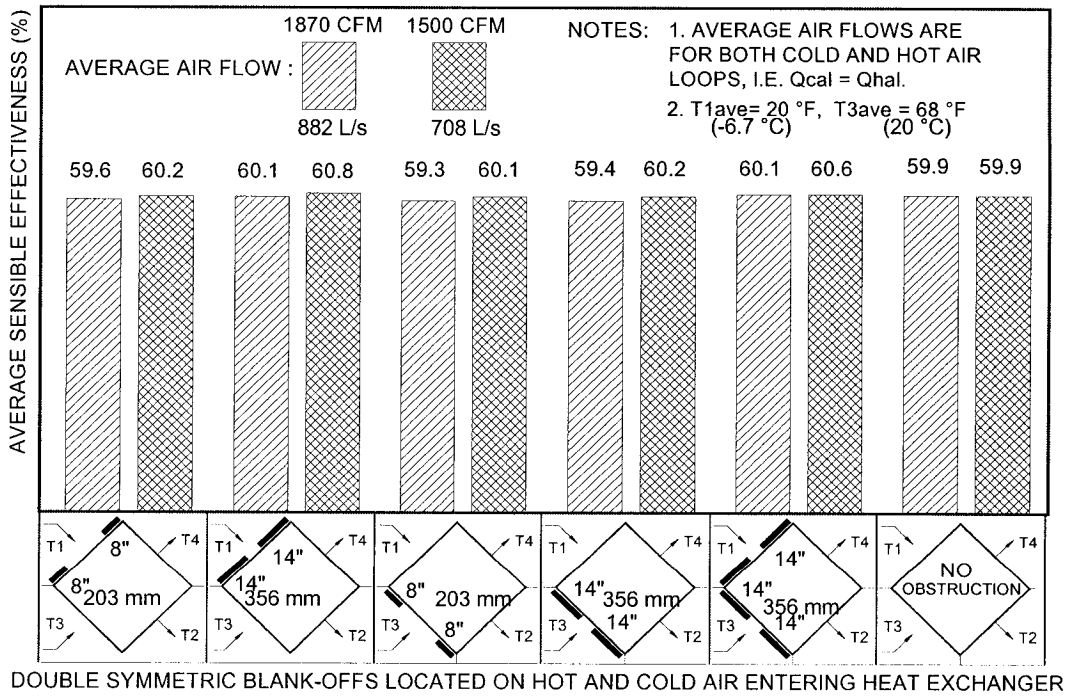

Figure 6.8 Average sensible effectiveness for double symmetric blank-off plates located on both the cold air and the hot air entering side of the heat exchanger

Moreover, as the size of the obstruction area increases, in some tests the sensible effectiveness unexpectedly increases. The largest increase over the base case is marginal, but the fact that the sensible effectiveness appears to increase is an unexpected result. As a further observation of all the obstruction tests, as expected the sensible effectiveness is slightly higher for the lower airflow rate of 1500 CFM (708 L/s). The cold loop and hot loop airflow rates were maintained within 0.5% of each other. In reference to figure 6.6 for the asymmetric obstructions located on the cold loop entering side of the heat exchanger for 1500 CFM (708 L/s), the largest increase in sensible effectiveness is from zero obstruction ($\varepsilon_s = 59.9\ \%$) to the 24" (610 mm) obstruction on the side of the center wall ($\varepsilon_s = 61.3\ \%$). The base case of zero obstruction is the last bar chart located in figure 6.8. For all the asymmetric obstructions, the largest increase of sensible effectiveness for both airflow rates is associated with the 24" (610 mm) obstruction located nearest the center wall on the cold loop side. This result could be written off simply as an experimental error or an anomaly, but the fact that it consistently occurs for both airflow rates does add credibility to the result and warrants further study. At this stage the exact reasons for this result are not clear. One possible reason is that this obstruction configuration causes an increased overall heat transfer coefficient as the result of the increase in air velocity at the entrance of the cold loop. Another possible explanation can be based on the results of the paper by that demonstrates through a numerical mathematical model, the principal heat transfer zone within a cross flow plate heat exchanger is concentrated through a diagonal zone. There appears to be less variation between the sensible effectiveness for the asymmetric obstructions on the hot air loop side than on the cold air loop side. For 1500 CFM (708 L/s), ε_s varies between 59.6% to 60.1%, only 0.5% difference. For 1870 CFM (882 L/s), ε_s varies between 59.7% to 60.1%, only 0.4% difference. In comparison with the cold loop, for 1500 CFM (708 L/s), ε_s varies between 60.0 % to 61.3%, 1.3 % difference. For 1870 CFM (882 (L/s), ε_s varies between 59.8% to 61.0 %, 2.1 % difference. This small difference is less than the 95% uncertainty levels, as that will be presented in section 6.6. The sensible effectiveness for asymmetric obstructions on the cold loop side is slightly higher than on the hot loop side. When comparing, for example, the 16" (406 mm) obstruction nearest the exterior wall for both the hot and cold loop sides, the cold loop side ε_s is

0.1% higher for 1500 CFM (708 L/s) and 0.7% higher for 1870 CFM (882 L/s). The obstructions on the cold loop side appear to have a greater influence on the sensible effectiveness. However, the differences are slight.

Symmetric Obstructions:

The double 8" (203 mm) obstructions located either on the cold loop or hot loop side has almost negligible effect on the sensible effectiveness compared to the base case as shown in figure 6.7. The largest difference occurs for the double 14" (356 mm) obstructions located on the cold loop side. This result reflects the effect seen in figure 6.6 with the 24" (610 mm) obstruction located on the cold loop side. The most remarkable result is in reference to the double 14" (356 mm) obstructions located on both the cold and the hot air loop sides simultaneously. These obstructions represent 84.5% blockage of the open area heat exchanger on both sides, and yet the sensible effectiveness is higher by 0.7% for 1500 CFM (708 L/s) and 0.2% for 1870 CFM (882 L/s). The increase in air velocity at the entrance of the heat exchanger and the resulting increase in the heat transfer coefficient may partially explain this effect. A thorough analysis of the dynamics of this effect is beyond the scope of the present work and requires more detailed analytical and experimental study.

6.5 Temperature Distribution within the Heat Exchanger

In all tests, the data for the temperature distribution within the heat exchanger was collected, processed and formatted. The visual basic program used for post-test data processing as depicted in the flow chart in figure 6.2 contains a subroutine that is used to organize the heat exchanger temperature measurements in a grid representing the actual layout of sensors. The subroutine works by extracting individual temperature measurements from a specific channel located on the corresponding spreadsheet and inserting it on a separate Microsoft Excel™ spreadsheet in a cell location that represents the physical location inside the heat exchanger. Once the program completes its execution, temperature distributions for the top, middle, and bottom grids on both the cold and the hot loop side is provided for the number of samples for a

particular test. If a test contains 120 samples, then there will be 6 temperature grids times 120, i.e., 720 grids. Since the tests were performed under steady state conditions, the grids will be very similar, and it is necessary only to choose one sample of 6 grids and erase the remaining to save computer memory. The raw data temperature grids can be analyzed by themselves but, in order to understand the distribution more clearly and for presentation purposes, temperature contour maps containing iso-temperatures ranges are created in Microsoft Excel™. Five ranges of temperatures were defined to represent the distribution. The ranges begin at 15 °F (-9.4 °C) and are at 10 °F (5.6 °C) intervals. The ranges and the corresponding symbols are defined in figure 6.9. The top and bottom grids contain only 9 points, and therefore will provide only a rough approximation of the temperature distribution. The middle grid, containing 16 points, will provide a better approximation.

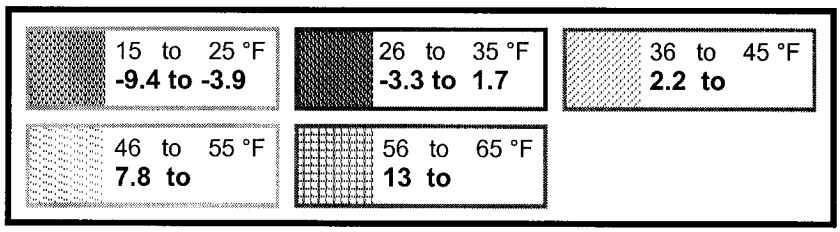

Figure 6.9 Five ranges of temperature for the temperature contour map within the plate heat exchanger

Balanced Airflow Temperature Distribution

Temperature distributions within the heat exchanger on both the cold and hot loop sides for the three principal planes, top, middle and bottom are presented in figure 6.10. The airflow rates for both the cold and the hot loops are within 0.2% of each other and are therefore considered balanced. It is clear that the temperature distributions are non-uniform in all cases. Two main divisions characterize the distributions: a cold and a hot corner. These corner effects tend to be more distinct on the leaving side of the heat exchanger. The cold corner phenomenon can be clearly observed on the hot loop leaving side of the heat exchanger on all three planes.

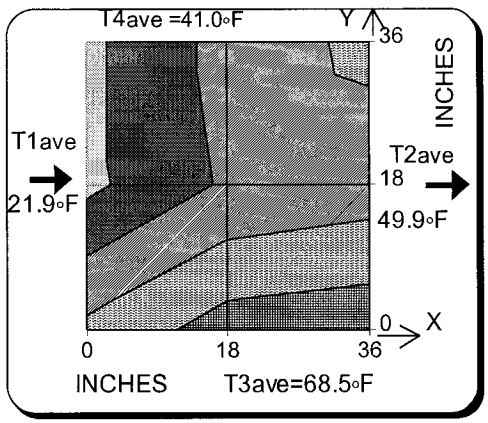

a) Cold air loop, top plane

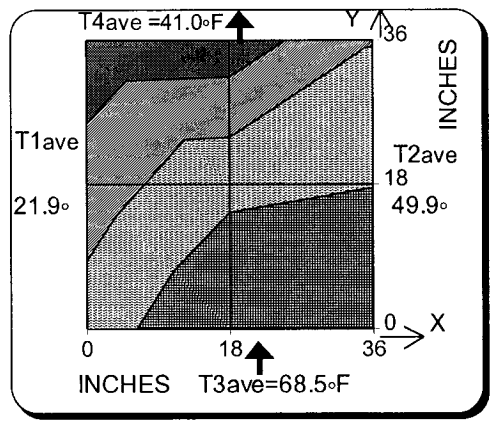

b) Hot air loop, top plane

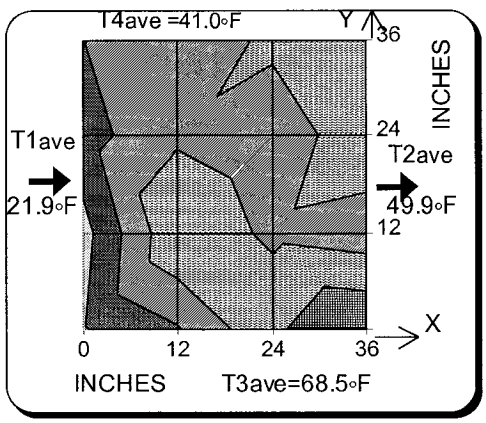

c) Cold air loop, middle plane

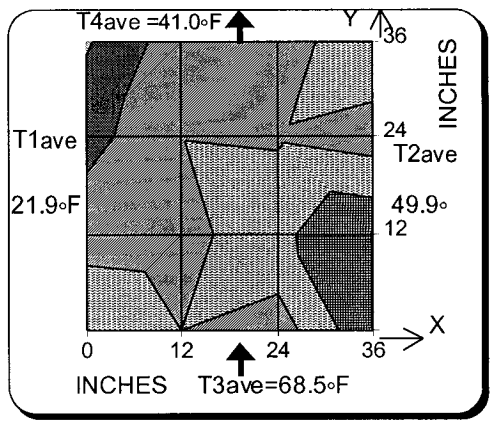

d) Hot air loop, middle plane

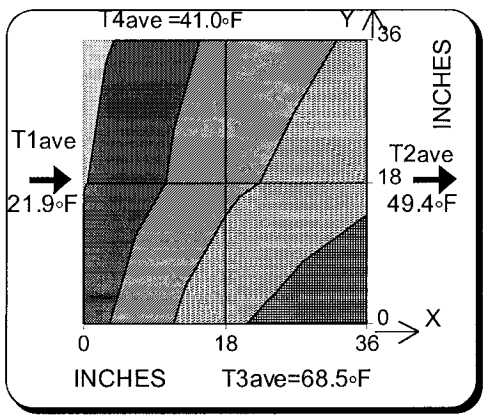

e) Cold air loop, bottom plane

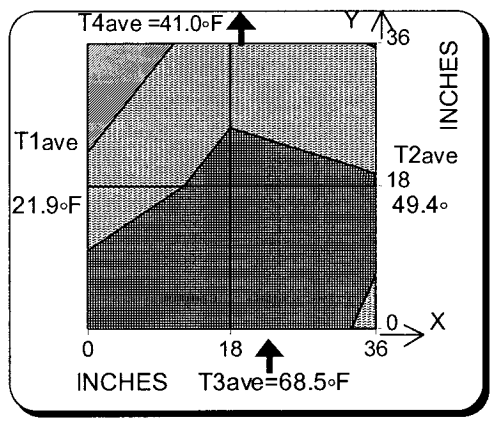

f) Hot air loop, bottom plane

Figure 6.10 Temperature distribution for balanced airflows, Qcal=1499 CFM (707 L/s) and Qhal=1502 CFM (709 L/s) at top, middle, and bottom planes on both the cold air and hot air loop side

The cold corner tends to occupy the corner zone in which the hot air has passes through the heat exchanger closest to the cold air entering side. The cold corner can be defined as a zone within the heat exchanger in which the temperatures are significantly colder than in the rest of the heat exchanger. Typically, the temperatures are below freezing, and the dewpoint, thus permitting frost to form. The tests were performed without the addition of humidity to the hot loop side. Very little frost formed, and its effect on the thermal performance of the heat exchanger can be considered negligible. The distribution on the cold loop side entering the heat exchanger varies from the top, middle to bottom plane. The cold zone increases in size until it is spread throughout the entire entrance on the bottom plane. This shift of the distribution may signify stratification in air density between the top and bottom planes. The colder air will be denser and tend to sink toward the floor of the unit upon entering the heat exchanger. This may also explain the difference in non-uniform temperature distribution on the top plane in comparison with the middle and bottom planes.

Temperature Distribution for various Obstructions

The temperature distributions within the heat exchanger vary widely for the different obstruction tests. The temperature distributions will be examined for two balanced airflow cases of approximately 1500 CFM (708 L/s) and 1870 CFM (882 L/s). The base case for the obstruction test is zero obstruction, as presented above for 1500 CFM (780 L/s). The results for 1870 CFM (882 L/s) at top, middle and bottom planes are presented in Appendix D. The entering air temperature on the cold loop was maintained at approximately 20 °F (-6.7 °C), and at 68 °F (20 °C) on the hot loop side. Airflow was adjusted for each test in order to maintain approximately 1500 CFM (708 L/s) on both sides. The distributions for the middle plane are presented exclusively. Figures 6.11 present the heat exchanger temperature distributions for all the different asymmetric obstructions located on the cold loop side. A thick black line on either the cold or hot loop side symbolizes the obstructions. The respective dimension of the vertical obstruction is placed next to the thick black line. Observing the temperature distributions on the cold loop side in figure 6.11 (a), (c), (e), (g), (i), and (k), the air temperature within the first 3 to 4

inches (76.2 mm to 102 mm) of the entrance of the heat exchanger is more or less uniform. However, it becomes less uniform as the air travels through the heat exchanger channel. At the exit of the heat exchanger on the cold loop side, as expected, there is a warm corner. The largest variation between the warmest and coldest temperatures exiting the heat exchanger on the cold loop is approximately 25 °F (13.9 °C). The largest variation on the entering side is approximately half that of the leaving side, i.e. 12 °F (6.7 °C). The temperature distributions vary little on the cold air loop side for all obstruction cases, with exception of the 24" (610 mm) obstruction located near the center wall in figure 6.11 (e). There is a slight shift of the 25 to 35 °F (-3.9 to 1.7 °C) contour on the entering side near the exterior wall. It should be noted that the temperature distribution does not change significantly for the 24" (610 mm) obstruction located near the exterior wall, as shown in figure 6.11 (k), as compared with the 24" (610 mm) obstruction located near the center wall figure 6.11 (e). The temperature distributions on the hot loop side of the heat exchanger display much greater variation as compared with those on the cold loop side. In particular, the cold corner region located on the hot loop side of the heat exchanger exhibits a remarkable change in size as a result of the obstructions located near the center wall. It is clearly evident that the cold corner region shrinks in size as the obstruction area increases from the center wall. In viewing figure 6.11 (b) for the 8" (203 mm) obstruction and comparing it with figure 6.11 (f) for the 24" (610 mm) obstruction, there is a dramatic reduction of the cold corner region. The size of the region is smaller than the zero obstruction case for the middle plane as illustrated in figure 6.9 (d).

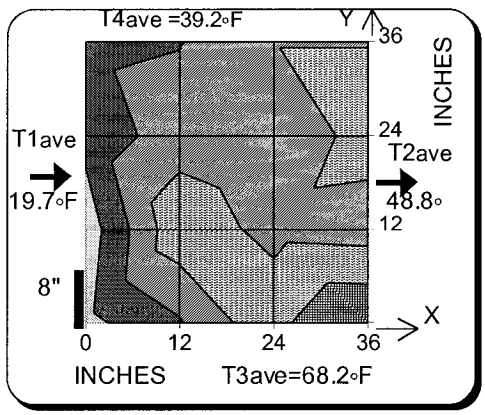

a) Cold loop temperature distribution for single Asymmetric 8" (203 mm) obstruction near center wall on cold loop side.

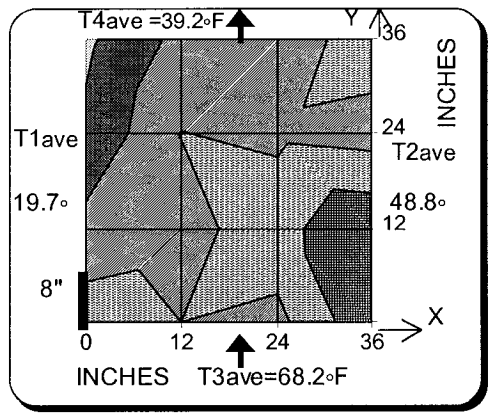

b) Hot loop temperature distribution for single Asymmetric 8" (203 mm) obstruction near center wall on cold loop side.

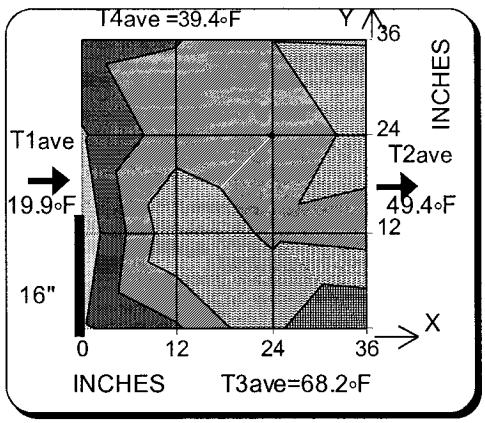

c) Cold loop temperature distribution for single Asymmetric 16" (406 mm) obstruction near center wall on cold loop side.

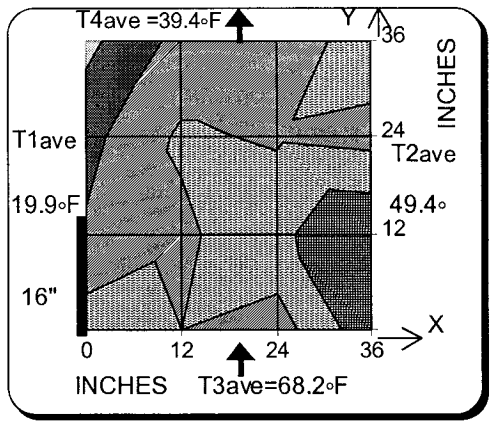

d) Hot loop temperature distribution for single Asymmetric 16" (406 mm) obstruction near center wall on cold loop side.

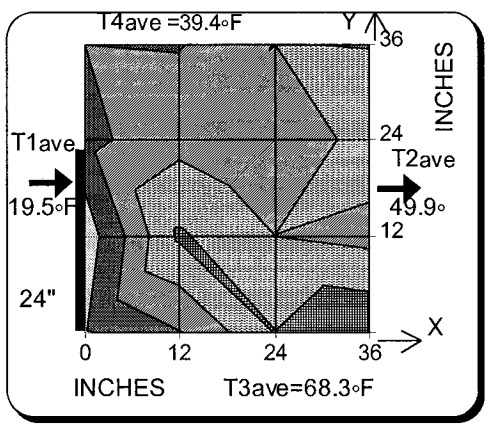

e) Cold loop temperature distribution for single Asymmetric 24" (610 mm) obstruction near center wall on cold loop side.

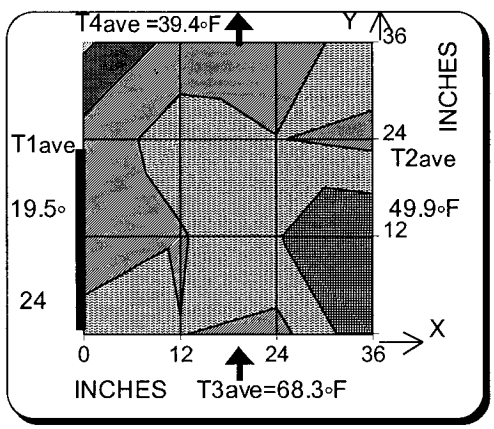

f) Hot loop temperature distribution for single Asymmetric 24" (610 mm) obstruction near center wall on cold loop side.

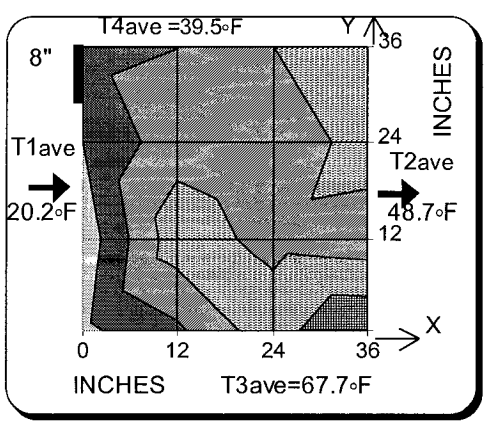

g) Cold loop temperature distribution for single Asymmetric 8" (203 mm) obstruction near exterior wall on cold loop side.

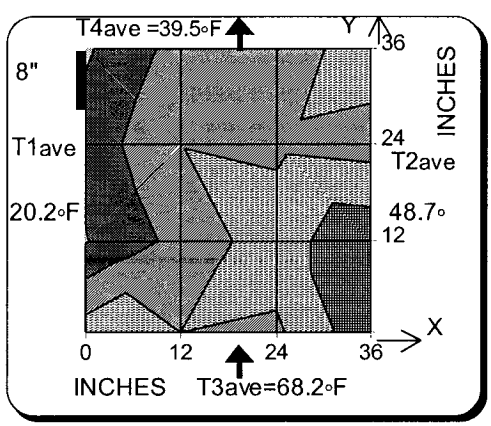

h) Hot loop temperature distribution for single Asymmetric 8" (203 mm) obstruction near exterior wall on cold loop side.

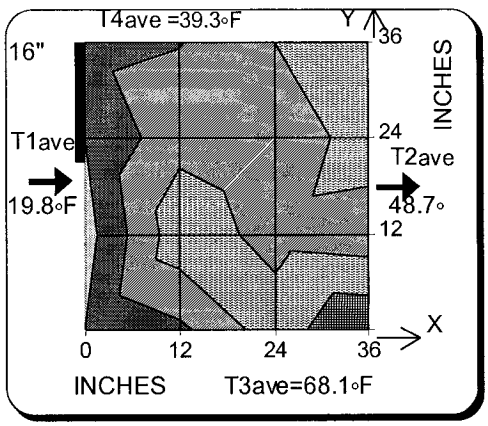

i) Cold loop temperature distribution for single Asymmetric 16" (406 mm) obstruction near exterior wall on cold loop side.

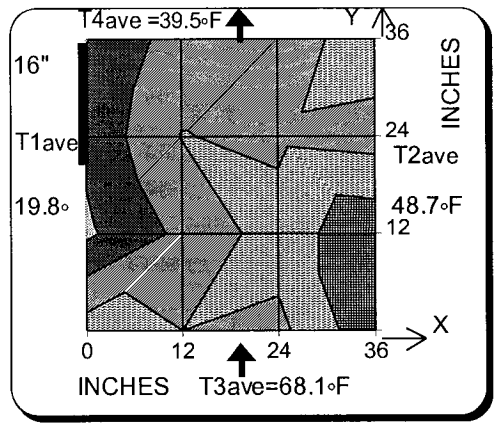

j) Hot loop temperature distribution for single Asymmetric 16" (406 mm) obstruction near exterior wall on cold loop side.

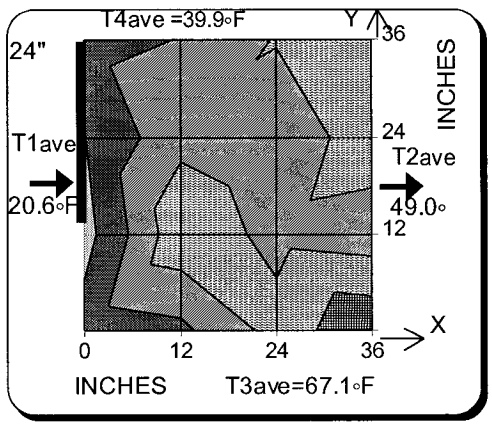

k) Cold loop temperature distribution for single Asymmetric 24" (610 mm) obstruction near exterior wall on cold loop side.

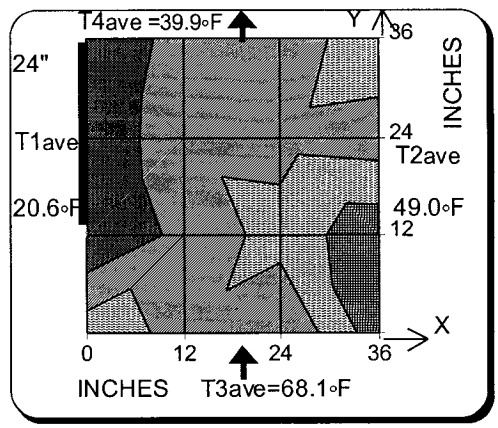

l) Hot loop temperature distribution for single Asymmetric 24" (610 mm) obstruction near exterior wall on cold loop side.

Figure 6.11 Temperature distributions within the plate heat exchanger for asymmetric obstructions located on the cold loop side for 1500 CFM (708 L/s) on cold and hot loop sides

In contrast, the hot corner region on the hot loop side does not vary noticeably. The same effect is not observed when the 24" (610 mm) asymmetric obstruction is located on the hot air loop side. Figure 6.12 depicts the temperature distributions for the 24" (610 mm) asymmetric obstruction in two locations on the hot air loop side: near the center wall and near the exterior wall. It can be seen that the cold corner is larger than in the zero obstruction case. This indicates that an obstruction located on the hot loop side entering the heat exchanger appears to exacerbate the cold corner effect.

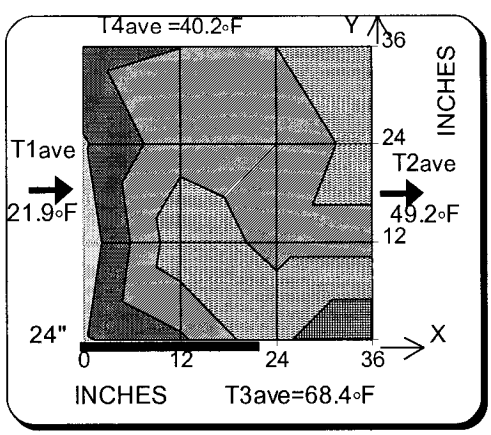

a) Cold loop temperature distribution

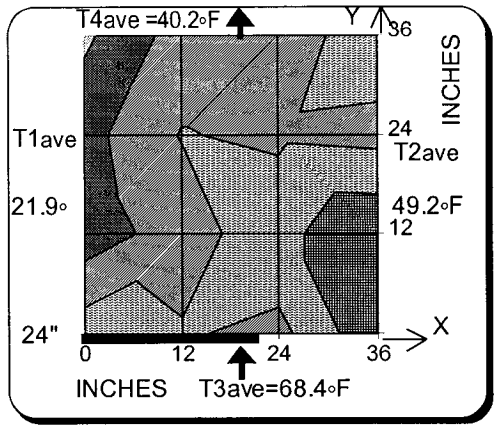

b) Hot loop temperature distribution

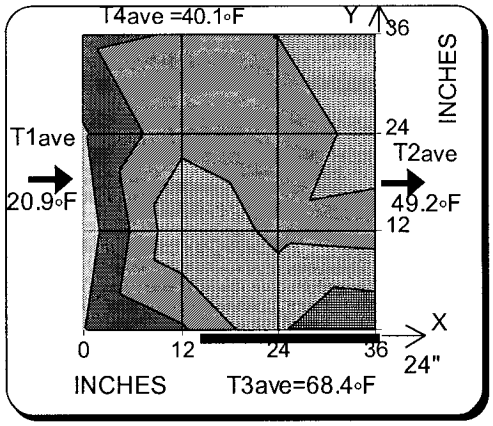

c) Cold loop temperature distribution

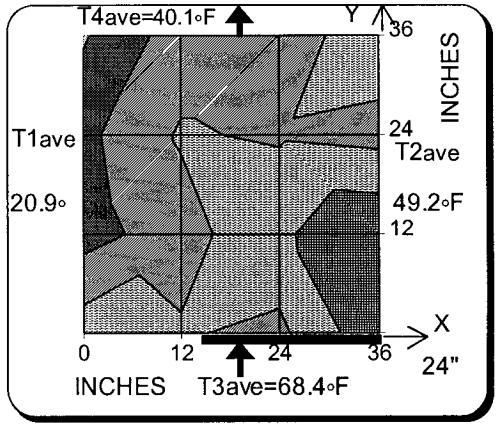

d) Hot loop temperature distribution

Figure 6.12 Temperature distributions within the plate heat exchanger for asymmetric 24" obstructions located on the hot loop side for 1500 CFM (708 L/s) balanced airflow

There is very little difference between the temperature distributions for the 24" (610 mm) obstruction located near either the center wall or the exterior wall as shown in figure 6.12 (b) and (d). Appendix E contains the temperature distributions for the remaining asymmetric obstruction locations on the hot air loop side. This shrinking effect of the cold corner region on the hot air loop is also observed for the temperature distributions produced at 1870 CFM (883 L/s) for both hot and cold loop airflow rates as presented in figure 6.13. The same pattern of shrinking occurs from the 8" (203 mm) to the 24" (610 mm) obstruction located near the center wall on the cold air loop side.

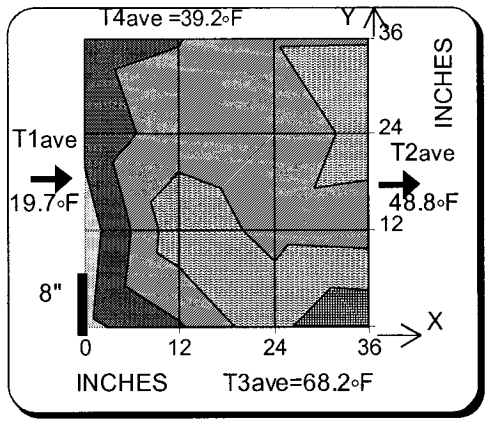

a) Cold loop temperature distribution

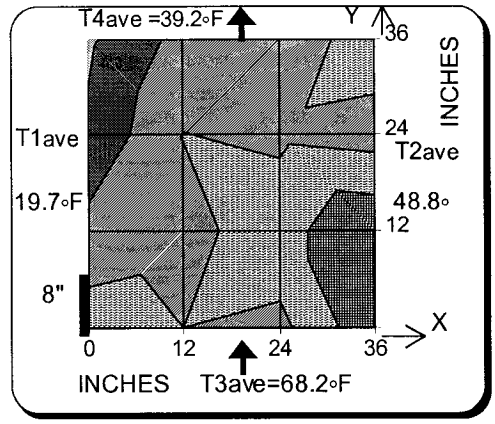

b) Hot loop temperature distribution

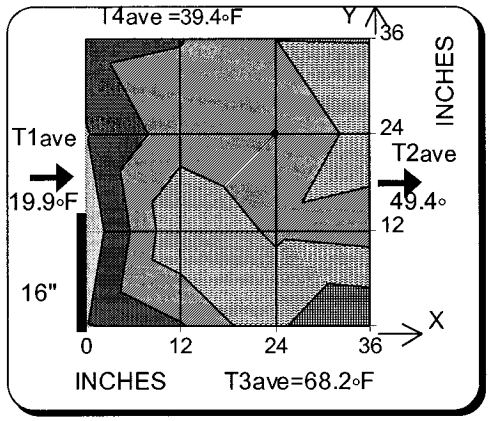

c) Cold loop temperature distribution

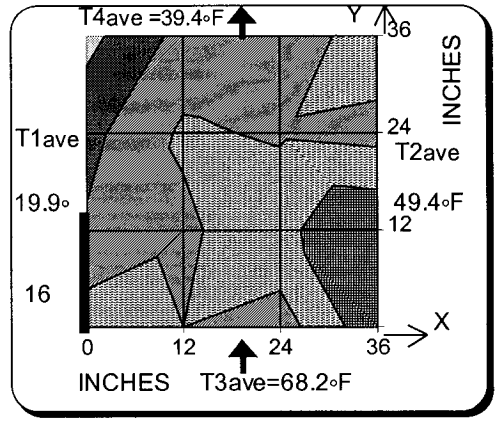

d) Hot loop temperature distribution

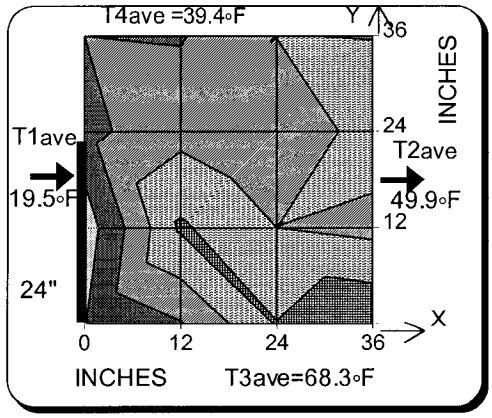

e) Cold loop temperature distribution

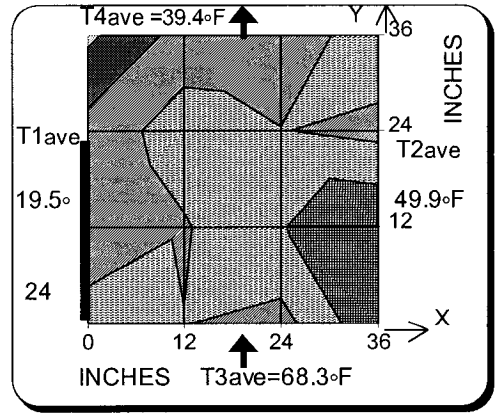

f) Hot loop temperature distribution

Figure 6.13 Temperature distributions within the plate heat exchanger for asymmetric 24" (610 mm) obstruction located on the cold loop side near the center wall for 1870 CFM (883 L/s) balanced airflow.

There appears to be some link between the slight increase in average sensible effectiveness as seen in figures 6.5 and the decreased cold corner area as a result of the 24" (610 mm) obstruction located near the center wall obstructions. Three of the symmetric obstruction cases are presented in figure 6.14. In the first instance, two 14" (356 mm) obstructions are located at entrance of the heat exchanger on the cold air loop side. A familiar pattern emerges with regard to the reduced area for the cold corner, as seen in figure 6.14 (b), since one of the 14" (356 mm) obstructions is located near the center wall. In contrast when there are 14" (356 mm) double obstructions located on both the cold and hot loop sides of the heat exchanger, the cold corner area increases in reference to the zero obstruction case.

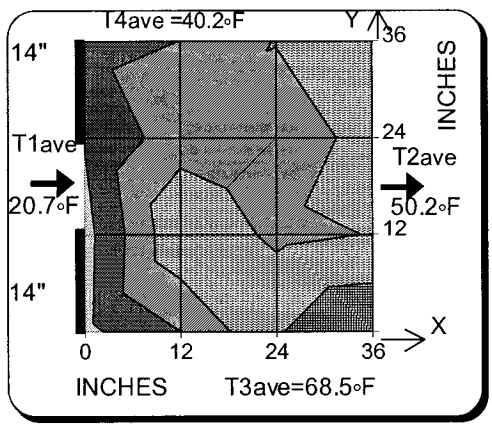

a) Cold loop temperature distribution for double symmetric 14" (356 mm) obstruction on cold loop side.

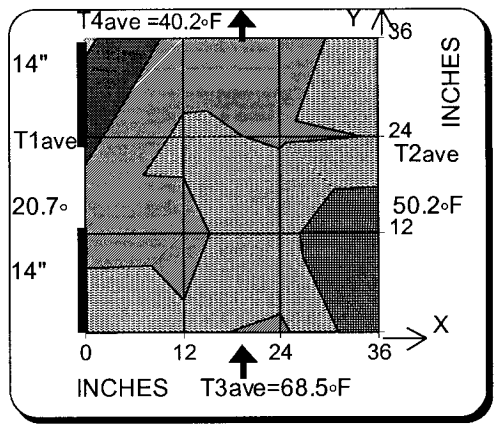

b) Hot loop temperature distribution for double symmetric 14" (356 mm) obstruction on cold loop side.

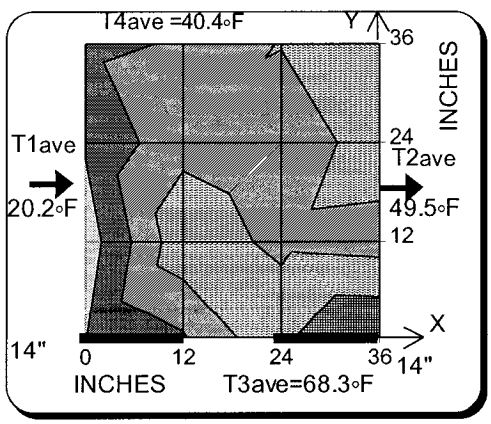

c) Cold loop temperature distribution for double symmetric 14" (356 mm) obstruction on hot loop side.

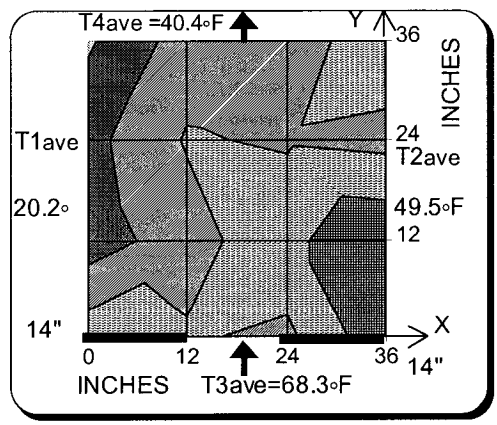

d) Hot loop temperature distribution for double symmetric 14" (356 mm) obstruction on hot loop side.

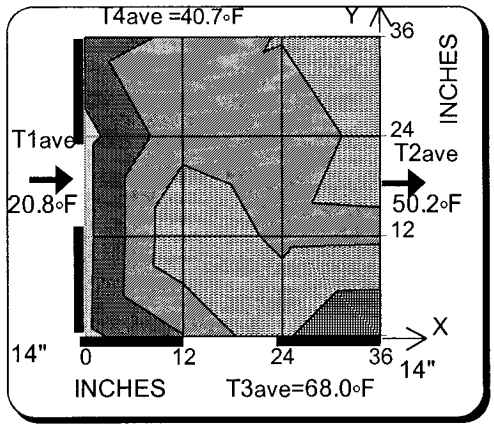

e) Cold loop temperature distribution for double symmetric 14" (356 mm) obstruction on hot loop side and cold loop side.

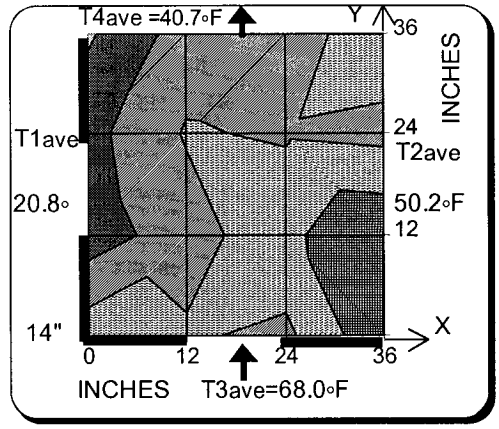

f) Hot loop temperature distribution for double symmetric 14" (356 mm) obstruction on hot loop side and cold loop side.

Figure 6.14 Temperature distributions within the plate heat exchanger for double symmetric 14" (356 mm) obstructions located on the (a), (b) cold loop side (c), (d) hot loop side (e), (f) on both sides for 1500 CFM (708 L/s) balanced airflow

The increase in the cold corner area may suggest that the obstructions located on the hot loop side override the effect of the obstruction located on the cold loop side near the center wall. It is of interest to note that the temperature distribution for the double 14" (356 mm) obstructions, as presented in figure 6.14 (e) and (f), does not vary much from the asymmetric obstructions and the zero obstruction case. The open entrance area is reduced by 84.5% for the double obstruction case. The entrance velocity for 1500 CFM (708 L/s) increases from 424 fpm (2.12 m/s) at zero obstruction to approximately 2700 fpm (12.5 m/s) at 84.5% blockage. The grid of 16 temperature sensors located on the middle plane will not allow for an accurate temperature distribution representation at the entrance of the heat exchanger where the entrance velocity rapidly increases and then diffuses throughout the heat exchanger towards the exit.

6.6 Post Test Uncertainty Analysis

Fancy graphs and impressive results will not be valid unless the experiments have been performed within acceptable uncertainty boundaries as defined by ASHRAE Guideline 2-1986 (RA 96) or NIST TH 1297. In chapter 3, the pre-test uncertainty analysis guided the choice of the instrumentation and the accuracy of the sensors. It also provided a prediction as to the

acceptable level of uncertainty in evaluating the sensible effectiveness. The heat recovery standards, ASHRAE std 84-1991 and CSA C439-00, do not prescribe the overall uncertainty limits for the heat recovery testing. However, Ciepliski, Besant, and Simonson (1998) established that 95% uncertainty for sensible effectiveness should not exceed 5%, i.e. $U_{\varepsilon s} < \pm 5\%$. This level of uncertainty is used as the limit for the present research. The average sensible effectiveness is used to evaluate the thermal performance of the plate heat exchanger, and is defined as follows:

$$\varepsilon_{s,\,ave} = \frac{\left[\dot{m}_s \times (t_{co} - t_{ci}) + \dot{m}_e \times (t_{hi} - t_{ho})\right]}{\dot{m}_{\min} \times (t_{hi} - t_{ci})} \qquad \textbf{(6.1)}$$

The variables in equation (6.1) have been defined in chapter 2. The 95% root-sum-square uncertainty for the average sensible effectiveness is defined as follows:

$$U_{\varepsilon s,\,ave,95\%} = \left[(tU_{\varepsilon s,\,ave,\,P})^2 + (U_{\varepsilon s,\,ave,\,B})^2\right]^{1/2} \qquad \textbf{(6.2)}$$

where $U_{\varepsilon s,\,ave,\,P}$ is the precision uncertainty, and t is the two-tailed student t distribution. The value of t is determined from the number of degrees of freedom, υ. In the case of large samples, $\upsilon \geq 30$, t=2. The number of samples per test ranges from 50 to 120 points. The precision uncertainty is calculated for the parameters that are used to derive the average sensible effectiveness using the root-sum square method.

$$U_{\varepsilon s,\,ave,\,P} = \left(\left(\frac{\partial \varepsilon_{s,\,ave}}{\partial \dot{m}_{cal}} U_{\dot{m}cal,\,P}\right)^2 + \left(\frac{\partial \varepsilon_{s,\,ave}}{\partial \dot{m}_{\min}} U_{\dot{m}al,\,P}\right)^2 + \left(\frac{\partial \varepsilon_{s,\,ave}}{\partial t_{ci}} U_{Tci,\,P}\right)^2 + \left(\frac{\partial \varepsilon_{s,\,ave}}{\partial t_{co}} U_{Tco,\,P}\right)^2 + \left(\frac{\partial \varepsilon_{s,\,ave}}{\partial t_{hi}} U_{Thi,\,P}\right)^2 \times 2\right)^{1/2} \qquad \textbf{(6.3)}$$

The individual parameters are either measured values or are derived from measured variables. The standard deviation for each measured variable is calculated based on the following equation:

$$S = \sqrt{\frac{n \times \sum_{i=1}^{n} X_i^2 - \left(\sum_{i=1}^{n} X_i\right)^2}{n \times (n-1)}} \qquad \textbf{(6.4)}$$

For example, the precision uncertainty for the cold air inlet temperature, $U_{Tci,\,P}$, is calculated as follows:

$$U_{T_{ci},P} = \sqrt{\frac{n \times \sum_{i=1}^{n} t_{ci}^{\,2} - \left(\sum_{i=1}^{n} t_{ci}\right)^2}{n \times (n-1)}} \qquad \textbf{(6.5)}$$

The number of data points collected for a particular test is *n*. Notice that the *t* factor is not incorporated into the individual parameter precision uncertainty. It is factored out and used in the final equation to calculate the overall precision uncertainty, $tU_{s,ave,P}$. The precision uncertainty for the average air temperature at the four locations entering and exiting the heat exchanger is presented in figure 6.15. It is recalled that the average air temperature at the entering and exiting grids is calculated from the 12 individual thermocouples. The bias uncertainty for air temperature of 0.5 °F (0.3 °C), which is constant, is included in figure 6.15 to provide a comparison between the two uncertainty parameters. As expected, the precision uncertainty is smaller than the bias uncertainty in most cases. This indicates that the random fluctuation of the average air temperature was low, and therefore the fluctuation of the individual thermocouples was within acceptable limits. The highest value of the precision uncertainty occurs for t_{1ave}, 0.77 °F (0.43 °C), at a face velocity of 519 fpm (2.6 m/s), while the lowest precision uncertainty occurs for T_{2ave},

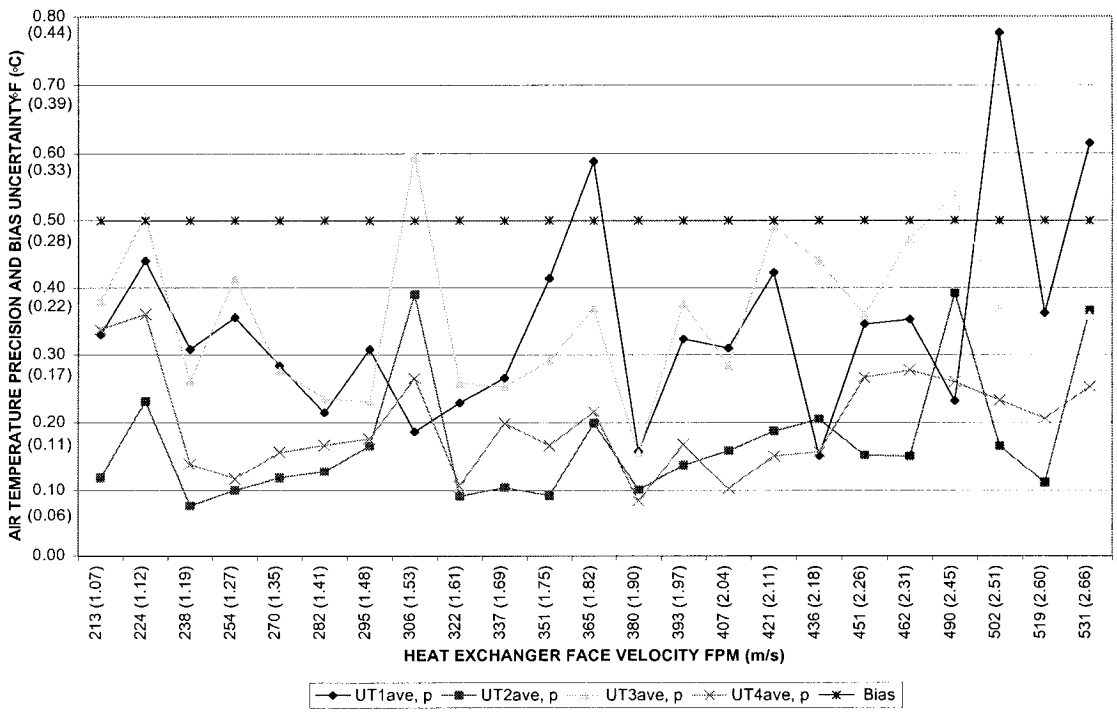

Figure 6.15 Average air temperature precision and bias uncertainty for a series of balanced airflow heat recovery tests.

approximately 0.07 °F (0.04 °C). The fluctuation in the average air temperature is attributed to varying loading conditions within the loops. Electronic noise and other uncertainty factors are considered to have a negligible effect on the random fluctuations of air temperature. In both the cold and the hot loops, the electric heater is responsible for the fine tune temperature control. The heater controls cannot maintain the air temperature at a 100% constant condition as a result of the PI temperature controller and the varying airflow rates. The temperature controller is set for a fast integral response, since electric resistance heaters respond instantaneously. As the airflow fluctuates, the load on the electric heater changes, and the controller will lag behind the change as the temperature deviates from the setpoint. The system achieved a reasonably steady state condition, as is reflected in the low temperature precision uncertainty. Airflow rate uncertainty precision increases marginally with increasing airflow, as depicted in figure 6.16.

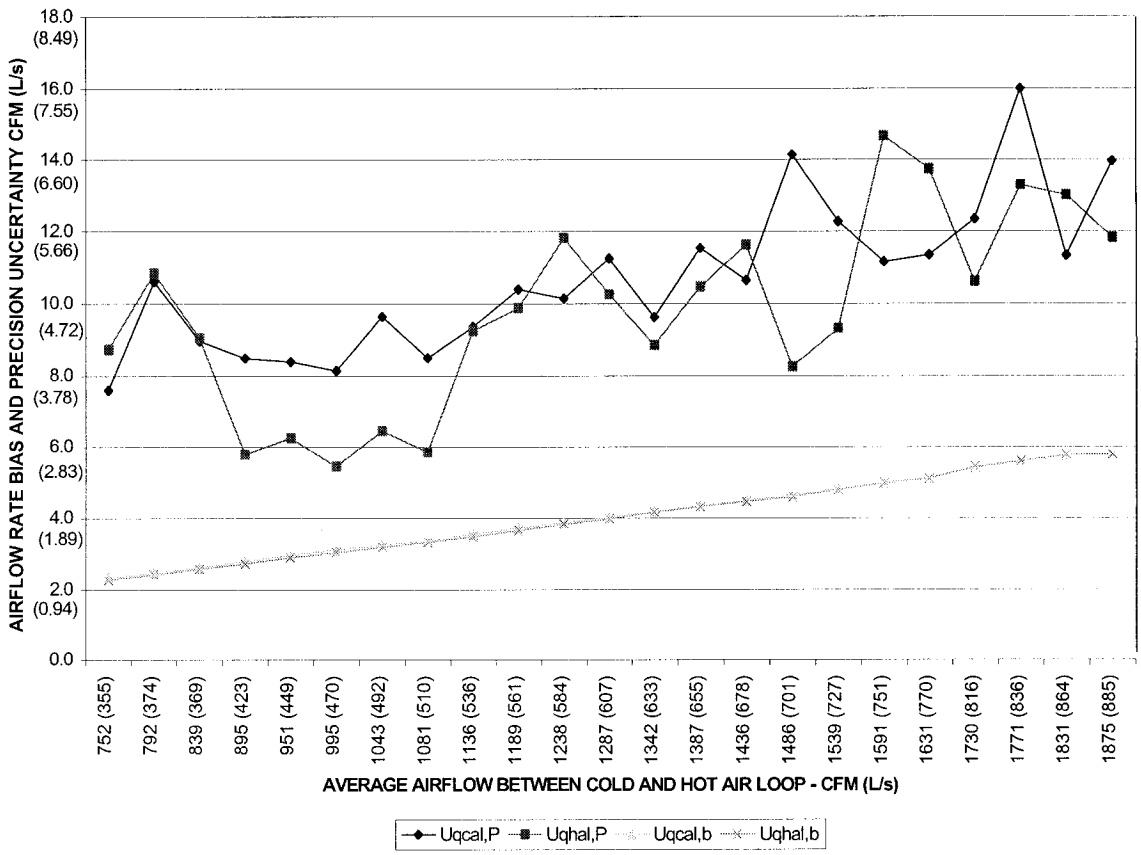

Figure 6.16 Airflow rate precision and bias uncertainty for the average airflow rate between cold and hot air loops

This is the result of increased turbulence and fluctuation at the airflow station due to higher air velocities. The airflow rate uncertainty precision is higher than the bias uncertainty, implying that the random fluctuations at the airflow measuring stations are significant. The airflow measuring stations in both loops exhibit a similar pattern of uncertainty precision increase with increasing airflow rate. The maximum uncertainty precision, which occurs at the cold loop airflow, is 16 CFM (7.55 L/s) out of 1771 CFM (836 L/s), representing only ± 0.9% of the airflow. The lowest uncertainty precision of 5.46 CFM (2.58 L/s) occurs at the hot loop airflow station for 995 CFM (470 L/s). This represents ± 0.54% of the airflow. The bias uncertainty is expected to be low since the pressure transducers are very accurate, i.e., 0.4% of full scale 0 to 0.5 in. w.c. (0 to 124 Pa). The bias uncertainty increases linearly for increasing airflow. In order to understand why the bias uncertainty increases with increasing airflow rate, the following equation needs to be examined:

$$U_{Q_{cal,\,B}} = \left(\left(\frac{\partial Q_{cal}}{\partial V_{cal}} U_{V_{cal,\,B}} \right)^2 + \left(\frac{\partial Q_{cal}}{\partial A_d} U_{A_d} \right)^2 \right)^{1/2} \qquad \textbf{(6.6)}$$

The basic equation for calculating airflow rate is as follows:

$$Q_{cal} = V_{cal} \times A_d \qquad \textbf{(6.7)}$$

Taking the first derivative of Q_{cal} with respect to V_{cal} and then to A_d:

$$\frac{\partial Q_{cal}}{\partial V_{cal}} = A_d \text{ and } \frac{\partial Q_{cal}}{\partial A_d} = V_{cal} \qquad \textbf{(6.8)}$$

A_d is constant and V_{cal} will vary with increasing airflow rate as a function of the velocity pressure, h_{cal}. However the bias uncertainty of the velocity pressure transducer is constant. The low precision and bias uncertainty for the airflow rate indicates two important points:

1. The airflow in both the cold and the hot air loops is steady during the period of a test
2. The airflow measuring station is providing precise and accurate measurements that are crucial in the evaluation of the sensible effectiveness.

As revealed in chapter 3, the sensible effectiveness uncertainty is very sensitive to the airflow rate, the velocity pressure transducer uncertainty and the temperature uncertainty. It has been demonstrated above that both of these uncertainties have achieved low values. The resulting

average sensible effectiveness bias, precision, 95% and 99% uncertainties are all presented in the figure 6.17.

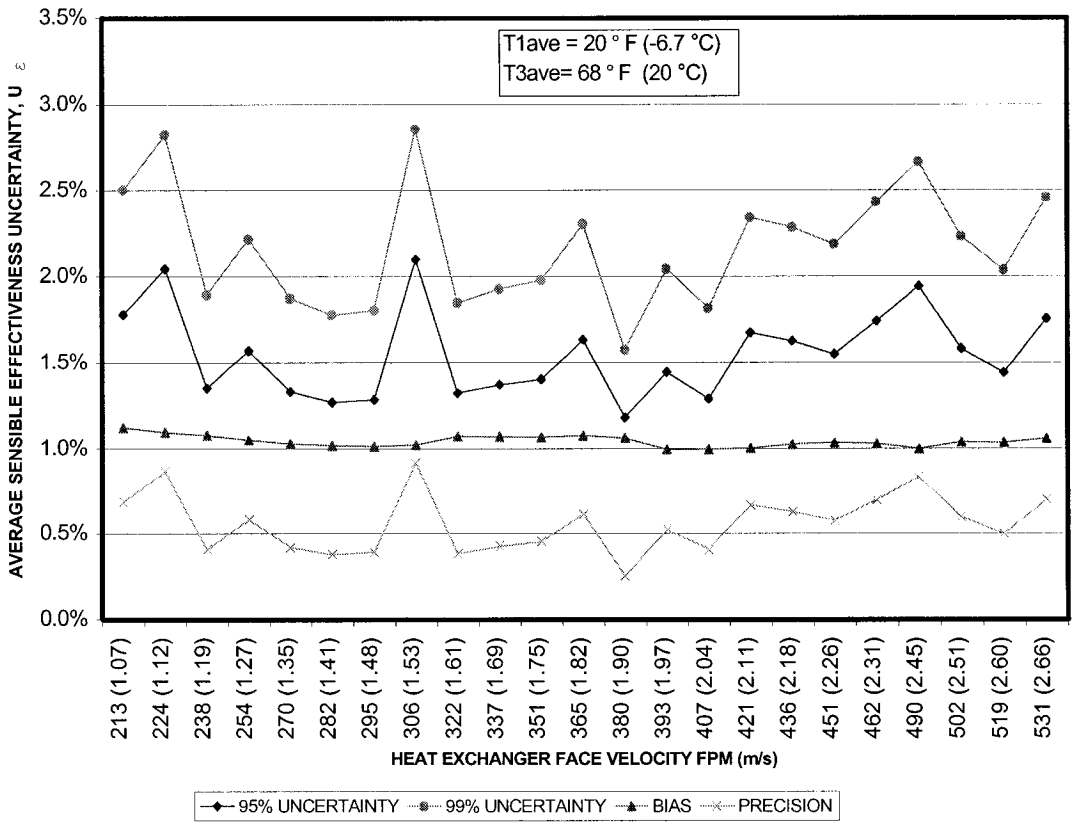

Figure 6.17 Sensible effectiveness uncertainty for balanced airflow tests ranging from 752 CFM (355 L/s) to 1875 CFM (885 L/s)

The objective to obtain 95% uncertainty for the average sensible effectiveness below 5% has been realized for all tests. Figure 6.17 is based on the balanced airflow tests for T_{1ave}=20 °F (6.7 °C). The 99% uncertainty is calculated as follows:

$$U_{\varepsilon,\,ave99\%} = tU_{\varepsilon,\,ave\,P} + U_{\varepsilon,\,ave\,B} \qquad \textbf{(6.9)}$$

The highest 95% uncertainty in the above series of balanced airflow tests is ± 2.1%. The 99% uncertainty does not exceed 3%, which reflects very accurate and precise measurements. Appendix F contains uncertainty values for the unbalanced airflow tests. The Visual Basic program that was developed to process the data collected from tests contains subroutines to calculate various statistical variables regarding the resulting sensible effectiveness including the bias, precision , 95% uncertainty and 99% uncertainty, and can be found in appendix C.

7.0 SUMMARY, CONCLUSIONS, AND RECOMMENDATIONS FOR FUTURE RESEARCH

The focus of the present thesis has been on the theoretical and experimental evaluation of the sensible effectiveness, ϵ_s, of an air-to-air cross flow plate type heat exchanger. A general review and comparison of all heat recovery devices has been undertaken. A detailed description of plate type heat exchangers was presented including a review of the various types. It was revealed that a true counter flow plate type air-to-air heat exchanger is impossible to fabricate. Although manufacturers call them counter-flow heat exchangers, their true airflow configuration is a combination of cross flow and counter-flow. The general characteristics and applications of cross flow plate heat exchangers have been explained in detail. The literature review indicates that there is a startling lack of research regarding air-to-air plate heat exchangers used in commercial HVAC applications. The only known research paper incorporating an attempt to experimentally study the temperature distribution within a plate heat exchanger is for counter flow configuration by M. Bantle, (1987). Otherwise, there is no research to date regarding the experimental study of the temperature distribution within an air-to-air cross flow plate heat exchanger which is known to exhibit what is commonly referred to as the cold corner effect. In reference to theoretical work, the various well-known formulations of ϵ_s for cross flow configurations have been presented as a possible model for the specific cross flow heat exchanger in the present work. These formulations are based on the NTU-ε relationships. As established by Kays and London (1984), there are four different relationships as a function of whether the airflow on both or either side is mixed or unmixed. The relationship that produces the highest sensible effectiveness is the case in which both airflows are unmixed; followed by the case in which one airflow is mixed and the other is unmixed. The lowest sensible effectiveness occurs for the case in which both airflows are mixed. The range of NTU for the series of curves is from 0.3 to 9.8. It is noted that the effectiveness curve for the case of one airflow mixed, and the other unmixed reaches its asymptotic effectiveness value of 0.63 at approximately NTU=3.0. These established formulations are based on the assumption that the airflow is uniform on both sides.

A model for the effect of non-uniform airflow using a two parallel path method has also been presented. This model has been expanded to a three path parallel model, and various permutations of non-uniform airflow have been simulated and presented in graphical format for a range of airflows. The results of the curves for the two path model indicate that a large non-uniformity occurring between two equal heat exchanger areas produces the largest reduction of sensible effectiveness, as large as 11.1 % reduction. This result is based on the assumption that the smaller airflow will flow through the smaller path area. If this assumption is not considered, then the sensible effectiveness reduction will increase dramatically for permutations involving large non-uniform airflow through small path areas, which is less likely to occur in real applications. The same results were found for the three path method.

The bulk of the research revolved around the design, fabrication, installation and commissioning of a new innovative heat recovery test facility and the subsequent testing of the cross flow plate heat exchanger. The design of the heat recovery test facility was preceded by a pre-test uncertainty analysis to determine the operating conditions and instrumentation required for achieving 95% uncertainty below 5%. The current North American standards for testing air-to-air heat recovery devices, ASHRAE Standard 84-1991, Method of Testing Air-to-Air Heat Exchangers, CSA Standard C439-00, 2000, Standard Laboratory Methods of Test for Rating the Performance of Heat/Energy-Recovery Ventilators, do not provide guidelines for either pre or post test uncertainty analysis. The standards ANSI/ASME PTC 19.1-1985 and NIST TN 1297 provide detailed guidelines for uncertainty analysis. Further to the research by Ciepliski, Besant, and Simonson (1998), uncertainty analysis before and after a heat recovery test is relevant. The pre-test uncertainty analysis is more appropriate during the initial design stage of a heat recovery test facility. However, once the facility has been put into operation and is producing results within acceptable uncertainty boundaries, then only post-test uncertainty analysis is required. A detailed derivation of the equations for establishing the pre-test uncertainty has been undertaken. In order to understand the effect of measurement instrument accuracy on the uncertainty of effectiveness uncertainty, sensitivity curves were generated for sensors having different accuracy values, also known as Bias. The sensors included air temperature, relative humidity, barometric pressure and

velocity pressure for airflow measurements. The accuracy of the tape measure used to measure the physical dimensions of the duct containing the airflow measuring stations is also considered. The sensitivity curves revealed that velocity pressure accuracy has the greatest effect on sensible effectiveness, followed by the duct dimension measurement and air temperature measurements. In all cases, non-covariance of all the variables produced less effect on sensible effectiveness than variables having covariance. The accuracy of the relative humidity sensors and the barometric pressure gage had little impact on sensible effectiveness uncertainty. A study of the operating conditions revealed that the airflow range has the greatest influence on the sensible effectiveness uncertainty for a velocity pressure transducer of a specific accuracy and the type of airflow measuring station. Lower airflow rates produced the greatest sensible effectiveness uncertainty. As a result, the minimum airflow rate of the heat recovery test facility was maintained above 750 CFM (354 L/s) for a rectangular grid airflow measuring station with a 14" x 14" (356mm x 356 mm) cross section and a velocity pressure transducer accuracy of ± 0.002 in. w.c. (± 0.5 Pa). Another operating condition that was studied in relation to the effectiveness uncertainty was the difference in temperature between the cold air entering, t_{ci}, and the hot air entering, t_{hi}. It was found that as the temperature difference between t_{ci} and t_{hi} decreased, the sensible effectiveness uncertainty increased. The initial basis of design of the heat recovery test facility stemmed from both ASHRAE Standard 84-1991, and CSA Standard C439-00, 2000. However, the following modifications were incorporated into the design:

1. A double tunnel system was used. Each tunnel is closed loop and completely independent of the other tunnel.
2. A single airflow station was used for each tunnel in order to reduce the number of velocity pressure transducers.
3. Variable frequency drives were used for both the cold and hot loop fan motors. This allowed for excellent control of the airflow.
4. Electric duct heaters controlled by a SCR provided fine-tuned control of the air temperature.

One of the essential features of the test facility is the instrumentation and data acquisition system. In light of the large number of measurement points required, a 4 channel multiplexer was

conceived and built in order to expand the existing data acquisition system from 48 to 129 points. Some of the key highlights of the instrumentation and data acquisition system include:

1. All instrumentation was calibrated and verified as part of the commissioning process.
2. The airflow stations, which are critical for accurate determination of effectiveness, were found to have excellent agreement with reference air velocity measurements using a hand held calibrated hot wire anemometer.
3. The plate heat exchanger contains 3 temperature grids located at the top, middle, and bottom on both the cold and hot loop sides. A total number of 68 points of temperature were collected to evaluate the temperature distribution within the plate heat exchanger.
4. A total number of 129 automated measurement points were collected from the test facility every 4 seconds. The limiting factor for the sampling rate was the relay switching on the multiplexer.
5. A comprehensive program was developed using the software Labview to manage the data collection and to provide real time data logging and calculations including effectiveness. A program in Excel Visual basic was developed to format, calculate and direct the data to specific tables for use in charts and statistics.
6. Based on the accuracy of the sensors utilized, the combined effectiveness uncertainty for the tests was estimated to be below $\pm 5\%$.

The fully functional heat recovery test facility was used to carry out 3 main types of tests on the cross flow plate heat exchanger:

1. Balance airflow tests for a range of airflow and cold loop air entering temperature. The hot loop air entering temperature was held relatively constant. 92 tests were completed.
2. Unbalanced airflow test for a range of Q_{cal}/Q_{hal} from 0.5 to 2.0 for constant cold and hot loop entering air temperatures. 33 tests were completed.
3. The effect of obstructions located in front of the plate heat exchanger on the cold and hot loop air entering side on effectiveness. 36 tests were completed

The minimum time for each test was 20 minutes, not including the time for setting up and establishing steady state conditions for airflow and temperature. A total number of 161 tests were

conducted. This corresponds to more than 54 hours of testing, not including time required for tests that were discarded for reasons of faulty readings, data acquisition fault or human error. For each of the tests, temperature distributions were developed and compared.

7.1 Summary of Experimental Results

Balanced Airflow Tests:

The tests conducted with balanced airflows on the specific cross flow plate heat exchanger revealed the following results:

1- The sensible effectiveness for the cross plate heat exchanger in the present study obtained a maximum sensible effectiveness of 0.63 at an average face velocity of 210 fpm (1.05 m/s), which corresponds to an NTU of approximately 9.8.

2- The sensible effectiveness decreased not more than 7.2% when the face velocity reached its maximum value of approximately 538 fpm (2.69 m/s).

3- The experimental sensible effectiveness most closely agreed with the cross flow NTU-ε relationship when one airflow is mixed and the other unmixed.

4- The experimental results indicate that the temperature difference between the cold and hot entering sides of the heat exchanger, $\Delta t_{1,3} = t_{3ave} - t_{1ave}$, ranging from 58 to 28 °F (32.2 to 15.6 °C) does not affect the sensible effectiveness, for approximately NTU= 3.0 to NTU=9.8. This is the case when t_{3ave} is held constant at approximately 68 °F (20 °F).

Unbalanced Airflow Tests:

The next series of tests involved a study of the effect of unbalanced airflow conditions on the sensible effectiveness. The results of these tests are summarized as follows:

1- As expected, the maximum sensible effectiveness of 0.784 occurs at an unbalanced airflow condition of $Q_{cal}/Q_{hal} = 2.0$. The sensible effectiveness also reaches a maximum value of 0.764 at $Q_{cal}/Q_{hal} = 0.5$.

2- The minimum sensible effectiveness of 0.595 occurs for the case of $Q_{cal}/Q_{hal} = 1.0$, at the bottom of the parabolic shaped curve.

3- The theoretical sensible effectiveness does not vary more than 7.8% from the experimental results. There is a much closer agreement with the sensible effectiveness as the unbalanced ratio, Q_{cal}/Q_{hal}, approaches either 0.5 or 2.0.

Obstruction Tests:

The sensible effectiveness has been evaluated for both balanced and unbalanced airflow conditions as might be expected in real applications. It is known that in real systems there is often uneven airflow entering the heat exchanger due to geometrically undesirable transitions from ductwork or other components such as filters or coils. The next step of testing was to evaluate ϵ_s for various sizes of simple rectangular-shaped obstructions. These obstructions were placed on the entrance of the cold and hot sides of the heat exchanger. The summarized results of those tests are listed as follows:

1- It was observed that all obstructions located on both the cold and hot entering side of the horizontal orientated plate heat exchanger did not cause ϵ_s to decrease in reference to the baseline test involving no obstructions. This observation includes the largest obstruction, the double 14" (356 mm) symmetric obstruction that blocked 84.5% of the open area to the entrance of the heat exchanger.

2- An unexpected 2.3 % increase in ϵ_s relative to the zero obstruction case was observed for the case involving the 24" (610 mm) obstruction located nearest the center wall on the cold loop side entering the heat exchanger. The case involving the 16" (406 mm) obstruction also located nearest the center wall on the cold loop side entering the heat exchanger exhibited a 1.3 % increase.

3- The obstructions located on the cold loop entering side of the heat exchanger have a greater effect on ϵ_s than the obstructions located on the hot loop side.

4- As expected ϵ_s is slightly higher for the various obstruction cases for the lower airflow rate of 1500 CFM (708 L/s) as compared with the higher airflow rate of 1870 CFM (882 L/s).

Temperature Distributions within Plate Heat Exchanger:

In all tests the temperatures within the plate heat exchanger were measured in order to develop the temperature distribution profiles. Several important observations regarding the temperature distributions are recorded as follows:

1- The air temperature distributions in cross flow heat exchangers were non-uniform in reference to the plane perpendicular to the airflow direction for all tests without obstructions.

2- The obstructions located on the cold side of the heat exchanger caused an initial uniform distribution on the cold side only but within a short distance returned to a non-uniform condition.

3- In all tests, on the hot side of the heat exchanger, there was a consistent pattern that developed in which there was a cold corner and corresponding hot corner.

4- In reference to the tests involving the obstructions, there is clear evidence of the cold corner region significantly shrinking in size as the obstruction area increases from the center wall on the cold side of the heat exchanger. The maximum reduction in the size of the cold corner occurred for the 24" (610 mm) obstruction located nearest the center wall on the cold air loop side.

7.2 Conclusions

The present research has focused on air-to-air cross flow plate heat exchangers, because of the lack of research for one of the most common type of heat recovery devices used in the HVAC industry. It can be concluded that the six objectives stated in section 1.5 have been realized. The contributions cover theoretical, experimental, and practical aspects in relation to air-to-air heat recovery. The 95% effectiveness uncertainty for all the tests successfully remained below ± 5%. It can be concluded that the present heat recovery test facility is functional and acceptable for thermal performance evaluation of heat recovery devices. In future tests some improvements should be implemented to further reduce the precision and the bias Uncertainty. In particular, a longer section of ductwork could be provided before and after the airflow station.

Four airflow stations could be used instead of two to determine the airflow at all four entering and exit points of the heat exchanger.

7.3 Recommendations for Future Work

The most revealing aspect of the present research revolves around two points:

1- The sensible effectiveness results of the obstruction tests.

2- The temperature distributions resulting from the obstruction tests.

The results of the obstruction tests warrant a more detailed study to determine if it is possible to optimize the sensible effectiveness through a cross flow plate heat exchanger. The present research did not touch on the subject of frost control. The results from the obstruction tests indicated there is a potential application to minimize the cold corner zone by diverting air through the cold air entering side. Currently there is no published research on this type of innovative frost control strategy. The conventional type of frost control method involves bypassing a percentage of the cold air around the heat exchanger in order to prevent frost from forming on the exhaust air side. This technique is not efficient, and, therefore, an extensive study of other frost control techniques for cross flow plate heat exchangers, including traversing defrost, is recommended. In conjunction with these future studies, the bulk air temperature distribution within the heat exchanger and the core temperature distribution could be measured at more points than in the present research to obtain an accurate picture of the dynamics occurring under frost control conditions.

REFERENCES

Abnerthy, R.B., Benedict, R.P.,and Dowdell, R.B., 1985, *ASME Measurement Uncertainty*, Trans. ASME, Journal of Fluids Engineering, 107, 161-164

Anantapantula, V.S., Sauer, H.J., 1994, Heat Recovery and the Economizer for HVAC Systems, ASHRAE journal, November, 1994, 48-53

ANSI/ASME Standard 41.1-1986 (RA 2001), Standard Method for Temperature Measurement, The American Society of Mechanical Engineers, New York, N.Y.

ANSI/ASME Standard PTC 19.1-1985, Measurement Uncertainty, Part 1, The American Society of Mechanical Engineers, New York, N.Y., 1985

ANSI/ASME Standard PTC 30-1991, Air Cooled Heat Exchangers, The American Society of Mechanical Engineers, New York, N.Y.

ANSI/ASME Standard 210-85, Laboratory Methods of Testing Fans for Rating, Air Movement and Control Association, Inc., The American Society of Mechanical Engineers, New York, N.Y.

ASHRAE 2000, *handbook-fundamentals*, American Society of Heating, Refrigeration and Air Conditioning Engineers Inc., Atlanta

ASHRAE 2000, *HVAC Systems and Equipment Handbook*, chapter 44, American Society of Heating, Refrigeration and Air Conditioning Engineers Inc., Atlanta

ASHRAE 1989 ANSI/ASHRAE Standard 62-1989, Ventilation for Acceptable Indoor Air Quality, American Society of Heating, Refrigeration and Air Conditioning Engineers Inc., Atlanta

ASHRAE Guideline 2-1986 (RA 96), *Engineering Analysis of Experimental Data*, American Society of Heating, Refrigeration and Air Conditioning Engineers Inc., Atlanta

ASHRAE Standard 84-1991, *Method of Testing Air-to-Air Heat Exchangers*, American Society of Heating, Refrigeration and Air Conditioning Engineers Inc., Atlanta

ASTM E 220-86, *Standard Method for Calibration of Thermocouples By Comparison Techniques*

ARI Standard 1060, *Rating Air-to-Air Energy Recovery Ventilation Equipment*, 1997, Air-Conditioning and Refrigeration Institute, Arlington Virginia

Bantle, M.R., 1987, Prediction and Control of Frost Formation in Air to Air Heat Exchanger, M. S.C., thesis in mechanical Engineering, University of Saskatchewan, Canada.

Bell, K.J.., 1981, *Plate Heat Exchangers*, Heat Exchangers Thermal-Hydraulic Fundamentals and Design, McGraw-Hill, New York, N.Y.

Benedict, R.P., Wyler, J.S., 1979, *Engineering Statistics-with Particular Reference to Performance Test Code Work*, Trans. of ASME, Vol 101, 662-669

Besant, R.W., Simonson, C.J.,2000, Air-to-Air Energy Recovery, ASHRAE Journal, May 2000, 31-42

Carnes, L., 1984, *Air-to-Air Heat Recovery Systems for Research Laboratories*, ASHRAE Trans., 90(2A), 327-340

Chiou, J.P., 1978, Thermal Performance Deterioration in Crossflow Heat Exchanger due to the Flow Non-uniformity, ASME Trans. Journal of Heat Transfer, Vol. 100, 580-587

Ciepliski, D.L., 1997, *Testing an Air-to-Air Energy Recovery Device Using Performance Test Standards,* M. S.C., thesis in mechanical Engineering, University of Saskatchewan, Canada

Ciepliski, D.L., Simonson, C.J. and Besant, R.W., 1998, *Some Recommendations for Improvements to ASHRAE standard 84-1991,* ASHRAE Trans. 104(1)

Coleman, H.W. and Steel, W.G., 1989, *Experimentation and Uncertainty Analysis for Engineers*, Wiley-Interscience, New York

CSA Standard C439-00, 2000, *Standard Laboratory Methods of Test for Rating the Performance of Heat/Energy-Recovery Ventilators*, Canadian Standards Association, Rexdale, Ontario, Canada

Dhital, P., Besant, R.W., and Schoenau, G.J., 1995, *Integrating Run-Around heat Exchanger Systems into the Design of Large Office Buildings*, ASHRAE Trans., 101, 978-990

Energy Recovery Equipment and Systems, SMACNA Sheet Metal and Air Conditioning Contractors National Association, Inc.

ENV. 1996. Standard 308-1996, Heat Exchangers-Test Procedures for Establishing Performance of Air-to-Air and Flue Gases Heat Recovery Devices, European Committee for Standardization

Gawley, H.N., and Fisher, D.R., 1975, *The Effectiveness and Rating of Air-to-Air Heat Exchangers*, ASHRAE Trans., Vol 81, 401-409

Gudac, G.J., Mueller, M.A., Sauer, H.J., et al, 1981, *Effectiveness and Pressure Drop Characteristics of Various Types of Air-to-Air Energy Recovery Systems*, ASHRAE Trans. Vol. 87, 199-210

Guo, P., Ciepliski, D.L., and Besant, R.W., 1998, *A Testing and HVAC Methodology for Air-to-Air Heat Pipe Heat Exchangers*, Int. J. HVAC & Research, 4(1), 3-26

Huang, P.H., 1989, *Humidity Measurements and Calibration Standards*, ISA, 298-304

Johnson, A.B., Simonson, C.J., and Besant, R.W., 1998, *Uncertainty Analysis in the Testing of Air-to-Air Heat/Energy Exchangers Installed in Buildings*, ASHRAE Trans. 104, 1639-1650

Kays, W.M., and London, A.L., 1984, *Compact Heat Exchangers*, Third Edition, McGraw-Hill, New York

Kitto, J.B., and Robertson, J.M., 1989, Effects of Maldistribution of flow on Heat Transfer Equipment Performance, Journal of Heat Transfer Engineering, 10(1), 18-25

Kline, S.J., 1983, *1983 Symposium on Uncertainty Analysis Closure*, Trans. ASME, Journal of Fluids Engineering, Vol. 107

Lassahn, G.D., 1985, *Uncertainty Definition*, Trans. ASME, Journal of Fluids Engineering, Vol. 107

McFarland, J.K., Jeter, S.M. and Abdel-Khalik, S.I., 1996, Effect of a Heat Pipe on Dehumification of a Controlled Air Space, ASHRAE Trans., Vol. 102(1), 132-139

Meckler, M., 1995, Maximizing Ventilation Potential for Heat Recovery, ASHRAE Journal, Nov. 1995, p. 42-47

Moffat, R.J., 1982, *Contributions to the Theory of Single-Sample Uncertainty Analysis*, Trans. ASME, Journal of Fluids Engineering, Vol. 104, 250-260

Moffat, R.J., 1985, *Using Uncertainty Analysis in the Planning of an Experiment*, Trans. ASME, Journal of Fluids Engineering, Vol. 107, 173-178

Mueller, M.A., Howell R.H, Gudac G.J., and Sauer, H.J., 1981, Development of a Standard Test Facility for Evaluation of all Types of Air-to-Air Energy Recovery Systems, ASHRAE Trans., Vol 87, 183-198

NIST Technical Note 1297, 1994 Edition, *Guidelines for Evaluating and Expressing the Uncertainty of NIST Measurements Results*, Physics Laboratory, National Institute and Technology, Gaithersburg, MD

Price, B.A., Smith, T.F., and Suby, A.A., 2000, Uncertainty Analysis-Estimating the Errors of Measured Variables and Determining How the Errors Propogate, Journal of Heating/Piping/Air Conditioning Engineering, October 2000, 34-43

Uddin, M.A., Bell, K.J., 1988, Effect of Uncertainties on the Design and Operation of Systems of Heat Exchangers, In: Heat transfer Equipment Design, (Edited by R.K. Shah, E. K. Subbarao and R.A. Mashelkar), Hemisphere, New York, 39-47

Rousseau, W.H., Milgram, E.L., 1974, Estimating Precision in Heat Rate Testing, Trans. ASME, Journal of Fluids Engineering,July 1974

Sauer, H.J., and Howell, R.H., 1981, *Promise and Potential of Air-to-Air Energy Recovery Systems*, ASHRAE Trans., Vol. 87(1), 167-182

Savadkouhian, M., 1981, *A Report on the Experimental Performance Evaluation of a Fixed Plate Air-to-Air Heat Exchanger*, M.Eng., Concordia University

Shah R.K., 1981, *Compact Heat Exchangers*, Heat Exchangers Thermal-Hydraulic Fundamentals and Design, McGraw-Hill, New York, N.Y.

Simonson, C.J., 1998, *Heat and Moisture Transfer in Energy Wheels*, Ph.D. thesis in the Department of Mechanical Engineering, University of Saskatchewan, Saskatoon, Canada.

Simonson, C.J., Shang, W., and Besant, R.W., 2000, Part-Load Performance of Energy Wheels: Part I – Wheel Speed Control, ASHRAE Trans., Vol. 106, 286-300

Simonson, C.J., Shang, W., and Besant, R.W., 2000, Part-Load Performance of Energy Wheels: Part II – Bypass Control and Correlations, ASHRAE Trans., Vol. 106 (1), 301-310

Sparrow, E.M., Martin, G.L., Abraham, J.P., and Tong, J.C.,2000, *Air-to-Air Energy Exchanger Test Facility for Mass and Energy Transfer Performance*, ASHRAE Trans

Van den Buick, E., 1991, Optimal Design of Cross Flow Heat Exchangers, ASME Trans., Journal of Heat Transfer, Vol 113, 341-347

APPENDIX A : MATHCAD PROGRAM FOR CALCULATING EFFECTIVENESS UNCERTAINTY

$Tcal := 50$ Dry bulb Air temperature in °F in cold air loop airflow measuring station

$T := (Tcal + 459.67)$ Conversion to R

$C8 := -10440.397$ Coefficients for
$C9 := -11.29465$ calculating saturated
$C10 := -0.027022355$ water vapor pressure
$C11 := 0.00001289036$
$C12 := -0.000000002478068$
$C13 := 6.5459673$

*****This MathCad program is used to simulate conditions to calculate the sensible effectiveness, 95% and 99% uncertainty of a heat recovery devices using ASHRAE standard 84-1991 equations, and fundamental pyschometric relationships for calculating air density and hence airflow.*****

$$pws := \exp\left(\frac{C8}{T} + C9 + C10 \cdot T + C11 \cdot T^2 + C12 \cdot T^3 + C13 \cdot \ln(T)\right) \cdot 2.036$$

$pws = 0.36262$ Calculation of saturated water vapor pressure on cold air loop side, psi

$UT := 0.5$ Temperature uncertainty - input deg F

$$dpws := \frac{d}{dT} \exp\left(\frac{C8}{T} + C9 + C10 \cdot T + C11 \cdot T^2 + C12 \cdot T^3 + C13 \cdot \ln(T)\right) \cdot 2.036$$

$Upws := UT \cdot dpws$ Calculation of saturated water vapor pressure uncertainty

$Upws = 0.00675$

$\phi cal := 0.30$ Relative Humidity in cold air loop - input

$U\phi := 0.02$ Relative Humidity uncertainty - input

$pw := \phi cal \cdot pws$ Calculation of water vapor pressure, psi

$$Upw := \left[\left[\left(\frac{d}{d\phi cal} \phi cal \cdot pws\right) \cdot U\phi\right]^2 + \left[\left(\frac{d}{dpws} \phi cal \cdot pws\right) \cdot Upws\right]^2\right]$$

$Upw = 0.00753$ Calculation of water vapor pressure uncertainty

$Pb := 29.921$ Barometric Pressure - input in. Hg

$UPb := 0.01$ Barometric Pressure uncertainty - input in. Hg

$$Wcal := 0.62198 \cdot \frac{pw}{(Pb - pw)}$$ Calculate humidity ratio for cold air loop

$Wcal = 0.002$

$$UWcal := \left[\left[\left[\frac{d}{dpw} 0.62198 \cdot \frac{pw}{(Pb - pw)}\right] \cdot Upw\right]^2 + \left[\left[\frac{d}{dPb} 0.62198 \cdot \frac{pw}{(Pb - pw)}\right] \cdot UPb\right]^2\right]^{\frac{1}{2}}$$

$UWcal = 1.577 \cdot 10^{-4}$

$\frac{UWcal}{Wcal} \cdot 100 = 6.947$ Calculate humidity ratio uncertainty for cold air loop

$$\rho cal := \frac{Pb}{(0.7543 \cdot T) \cdot (1 + 1.6078 \cdot Wcal)}$$ Calculate air density in cold air loop, lb/cuft

$\rho cal = 0.07755$

$$vcal := \frac{1}{\rho cal}$$ Calculate specific density in cold air loop, cuft/lb

$vcal = 12.896$

$$UT\rho cal := \left[\left[\frac{d}{dT}\frac{Pb}{(0.7543 \cdot T) \cdot (1 + 1.6078 \cdot Wcal)}\right] \cdot UT\right]$$ Calculate dry bulb temperature uncertainty with respect to air density

$$UWcal\rho cal := \left[\left[\frac{d}{dWcal}\frac{Pb}{(0.7543 \cdot T) \cdot (1 + 1.6078 \cdot Wcal)}\right] \cdot UWcal\right]$$ Calculate humidity ratio uncertainty with respect air density on cold air loop side

$$UPb\rho cal := \left[\left[\frac{d}{dPb}\frac{Pb}{(0.7543 \cdot T) \cdot (1 + 1.6078 \cdot Wcal)}\right] \cdot UPb\right]$$ Calculate barometric pressure uncertainty with respect to air density on cold air loop side

$$U\rho cal := \left[(UT\rho cal)^2 + (UWcal\rho cal)^2 + (UPb\rho cal)^2\right]^{\frac{1}{2}}$$

$U\rho cal = 8.272 \cdot 10^{-5}$ air density uncertainty on the cold air loop side

$$\frac{U\rho cal}{\rho cal} \cdot 100 = 0.107$$

$Thal := 45$ Dry bulb Air temperature in °F in cold air loop airflow measuring station

$T := (Thal + 459.67)$ Conversion to R

$C8 := -10440.397$
$C9 := -11.29465$ Coefficients for
$C10 := -0.027022355$ calculating saturated
$C11 := 0.00001289036$ water vapor pressure
$C12 := -0.000000002478068$
$C13 := 6.5459673$

$$pws := \exp\left(\frac{C8}{T} + C9 + C10 \cdot T + C11 \cdot T^2 + C12 \cdot T^3 + C13 \cdot \ln(T)\right) \cdot 2.036$$

$pws = 0.30042$ Calculation of saturated water vapor pressure on cold air loop side, psi

$$dpws := \frac{d}{dT}\exp\left(\frac{C8}{T} + C9 + C10 \cdot T + C11 \cdot T^2 + C12 \cdot T^3 + C13 \cdot \ln(T)\right) \cdot 2.036$$

$Upws := UT \cdot dpws$ Calculation of saturated water vapor pressure uncertainty

$Upws = 0.00572$ Relative Humidity in hot air loop - input

$\phi hal := 0.70$ Relative Humidity uncertainty - input

$pw := \phi hal \cdot pws$

$pw = 0.21$ Calculation of water vapor pressure, psi

$$Upw := \left[\left[\left(\frac{d}{d\phi hal}\phi hal \cdot pws\right)\cdot U\phi\right]^2 + \left[\left(\frac{d}{dpws}\phi hal \cdot pws\right)\cdot Upws\right]^2\right]^{\frac{1}{2}}$$

$Upw = 0.00722$ Calculation of water vapor pressure uncertainty

$Pb := 29.921$ Barometric Pressure - input in. Hg

$$Whal := 0.62198\cdot\frac{pw}{(Pb - pw)}$$ Calculate humidity ratio for hot air loop

$Whal = 0.004$

$$UWhal := \left[\left[\left[\frac{d}{dpw}0.62198\cdot\frac{pw}{(Pb - pw)}\right]\cdot Upw\right]^2 + \left[\left[\frac{d}{dPb}0.62198\cdot\frac{pw}{(Pb - pw)}\right]\cdot UPb\right]^2\right]^{\frac{1}{2}}$$

$UWhal = 1.522\cdot10^{-4}$ Calculate humidity ratio uncertainty for hot air loop

$\frac{UWhal}{Whal}\cdot 100 = 3.457$

+

$$\rho hal := \frac{Pb}{(0.7543\cdot T)\cdot(1 + 1.6078\cdot Whal)}$$ Calculate air density in hot air loop, lb/cuft

$\rho hal = 0.07805$

$$\nu hal := \frac{1}{\rho hal}$$ Calculate specific density in hot air loop, cuft/lb

$\nu hal = 12.813$

$$UT\rho hal := \left[\left[\frac{d}{dT}\frac{Pb}{(0.7543\cdot T)\cdot(1 + 1.6078\cdot Whal)}\right]\cdot UT\right]$$ Calculate dry bulb temperature uncertainty with respect to air density

$$UWcal\rho hal := \left[\left[\frac{d}{dWhal}\frac{Pb}{(0.7543\cdot T)\cdot(1 + 1.6078\cdot Whal)}\right]\cdot UWhal\right]$$ Calculate humidity ratio uncertainty with respect air density on hot air loop side

$$UPb\rho hal := \left[\left[\frac{d}{dPb}\frac{Pb}{(0.7543\cdot T)\cdot(1 + 1.6078\cdot Whal)}\right]\cdot UPb\right]$$ Calculate barometric pressure uncertainty with respect to air density on hot air loop side

$$U\rho hal := \left[(UT\rho hal)^2 + (UWcal\rho hal)^2 + (UPb\rho hal)^2\right]^{\frac{1}{2}}$$

$U\rho hal = 8.378\cdot10^{-5}$ air density uncertainty on the hot air loop side

$\frac{U\rho hal}{\rho hal}\cdot 100 = 0.107$

$hcal := 0.08$ Velocity pressure at air flow measuring station on cold air loop side, inches w.c.

$Uhcal := 0.002$ Velocity pressure uncertainty at air flow measuring station on cold air loop side, inches w.c.

$hhal := 0.0805168$ Velocity pressure at air flow measuring station on hot air loop side, inches w.c.

$Uhhal := 0.002$ Velocity pressure uncertainty at air flow measuring station on hot air loop side, inches w.c.

$vcal := 1096 \cdot \sqrt{\frac{hcal}{\rho cal}}$ Air Velocity at air flow measuring station on cold air loop side, fpm

$vcal = 1113.2$

$vhal := 1096 \cdot \sqrt{\frac{hhal}{\rho hal}}$ Air Velocity at air flow measuring station on hot air loop side, fpm

$vhal = 1113.2$

$$Uvcal := \left[\left[\left(\frac{d}{dhcal} 1096 \cdot \sqrt{\frac{hcal}{\rho cal}}\right) \cdot Uhcal\right]^2 + \left[\left(\frac{d}{d\rho cal} 1096 \cdot \sqrt{\frac{hcal}{\rho cal}}\right) \cdot U\rho cal\right]^2\right]^{\frac{1}{2}}$$

$\frac{Uvcal}{vcal} \cdot 100 = 1.251$ Air Velocity uncertainty at air flow measuring station on cold air loop side, fpm

$$Uvhal := \left[\left[\left(\frac{d}{dhhal} 1096 \cdot \sqrt{\frac{hhal}{\rho hal}}\right) \cdot Uhhal\right]^2 + \left[\left(\frac{d}{d\rho hal} 1096 \cdot \sqrt{\frac{hhal}{\rho hal}}\right) \cdot U\rho hal\right]^2\right]^2$$

$\frac{Uvhal}{vhal} \cdot 100 = 1.243$ Air Velocity uncertainty at air flow measuring station on hot air loop side, fpm

$Ld := 14$ Duct dimension, Ld, inches

$Wd := 14$ Duct dimension, Wd, inches

$ULd := 0.03125$ Duct dimension uncertainty, Ld, inches

$UWd := 0.03125$ Duct dimension uncertainty, Wd, inches

$Ad := Ld \cdot \frac{Wd}{144}$ Duct cross sectional area, Ad, sqft

$Ad = 1.361$

$$UAd := \left[\left[\left(\frac{d}{dLd} Ld \cdot \frac{Wd}{144} \right) \cdot ULd \right]^2 + \left[\left(\frac{d}{dWd} Ld \cdot \frac{Wd}{144} \right) \cdot UWd \right]^2 \right]^{\frac{1}{2}}$$

$\frac{UAd}{Ad} \cdot 100 = 0.316$ Duct cross sectional area Uncertainty, Ad, sqft

$qcal := vcal \cdot Ad$ Airflow rate uncertainty on the cold air loop side

$qcal = 1515$

$Ccal := 0.24 \cdot \rho cal \cdot vcal \cdot Ad$ Specific heat on the cold air loop side

$qhal := vhal \cdot Ad$

$qhal = 1515$ Airflow rate uncertainty on the hot air loop side

$Chal := 0.24 \cdot \rho hal \cdot vhal \cdot Ad$ Specific heat on the cold air loop side

$$Uqcal := \left[\left[\left(\frac{d}{dvcal} vcal \cdot Ad \right) \cdot Uvcal \right]^2 + \left[\left(\frac{d}{dAd} vcal \cdot Ad \right) \cdot UAd \right]^2 \right]^{\frac{1}{2}}$$

$Uqcal = 19.551$ Airflow rate uncertainty on the cold air loop side

$\frac{Uqcal}{qcal} \cdot 100 = 1.29$

$$U\rho calCcal := \left[\left(\frac{d}{d\rho cal} 0.24 \cdot \rho cal \cdot vcal \cdot Ad \right) \cdot U\rho cal \right]$$ Air density uncertainty w.r.t. specific heat on cold air loop side

$$U\rho calCcal := \left[\left(\frac{d}{d\rho cal} 0.24 \cdot \rho cal \cdot vcal \cdot Ad \right) \cdot U\rho cal \right]$$ Air density uncertainty w.r.t. specific heat on cold air loop side

$$UvcalCcal := \left(\frac{d}{dvcal} 0.24 \cdot \rho cal \cdot vcal \cdot Ad \right) \cdot Uvcal$$ Air velocity uncertainty w.r.t. specific heat on cold air loop side

$$UAdCcal := \left[\left(\frac{d}{dAd} 0.24 \cdot \rho cal \cdot vcal \cdot Ad \right) \cdot UAd \right]$$ Duct Area uncertainty w.r.t. specific heat on cold air loop side

$$UCcal := \left[(U\rho calCcal)^2 + (UvcalCcal)^2 + (UAdCcal)^2 \right]^{\frac{1}{2}}$$

$\frac{UCcal}{Ccal} \cdot 100 = 1.295$ Specific heat uncertainty on the cold air loop side

$$U\rho halChal := \left[\left(\frac{d}{d\rho hal} 0.24 \cdot \rho hal \cdot vhal \cdot Ad \right) \cdot U\rho hal \right]$$ Air density uncertainty w.r.t. specific heat on hot air loop side

$$UvhalChal := \left(\frac{d}{dvhal} 0.24 \cdot \rho hal \cdot vhal \cdot Ad \right) \cdot Uvhal$$ Air velocity uncertainty w.r.t. specific heat on hot air loop side

$$UAdChal := \left[\left(\frac{d}{dAd} 0.24 \cdot \rho hal \cdot vhal \cdot Ad \right) \cdot UAd \right]$$ Duct Area uncertainty w.r.t. specific heat on hot air loop side

$$UChal := \left[(U\rho halChal)^2 + (UvhalChal)^2 + (UAdChal)^2 \right]^{\frac{1}{2}}$$

$\frac{UChal}{Chal} \cdot 100 = 1.287$ Specific heat uncertainty on the hot air loop side

$ms := \rho cal \cdot vcal \cdot Ad$ Mass airflow rate on the cold air loop side

$ms = 117.498$

$me := \rho hal \cdot vhal \cdot Ad$ Mass airflow rate on the hot air loop side

$me = 118.257$

$$Ums := \left[\left[\left(\frac{d}{d\rho cal} \rho cal \cdot vcal \cdot Ad \right) \cdot U\rho cal \right]^2 + \left[\left(\frac{d}{dvcal} \rho cal \cdot vcal \cdot Ad \right) \cdot Uvcal \right]^2 + \left[\left(\frac{d}{dAd} \rho cal \cdot vcal \cdot Ad \right) \cdot UAd \right]^2 \right]$$

$Ums = 2.3144$ Mass airflow rate uncertainty on the cold air loop side

$$Ume := \left[\left[\left(\frac{d}{d\rho hal} \rho hal \cdot vhal \cdot Ad \right) \cdot U\rho hal \right]^2 + \left[\left(\frac{d}{dvhal} \rho hal \cdot vhal \cdot Ad \right) \cdot Uvhal \right]^2 + \left[\left(\frac{d}{dAd} \rho hal \cdot vhal \cdot Ad \right) \cdot UAd \right]^2 \right]$$

$Ume = 2.3167$ Mass airflow rate uncertainty on the hot air loop side

$Tci := 20$	Cold air inlet temperature to hx
$Tco := 47.35$	Cold air outlet temperature to hx
$Thi := 72$	Hot air inlet temperature to hx
$Tho := 44.65$	Hot air outlet temperature to hx
$Ccal = 28.199$	Hot air outlet temperature to hx
$Chal = 28.382$	Hot air outlet temperature to hx
$UTci := UT$	Cold air inlet temperature to hx uncertainty
$UTco := UT$	Cold air outlet temperature to hx uncertainty
$UThi := UT$	Hot air inlet temperature to hx uncertainty
$UTho := UT$	Hot air outlet temperature to hx uncertainty

$me := if(ms \le me, ms, me)$ $ms := if(me \le ms, me, ms)$

$\varepsilon := \frac{ms}{me} \cdot \frac{Tco - Tci}{(Thi - Tci)}$ Sensible effectiveness on cold air loop side

$\varepsilon e := \frac{me}{ms} \cdot \frac{Thi - Tho}{Thi - Tci}$ Sensible effectiveness on hot air loop side

$\frac{ms}{me} = 1$ $\frac{me}{ms} = 1$

$\varepsilon = 0.526$

$\varepsilon e = 0.526$

$$Ums\varepsilon := \left[\left[\frac{d}{dms\,me}\frac{ms}{}\cdot\frac{Tco - Tci}{(Thi - Tci)}\right]\cdot Ums\right]$$ Uncertainty of cold air loop mass flow rate w.r.t. sensible effectiveness

$$Ume\varepsilon := \left[\frac{d}{dme\,me}\frac{ms}{}\cdot\frac{Tco - Tci}{(Thi - Tci)}\right]\cdot Ume$$ Uncertainty of hot air loop mass flow rate w.r.t. sensible effectiveness

$$UTco\varepsilon := \left[\left[\frac{d}{dTco\,me}\frac{ms}{}\cdot\frac{Tco - Tci}{(Thi - Tci)}\right]\cdot UTco\right]$$ Uncertainty of cold air temperature leaving hx w.r.t. sensible effectiveness

$$UTci\varepsilon := \left[\left[\frac{d}{dTci\,me}\frac{ms}{}\cdot\frac{Tco - Tci}{(Thi - Tci)}\right]\cdot UTci\right]$$ Uncertainty of cold air temperature entering hx w.r.t. sensible effectiveness

$$UThi\varepsilon := \left[\left[\frac{d}{dThi\,me}\frac{ms}{}\cdot\frac{Tco - Tci}{(Thi - Tci)}\right]\cdot UThi\right]$$ Uncertainty of hot air temperature entering hx w.r.t. sensible effectiveness

$$U\varepsilon := \left[(Ums\varepsilon)^2 + (Ume\varepsilon)^2 + (UTco\varepsilon)^2 + (UTci\varepsilon)^2 + \left[(UThi\varepsilon)^2\right]\right]^{\frac{1}{2}}$$

$U\varepsilon = 0.01881$ Sensible effectiveness uncertainty for the cold air loop side

$$Ums\varepsilon c := \left[\left[\frac{d}{dms\,me}\frac{ms}{}\cdot\frac{Tco - Tci}{(Thi - Tci)}\right]\cdot Ums\right]$$ Uncertainty of cold air loop mass flow rate w.r.t. sensible effectiveness

$$Ume\varepsilon c := \left[\left[\frac{d}{dme\,me}\frac{ms}{}\cdot\frac{Tco - Tci}{(Thi - Tci)}\right]\cdot Ume\right]$$ Uncertainty of hot air loop mass flow rate w.r.t. sensible effectiveness

$$UTco\varepsilon c := \left[\left[\frac{d}{dTco\,me}\frac{ms}{}\cdot\frac{Tco - Tci}{(Thi - Tci)}\right]\cdot UTco\right]$$ Uncertainty of cold air temperature leaving hx w.r.t. sensible effectiveness

$$UTci\varepsilon c := \left[\frac{d}{dTci\,me}\frac{ms}{}\cdot\frac{Tco - Tci}{(Thi - Tci)}\right]\cdot UTci$$ Uncertainty of cold air temperature entering hx w.r.t. sensible effectiveness

$$UThi\varepsilon c := \left[\frac{d}{dThi\,me}\frac{ms}{}\cdot\frac{Tco - Tci}{(Thi - Tci)}\right]\cdot UThi$$ Uncertainty of hot air temperature entering hx w.r.t. sensible effectiveness

$$Umsme\varepsilon c := \left|\left[\frac{d}{dms\,me}\frac{ms}{}\cdot\frac{Tco - Tci}{(Thi - Tci)}\right]\cdot\left[\frac{d}{dme\,me}\frac{ms}{}\cdot\frac{Tco - Tci}{(Thi - Tci)}\right]\cdot Ums\cdot Ume\right|$$

Uncertainty co-variance of hot air mass flow rate and cold air mass flow rate w.r.t. sensible effectiveness

$$U\varepsilon c := \left[(Ums\varepsilon c)^2 + (Ume\varepsilon c)^2 + (UTco\varepsilon c)^2 + (UTci\varepsilon c)^2 + (UThi\varepsilon c)^2 + 2\cdot(Umsme\varepsilon c)\right]^{\frac{1}{2}}$$

$U\varepsilon c = 0.024$ Sensible effectiveness uncertainty for the cold air loop side containing co-variance between cold and hot air loop mass flow rates

$$\theta\varepsilon := \frac{U\varepsilon}{\varepsilon}\cdot 100$$ Normalized effectiveness uncertainty (non co-variance)

$\theta\varepsilon = 3.576$

$$\theta\varepsilon c := \frac{U\varepsilon c}{\varepsilon}\cdot 100$$ Normalized effectiveness uncertainty with co-variance

$\theta\varepsilon c = 4.533$

$$\varepsilon ave := \frac{ms\cdot(Tco - Tci) + me\cdot(Thi - Tho)}{2\cdot ms\cdot(Thi - Tci)}$$

$\varepsilon ave = 0.526$ Average effectiveness

$$Ums\varepsilon ave := \left[\frac{d}{dms}\frac{ms\cdot(Tco - Tci) + me\cdot(Thi - Tho)}{2\cdot ms\cdot(Thi - Tci)}\right]\cdot Ums$$ Uncertainty of cold air loop mass flow rate w.r.t. average sensible effectiveness

$$UTco\varepsilon ave := \left[\left[\frac{d}{dTco}\frac{ms\cdot(Tco - Tci) + me\cdot(Thi - Tho)}{2\cdot ms\cdot(Thi - Tci)}\right]\cdot UTco\right]$$ Uncertainty of cold air temperature leaving hx w.r.t. average sensible effectiveness

$$UTci\varepsilon ave := \left[\frac{d}{dTci}\frac{ms\cdot(Tco - Tci) + me\cdot(Thi - Tho)}{2\cdot ms\cdot(Thi - Tci)}\right]\cdot UTci$$ Uncertainty of cold air temperature entering hx w.r.t. average sensible effectiveness

$$UThi\varepsilon ave := \left[\left[\frac{d}{dThi}\frac{ms\cdot(Tco - Tci) + me\cdot(Thi - Tho)}{2\cdot ms\cdot(Thi - Tci)}\right]\cdot UThi\right]$$ Uncertainty of hot air temperature entering hx w.r.t. average sensible effectiveness

$$UTho\varepsilon ave := \left[\left[\frac{d}{dTho}\frac{ms\cdot(Tco - Tci) + me\cdot(Thi - Tho)}{2\cdot ms\cdot(Thi - Tci)}\right]\cdot UTho\right]$$ Uncertainty of hot air temperature leaving hx w.r.t. average sensible effectiveness

$$Ume\varepsilon ave := \left[\frac{d}{dme}\frac{ms\cdot(Tco - Tci) + me\cdot(Thi - Tho)}{2\cdot ms\cdot(Thi - Tci)}\right]\cdot Ume$$ Uncertainty of hot air loop mass flow rate w.r.t. average sensible effectiveness

$$U\varepsilon ave := \left[(Ums\varepsilon ave)^2 + UTco\varepsilon ave^2 + (UTci\varepsilon ave)^2 + (UThi\varepsilon ave)^2 + (UTho\varepsilon ave)^2 + (Ume\varepsilon ave)^2\right]^{\frac{1}{2}}$$

$$Umems\varepsilon ave := \left|\left[\frac{d}{dms}\frac{ms\cdot(Tco - Tci) + me\cdot(Thi - Tho)}{2\cdot ms\cdot(Thi - Tci)}\right]\cdot\left[\frac{d}{dme}\frac{ms\cdot(Tco - Tci) + me\cdot(Thi - Tho)}{2\cdot ms\cdot(Thi - Tci)}\right]\cdot Ums\cdot Ume\right|$$

$$Ua := \left[(Ums\varepsilon ave)^2 + UTco\varepsilon ave^2 + (UTci\varepsilon ave)^2 + (UThi\varepsilon ave)^2 + (UTho\varepsilon ave)^2 + (Ume\varepsilon ave)^2\right]$$

$$U\varepsilon avec := \left(Ua^2 + 2 \cdot Umems\varepsilon ave\right)^{\frac{1}{2}}$$

Average sensible effectiveness uncertainty with covariance

$U\varepsilon ave = 0.01$

$U\varepsilon avec = 0.007$

$\theta\varepsilon ave := \frac{U\varepsilon ave}{\varepsilon ave} \cdot 100$ Normalized average sensible effectiveness uncertainty (non co-variance)

$\theta\varepsilon avec := \frac{U\varepsilon avec}{\varepsilon ave} \cdot 100$ Normalized average sensible effectiveness uncertainty with co-variance

$\theta\varepsilon ave = 1.902$

$\theta\varepsilon avec = 1.394$

$$UThi\varepsilon ave := \left[\left[\frac{d}{dThi}\frac{ms\cdot(Tco - Tci) + me\cdot(Thi - Tho)}{2\cdot ms\cdot(Thi - Tci)}\right]\cdot UThi\right]$$ Uncertainty of hot air temperature entering hx w.r.t. average sensible effectiveness

$$UTho\varepsilon ave := \left[\left[\frac{d}{dTho}\frac{ms\cdot(Tco - Tci) + me\cdot(Thi - Tho)}{2\cdot ms\cdot(Thi - Tci)}\right]\cdot UTho\right]$$ Uncertainty of hot air temperature leaving hx w.r.t. average sensible effectiveness

$$Ume\varepsilon ave := \left[\frac{d}{dme}\frac{ms\cdot(Tco - Tci) + me\cdot(Thi - Tho)}{2\cdot ms\cdot(Thi - Tci)}\right]\cdot Ume$$ Uncertainty of hot air loop mass flow rate w.r.t. average sensible effectiveness

$$U\varepsilon ave := \left[(Ums\varepsilon ave)^2 + UTco\varepsilon ave^2 + (UTci\varepsilon ave)^2 + (UThi\varepsilon ave)^2 + (UTho\varepsilon ave)^2 + (Ume\varepsilon ave)^2\right]^{\frac{1}{2}}$$

$$Umems\varepsilon ave := \left[\left[\frac{d}{dms}\frac{ms\cdot(Tco - Tci) + me\cdot(Thi - Tho)}{2\cdot ms\cdot(Thi - Tci)}\right]\cdot\left[\frac{d}{dme}\frac{ms\cdot(Tco - Tci) + me\cdot(Thi - Tho)}{2\cdot ms\cdot(Thi - Tci)}\right]\cdot Ums\cdot Ume\right]$$

$$Ua := \left[(Ums\varepsilon ave)^2 + UTco\varepsilon ave^2 + (UTci\varepsilon ave)^2 + (UThi\varepsilon ave)^2 + (UTho\varepsilon ave)^2 + (Ume\varepsilon ave)^2\right]$$

APPENDIX B: ELECTRICAL SCHEMATICS FOR HEAT RECOVERY TEST FACILITY

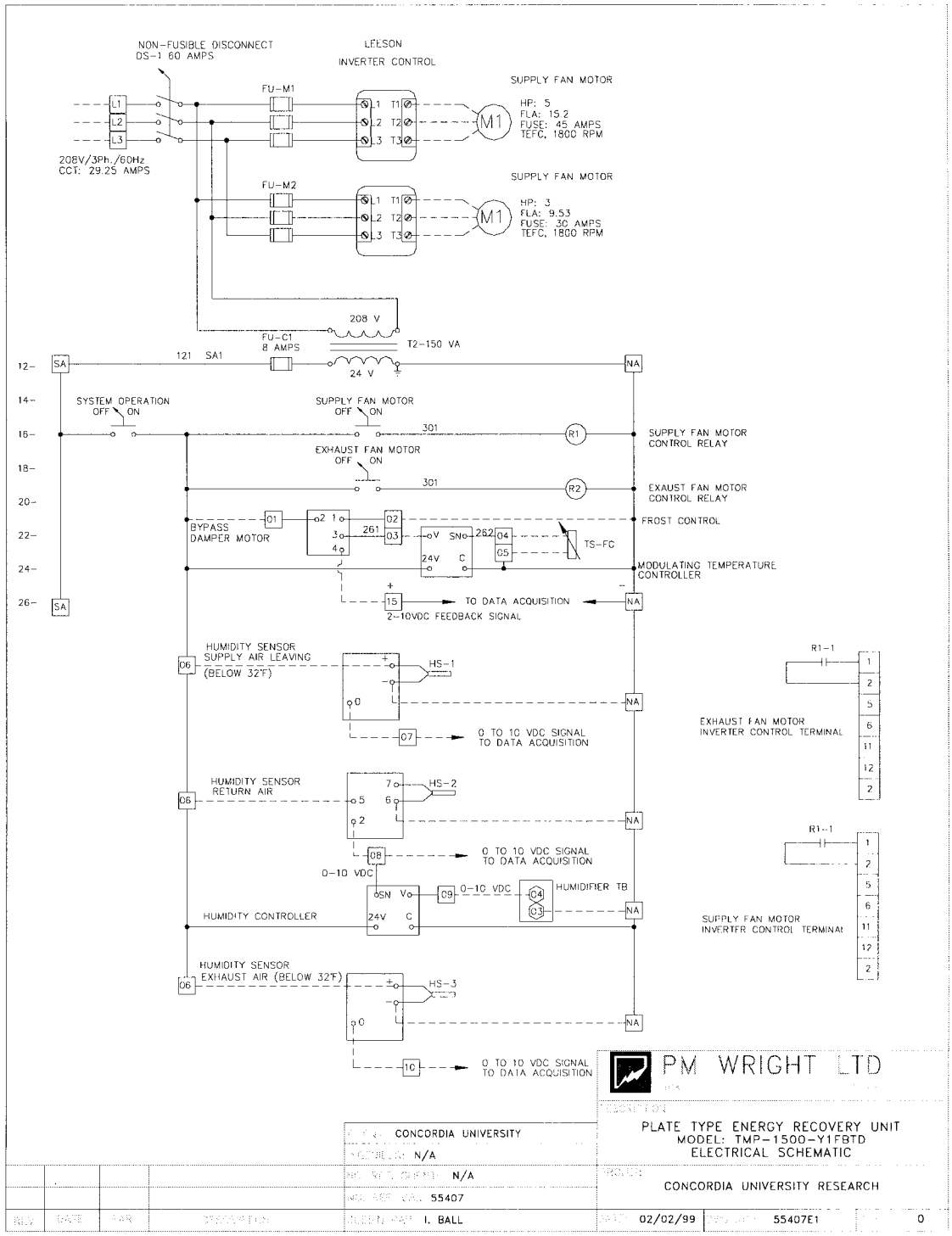

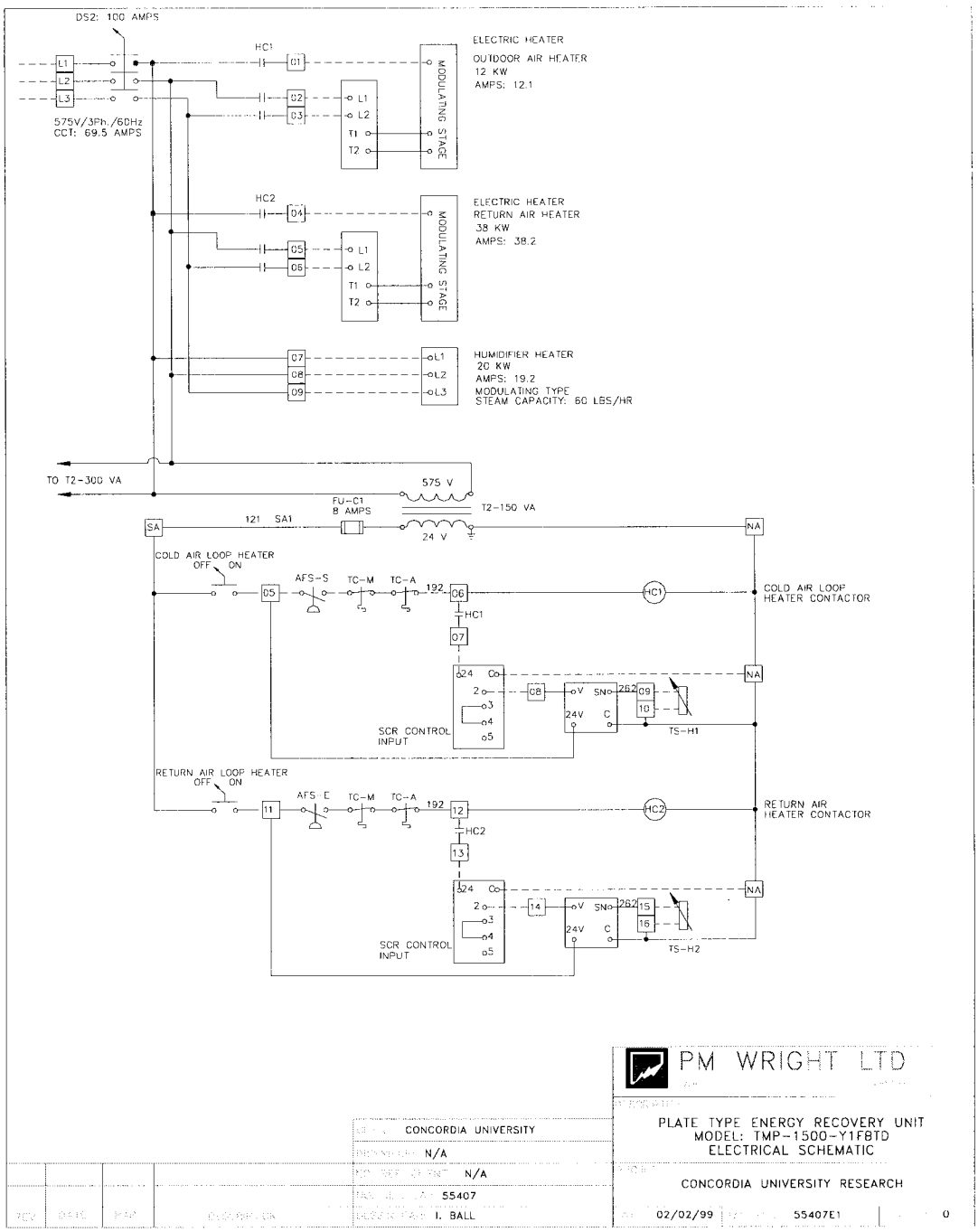

ELECTRICAL SCHEMATIC FOR HEAT RECOVERY TEST FACILITY

APPENDIX C: VISUAL BASIC PROGRAM FOR FORMATTING DATA, CALCULATIONS, AND POST TEST UNCERTAINTY ANALYSIS

```
*** PROGRAM FOR DATA PROCESSING FOR HEAT RECOVERY TEST DATA ***
Sub tempdist()

Dim irow As Integer, irowtot As Integer, endrow As Boolean
Dim SUMT1 As Single, SUMT2 As Single, SUMT3 As Single, SUMT4 As Single
Dim T1ave As Single, T2ave As Single, T3ave As Single, T4ave As Single, PB As Single
Dim T1CELL As Single, T2CELL As Single, T3CELL As Single, T4CELL As Single
Dim T1MIN As Single, T2MIN As Single, T3MIN As Single, T4MIN As Single
Dim T1MAX As Single, T2MAX As Single, T3MAX As Single, T4MAX As Single
Dim C8 As Single, C9 As Single, C10 As Single, C11 As Single, C12 As Single, C13 As Single
Dim PWSCALC8 As Single, PWSCALC9 As Single, PWSCALC10 As Single, PWSCALC11 As Single
Dim PWSCALC12 As Single, PWSCALC13 As Single
Dim PWSHALC8 As Single, PWSHALC9 As Single, PWSHALC10 As Single, PWSHALC11 As Single
Dim PWSHALC12 As Single, PWSHALC13 As Long
Dim CALDENS As Single, HALDENS As Single
Dim VPCAL As Single, VPHAL As Single, DUCTAREA As Single, HXAREA As Single
Dim SPCAL1 As Single, SPCAL2 As Single, SPHAL3 As Single, SPHAL4 As Single
Dim T1AVESUM As Single, T1aveMIN As Single, T1aveMAX As Single, T1MAXSUM As Single
Dim T1MAXMIN As Single, T1MAXMAX As Single, T1MINSUM As Single, T1MINMIN As Single
Dim T1MINMAX As Single, T1RANGESUM As Single, T1RANGEMIN As Single, T1RANGEMAX As Single
Dim T2AVESUM As Single, T2aveMIN As Single, T2aveMAX As Single, T2MAXSUM As Single
Dim T2MAXMIN As Single, T2MAXMAX As Single, T2MINSUM As Single, T2MINMIN As Single
Dim T2MINMAX As Single, T2RANGESUM As Single, T2RANGEMIN As Single, T2RANGEMAX As Single
Dim T3AVESUM As Single, T3aveMIN As Single, T3aveMAX As Single, T3MAXSUM As Single
Dim T3MAXMIN As Single, T3MAXMAX As Single, T3MINSUM As Single, T3MINMIN As Single
Dim T3MINMAX As Single, T3RANGESUM As Single, T3RANGEMIN As Single, T3RANGEMAX As Single
Dim T4AVESUM As Single, T4aveMIN As Single, T4aveMAX As Single, T4MAXSUM As Single
Dim T4MAXMIN As Single, T4MAXMAX As Single, T4MINSUM As Single, T4MINMIN As Single
Dim T4MINMAX As Single, T4RANGESUM As Single, T4RANGEMIN As Single, T4RANGEMAX As Single
Dim CALDENSSUM As Single, CALDENSMIN As Single, CALDENSMAX As Single, HALDENSSUM As Single
Dim HALDENSMIN As Single, HALDENSMAX As Single, CFMCALSUM As Single, CFMCALMIN As Single
Dim CFMCALMAX As Single, CFMHALSUM As Single, CFMHALMIN As Single, CFMHALMAX As Single
Dim EFFSUM As Single, EFFMIN As Single, EFFMAX As Single, VHXCALSUM As Single
Dim VHXCALMIN As Single, VHXCALMAX As Single, VHXHALSUM As Single, VHXHALMIN As Single
Dim VHXHALMAX As Single, DELTASPCALSUM As Single, DELTASPCALMIN As Single
Dim DELTASPCALMAX As Single, DELTASPHALSUM As Single, DELTASPHALMIN As Single
Dim DELTASPHALMAX As Single, TEMPEFF As Single, TEMPEFFSUM As Single, TEMPEFFMIN As Single
Dim TEMPEFFMAX As Single, CFMCALCFMHALSUM As Single, CFMCALCFMHALMIN As Single
Dim CFMCALCFMHALMAX As Single, T1AVESQSUM As Single, T1MINSQSUM As Single, T1MAXSQSUM As Single
Dim T1RANGESQSUM As Single, T2AVESQSUM As Single, T2MINSQSUM As Single, T2MAXSQSUM As Single
Dim T2RANGESQSUM As Single, T3AVESQSUM As Single, T3MINSQSUM As Single, T3MAXSQSUM As Single
Dim T3RANGESQSUM As Single, T4AVESQSUM As Single, T4MINSQSUM As Single, T4MAXSQSUM As Single
Dim T4RANGESQSUM As Single, CALDENSSQSUM As Single, HALDENSSQSUM As Single, CFMCALSQSUM As
Single
Dim CFMHALSQSUM As Single, VHXCALSQSUM As Single, VHXHALSQSUM As Single
Dim DELTASPHALSQSUM As Single, DELTASPCALSQSUM As Single, CFMCALCFMHALSQSUM As Single
Dim TEMPEFFSQSUM As Single, T1AVESTD As Single, T1MINSTD As Single, T1MAXSTD As Single
Dim T1RANGESTD As Single, T2AVESTD As Single, T2MINSTD As Single, T2MAXSTD As Single
Dim T2RANGESTD As Single, T3AVESTD As Single, T3MINSTD As Single, T3MAXSTD As Single
Dim T3RANGESTD As Single, T4AVESTD As Single, T4MINSTD As Single, T4MAXSTD As Single
Dim T4RANGESTD As Single, CALDENSSTD As Double, HALDENSSTD As Double, CFMCALSTD As Single
Dim CFMHALSTD As Single, VHXCALSTD As Single, VHXHALSTD As Single, DELTASPCALSTD As Single
Dim DELTASPHALSTD As Single, CFMCALCFMHALSTD As Single, TEMPEFFSTD As Single, EFFSTD As Single


UserForm1.Show
'ENTER BAROMETRIC PRESSURE
PB = UserForm1.TextBox1.Value
TBIAS = UserForm1.TextBox2.Value
RHBIAS = UserForm1.TextBox3.Value
VPBIAS = UserForm1.TextBox4.Value
SPBIAS = UserForm1.TextBox5.Value
PBBIAS = UserForm1.TextBox6.Value
```

```
LBIAS = UserForm1.TextBox7.Value

TBIAS = 0.5
RHBIAS = 0.02
VPBIAS = 0.002
SPBIAS = 0.05
PBBIAS = 0.01
LBIAS = 0.03125 / 12
Worksheets("temp dist").Cells(1, 1).Value = PB

rowcount = 0
endrow = True
'TRANSFER COLUMN LETTERS TO NUMBERS
A = 11
B = 12
C = 13
D = 14
E = 15
F = 16
G = 17
H = 18
I = 19
J = 20
K = 21
L = 22
M = 23
N = 24
O = 25
P = 26
Q = 27
R = 28

'COEFFICIENTS FOR CALCULATING WATER VAPOR PRESSURE FROM ASHRAE
C8 = -10440.397
C9 = -11.29465
C10 = -0.027022355
C11 = 0.00001289036
C12 = -0.000000002478068
C13 = 6.5459673

'DUCT AREA = (14 INCHES X 14 INCHES) / 144
DUCTAREA = 1.361111
Length = 1.167
'HEAT EXCHANGER AREA = 15.375 X 33.125/144 SQFT
HXAREA = 3.5368

'DETERMINE THE NUMBER OF ROWS IN SPREADSHEET
For irow = 1 To 999


rowcount = Worksheets("ch1").Cells(irow, 1).Value
endrow = IsNumeric(rowcount)
rowcheck = 65 - rowcount

If rowcheck > 40 Then
irowtot = irow - 4
GoTo line700
End If

Next

line700:
'Worksheets("temp dist").Cells(2, 1).Value = irow
'Worksheets("temp dist").Cells(4, 1).Value = irowtot
nrow = -5

'Initialize variables

T1AVESUM = 0
T1AVESQSUM = 0
```

T1aveMIN = 9999
T1aveMAX = -40

T1MAXSUM = 0
T1MAXSQSUM = 0
T1MAXMIN = 9999
T1MAXMAX = -40

T1MINSUM = 0
T1MINSQSUM = 0
T1MINMIN = 9999
T1MINMAX = -40

T1RANGESUM = 0
T1RANGESQSUM = 0
T1RANGEMIN = 9999
T1RANGEMAX = -40

T2AVESUM = 0
T2AVESQSUM = 0
T2aveMIN = 9999
T2aveMAX = -40

T2MAXSUM = 0
T2MAXSQSUM = 0
T2MAXMIN = 9999
T2MAXMAX = -40

T2MINSUM = 0
T2MINSQSUM = 0
T2MINMIN = 9999
T2MINMAX = -40

T2RANGESUM = 0
T2RANGESQSUM = 0
T2RANGEMIN = 9999
T2RANGEMAX = -40

RH2SUM = 0
RH2SQSUM = 0

T3AVESUM = 0
T3AVESQSUM = 0
T3aveMIN = 9999
T3aveMAX = -40

T3MAXSUM = 0
T3MAXSQSUM = 0
T3MAXMIN = 9999
T3MAXMAX = -40

T3MINSUM = 0
T3MINSQSUM = 0
T3MINMIN = 9999
T3MINMAX = -40

T3RANGESUM = 0
T3RANGESQSUM = 0
T3RANGEMIN = 9999
T3RANGEMAX = -40

T4AVESUM = 0
T4AVESQSUM = 0
T4aveMIN = 9999
T4aveMAX = -40

T4MAXSUM = 0
T4MAXSQSUM = 0
T4MAXMIN = 9999

T4MAXMAX = -40

T4MINSUM = 0
T4MINSQSUM = 0
T4MINMIN = 9999
T4MINMAX = -40

T4RANGESUM = 0
T4RANGESQSUM = 0
T4RANGEMIN = 9999
T4RANGEMAX = -40

RH4SUM = 0
RH4SQSUM = 0

CALDENSSUM = 0
CALDENSSQSUM = 0
CALDENSMIN = 9999
CALDENSMAX = -40

HALDENSSUM = 0
HALDENSSQSUM = 0
HALDENSMIN = 9999
HALDENSMAX = -40

CFMCALSUM = 0
CFMCALSQSUM = 0
CFMCALMIN = 9999
CFMCALMAX = -40

CFMHALSUM = 0
CFMHALSQSUM = 0
CFMHALMIN = 9999
CFMHALMAX = -40

EFFSUPSUM = 0
EFFSUPSQSUM = 0
EFFSUPMIN = 9999
EFFSUPMAX = -40

EFFEXHSUM = 0
EFFEXHSQSUM = 0
EFFEXHMIN = 9999
EFFEXHMAX = -40

EFFAVESUM = 0
EFFAVESQSUM = 0
EFFAVEMIN = 9999
EFFAVEMAX = -40

VHXCALSUM = 0
VHXCALSQSUM = 0
VHXCALMIN = 9999
VHXCALMAX = -40

VHXHALSUM = 0
VHXHALSQSUM = 0
VHXHALMIN = 9999
VHXHALMAX = -40

VPCALSUM = 0
VPHALSUM = 0

DELTASPCALSUM = 0
DELTASPCALSQSUM = 0
DELTASPCALMIN = 9999
DELTASPCALMAX = -40

DELTASPHALSUM = 0

```
DELTASPHALSQSUM = 0
DELTASPHALMIN = 9999
DELTASPHALMAX = -40

CFMCALCFMHALSUM = 0
CFMCALCFMHALSQSUM = 0
CFMCALCFMHALMIN = 9999
CFMCALCFMHALMAX = -40

TEMPEFFSUPSUM = 0
TEMPEFFSUPSQSUM = 0
TEMPEFFSUPMIN = 9999
TEMPEFFSUPMAX = -40

For irow = 1 To irowtot


'INSERT TIME COLUMN
If irow = 1 Then
Worksheets("results").Cells(irow + 2, 1).Value = 0
timeinc = 0
Else

time1 = Worksheets("time").Cells(irow, 1).Value
time2 = Worksheets("time").Cells((irow - 1), 1).Value

Worksheets("time").Cells(irow, 2).Value = time1 - time2
timeinc = timeinc + (time1 - time2)
Worksheets("results").Cells(irow + 2, 1).Value = timeinc
End If

'intialize variables
SUMT1 = 0
SUMT2 = 0
SUMT3 = 0
SUMT4 = 0
T1MIN = 999
T2MIN = 999
T3MIN = 999
T4MIN = 999

T1MAX = -40
T2MAX = -40
T3MAX = -40
T4MAX = -40


'--------------------------------------
For icol = 1 To 11

'SUM POINTS IN GRID 2, THAT HAS 12 EXTRA POINTS
T2CELL = Worksheets("ch2").Cells(irow, icol).Value
SUMT2 = SUMT2 + T2CELL
If T2CELL < T2MIN Then T2MIN = T2CELL
If T2CELL > T2MAX Then T2MAX = T2CELL

Next

For icol = 29 To 40


If icol < 40 Then
T2CELL = Worksheets("ch2").Cells(irow, icol).Value
If T2CELL < T2MIN Then T2MIN = T2CELL
If T2CELL > T2MAX Then T2MAX = T2CELL
SUMT2 = SUMT2 + T2CELL
End If

If icol = 40 Then
T2CELLA = Worksheets("ch1").Cells(irow, 41).Value
```

```
If T2CELLA < T2MIN Then T2MIN = T2CELLA
If T2CELLA > T2MAX Then T2MAX = T2CELLA
T2CELLB = Worksheets("ch2").Cells(irow, 41).Value
If T2CELLB < T2MIN Then T2MIN = T2CELLB
If T2CELLB > T2MAX Then T2MAX = T2CELLB
SUMT2 = SUMT2 + T2CELLA + T2CELLB
End If

'SUM ENTERING AND LEAVING TEMPERATURES FROM 12 POINT TEMP GRID
T1CELL = Worksheets("ch1").Cells(irow, icol).Value
SUMT1 = SUMT1 + T1CELL
T3CELL = Worksheets("ch3").Cells(irow, icol).Value
SUMT3 = SUMT3 + T3CELL
T4CELL = Worksheets("ch4").Cells(irow, icol).Value
SUMT4 = SUMT4 + T4CELL

'DETERMINE MAX AND MIN FOR T1, T3 AND T4
If T1CELL < T1MIN Then T1MIN = T1CELL
If T1CELL > T1MAX Then T1MAX = T1CELL

If T3CELL < T3MIN Then T3MIN = T3CELL
If T3CELL > T3MAX Then T3MAX = T3CELL

If T4CELL < T4MIN Then T4MIN = T4CELL
If T4CELL > T4MAX Then T4MAX = T4CELL

Next

'---------------------------------------
'CALCULATING AVERAGE : T1, T2, T3, and T4
Worksheets("results").Cells(irow + 2, 2).Value = SUMT1 / 12
T1ave = SUMT1 / 12
T1AVESUM = T1AVESUM + T1ave
T1AVESQSUM = T1AVESQSUM + (T1ave) ^ 2
If T1ave < T1aveMIN Then T1aveMIN = T1ave
If T1AVESUM > T1aveMAX Then T1aveMAX = T1ave

Worksheets("results").Cells(irow + 2, 6).Value = SUMT2 / 24
T2ave = SUMT2 / 24
T2AVESUM = T2AVESUM + T2ave
T2AVESQSUM = T2AVESQSUM + (T2ave) ^ 2
If T2AVESUM < T2aveMIN Then T2aveMIN = T2ave
If T2AVESUM > T2aveMAX Then T2aveMAX = T2ave

Worksheets("results").Cells(irow + 2, 12).Value = SUMT3 / 12
T3ave = SUMT3 / 12
T3AVESUM = T3AVESUM + T3ave
T3AVESQSUM = T3AVESQSUM + (T3ave) ^ 2
If T3AVESUM < T3aveMIN Then T3aveMIN = T3ave
If T3AVESUM > T3aveMAX Then T3aveMAX = T3ave

Worksheets("results").Cells(irow + 2, 16).Value = SUMT4 / 12
T4ave = SUMT4 / 12
T4AVESUM = T4AVESUM + T4ave
T4AVESQSUM = T4AVESQSUM + (T4ave) ^ 2
If T4AVESUM < T4aveMIN Then T4aveMIN = T4ave
If T4AVESUM > T4aveMAX Then T4aveMAX = T4ave

'INSERTING MIN, MAX AND MAX-MIN : T1, T2, T3, and T4
Worksheets("results").Cells(irow + 2, 3).Value = T1MAX
T1MAXSUM = T1MAXSUM + T1MAX
T1MAXSQSUM = T1MAXSQSUM + (T1MAX) ^ 2
If T1MAX < T1MAXMIN Then T1MAXMIN = T1MAX
If T1MAX > T1MAXMAX Then T1MAXMAX = T1MAX

Worksheets("results").Cells(irow + 2, 4).Value = T1MIN
T1MINSUM = T1MINSUM + T1MIN
T1MINSQSUM = T1MINSQSUM + (T1MIN) ^ 2
If T1MIN < T1MINMIN Then T1MINMIN = T1MIN
If T1MIN > T1MINMAX Then T1MINMAX = T1MIN
```

```
Worksheets("results").Cells(irow + 2, 5).Value = Abs(T1MAX - T1MIN)
T1RANGESUM = T1RANGESUM + Abs(T1MAX - T1MIN)
T1RANGESQSUM = T1RANGESQSUM + (T1MAX - T1MIN) ^ 2
If Abs(T1MAX - T1MIN) < T1RANGEMIN Then T1RANGEMIN = Abs(T1MAX - T1MIN)
If Abs(T1MAX - T1MIN) > T1RANGEMAX Then T1RANGEMAX = Abs(T1MAX - T1MIN)

Worksheets("results").Cells(irow + 2, 7).Value = T2MAX
T2MAXSUM = T2MAXSUM + T2MAX
T2MAXSQSUM = T2MAXSQSUM + (T2MAX) ^ 2
If T2MAX < T2MAXMIN Then T2MAXMIN = T2MAX
If T2MAX > T2MAXMAX Then T2MAXMAX = T2MAX

Worksheets("results").Cells(irow + 2, 8).Value = T2MIN
T2MINSUM = T2MINSUM + T2MIN
T2MINSQSUM = T2MINSQSUM + (T2MIN) ^ 2
If T2MIN < T2MINMIN Then T2MINMIN = T2MIN
If T2MIN > T2MINMAX Then T2MINMAX = T2MIN

Worksheets("results").Cells(irow + 2, 9).Value = Abs(T2MAX - T2MIN)
T2RANGESUM = T2RANGESUM + Abs(T2MAX - T2MIN)
T2RANGESQSUM = T2RANGESQSUM + (T2MAX - T2MIN) ^ 2
If Abs(T2MAX - T2MIN) < T2RANGEMIN Then T2RANGEMIN = Abs(T2MAX - T2MIN)
If Abs(T2MAX - T2MIN) > T2RANGEMAX Then T2RANGEMAX = Abs(T2MAX - T2MIN)

Worksheets("results").Cells(irow + 2, 13).Value = T3MAX
T3MAXSUM = T3MAXSUM + T3MAX
T3MAXSQSUM = T3MAXSQSUM + (T3MAX) ^ 2
If T3MAX < T3MAXMIN Then T3MAXMIN = T3MAX
If T3MAX > T3MAXMAX Then T3MAXMAX = T3MAX

Worksheets("results").Cells(irow + 2, 14).Value = T3MIN
T3MINSUM = T3MINSUM + T3MIN
T3MINSQSUM = T3MINSQSUM + (T3MIN) ^ 2
If T3MIN < T3MINMIN Then T3MINMIN = T3MIN
If T3MIN > T3MINMAX Then T3MINMAX = T3MIN

Worksheets("results").Cells(irow + 2, 15).Value = Abs(T3MAX - T3MIN)
T3RANGESUM = T3RANGESUM + Abs(T3MAX - T3MIN)
T3RANGESQSUM = T3RANGESQSUM + Abs(T3MAX - T3MIN) ^ 2
If Abs(T3MAX - T3MIN) < T3RANGEMIN Then T3RANGEMIN = Abs(T3MAX - T3MIN)
If Abs(T3MAX - T3MIN) > T3RANGEMAX Then T3RANGEMAX = Abs(T3MAX - T3MIN)

Worksheets("results").Cells(irow + 2, 17).Value = T4MAX
T4MAXSUM = T4MAXSUM + T4MAX
T4MAXSQSUM = T4MAXSQSUM + (T4MAX) ^ 2
If T4MAX < T4MAXMIN Then T4MAXMIN = T4MAX
If T4MAX > T4MAXMAX Then T4MAXMAX = T4MAX

Worksheets("results").Cells(irow + 2, 18).Value = T4MIN
T4MINSUM = T4MINSUM + T4MIN
T4MINSQSUM = T4MINSQSUM + (T4MIN) ^ 2
If T4MIN < T4MINMIN Then T4MINMIN = T4MIN
If T4MIN > T4MINMAX Then T4MINMAX = T4MIN

Worksheets("results").Cells(irow + 2, 19).Value = Abs(T4MAX - T4MIN)
T4RANGESUM = T4RANGESUM + Abs(T4MAX - T4MIN)
T4RANGESQSUM = T4RANGESQSUM + Abs(T4MAX - T4MIN) ^ 2
If Abs(T4MAX - T4MIN) < T4RANGEMIN Then T4RANGEMIN = Abs(T4MAX - T4MIN)
If Abs(T4MAX - T4MIN) > T4RANGEMAX Then T4RANGEMAX = Abs(T4MAX - T4MIN)

'RELATIVE HUMIDITY RH2 AND RH4 TO BE USED FOR AIR DENSITY CALCULATIONS
RH2 = Worksheets("ch1").Cells(irow, 44).Value / 100
Worksheets("results").Cells(irow + 2, 10).Value = RH2
RH2SUM = RH2SUM + RH2
RH2SQSUM = RH2SQSUM + (RH2) ^ 2

RH4 = Worksheets("ch1").Cells(irow, 46).Value / 100
Worksheets("results").Cells(irow + 2, 20).Value = RH4
RH4SUM = RH4SUM + RH4
```

```
RH4SQSUM = RH4SQSUM + (RH4) ^ 2

'CALCULATION OF SATURATED WATER VAPOR PRESSURE FOR CAL
TCAL = Worksheets("ch3").Cells(irow, 41).Value
PWSCALC8 = (C8) / (TCAL + 459.67)
PWSCALC10 = C10 * (TCAL + 459.67)
PWSCALC11 = C11 * ((TCAL + 459.67) ^ 2)
PWSCAL12 = C12 * ((TCAL + 459.67) ^ 3)
PWSCAL13 = C13 * ((Log(TCAL + 459.67) / Log(2.718282)))
PWSCAL = (2.036) * Exp(PWSCALC8 + C9 + PWSCALC10 + PWSCALC11 + PWSCAL12 + PWSCAL13)
PWSCALSUM = PWSCALSUM + PWSCAL

' CALCULATION OF CAL AIR DENSITY
CALDENS = 1 / (0.7543 * (TCAL + 459.67) * (1 + 1.6078 * (0.62198 * (RH2 * (2.036) * Exp((C8) / (TCAL + 459.67) + (C9)
+ (C10) * (TCAL + 459.67) + (C11) * ((TCAL + 459.67) ^ 2) + (C12) * ((TCAL + 459.67) ^ 3) + (C13) * ((Log(TCAL +
459.67) / Log(2.718282))))) / (PB - (RH2 * (2.036) * Exp((C8) / (TCAL + 459.67) + (C9) + (C10) * (TCAL + 459.67) + (C11)
* ((TCAL + 459.67) ^ 2) + (C12) * ((TCAL + 459.67) ^ 3) + (C13) * ((Log(TCAL + 459.67) / Log(2.718282)))))))) / PB)
'CALDENS = 1 / (0.7543 * (T2ave + 459.67) * (1 + 1.6078 * (0.62198 * (RH2 * PWSCAL) / (PB - (RH2 * PWSCAL)) / PB)))
Worksheets("results").Cells(irow + 2, 11).Value = CALDENS
CALDENSSUM = CALDENSSUM + CALDENS
CALDENSSQSUM = CALDENSSQSUM + (CALDENS) ^ 2
If CALDENS < CALDENSMIN Then CALDENSMIN = CALDENS
If CALDENS > CALDENSMAX Then CALDENSMAX = CALDENS

'CALCULATION OF SATURATED WATER VAPOR PRESSURE FOR HAL
THAL = Worksheets("ch4").Cells(irow, 41).Value
PWSHALC8 = (C8) / (THAL + 459.67)
PWSHALC10 = C10 * (THAL + 459.67)
PWSHALC11 = C11 * ((THAL + 459.67) ^ 2)
PWSHALC12 = C12 * ((THAL + 459.67) ^ 3)
PWSHALC13 = C13 * ((Log(THAL + 459.67) / Log(2.718282)))
PWSHAL = (2.036) * Exp(PWSHALC8 + C9 + PWSHALC10 + PWSHALC11 + PWSHALC12 + PWSHALC13)
PWSHALSUM = PWSHALSUM + PWSHAL

' CALCULATION OF HAL AIR DENSITY
HALDENS = 1 / (0.7543 * (THAL + 459.67) * (1 + 1.6078 * (0.62198 * (RH4 * (2.036) * Exp((C8) / (THAL + 459.67) + (C9)
+ (C10) * (THAL + 459.67) + (C11) * ((THAL + 459.67) ^ 2) + (C12) * ((THAL + 459.67) ^ 3) + (C13) * ((Log(THAL +
459.67) / Log(2.718282))))) / (PB - (RH4 * (2.036) * Exp((C8) / (THAL + 459.67) + (C9) + (C10) * (THAL + 459.67) + (C11)
* ((THAL + 459.67) ^ 2) + (C12) * ((THAL + 459.67) ^ 3) + (C13) * ((Log(THAL + 459.67) / Log(2.718282)))))))) / PB)
'HALDENS = 1 / (0.7543 * (T4ave + 459.67) * (1 + 1.6078 * (0.62198 * ((RH4 / 100) * PWSHAL) / (PB - ((RH4 / 100) *
PWSHAL)) / PB)))
Worksheets("results").Cells(irow + 2, 21).Value = HALDENS
HALDENSSUM = HALDENSSUM + HALDENS
HALDENSSQSUM = HALDENSSQSUM + (HALDENS) ^ 2
If HALDENS < HALDENSMIN Then HALDENSMIN = HALDENS
If HALDENS > HALDENSMAX Then HALDENSMAX = HALDENS

' CALCULATION OF CAL AND HAL CFM
VPCAL = Worksheets("ch1").Cells(irow, 42).Value
VPHAL = Worksheets("ch2").Cells(irow, 42).Value
VPCALSUM = VPCALSUM + VPCAL
VPCALSQSUM = VPCALSQSUM + (VPCAL) ^ 2
VPHALSUM = VPHALSUM + VPHAL
VPHALSQSUM = VPHALSQSUM + (VPHAL) ^ 2

CFMCAL = (1096 * Sqr(VPCAL / CALDENS)) * DUCTAREA
If CFMCAL = 0 Then GoTo line999
Worksheets("results").Cells(irow + 2, 22).Value = CFMCAL
CFMCALSUM = CFMCALSUM + CFMCAL
CFMCALSQSUM = CFMCALSQSUM + (CFMCAL) ^ 2
If CFMCAL < CFMCALMIN Then CFMCALMIN = CFMCAL
If CFMCAL > CFMCALMAX Then CFMCALMAX = CFMCAL

CFMHAL = (1096 * Sqr(VPHAL / HALDENS)) * DUCTAREA
Worksheets("results").Cells(irow + 2, 23).Value = CFMHAL
CFMHALSUM = CFMHALSUM + CFMHAL
CFMHALSQSUM = CFMHALSQSUM + (CFMHAL) ^ 2
If CFMHAL < CFMHALMIN Then CFMHALMIN = CFMHAL
If CFMHAL > CFMHALMAX Then CFMHALMAX = CFMHAL
```

```
'EFFECTIVENESS CALCULATION - SUPPLY, EXHAUST AND AVERAGE
If CFMHAL = 0 Then GoTo line999
TEMPEFFSUP = (T2ave - T1ave) / (T3ave - T1ave)
TEMPEFFEXH = (T3ave - T4ave) / (T3ave - T1ave)
Worksheets("results").Cells(irow + 2, 24).Value = (CALDENS * CFMCAL) / (HALDENS * CFMHAL)
Worksheets("results").Cells(irow + 2, 25).Value = TEMPEFFSUP
MSUP = CFMCAL * CALDENS
MEXH = CFMHAL * HALDENS
If MSUP < MEXH Then MMIN = MSUP
If MEXH < MSUP Then MMIN = MEXH

EFFSUP = (MSUP / MMIN) * TEMPEFFSUP
EFFEXH = (MEXH / MMIN) * TEMPEFFEXH
EFFAVE = (MSUP * (T2ave - T1ave) + MEXH * (T3ave - T4ave)) / (2 * MMIN * (T3ave - T1ave))
Worksheets("CHECK").Cells(irow + 2, 1).Value = (MSUP * (T2ave - T1ave) + MEXH * (T3ave - T4ave))
Worksheets("CHECK").Cells(irow + 2, 2).Value = (MMIN * (T3ave - T1ave))
CFMCALCFMHALSUM = CFMCALCFMHALSUM + (CFMCAL / CFMHAL)
CFMCALCFMHALSQSUM = CFMCALCFMHALSQSUM + (CFMCAL / CFMHAL) ^ 2
If (CFMCAL / CFMHAL) < CFMCALCFMHALMIN Then CFMCALCFMHALMIN = (CFMCAL / CFMHAL)
If (CFMCAL / CFMHAL) > CFMCALCFMHALMAX Then CFMCALCFMHALMAX = (CFMCAL / CFMHAL)

TEMPEFFSUPSUM = TEMPEFFSUPSUM + TEMPSUPEFF
TEMPEFFSUPSQSUM = TEMPEFFSUPSQSUM + (TEMPSUPEFF) ^ 2
If TEMPEFFSUP < TEMPEFFSUPMIN Then TEMPEFFSUPMIN = TEMPEFFSUP
If TEMPEFFSUP > TEMPEFFSUPMAX Then TEMPEFFSUPMAX = TEMPEFFSUP

Worksheets("results").Cells(irow + 2, 26).Value = EFFSUP
Worksheets("results").Cells(irow + 2, 27).Value = EFFEXH
Worksheets("results").Cells(irow + 2, 28).Value = EFFAVE
EFFSUPSUM = EFFSUPSUM + EFFSUP
EFFSUPSQSUM = EFFSUPSQSUM + (EFFSUP) ^ 2
If EFFSUP < EFFSUPMIN Then EFFSUPMIN = EFFSUP
If EFFSUP > EFFSUPMAX Then EFFSUPMAX = EFFSUP

EFFEXHSUM = EFFEXHSUM + EFFEXH
EFFEXHSQSUM = EFFEXHSQSUM + (EFFEXH) ^ 2
If EFFEXH < EFFEXHMIN Then EFFEXHMIN = EFFEXH
If EFFEXH > EFFEXHMAX Then EFFEXHMAX = EFFEXH

EFFAVESUM = EFFAVESUM + EFFAVE
EFFAVESQSUM = EFFAVESQSUM + (EFFAVE) ^ 2
If EFFAVE < EFFAVEMIN Then EFFAVEMIN = EFFAVE
If EFFAVE > EFFAVEMAX Then EFFAVEMAX = EFFAVE
'FACE VELOCITY AND STATIC PRESSURE DROP ACROSS HX FOR CAL AND HAL
VHXCAL = CFMCAL / HXAREA
VHXCALSUM = VHXCALSUM + VHXCAL
VHXCALSQSUM = VHXCALSQSUM + (VHXCAL) ^ 2
If VHXCAL < VHXCALMIN Then VHXCALMIN = VHXCAL
If VHXCAL > VHXCALMAX Then VHXCALMAX = VHXCAL

VHXHAL = CFMHAL / HXAREA
VHXHALSUM = VHXHALSUM + VHXHAL
VHXHALSQSUM = VHXHALSQSUM + (VHXHAL) ^ 2
If VHXHAL < VHXHALMIN Then VHXHALMIN = VHXHAL
If VHXHAL > VHXHALMAX Then VHXHALMAX = VHXHAL

Worksheets("results").Cells(irow + 2, 29).Value = VHXCAL
Worksheets("results").Cells(irow + 2, 30).Value = VHXHAL
SPCAL1 = Worksheets("ch1").Cells(irow, 43).Value
SPCAL2 = Worksheets("ch2").Cells(irow, 43).Value
SPHAL3 = Worksheets("ch3").Cells(irow, 43).Value
SPHAL4 = Worksheets("ch4").Cells(irow, 43).Value

DELTASPCAL = SPCAL2 - SPCAL1
DELTASPCALSUM = DELTASPCALSUM + DELTASPCAL
DELTASPCALSQSUM = DELTASPCALSQSUM + (DELTASPCAL) ^ 2
If DELTASPCAL < DELTASPCALMIN Then DELTASPCALMIN = DELTASPCAL
If DELTASPCAL > DELTASPCALMAX Then DELTASPCALMAX = DELTASPCAL

DELTASPHAL = SPHAL4 - SPHAL3
```

```
DELTASPHALSUM = DELTASPHALSUM + DELTASPHAL
DELTASPHALSQSUM = DELTASPHALSQSUM + (DELTASPHAL) ^ 2
If DELTASPHAL < DELTASPHALMIN Then DELTASPHALMIN = DELTASPHAL
If DELTASPHAL > DELTASPHALMAX Then DELTASPHALMAX = DELTASPHAL

Worksheets("results").Cells(irow + 2, 31).Value = DELTASPCAL
Worksheets("results").Cells(irow + 2, 32).Value = DELTASPHAL
nrow = nrow + 5


   'ENTERING COLD LOOP AIR TEMPERATURE
sumcoldEAT = SUMT1
   'LEAVING COLD LOOP AIR TEMPERATURE
sumcoldLAT = SUMT2 / 2

   'ENTERING HOT LOOP AIR TEMPERATURE
sumhotEAT = SUMT3

   'LEAVING HOT LOOP AIR TEMPERATURE
sumhotLAT = SUMT4


'**********COLD TOP**********************
Worksheets("temp dist").Cells(irow + nrow, 3) = sumcoldEAT / 12
Worksheets("temp dist").Cells(irow + nrow + 4, 3) = sumcoldLAT / 12
Worksheets("temp dist").Cells(irow + nrow + 2, 1) = sumhotEAT / 12
Worksheets("temp dist").Cells(irow + nrow + 2, 5) = sumhotLAT / 12

   ' tc10/ch1-b
Worksheets("temp dist").Cells(irow + nrow + 1, 2).Value = Worksheets("ch1").Cells(irow, B).Value

   'tc11/ch1-c+
Worksheets("temp dist").Cells(irow + nrow + 1, 3).Value = Worksheets("ch1").Cells(irow, C).Value

   'tc12/ch1-d
Worksheets("temp dist").Cells(irow + nrow + 1, 4).Value = Worksheets("ch1").Cells(irow, D).Value

   'tc13/ch1-e
Worksheets("temp dist").Cells(irow + nrow + 2, 2).Value = Worksheets("ch1").Cells(irow, E).Value

   'tc14/ch1-f
Worksheets("temp dist").Cells(irow + nrow + 2, 3).Value = Worksheets("ch1").Cells(irow, F).Value

   'tc15/ch1-g
Worksheets("temp dist").Cells(irow + nrow + 2, 4).Value = Worksheets("ch1").Cells(irow, G).Value

'tc16/ch1-h
Worksheets("temp dist").Cells(irow + nrow + 3, 2).Value = Worksheets("ch1").Cells(irow, H).Value

'tc17/ch1-i
Worksheets("temp dist").Cells(irow + nrow + 3, 3).Value = Worksheets("ch1").Cells(irow, I).Value

'tc18/ch1-j
Worksheets("temp dist").Cells(irow + nrow + 3, 4).Value = Worksheets("ch1").Cells(irow, J).Value

'**********COLD MIDDLE **********************
'INSERT AVERAGE COLD LOOP EAT/LAT AND HOT LOOP EAT/LAT FOR EACH TEMP GRID
Worksheets("temp dist").Cells(irow + nrow, 9) = sumcoldEAT / 12
Worksheets("temp dist").Cells(irow + nrow + 5, 9) = sumcoldLAT / 12
Worksheets("temp dist").Cells(irow + nrow + 2, 7) = sumhotEAT / 12
Worksheets("temp dist").Cells(irow + nrow + 2, 12) = sumhotLAT / 12

   ' tc300/ch2-C
Worksheets("temp dist").Cells(irow + nrow + 1, 8).Value = Worksheets("ch2").Cells(irow, C).Value

   'tc301/ch2-D
Worksheets("temp dist").Cells(irow + nrow + 1, 9).Value = Worksheets("ch2").Cells(irow, D).Value

   'tc302/ch1-E
Worksheets("temp dist").Cells(irow + nrow + 1, 10).Value = Worksheets("ch2").Cells(irow, E).Value
```

```
    'tc303/ch1-F
Worksheets("temp dist").Cells(irow + nrow + 1, 11).Value = Worksheets("ch2").Cells(irow, F).Value

    'tc304/ch1-G
Worksheets("temp dist").Cells(irow + nrow + 2, 8).Value = Worksheets("ch2").Cells(irow, G).Value

    'tc305/ch1-H
Worksheets("temp dist").Cells(irow + nrow + 2, 9).Value = Worksheets("ch2").Cells(irow, H).Value

    'tc306/ch1-I
Worksheets("temp dist").Cells(irow + nrow + 2, 10).Value = Worksheets("ch2").Cells(irow, I).Value

    'tc307/ch1-J
Worksheets("temp dist").Cells(irow + nrow + 2, 11).Value = Worksheets("ch2").Cells(irow, J).Value

    'tc308/ch1-K
Worksheets("temp dist").Cells(irow + nrow + 3, 8).Value = Worksheets("ch2").Cells(irow, K).Value

    'tc309/ch1-L
Worksheets("temp dist").Cells(irow + nrow + 3, 9).Value = Worksheets("ch2").Cells(irow, L).Value

    'tc310/ch1-M
Worksheets("temp dist").Cells(irow + nrow + 3, 10).Value = Worksheets("ch2").Cells(irow, M).Value

    'tc311/ch1-N
Worksheets("temp dist").Cells(irow + nrow + 3, 11).Value = Worksheets("ch2").Cells(irow, N).Value

    'tc312/ch1-O
Worksheets("temp dist").Cells(irow + nrow + 4, 8).Value = Worksheets("ch2").Cells(irow, O).Value

    'tc313/ch1-P
Worksheets("temp dist").Cells(irow + nrow + 4, 9).Value = Worksheets("ch2").Cells(irow, P).Value

    'tc314/ch1-Q
Worksheets("temp dist").Cells(irow + nrow + 4, 10).Value = Worksheets("ch2").Cells(irow, Q).Value

    'tc315/ch1-R
Worksheets("temp dist").Cells(irow + nrow + 4, 11).Value = Worksheets("ch2").Cells(irow, R).Value

'***********COLD BOTTOM **********************
'INSERT AVERAGE COLD LOOP EAT/LAT AND HOT LOOP EAT/LAT FOR EACH TEMP GRID
Worksheets("temp dist").Cells(irow + nrow, 16) = sumcoldEAT / 12
Worksheets("temp dist").Cells(irow + nrow + 4, 16) = sumcoldLAT / 12
Worksheets("temp dist").Cells(irow + nrow + 2, 14) = sumhotEAT / 12
Worksheets("temp dist").Cells(irow + nrow + 2, 18) = sumhotLAT / 12

    ' tc50/ch3-R
Worksheets("temp dist").Cells(irow + nrow + 1, 15).Value = Worksheets("ch3").Cells(irow, R).Value

    ' tc51/ch4-B
Worksheets("temp dist").Cells(irow + nrow + 1, 16).Value = Worksheets("ch4").Cells(irow, B).Value

   ' tc52/ch4-C
Worksheets("temp dist").Cells(irow + nrow + 1, 17).Value = Worksheets("ch4").Cells(irow, C).Value

   ' tc553/ch4-D
Worksheets("temp dist").Cells(irow + nrow + 2, 15).Value = Worksheets("ch4").Cells(irow, D).Value

   ' tc54/ch4-E
Worksheets("temp dist").Cells(irow + nrow + 2, 16).Value = Worksheets("ch4").Cells(irow, E).Value

   ' tc55/ch4-F
Worksheets("temp dist").Cells(irow + nrow + 2, 17).Value = Worksheets("ch4").Cells(irow, F).Value

   ' tc56/ch4-G
Worksheets("temp dist").Cells(irow + nrow + 3, 15).Value = Worksheets("ch4").Cells(irow, G).Value

   ' tc57/ch4-H
Worksheets("temp dist").Cells(irow + nrow + 3, 16).Value = Worksheets("ch4").Cells(irow, H).Value
```

```
  ' tc58/ch4-I
Worksheets("temp dist").Cells(irow + nrow + 3, 17).Value = Worksheets("ch4").Cells(irow, I).Value


'**********HOT TOP**********
Worksheets("temp dist").Cells(irow + nrow, 22) = sumcoldEAT / 12
Worksheets("temp dist").Cells(irow + nrow + 4, 22) = sumcoldLAT / 12
Worksheets("temp dist").Cells(irow + nrow + 2, 20) = sumhotEAT / 12
Worksheets("temp dist").Cells(irow + nrow + 2, 24) = sumhotLAT / 12

  ' tc20/ch1-K
Worksheets("temp dist").Cells(irow + nrow + 1, 21).Value = Worksheets("ch1").Cells(irow, K).Value

  'tc21/ch1-L
Worksheets("temp dist").Cells(irow + nrow + 1, 22).Value = Worksheets("ch1").Cells(irow, L).Value

  'tc22/ch1-M
Worksheets("temp dist").Cells(irow + nrow + 1, 23).Value = Worksheets("ch1").Cells(irow, M).Value

  'tc23/ch1-N
Worksheets("temp dist").Cells(irow + nrow + 2, 21).Value = Worksheets("ch1").Cells(irow, N).Value

  'tc24/ch1-O
Worksheets("temp dist").Cells(irow + nrow + 2, 22).Value = Worksheets("ch1").Cells(irow, O).Value

  'tc25/ch1-P
Worksheets("temp dist").Cells(irow + nrow + 2, 23).Value = Worksheets("ch1").Cells(irow, P).Value

'tc26/ch1-Q
Worksheets("temp dist").Cells(irow + nrow + 3, 21).Value = Worksheets("ch1").Cells(irow, Q).Value

'tc27/ch1-R
Worksheets("temp dist").Cells(irow + nrow + 3, 22).Value = Worksheets("ch1").Cells(irow, R).Value

'tc28/ch2-B
Worksheets("temp dist").Cells(irow + nrow + 3, 23).Value = Worksheets("ch2").Cells(irow, B).Value

'**********HOT MIDDLE **********
'INSERT AVERAGE COLD LOOP EAT/LAT AND HOT LOOP EAT/LAT FOR EACH TEMP GRID
Worksheets("temp dist").Cells(irow + nrow, 28) = sumcoldEAT / 12
Worksheets("temp dist").Cells(irow + nrow + 5, 28) = sumcoldLAT / 12
Worksheets("temp dist").Cells(irow + nrow + 2, 26) = sumhotEAT / 12
Worksheets("temp dist").Cells(irow + nrow + 2, 31) = sumhotLAT / 12

  ' tc400/ch3-B
Worksheets("temp dist").Cells(irow + nrow + 1, 27).Value = Worksheets("ch3").Cells(irow, B).Value

  'tc401/ch3-C
Worksheets("temp dist").Cells(irow + nrow + 1, 28).Value = Worksheets("ch3").Cells(irow, C).Value

  'tc402/ch3-D
Worksheets("temp dist").Cells(irow + nrow + 1, 29).Value = Worksheets("ch3").Cells(irow, D).Value

  'tc403/ch3-E
Worksheets("temp dist").Cells(irow + nrow + 1, 30).Value = Worksheets("ch3").Cells(irow, E).Value

  'tc404/ch3-F
Worksheets("temp dist").Cells(irow + nrow + 2, 27).Value = Worksheets("ch3").Cells(irow, F).Value

  'tc405/ch3-G
Worksheets("temp dist").Cells(irow + nrow + 2, 28).Value = Worksheets("ch3").Cells(irow, G).Value

  'tc406/ch3-H
Worksheets("temp dist").Cells(irow + nrow + 2, 29).Value = Worksheets("ch3").Cells(irow, H).Value

  'tc407/ch3-I
Worksheets("temp dist").Cells(irow + nrow + 2, 30).Value = Worksheets("ch3").Cells(irow, I).Value

  'tc408/ch3-J
```

```
Worksheets("temp dist").Cells(irow + nrow + 3, 27).Value = Worksheets("ch3").Cells(irow, J).Value

   'tc409/ch3-K
Worksheets("temp dist").Cells(irow + nrow + 3, 28).Value = Worksheets("ch3").Cells(irow, K).Value

   'tc410/ch3-L
Worksheets("temp dist").Cells(irow + nrow + 3, 29).Value = Worksheets("ch3").Cells(irow, L).Value

   'tc411/ch3-M
Worksheets("temp dist").Cells(irow + nrow + 3, 30).Value = Worksheets("ch3").Cells(irow, M).Value

   'tc412/ch3-N
Worksheets("temp dist").Cells(irow + nrow + 4, 27).Value = Worksheets("ch3").Cells(irow, N).Value

   'tc413/ch3-O
Worksheets("temp dist").Cells(irow + nrow + 4, 28).Value = Worksheets("ch3").Cells(irow, O).Value

   'tc414/ch3-P
Worksheets("temp dist").Cells(irow + nrow + 4, 29).Value = Worksheets("ch3").Cells(irow, P).Value

   'tc415/ch1-Q
Worksheets("temp dist").Cells(irow + nrow + 4, 30).Value = Worksheets("ch3").Cells(irow, Q).Value

'**********HOT BOTTOM **********
'INSERT AVERAGE COLD LOOP EAT/LAT AND HOT LOOP EAT/LAT FOR EACH TEMP GRID

Worksheets("temp dist").Cells(irow + nrow, 35) = sumcoldEAT / 12
Worksheets("temp dist").Cells(irow + nrow + 4, 35) = sumcoldLAT / 12
Worksheets("temp dist").Cells(irow + nrow + 2, 33) = sumhotEAT / 12
Worksheets("temp dist").Cells(irow + nrow + 2, 37) = sumhotLAT / 12

   ' tc60/ch4-J
Worksheets("temp dist").Cells(irow + nrow + 1, 34).Value = Worksheets("ch4").Cells(irow, J).Value

   ' tc61/ch4-K
Worksheets("temp dist").Cells(irow + nrow + 1, 35).Value = Worksheets("ch4").Cells(irow, K).Value

  ' tc62/ch4-L
Worksheets("temp dist").Cells(irow + nrow + 1, 36).Value = Worksheets("ch4").Cells(irow, L).Value

  ' tc63/ch4-M
Worksheets("temp dist").Cells(irow + nrow + 2, 34).Value = Worksheets("ch4").Cells(irow, M).Value

  ' tc64/ch4-N
Worksheets("temp dist").Cells(irow + nrow + 2, 35).Value = Worksheets("ch4").Cells(irow, N).Value

  ' tc65/ch4-O
Worksheets("temp dist").Cells(irow + nrow + 2, 36).Value = Worksheets("ch4").Cells(irow, O).Value

  ' tc66/ch4-P
Worksheets("temp dist").Cells(irow + nrow + 3, 34).Value = Worksheets("ch4").Cells(irow, P).Value

  ' tc67/ch4-Q
Worksheets("temp dist").Cells(irow + nrow + 3, 35).Value = Worksheets("ch4").Cells(irow, Q).Value

  ' tc58/ch4-R
Worksheets("temp dist").Cells(irow + nrow + 3, 36).Value = Worksheets("ch4").Cells(irow, R).Value

line999:

Next
Worksheets("results_summary").Cells(2, 4).Value = irowtot
'Worksheets("results_summary").Cells(2, 9).Value = irow

'CALCULATE THE OVERALL AVERAGE, MIN, MAX, VALUES FOR EACH PARAMETER

Worksheets("results_summary").Cells(4, 4).Value = T1AVESUM / irowtot
T1AVETOT = T1AVESUM / irowtot
Worksheets("results_summary").Cells(4, 5).Value = T1aveMIN
Worksheets("results_summary").Cells(4, 6).Value = T1aveMAX
```

```
Worksheets("results_summary").Cells(4, 7).Value = Abs(T1aveMAX - T1aveMIN)
T1AVESTD = (((irowtot * T1AVESQSUM) - (T1AVESUM) ^ 2) / (irowtot * (irowtot - 1))) ^ 0.5
Worksheets("results_summary").Cells(4, 8).Value = T1AVESTD
T1AVE95 = ((T1AVESTD * 2) ^ 2 + (TBIAS) ^ 2) ^ 0.5
T1AVE99 = ((T1AVESTD * 2) + (TBIAS))
Worksheets("results_summary").Cells(4, 10).Value = T1AVE95
Worksheets("results_summary").Cells(4, 11).Value = T1AVE99

Worksheets("results_summary").Cells(5, 4).Value = T1MINSUM / irowtot
Worksheets("results_summary").Cells(5, 5).Value = T1MINMIN
Worksheets("results_summary").Cells(5, 6).Value = T1MINMAX
Worksheets("results_summary").Cells(5, 7).Value = Abs(T1MINMAX - T1MINMIN)
T1MINSTD = (((irowtot * T1MINSQSUM) - (T1MINSUM) ^ 2) / (irowtot * (irowtot - 1))) ^ 0.5
Worksheets("results_summary").Cells(5, 8).Value = T1MINSTD
T1MIN95 = ((T1MINSTD * 2) ^ 2 + (TBIAS) ^ 2) ^ 0.5
T1MIN99 = ((T1MINSTD * 2) + (TBIAS))
Worksheets("results_summary").Cells(5, 10).Value = T1MIN95
Worksheets("results_summary").Cells(5, 11).Value = T1MIN99

Worksheets("results_summary").Cells(6, 4).Value = T1MAXSUM / irowtot
Worksheets("results_summary").Cells(6, 5).Value = T1MAXMIN
Worksheets("results_summary").Cells(6, 6).Value = T1MAXMAX
Worksheets("results_summary").Cells(6, 7).Value = Abs(T1MAXMAX - T1MAXMIN)
T1MAXSTD = (((irowtot * T1MAXSQSUM) - (T1MAXSUM) ^ 2) / (irowtot * (irowtot - 1))) ^ 0.5
Worksheets("results_summary").Cells(6, 8).Value = T1MAXSTD
T1MAX95 = ((T1MAXSTD * 2) ^ 2 + (TBIAS) ^ 2) ^ 0.5
T1MAX99 = ((T1MAXSTD * 2) + (TBIAS))
Worksheets("results_summary").Cells(6, 10).Value = T1MAX95
Worksheets("results_summary").Cells(6, 11).Value = T1MAX99

Worksheets("results_summary").Cells(7, 4).Value = T1RANGESUM / irowtot
Worksheets("results_summary").Cells(7, 5).Value = T1RANGEMIN
Worksheets("results_summary").Cells(7, 6).Value = T1RANGEMAX
Worksheets("results_summary").Cells(7, 7).Value = Abs(T1RANGEMAX - T1RANGEMIN)
T1RANGESTD = (((irowtot * T1RANGESQSUM) - (T1RANGESUM) ^ 2) / (irowtot * (irowtot - 1))) ^ 0.5
Worksheets("results_summary").Cells(7, 8).Value = T1RANGESTD
T1RANGE95 = ((T1RANGESTD * 2) ^ 2 + (TBIAS) ^ 2) ^ 0.5
T1RANGE99 = ((T1RANGESTD * 2) + (TBIAS))
Worksheets("results_summary").Cells(7, 10).Value = T1RANGE95
Worksheets("results_summary").Cells(7, 11).Value = T1RANGE99

T2AVETOT = T2AVESUM / irowtot
Worksheets("results_summary").Cells(8, 4).Value = T2AVETOT
Worksheets("results_summary").Cells(8, 5).Value = T2aveMIN
Worksheets("results_summary").Cells(8, 6).Value = T2aveMAX
Worksheets("results_summary").Cells(8, 7).Value = Abs(T2aveMAX - T2aveMIN)
T2AVESTD = (((irowtot * T2AVESQSUM) - (T2AVESUM) ^ 2) / (irowtot * (irowtot - 1))) ^ 0.5
Worksheets("results_summary").Cells(8, 8).Value = T2AVESTD
T2AVE95 = ((T2AVESTD * 2) ^ 2 + (TBIAS) ^ 2) ^ 0.5
T2AVE99 = ((T2AVESTD * 2) + (TBIAS))
Worksheets("results_summary").Cells(8, 10).Value = T2AVE95
Worksheets("results_summary").Cells(8, 11).Value = T2AVE99

RH2AVETOT = RH2SUM / irowtot
RH2AVESTD = (((irowtot * RH2SQSUM) - (RH2AVETOT) ^ 2) / (irowtot * (irowtot - 1))) ^ 0.5

Worksheets("results_summary").Cells(9, 4).Value = T2MINSUM / irowtot
Worksheets("results_summary").Cells(9, 5).Value = T2MINMIN
Worksheets("results_summary").Cells(9, 6).Value = T2MINMAX
Worksheets("results_summary").Cells(9, 7).Value = Abs(T2MINMAX - T2MINMIN)
T2MINSTD = (((irowtot * T2MINSQSUM) - (T2MINSUM) ^ 2) / (irowtot * (irowtot - 1))) ^ 0.5
Worksheets("results_summary").Cells(9, 8).Value = T2MINSTD
T2MIN95 = ((T2MINSTD * 2) ^ 2 + (TBIAS) ^ 2) ^ 0.5
T2MIN99 = ((T2MINSTD * 2) + (TBIAS))
Worksheets("results_summary").Cells(9, 10).Value = T2MIN95
Worksheets("results_summary").Cells(9, 11).Value = T2MIN99

Worksheets("results_summary").Cells(10, 4).Value = T2MAXSUM / irowtot
Worksheets("results_summary").Cells(10, 5).Value = T2MAXMIN
Worksheets("results_summary").Cells(10, 6).Value = T2MAXMAX
```

```
Worksheets("results_summary").Cells(10, 7).Value = Abs(T2MAXMAX - T2MAXMIN)
T2MAXSTD = (((irowtot * T2MAXSQSUM) - (T2MAXSUM) ^ 2) / (irowtot * (irowtot - 1))) ^ 0.5
Worksheets("results_summary").Cells(10, 8).Value = T2MAXSTD
T2MAX95 = ((T2MAXSTD * 2) ^ 2 + (TBIAS) ^ 2) ^ 0.5
T2MAX99 = ((T2MAXSTD * 2) + (TBIAS))
Worksheets("results_summary").Cells(10, 10).Value = T2MAX95
Worksheets("results_summary").Cells(10, 11).Value = T2MAX99

Worksheets("results_summary").Cells(11, 4).Value = T2RANGESUM / irowtot
Worksheets("results_summary").Cells(11, 5).Value = T2RANGEMIN
Worksheets("results_summary").Cells(11, 6).Value = T2RANGEMAX
Worksheets("results_summary").Cells(11, 7).Value = Abs(T2RANGEMAX - T2RANGEMIN)
T2RANGESTD = (((irowtot * T2RANGESQSUM) - (T2RANGESUM) ^ 2) / (irowtot * (irowtot - 1))) ^ 0.5
Worksheets("results_summary").Cells(11, 8).Value = T2RANGESTD
T2RANGE95 = ((T2RANGESTD * 2) ^ 2 + (TBIAS) ^ 2) ^ 0.5
T2RANGE99 = ((T2RANGESTD * 2) + (TBIAS))
Worksheets("results_summary").Cells(11, 10).Value = T2RANGE95
Worksheets("results_summary").Cells(11, 11).Value = T2RANGE99

Worksheets("results_summary").Cells(12, 4).Value = CALDENSSUM / irowtot
Worksheets("results_summary").Cells(12, 5).Value = CALDENSMIN
Worksheets("results_summary").Cells(12, 6).Value = CALDENSMAX
Worksheets("results_summary").Cells(12, 7).Value = CALDENSMAX - CALDENSMIN

CALDENSSTD = (Abs((((irowtot * CALDENSSQSUM) - (CALDENSSUM) ^ 2) / (irowtot * (irowtot - 1))))) ^ 0.5

Worksheets("results_summary").Cells(12, 8).Value = CALDENSSTD

Worksheets("results_summary").Cells(13, 4).Value = CFMCALSUM / irowtot
CFMCALAVETOT = CFMCALSUM / irowtot
Worksheets("results_summary").Cells(13, 5).Value = CFMCALMIN
Worksheets("results_summary").Cells(13, 6).Value = CFMCALMAX
Worksheets("results_summary").Cells(13, 7).Value = CFMCALMAX - CFMCALMIN
CFMCALSTD = (((irowtot * CFMCALSQSUM) - (CFMCALSUM) ^ 2) / (irowtot * (irowtot - 1))) ^ 0.5
Worksheets("results_summary").Cells(13, 8).Value = CFMCALSTD

Worksheets("results_summary").Cells(14, 4).Value = VHXCALSUM / irowtot
VHXCALAVE = VHXCALSUM / irowtot
Worksheets("results_summary").Cells(14, 5).Value = VHXCALMIN
Worksheets("results_summary").Cells(14, 6).Value = VHXCALMAX
Worksheets("results_summary").Cells(14, 7).Value = VHXCALMAX - VHXCALMIN
VHXCALSTD = (((irowtot * VHXCALSQSUM) - (VHXCALSUM) ^ 2) / (irowtot * (irowtot - 1))) ^ 0.5
Worksheets("results_summary").Cells(14, 8).Value = VHXCALSTD

Worksheets("results_summary").Cells(15, 4).Value = DELTASPCALSUM / irowtot
Worksheets("results_summary").Cells(15, 5).Value = DELTASPCALMIN
Worksheets("results_summary").Cells(15, 6).Value = DELTASPCALMAX
Worksheets("results_summary").Cells(15, 7).Value = DELTASPCALMAX - DELTASPCALMIN
DELTASPCALSTD = (((irowtot * DELTASPCALSQSUM) - (DELTASPCALSUM) ^ 2) / (irowtot * (irowtot - 1))) ^ 0.5

DELTASPCAL95 = ((DELTASPCALSTD * 2) ^ 2 + (SPBIAS ^ 2)) ^ 0.5
DELTASPCAL99 = (DELTASPCALSTD * 2) + SPBIAS
Worksheets("results_summary").Cells(15, 8).Value = DELTASPCALSTD
Worksheets("results_summary").Cells(15, 10).Value = DELTASPCAL95
Worksheets("results_summary").Cells(15, 11).Value = DELTASPCAL99
'---

Worksheets("results_summary").Cells(16, 4).Value = T3AVESUM / irowtot
T3AVETOT = T3AVESUM / irowtot
Worksheets("results_summary").Cells(16, 5).Value = T3aveMIN
Worksheets("results_summary").Cells(16, 6).Value = T3aveMAX
Worksheets("results_summary").Cells(16, 7).Value = Abs(T3aveMAX - T3aveMIN)
T3AVESTD = (((irowtot * T3AVESQSUM) - (T3AVESUM) ^ 2) / (irowtot * (irowtot - 1))) ^ 0.5
Worksheets("results_summary").Cells(16, 8).Value = T3AVESTD
T3AVE95 = ((T3AVESTD * 2) ^ 2 + (TBIAS) ^ 2) ^ 0.5
T3AVE99 = ((T3AVESTD * 2) + (TBIAS))
Worksheets("results_summary").Cells(16, 10).Value = T3AVE95
Worksheets("results_summary").Cells(16, 11).Value = T3AVE99

Worksheets("results_summary").Cells(17, 4).Value = T3MINSUM / irowtot
```

```
Worksheets("results_summary").Cells(17, 5).Value = T3MINMIN
Worksheets("results_summary").Cells(17, 6).Value = T3MINMAX
Worksheets("results_summary").Cells(17, 7).Value = Abs(T3MINMAX - T3MINMIN)
T3MINSTD = (((irowtot * T3MINSQSUM) - (T3MINSUM) ^ 2) / (irowtot * (irowtot - 1))) ^ 0.5
Worksheets("results_summary").Cells(17, 8).Value = T3MINSTD
T3MIN95 = ((T3MINSTD * 2) ^ 2 + (TBIAS) ^ 2) ^ 0.5
T3MIN99 = ((T3MINSTD * 2) + (TBIAS))
Worksheets("results_summary").Cells(17, 10).Value = T3MIN95
Worksheets("results_summary").Cells(17, 11).Value = T3MIN99

Worksheets("results_summary").Cells(18, 4).Value = T3MAXSUM / irowtot
Worksheets("results_summary").Cells(18, 5).Value = T3MAXMIN
Worksheets("results_summary").Cells(18, 6).Value = T3MAXMAX
Worksheets("results_summary").Cells(18, 7).Value = Abs(T3MAXMAX - T3MAXMIN)
T3MAXSTD = (((irowtot * T3MAXSQSUM) - (T3MAXSUM) ^ 2) / (irowtot * (irowtot - 1))) ^ 0.5
Worksheets("results_summary").Cells(18, 8).Value = T3MAXSTD
T3MAX95 = ((T3MAXSTD * 2) ^ 2 + (TBIAS) ^ 2) ^ 0.5
T3MAX99 = ((T3MAXSTD * 2) + (TBIAS))
Worksheets("results_summary").Cells(18, 10).Value = T3MAX95
Worksheets("results_summary").Cells(18, 11).Value = T3MAX99

Worksheets("results_summary").Cells(19, 4).Value = T3RANGESUM / irowtot
Worksheets("results_summary").Cells(19, 5).Value = T3RANGEMIN
Worksheets("results_summary").Cells(19, 6).Value = T3RANGEMAX
Worksheets("results_summary").Cells(19, 7).Value = Abs(T3RANGEMAX - T3RANGEMIN)
T3RANGESTD = (((irowtot * T3RANGESQSUM) - (T3RANGESUM) ^ 2) / (irowtot * (irowtot - 1))) ^ 0.5
Worksheets("results_summary").Cells(19, 8).Value = T3RANGESTD
T3RANGE95 = ((T3RANGESTD * 2) ^ 2 + (TBIAS) ^ 2) ^ 0.5
T3RANGE99 = ((T3RANGESTD * 2) + (TBIAS))
Worksheets("results_summary").Cells(19, 10).Value = T3RANGE95
Worksheets("results_summary").Cells(19, 11).Value = T3RANGE99

Worksheets("results_summary").Cells(20, 4).Value = T4AVESUM / irowtot
T4AVETOT = T4AVESUM / irowtot
Worksheets("results_summary").Cells(20, 5).Value = T4aveMIN
Worksheets("results_summary").Cells(20, 6).Value = T4aveMAX
Worksheets("results_summary").Cells(20, 7).Value = Abs(T4aveMAX - T4aveMIN)
T4AVESTD = (((irowtot * T4AVESQSUM) - (T4AVESUM) ^ 2) / (irowtot * (irowtot - 1))) ^ 0.5
Worksheets("results_summary").Cells(20, 8).Value = T4AVESTD
T4AVE95 = ((T4AVESTD * 2) ^ 2 + (TBIAS) ^ 2) ^ 0.5
T4AVE99 = ((T4AVESTD * 2) + (TBIAS))
Worksheets("results_summary").Cells(20, 10).Value = T4AVE95
Worksheets("results_summary").Cells(20, 11).Value = T4AVE99

RH4AVETOT = RH4SUM / irowtot
RH4AVESTD = (((irowtot * RH4SQSUM) - (RH4AVETOT) ^ 2) / (irowtot * (irowtot - 1))) ^ 0.5

Worksheets("results_summary").Cells(21, 4).Value = T4MINSUM / irowtot
Worksheets("results_summary").Cells(21, 5).Value = T4MINMIN
Worksheets("results_summary").Cells(21, 6).Value = T4MINMAX
Worksheets("results_summary").Cells(21, 7).Value = Abs(T4MINMAX - T4MINMIN)
T4MINSTD = (((irowtot * T4MINSQSUM) - (T4MINSUM) ^ 2) / (irowtot * (irowtot - 1))) ^ 0.5
Worksheets("results_summary").Cells(21, 8).Value = T4MINSTD
T4MIN95 = ((T4MINSTD * 2) ^ 2 + (TBIAS) ^ 2) ^ 0.5
T4MIN99 = ((T4MINSTD * 2) + (TBIAS))
Worksheets("results_summary").Cells(21, 10).Value = T4MIN95
Worksheets("results_summary").Cells(21, 11).Value = T4MIN99

Worksheets("results_summary").Cells(22, 4).Value = T4MAXSUM / irowtot
Worksheets("results_summary").Cells(22, 5).Value = T4MAXMIN
Worksheets("results_summary").Cells(22, 6).Value = T4MAXMAX
Worksheets("results_summary").Cells(22, 7).Value = Abs(T4MAXMAX - T4MAXMIN)
T4MAXSTD = (((irowtot * T4MAXSQSUM) - (T4MAXSUM) ^ 2) / (irowtot * (irowtot - 1))) ^ 0.5
Worksheets("results_summary").Cells(22, 8).Value = T4MAXSTD
T4MAX95 = ((T4MAXSTD * 2) ^ 2 + (TBIAS) ^ 2) ^ 0.5
T4MAX99 = ((T4MAXSTD * 2) + (TBIAS))
Worksheets("results_summary").Cells(22, 10).Value = T4MAX95
Worksheets("results_summary").Cells(22, 11).Value = T4MAX99

Worksheets("results_summary").Cells(23, 4).Value = T4RANGESUM / irowtot
```

```
Worksheets("results_summary").Cells(23, 5).Value = T4RANGEMIN
Worksheets("results_summary").Cells(23, 6).Value = T4RANGEMAX
Worksheets("results_summary").Cells(23, 7).Value = Abs(T4RANGEMAX - T4RANGEMIN)
T4RANGESTD = (((irowtot * T4RANGESQSUM) - (T4RANGESUM) ^ 2) / (irowtot * (irowtot - 1))) ^ 0.5
Worksheets("results_summary").Cells(23, 8).Value = T4RANGESTD
T4RANGE95 = ((T4RANGESTD * 2) ^ 2 + (TBIAS) ^ 2) ^ 0.5
T4RANGE99 = ((T4RANGESTD * 2) + (TBIAS))
Worksheets("results_summary").Cells(23, 10).Value = T4RANGE95
Worksheets("results_summary").Cells(23, 11).Value = T4RANGE99


Worksheets("results_summary").Cells(24, 4).Value = HALDENSSUM / irowtot
Worksheets("results_summary").Cells(24, 5).Value = HALDENSMIN
Worksheets("results_summary").Cells(24, 6).Value = HALDENSMAX
Worksheets("results_summary").Cells(24, 7).Value = HALDENSMAX - HALDENSMIN

HALDENSSTD = (Abs((((irowtot * HALDENSSQSUM) - (HALDENSSUM) ^ 2) / (irowtot * (irowtot - 1))))) ^ 0.5

Worksheets("results_summary").Cells(24, 8).Value = HALDENSSTD

Worksheets("results_summary").Cells(25, 4).Value = CFMHALSUM / irowtot
CFMHALAVETOT = CFMHALSUM / irowtot
Worksheets("results_summary").Cells(25, 5).Value = CFMHALMIN
Worksheets("results_summary").Cells(25, 6).Value = CFMHALMAX
Worksheets("results_summary").Cells(25, 7).Value = CFMHALMAX - CFMHALMIN
CFMHALSTD = (((irowtot * CFMHALSQSUM) - (CFMHALSUM) ^ 2) / (irowtot * (irowtot - 1))) ^ 0.5
Worksheets("results_summary").Cells(25, 8).Value = CFMHALSTD

Worksheets("results_summary").Cells(26, 4).Value = VHXHALSUM / irowtot
Worksheets("results_summary").Cells(26, 5).Value = VHXHALMIN
Worksheets("results_summary").Cells(26, 6).Value = VHXHALMAX
Worksheets("results_summary").Cells(26, 7).Value = VHXHALMAX - VHXHALMIN
VHXHALSTD = (((irowtot * VHXHALSQSUM) - (VHXHALSUM) ^ 2) / (irowtot * (irowtot - 1))) ^ 0.5
Worksheets("results_summary").Cells(26, 8).Value = VHXHALSTD

Worksheets("results_summary").Cells(27, 4).Value = DELTASPHALSUM / irowtot
Worksheets("results_summary").Cells(27, 5).Value = DELTASPHALMIN
Worksheets("results_summary").Cells(27, 6).Value = DELTASPHALMAX
Worksheets("results_summary").Cells(27, 7).Value = DELTASPHALMAX - DELTASPHALMIN
DELTASPHALSTD = (((irowtot * DELTASPHALSQSUM) - (DELTASPHALSUM) ^ 2) / (irowtot * (irowtot - 1))) ^ 0.5
DELTASPHAL95 = ((DELTASPHALSTD * 2) ^ 2 + (SPBIAS ^ 2)) ^ 0.5
DELTASPHAL99 = (DELTASPHALSTD * 2) + SPBIAS
Worksheets("results_summary").Cells(27, 8).Value = DELTASPHALSTD
Worksheets("results_summary").Cells(27, 10).Value = DELTASPHAL95
Worksheets("results_summary").Cells(27, 11).Value = DELTASPHAL99

Worksheets("results_summary").Cells(28, 4).Value = CFMCALCFMHALSUM / irowtot
Worksheets("results_summary").Cells(28, 5).Value = CFMCALCFMHALMIN
Worksheets("results_summary").Cells(28, 6).Value = CFMCALCFMHALMAX
Worksheets("results_summary").Cells(28, 7).Value = CFMCALCFMHALMAX - CFMCALCFMHALMIN
CFMCALCFMHALSTD = (((irowtot * CFMCALCFMHALSQSUM) - (CFMCALCFMHALSUM) ^ 2) / (irowtot * (irowtot - 1))) ^
0.5
Worksheets("results_summary").Cells(28, 8).Value = CFMCALCFMHALSTD

'Worksheets("results_summary").Cells(29, 4).Value = TEMPEFFSUPSUM / irowtot
'Worksheets("results_summary").Cells(29, 5).Value = TEMPEFFSUPMIN
'Worksheets("results_summary").Cells(29, 6).Value = TEMPEFFSUPMAX
'Worksheets("results_summary").Cells(29, 7).Value = TEMPEFFSUPMAX - TEMPEFFSUPMIN
'TEMPEFFSUPSTD = (((irowtot * TEMPEFFSUPSQSUM) - (TEMPEFFSUPSUM) ^ 2) / (irowtot * (irowtot - 1))) ^ 0.5
'Worksheets("results_summary").Cells(29, 8).Value = TEMPEFFSUPSTD

Worksheets("results_summary").Cells(29, 4).Value = EFFSUPSUM / irowtot
Worksheets("results_summary").Cells(29, 5).Value = EFFSUPMIN
Worksheets("results_summary").Cells(29, 6).Value = EFFSUPMAX
Worksheets("results_summary").Cells(29, 7).Value = EFFSUPMAX - EFFSUPMIN
'EFFSUPSTD = (((irowtot * EFFSUPSQSUM) - (EFFSUPSUM) ^ 2) / (irowtot * (irowtot - 1))) ^ 0.5
Worksheets("results_summary").Cells(29, 8).Value = EFFSUPSTD

Worksheets("results_summary").Cells(30, 4).Value = EFFEXHSUM / irowtot
Worksheets("results_summary").Cells(30, 5).Value = EFFEXHMIN
```

```
Worksheets("results_summary").Cells(30, 6).Value = EFFEXHMAX
Worksheets("results_summary").Cells(30, 7).Value = EFFEXHMAX - EFFEXHMIN

Worksheets("results_summary").Cells(31, 4).Value = EFFAVESUM / irowtot
Worksheets("results_summary").Cells(31, 5).Value = EFFAVEMIN
Worksheets("results_summary").Cells(31, 6).Value = EFFAVEMAX
Worksheets("results_summary").Cells(31, 7).Value = EFFAVEMAX - EFFAVEMIN

'CALCULATION OF PRECISION UNCERTAINTY VARIABLES
'  ***** COLD AIR LOOP  ********
'      SATURATED WATER VAPOR PRESSURE IN COLD AIR LOOP
PWSCALC8 = (C8) / (T2AVETOT + 459.67)
PWSCALC10 = C10 * (T2AVETOT + 459.67)
PWSCALC11 = C11 * ((T2AVETOT + 459.67) ^ 2)
PWSCALC12 = C12 * ((T2AVETOT + 459.67) ^ 3)
PWSCALC13 = C13 * ((Log(T2AVETOT + 459.67) / Log(2.718282)))
PWSCAL = (2.036) * Exp(PWSCALC8 + C9 + PWSCALC10 + PWSCALC11 + PWSCALC12 + PWSCALC13)
PWSCALC8D = C8 / ((T2AVETOT + 459.67) ^ 2)
PWSCALC11D = 2 * C11 * (T2AVETOT + 459.67)
PWSCALC12D = 3 * C12 * ((T2AVETOT + 459.67) ^ 2)
DPWSCALDT = PWSCAL * (C10 - PWSCALC8D + PWSCALC11D + PWSCALC12D + (C13 / (T2AVETOT + 459.67)))
UPWSCAL = DPWSCALDT * T2AVESTD
Worksheets("uncert").Cells(2, 3).Value = PWSCAL
Worksheets("uncert").Cells(2, 4).Value = UPWSCAL

'      VAPOR PRESSURE IN COLD AIR LOOP

UpwCAL = ((PWSCAL * RH2AVESTD) ^ 2 + (RH2AVETOT * UPWSCAL) ^ 2) ^ 0.5
PwCAL = RH2AVETOT * PWSCAL
Worksheets("uncert").Cells(3, 3).Value = PwCAL
Worksheets("uncert").Cells(3, 4).Value = UpwCAL

'      HUMIDITY RATIO IN COLD AIR LOOP
Wcal = 0.62198 * (PwCAL / (PB - PwCAL))
UWcal = 0.62198 * (1 / (PwCAL * (((PB / PwCAL) - 1) ^ 2))) * UpwCAL
Worksheets("uncert").Cells(4, 3).Value = Wcal
Worksheets("uncert").Cells(4, 4).Value = UWcal
Worksheets("uncert").Cells(5, 3).Value = RH2AVETOT
Worksheets("uncert").Cells(5, 4).Value = RH2AVESTD


'      MOIST AIR DENSITY IN COLD AIR LOOP
CALDENSAVE = PB / (0.7543 * (T2AVETOT + 459.67) * (1 + 1.6078 * Wcal))
UCALDENSAVE1 = (-PB / (0.7543 * (1 + 1.6078 * Wcal) * (T2AVETOT + 459.67) ^ 2) * T2AVESTD) ^ 2
UCALDENSAVE2 = (-PB / (0.7543 * ((1 + 1.6078 * Wcal) ^ 2) * (T2AVETOT + 459.67)) * UWcal) ^ 2
UCALDENSAVE = (UCALDENSAVE1 + UCALDENSAVE2) ^ 0.5
Worksheets("uncert").Cells(6, 3).Value = CALDENSAVE
Worksheets("uncert").Cells(6, 4).Value = UCALDENSAVE

'      VELOCITY PRESSURE IN COLD AIR LOOP
VPCALAVE = VPCALSUM / irowtot
VPCALSTD = (((irowtot * VPCALSQSUM) - (VPCALSUM) ^ 2) / (irowtot * (irowtot - 1))) ^ 0.5
Worksheets("uncert").Cells(7, 3).Value = VPCALAVE
Worksheets("uncert").Cells(7, 4).Value = VPCALSTD

'      AIR VELOCITY IN COLD AIR LOOP
VELCALAVE = 1096 * (VPCALAVE / CALDENSAVE) ^ 0.5
UVELCAL1 = ((0.5) * (VPCALAVE / CALDENSAVE) ^ (-0.5) * VPCALSTD) ^ 2
UVELCAL2 = ((-0.5) * (VPCALAVE / CALDENSAVE) ^ (-1.5) * UCALDENSAVE) ^ 2
UVELCAL = (UVELCAL1 + UVELCAL2) ^ 0.5
Worksheets("uncert").Cells(8, 3).Value = VELCALAVE
Worksheets("uncert").Cells(8, 4).Value = UVELCAL

'      MASS AIR FLOW RATE IN COLD AIR LOOP
MCALAVE = CALDENSAVE * VELCALAVE * DUCTAREA
UMCALAVE1 = (VELCALAVE * DUCTAREA * UCALDENSAVE) ^ 2
UMCALAVE2 = (CALDENSAVE * DUCTAREA * UVELCAL) ^ 2
UMCALAVE = (UMCALAVE1 + UMCALAVE2) ^ 0.5
Worksheets("uncert").Cells(9, 3).Value = MCALAVE
Worksheets("uncert").Cells(9, 4).Value = UMCALAVE
```

```
'********HOT AIR LOOP******
'     SATURATED WATER VAPOR PRESSURE IN HOT AIR LOOP
PWSHALC8 = (C8) / (T4AVETOT + 459.67)
PWSHALC10 = C10 * (T4AVETOT + 459.67)
PWSHALC11 = C11 * ((T4AVETOT + 459.67) ^ 2)
PWSHAL12 = C12 * ((T4AVETOT + 459.67) ^ 3)
PWSHAL13 = C13 * ((Log(T4AVETOT + 459.67) / Log(2.718282)))
PWSHAL = (2.036) * Exp(PWSHALC8 + C9 + PWSHALC10 + PWSHALC11 + PWSHAL12 + PWSHAL13)
PWSHALC8D = C8 / ((T4AVETOT + 459.67) ^ 2)
PWSHAL11D = 2 * C11 * (T4AVETOT + 459.67)
PWSHAL12D = 3 * C12 * ((T4AVETOT + 459.67) ^ 2)
DPWSHALDT = PWSHAL * (C10 - PWSHALC8D + PWSHAL11D + PWSHAL12D + (C13 / (T4AVETOT + 459.67)))
UPWSHAL = DPWSHALDT * T4AVESTD
Worksheets("uncert").Cells(10, 3).Value = PWSHAL
Worksheets("uncert").Cells(10, 4).Value = UPWSHAL

'     VAPOR PRESSURE IN HOLD AIR LOOP

UpwHAL = ((PWSHAL * RH4AVESTD) ^ 2 + (RH4AVETOT * UPWSHAL) ^ 2) ^ 0.5
PwHAL = RH4AVETOT * PWSHAL
Worksheets("uncert").Cells(11, 3).Value = PwHAL
Worksheets("uncert").Cells(11, 4).Value = UpwHAL

'     HUMIDITY RATIO IN HOLD AIR LOOP
Whal = 0.62198 * (PwHAL / (PB - PwHAL))
UWhal = 0.62198 * (1 / (PwHAL * (((PB / PwHAL) - 1) ^ 2))) * UpwHAL
Worksheets("uncert").Cells(12, 3).Value = Whal
Worksheets("uncert").Cells(12, 4).Value = UWhal
Worksheets("uncert").Cells(13, 3).Value = RH4AVETOT
Worksheets("uncert").Cells(13, 4).Value = RH4AVESTD

'     MOIST AIR DENSITY IN HOLD AIR LOOP
HALDENSAVE = PB / (0.7543 * (T4AVETOT + 459.67) * (1 + 1.6078 * Whal))
UHALDENSAVE1 = (-PB / (0.7543 * (1 + 1.6078 * Whal) * (T4AVETOT + 459.67) ^ 2) * T4AVESTD) ^ 2
UHALDENSAVE2 = (-PB / (0.7543 * ((1 + 1.6078 * Whal) ^ 2) * (T4AVETOT + 459.67)) * UWhal) ^ 2
UHALDENSAVE = (UHALDENSAVE1 + UHALDENSAVE2) ^ 0.5
Worksheets("uncert").Cells(14, 3).Value = HALDENSAVE
Worksheets("uncert").Cells(14, 4).Value = UHALDENSAVE

'     VELOCITY PRESSURE IN HOLD AIR LOOP
VPHALAVE = VPHALSUM / irowtot
VPHALSTD = (((irowtot * VPHALSQSUM) - (VPHALSUM) ^ 2) / (irowtot * (irowtot - 1))) ^ 0.5
Worksheets("uncert").Cells(15, 3).Value = VPHALAVE
Worksheets("uncert").Cells(15, 4).Value = VPHALSTD

'     AIR VELOCITY IN HOLD AIR LOOP
VELHALAVE = 1096 * (VPHALAVE / HALDENSAVE) ^ 0.5
UVELHAL1 = ((0.5) * (VPHALAVE / HALDENSAVE) ^ (-0.5) * VPHALSTD) ^ 2
UVELHAL2 = ((-0.5) * (VPHALAVE / HALDENSAVE) ^ (-1.5) * UHALDENSAVE) ^ 2
UVELHAL = (UVELHAL1 + UVELHAL2) ^ 0.5
Worksheets("uncert").Cells(16, 3).Value = VELHALAVE
Worksheets("uncert").Cells(16, 4).Value = UVELHAL


'     MASS AIR FLOW RATE IN HOLD AIR LOOP
MHALAVE = HALDENSAVE * VELHALAVE * DUCTAREA
UMHALAVE1 = (VELHALAVE * DUCTAREA * UHALDENSAVE) ^ 2
UMHALAVE2 = (HALDENSAVE * DUCTAREA * UVELHAL) ^ 2
UMHALAVE = (UMHALAVE1 + UMHALAVE2) ^ 0.5
Worksheets("uncert").Cells(17, 3).Value = MHALAVE
Worksheets("uncert").Cells(17, 4).Value = UMHALAVE

'     EFFECTIVENESS

If MHALAVE < MCALAVE Then
MMINA = MHALAVE
UMMINA = UMHALAVE
End If
If MCALAVE < MHALAVE Then
```

```
MMINA = MCALAVE
UMMINA = UMCALAVE
End If

EFFSUP = (MCALAVE / MMINA) * ((T2AVETOT - T1AVETOT) / (T3AVETOT - T1AVETOT))
EFFEXH = (MHALAVE / MMINA) * ((T3AVETOT - T4AVETOT) / (T3AVETOT - T1AVETOT))
EFFAVE1 = (MCALAVE * (T2AVETOT - T1AVETOT) + MHALAVE * (T3AVETOT - T4AVETOT))
EFFAVE2 = 2 * MMIN * (T3AVETOT - T1AVETOT)
EFFAVE = EFFAVE1 / EFFAVE2

UEFFSUP1 = ((1 / MMINA) * ((T2AVETOT - T1AVETOT) / (T3AVETOT - T1AVETOT))) * UMCALAVE
UEFFSUP2 = (((-MCALAVE) / (MMINA ^ 2)) * ((T2AVETOT - T1AVETOT) / (T3AVETOT - T1AVETOT))) * UMMINA
UEFFSUP3 = (MCALAVE / MMINA) * ((T2AVETOT - T1AVETOT) / ((T3AVETOT - T1AVETOT) ^ 2)) * T1AVESTD
UEFFSUP4 = ((MCALAVE / MMINA) * (1 / (T3AVETOT - T1AVETOT))) * T2AVESTD
UEFFSUP5 = (MCALAVE / MMINA) * ((T2AVETOT - T1AVETOT) / ((T3AVETOT - T1AVETOT) ^ 2)) * T3AVESTD
UEFFSUP = (UEFFSUP1 ^ 2 + UEFFSUP2 ^ 2 + UEFFSUP3 ^ 2 + UEFFSUP4 ^ 2 + UEFFSUP5 ^ 2) ^ 0.5
Worksheets("uncert").Cells(18, 3).Value = EFFSUP
Worksheets("uncert").Cells(18, 4).Value = UEFFSUP
Worksheets("results_summary").Cells(29, 8).Value = UEFFSUP

UEFFEXH1 = ((1 / MMINA) * ((T3AVETOT - T4AVETOT) / (T3AVETOT - T1AVETOT))) * UMHALAVE
UEFFEXH2 = (((-MHALAVE) / (MMINA ^ 2)) * ((T2AVETOT - T1AVETOT) / (T3AVETOT - T1AVETOT))) * UMMINA
UEFFEXH3 = ((-MHALAVE) / MMINA) * ((T3AVETOT - T4AVETOT) / ((T3AVETOT - T1AVETOT) ^ 2)) * T1AVESTD
UEFFEXH4 = ((MHALAVE / MMINA) * ((T4AVETOT - T1AVETOT) / ((T3AVETOT - T1AVETOT) ^ 2))) * T3AVESTD
UEFFEXH5 = (((-MHALAVE) / MMINA) * (1 / (T3AVETOT - T1AVETOT))) * T4AVESTD
UEFFEXH = (UEFFEXH1 ^ 2 + UEFFEXH2 ^ 2 + UEFFEXH3 ^ 2 + UEFFEXH4 ^ 2 + UEFFEXH5 ^ 2) ^ 0.5
Worksheets("uncert").Cells(19, 3).Value = EFFEXH
Worksheets("uncert").Cells(19, 4).Value = UEFFEXH
Worksheets("results_summary").Cells(30, 8).Value = UEFFEXH

UEFFAVE1 = ((T2AVETOT - T1AVETOT) / ((2 * MMINA) * (T3AVETOT - T1AVETOT))) * UMCALAVE
UEFFAVE2 = ((T3AVETOT - T4AVETOT) / ((2 * MMINA) * (T3AVETOT - T1AVETOT))) * UMHALAVE
UEFFAVE3A = (-1) * (MCALAVE * (T2AVETOT - T1AVETOT) + MHALAVE * (T3AVETOT - T4AVETOT))
UEFFAVE3 = ((UEFFAVE3A) / (2 * (MMINA ^ 2) * (T3AVETOT - T1AVETOT))) * UMMINA
UEFFAVE4A = (MCALAVE * (T2AVETOT - T3AVETOT) + MHALAVE * (T3AVETOT - T4AVETOT))
UEFFAVE4 = (UEFFAVE4A / (2 * MMINA * ((T3AVETOT - T1AVETOT) ^ 2))) * T1AVESTD
UEFFAVE5 = MCALAVE / (2 * MMINA * (T3AVETOT - T1AVETOT)) * T2AVESTD
UEFFAVE6A = MCALAVE * (T2AVETOT - T1AVETOT) + MHALAVE * (T3AVETOT - T4AVETOT)
UEFFAVE6 = (UEFFAVE6A / (2 * MMINA * ((T3AVETOT - T1AVETOT) ^ 2))) * T3AVESTD
UEFFAVE7 = (-MHALAVE) / (2 * MMINA * (T3AVETOT - T1AVETOT)) * T4AVESTD
UEFFAVET1 = UEFFAVE1 ^ 2 + UEFFAVE2 ^ 2 + UEFFAVE3 ^ 2 + UEFFAVE4 ^ 2 + UEFFAVE5 ^ 2
UEFFAVE = (UEFFAVET1 + UEFFAVE6 ^ 2 + UEFFAVE7 ^ 2) ^ 0.5
Worksheets("uncert").Cells(20, 3).Value = EFFAVE
Worksheets("uncert").Cells(20, 4).Value = UEFFAVE
Worksheets("results_summary").Cells(31, 8).Value = UEFFAVE

'BIAS CALCULATIONS
'  ***** COLD AIR LOOP  ********
'       TEMPERATURE
Worksheets("results_summary").Cells(4, 9).Value = TBIAS
Worksheets("results_summary").Cells(16, 9).Value = TBIAS

'     SATURATED WATER VAPOR PRESSURE IN COLD AIR LOOP
UPWSCALB = DPWSCALDT * TBIAS
Worksheets("uncert").Cells(2, 5).Value = UPWSCALB

'     VAPOR PRESSURE IN COLD AIR LOOP
UpwCALB = ((PWSCAL * RHBIAS) ^ 2 + (RH2AVETOT * UPWSCALB) ^ 2) ^ 0.5
Worksheets("uncert").Cells(3, 5).Value = UpwCALB

'     HUMIDITY RATIO IN COLD AIR LOOP
UWcalB1 = 0.62198 * (1 / (PwCAL * (((PB / PwCAL) - 1) ^ 2))) * UpwCALB
UWcalB2 = ((-0.62198) * (PwCAL) / ((PB - PwCAL) ^ 2)) * PBBIAS
UWcalB = ((UWcalB1 ^ 2) + (UWcalB2 ^ 2)) ^ 0.5
Worksheets("uncert").Cells(4, 5).Value = UWcalB

'     MOIST AIR DENSITY IN COLD AIR LOOP
UCALDENSAVEB1 = (-PB / (0.7543 * (1 + 1.6078 * Wcal) * (T2AVETOT + 459.67) ^ 2) * TBIAS) ^ 2
UCALDENSAVEB2 = (-PB / (0.7543 * ((1 + 1.6078 * Wcal) ^ 2) * (T2AVETOT + 459.67)) * UWcalB) ^ 2
UCALDENSAVEB3 = (1 / (0.7543 * (T2AVETOT + 459.67) * (1 + 1.6078 * Wcal)) * PBBIAS) ^ 2
```

```
UCALDENSAVEB = (UCALDENSAVEB1 + UCALDENSAVEB2 + UCALDENSAVEB3) ^ 0.5
UCALDENS95 = ((UCALDENSAVE * 2) ^ 2 + (UCALDENSAVEB ^ 2)) ^ 0.5
UCALDENS99 = (UCALDENSAVE * 2) + UCALDENSAVEB
Worksheets("uncert").Cells(5, 5).Value = RHBIAS
Worksheets("uncert").Cells(6, 5).Value = UCALDENSAVEB
Worksheets("results_summary").Cells(12, 9).Value = UCALDENSAVEB
Worksheets("results_summary").Cells(12, 10).Value = UCALDENS95
Worksheets("results_summary").Cells(12, 11).Value = UCALDENS99

'     AIR VELOCITY IN COLD AIR LOOP
UVELCALB1 = ((0.5) * (VPCALAVE / CALDENSAVE) ^ (-0.5) * VPBIAS) ^ 2
UVELCALB2 = ((-0.5) * (VPCALAVE / CALDENSAVE) ^ (-1.5) * UCALDENSAVEB) ^ 2
UVELCALB = (UVELCALB1 + UVELCALB2) ^ 0.5
Worksheets("uncert").Cells(7, 5).Value = VPBIAS
Worksheets("uncert").Cells(8, 5).Value = UVELCALB

'     MASS AIR FLOW RATE IN COLD AIR LOOP
UMCALAVEB1 = (VELCALAVE * DUCTAREA * UCALDENSAVEB) ^ 2
UMCALAVEB2 = (CALDENSAVE * DUCTAREA * UVELCALB) ^ 2
UMCALAVEB3 = (CALDENSAVE * VELCALAVE * (1.414 * Length * LBIAS)) ^ 2
UMCALAVEB = (UMCALAVEB1 + UMCALAVEB2 + UMCALAVEB3) ^ 0.5

UQCALAVEB1 = (DUCTAREA * UVELCALB) ^ 2
UQCALAVEB2 = (VELCALAVE * (1.414 * Length * LBIAS)) ^ 2
UQCALAVEB = (UQCALAVEB1 + UQCALAVEB2) ^ 0.5
UQCAL95 = ((CFMCALSTD * 2) ^ 2 + (UQCALAVEB ^ 2)) ^ 0.5
UQCAL99 = (CFMCALSTD * 2) + UQCALAVEB


Worksheets("results_summary").Cells(13, 9).Value = UQCALAVEB
Worksheets("results_summary").Cells(13, 10).Value = UQCAL95
Worksheets("results_summary").Cells(13, 11).Value = UQCAL99
Worksheets("results_summary").Cells(15, 9).Value = SPBIAS

'     FACE VELOCITY ACROSS HEAT EXCHANGER IN COLD LOOP
UVHXCALB1 = (((1 / HXAREA) * UQCALAVEB)) ^ 2
UVHXCALB2 = (((-UQCALAVEB) / (HXAREA ^ 2)) * (1.414 * Length * LBIAS)) ^ 2
UVHXCALB = (UVHXCALB1 + UVHXCALB2) ^ 0.5
UVHXCAL95 = ((VHXCALSTD * 2) ^ 2 + (UVHXCALB ^ 2)) ^ 0.5
UVHXCAL99 = (VHXCALSTD * 2) + (UVHXCALB ^ 2)
Worksheets("results_summary").Cells(14, 9).Value = UVHXCALB
Worksheets("results_summary").Cells(14, 10).Value = UVHXCAL95
Worksheets("results_summary").Cells(14, 11).Value = UVHXCAL99


'     HOT AIR LOOP BIAS

'     SATURATED WATER VAPOR PRESSURE IN HOT AIR LOOP
UPWSHALB = DPWSHALDT * TBIAS
Worksheets("uncert").Cells(10, 5).Value = UPWSHALB

'     VAPOR PRESSURE IN HOT AIR LOOP
UpwHALB = ((PWSHAL * RHBIAS) ^ 2 + (RH4AVETOT * UPWSHALB) ^ 2) ^ 0.5
Worksheets("uncert").Cells(11, 5).Value = UpwHALB

'     HUMIDITY RATIO IN HOT AIR LOOP
UWhalB1 = 0.62198 * (1 / (PwHAL * (((PB / PwHAL) - 1) ^ 2))) * UpwHALB
UWhalB2 = ((-0.62198) * (PwHAL) / ((PB - PwHAL) ^ 2)) * PBBIAS
UWhalB = ((UWhalB1 ^ 2) + (UWhalB2 ^ 2)) ^ 0.5
Worksheets("uncert").Cells(12, 5).Value = UWhalB

'     MOIST AIR DENSITY IN HOT AIR LOOP
UHALDENSAVEB1 = (-PB / (0.7543 * (1 + 1.6078 * Whal) * (T4AVETOT + 459.67) ^ 2) * TBIAS) ^ 2
UHALDENSAVEB2 = (-PB / (0.7543 * ((1 + 1.6078 * Whal) ^ 2) * (T4AVETOT + 459.67)) * UWhalB) ^ 2
UHALDENSAVEB3 = (1 / (0.7543 * (T4AVETOT + 459.67) * (1 + 1.6078 * Whal)) * PBBIAS) ^ 2
UHALDENSAVEB = (UHALDENSAVEB1 + UHALDENSAVEB2 + UHALDENSAVEB3) ^ 0.5
UHALDENS95 = ((UHALDENSAVE * 2) ^ 2 + (UHALDENSAVEB ^ 2)) ^ 0.5
UHALDENS99 = (UHALDENSAVE * 2) + UHALDENSAVEB
Worksheets("uncert").Cells(13, 5).Value = RHBIAS
Worksheets("uncert").Cells(14, 5).Value = UHALDENSAVEB
```

```
Worksheets("results_summary").Cells(24, 9).Value = UHALDENSAVEB
Worksheets("results_summary").Cells(24, 10).Value = UHALDENS95
Worksheets("results_summary").Cells(24, 11).Value = UHALDENS99

'      AIR VELOCITY IN HOT AIR LOOP
UVELHALB1 = ((0.5) * (VPHALAVE / HALDENSAVE) ^ (-0.5) * VPBIAS) ^ 2
UVELHALB2 = ((-0.5) * (VPHALAVE / HALDENSAVE) ^ (-1.5) * UHALDENSAVEB) ^ 2
UVELHALB = (UVELHALB1 + UVELHALB2) ^ 0.5
Worksheets("uncert").Cells(15, 5).Value = VPBIAS
Worksheets("uncert").Cells(16, 5).Value = UVELHALB



'      MASS AIR FLOW RATE IN HOT AIR LOOP
UMHALAVEB1 = (VELHALAVE * DUCTAREA * UHALDENSAVEB) ^ 2
UMHALAVEB2 = (CALDENSAVE * DUCTAREA * UVELHALB) ^ 2
UMHALAVEB3 = (HALDENSAVE * VELHALAVE * (1.414 * Length * LBIAS)) ^ 2
UMHALAVEB = (UMHALAVEB1 + UMHALAVEB2 + UMHALAVEB3) ^ 0.5
Worksheets("uncert").Cells(17, 5).Value = UMHALAVEB

UQHALAVEB1 = (DUCTAREA * UVELHALB) ^ 2
UQHALAVEB2 = (VELHALAVE * (1.414 * Length * LBIAS)) ^ 2
UQHALAVEB = (UQHALAVEB1 + UQHALAVEB2) ^ 0.5
UQHAL95 = ((CFMHALSTD * 2) ^ 2 + (UQHALAVEB ^ 2)) ^ 0.5
UQHAL99 = (CFMHALSTD * 2) + UQHALAVEB

UQCALQHALB1 = ((1 / (DUCTAREA * VELHALAVE)) * UQCALAVEB)
UQCALQHALB2 = (((-1) * DUCTAREA * VELCALAVE / ((DUCTAREA * VELHALAVE) ^ 2)) * UQHALAVEB)
UQCALQHALB = (UQCALQHALB1 ^ 2 + UQHALQHALB1 ^ 2) ^ 0.5
UQCALQHAL95 = (((CFMCALCFMHALSTD * 2) ^ 2) + (UQCALQHALB ^ 2)) ^ 0.5
UQCALQHAL99 = (CFMCALCFMHALSTD * 2) + UQCALQHALB

Worksheets("results_summary").Cells(25, 9).Value = UQHALAVEB
Worksheets("results_summary").Cells(25, 10).Value = UQHAL95
Worksheets("results_summary").Cells(25, 11).Value = UQHAL99
Worksheets("results_summary").Cells(28, 9).Value = UQCALQHALB
Worksheets("results_summary").Cells(28, 10).Value = UQCALQHAL95
Worksheets("results_summary").Cells(28, 11).Value = UQCALQHAL99
Worksheets("results_summary").Cells(27, 9).Value = SPBIAS

'      FACE VELOCITY ACROSS HX IN HOT AIR LOOP
UVHXHALB1 = (((1 / HXAREA) * UQHALAVEB)) ^ 2
UVHXHALB2 = (((-UQHALAVEB) / (HXAREA ^ 2)) * (1.414 * Length * LBIAS)) ^ 2
UVHXHALB = (UVHXHALB1 + UVHXHALB2) ^ 2
UVHXHAL95 = ((VHXHALSTD * 2) ^ 2 + (UVHXHALB ^ 2)) ^ 0.5
UVHXHAL99 = (VHXHALSTD * 2) + (UVHXHALB ^ 2)
Worksheets("results_summary").Cells(26, 9).Value = UVHXHALB
Worksheets("results_summary").Cells(26, 10).Value = UVHXHAL95
Worksheets("results_summary").Cells(26, 11).Value = UVHXHAL99

'      EFFECTIVENESS BIAS UNCERTAINTY
If MHALAVE < MCALAVE Then
UMMINAB = UMHALAVEB
End If
If MCALAVE < MHALAVE Then
UMMINAB = UMCALAVEB
End If
UEFFSUPB1 = ((1 / MMINA) * ((T2AVETOT - T1AVETOT) / (T3AVETOT - T1AVETOT))) * UMCALAVEB
UEFFSUPB2 = (((-MCALAVE) / (MMINA ^ 2)) * ((T2AVETOT - T1AVETOT) / (T3AVETOT - T1AVETOT))) * UMMINAB
UEFFSUPB3 = (MCALAVE / MMINA) * ((T2AVETOT - T1AVETOT) / ((T3AVETOT - T1AVETOT) ^ 2)) * TBIAS
UEFFSUPB4 = ((MCALAVE / MMINA) * (1 / (T3AVETOT - T1AVETOT))) * TBIAS
UEFFSUPB5 = (MCALAVE / MMINA) * ((T2AVETOT - T1AVETOT) / ((T3AVETOT - T1AVETOT) ^ 2)) * TBIAS
UEFFSUPB = (UEFFSUPB1 ^ 2 + UEFFSUPB2 ^ 2 + UEFFSUPB3 ^ 2 + UEFFSUPB4 ^ 2 + UEFFSUPB5 ^ 2) ^ 0.5
UEFFSUP95 = ((UEFFSUP * 2) ^ 2 + (UEFFSUPB) ^ 2) ^ 0.5
UEFFSUP99 = (UEFFSUP * 2) + UEFFSUPB
Worksheets("uncert").Cells(18, 5).Value = UEFFSUPB
Worksheets("results_summary").Cells(29, 9).Value = UEFFSUPB
Worksheets("results_summary").Cells(29, 10).Value = UEFFSUP95
Worksheets("results_summary").Cells(29, 11).Value = UEFFSUP99
```

```
UEFFEXHB1 = ((1 / MMINA) * ((T3AVETOT - T4AVETOT) / (T3AVETOT - T1AVETOT))) * UMHALAVEB
UEFFEXHB2 = (((-MHALAVE) / (MMINA ^ 2)) * ((T2AVETOT - T1AVETOT) / (T3AVETOT - T1AVETOT))) * UMMINAB
UEFFEXHB3 = ((-MHALAVE) / MMINA) * ((T3AVETOT - T4AVETOT) / ((T3AVETOT - T1AVETOT) ^ 2)) * TBIAS
UEFFEXHB4 = ((MHALAVE / MMINA) * ((T4AVETOT - T1AVETOT) / ((T3AVETOT - T1AVETOT) ^ 2))) * TBIAS
UEFFEXHB5 = (((-MHALAVE) / MMINA) * (1 / (T3AVETOT - T1AVETOT))) * TBIAS
UEFFEXHB = (UEFFEXHB1 ^ 2 + UEFFEXHB2 ^ 2 + UEFFEXHB3 ^ 2 + UEFFEXHB4 ^ 2 + UEFFEXHB5 ^ 2) ^ 0.5
UEFFEXH95 = ((UEFFEXH * 2) ^ 2 + (UEFFEXHB) ^ 2) ^ 0.5
UEFFEXH99 = (UEFFEXH * 2) + UEFFEXHB
Worksheets("uncert").Cells(19, 5).Value = UEFFEXHB
Worksheets("results_summary").Cells(30, 9).Value = UEFFEXHB
Worksheets("results_summary").Cells(30, 10).Value = UEFFEXH95
Worksheets("results_summary").Cells(30, 11).Value = UEFFEXH99

UEFFAVEB1 = ((T2AVETOT - T1AVETOT) / ((2 * MMINA) * (T3AVETOT - T1AVETOT))) * UMCALAVEB
UEFFAVEB2 = ((T3AVETOT - T4AVETOT) / ((2 * MMINA) * (T3AVETOT - T1AVETOT))) * UMHALAVEB
UEFFAVEB3A = (-1) * (MCALAVE * (T2AVETOT - T1AVETOT) + MHALAVE * (T3AVETOT - T4AVETOT))
UEFFAVEB3 = ((UEFFAVE3A) / (2 * (MMINA ^ 2) * (T3AVETOT - T1AVETOT))) * UMMINAB
UEFFAVEB4A = (MCALAVE * (T2AVETOT - T3AVETOT) + MHALAVE * (T3AVETOT - T4AVETOT))
UEFFAVEB4 = (UEFFAVE4A / (2 * MMINA * ((T3AVETOT - T1AVETOT) ^ 2))) * TBIAS
UEFFAVEB5 = MCALAVE / (2 * MMINA * (T3AVETOT - T1AVETOT)) * TBIAS
UEFFAVEB6A = MCALAVE * (T2AVETOT - T1AVETOT) + MHALAVE * (T3AVETOT - T4AVETOT)
UEFFAVEB6 = (UEFFAVE6A / (2 * MMINA * ((T3AVETOT - T1AVETOT) ^ 2))) * TBIAS
UEFFAVEB7 = (-MHALAVE) / (2 * MMINA * (T3AVETOT - T1AVETOT)) * TBIAS
UEFFAVEBT1 = UEFFAVEB1 ^ 2 + UEFFAVEB2 ^ 2 + UEFFAVEB3 ^ 2 + UEFFAVEB4 ^ 2 + UEFFAVEB5 ^ 2
UEFFAVEB = (UEFFAVEBT1 + UEFFAVEB6 ^ 2 + UEFFAVEB7 ^ 2) ^ 0.5
UEFFAVE95 = ((UEFFAVE * 2) ^ 2 + (UEFFAVEB) ^ 2) ^ 0.5
UEFFAVE99 = (UEFFAVE * 2) + UEFFAVEB
Worksheets("uncert").Cells(20, 5).Value = UEFFAVEB
Worksheets("results_summary").Cells(31, 9).Value = UEFFAVEB
Worksheets("results_summary").Cells(31, 10).Value = UEFFAVE95
Worksheets("results_summary").Cells(31, 11).Value = UEFFAVE99

End Sub
'Function STDEV(irowtot, XSQSUM, XSUM)
'STDEV = (((irowtot * XSQSUM) - (XSUM) ^ 2) / (irowtot * (irowtot - 1))) ^ 0.5
'End Function
```

APPENDIX D: TEMPERATURE DISTRIBUTION ON TOP, MIDDLE AND BOTTOM PLANE FOR 1870 CFM (882 L/s)

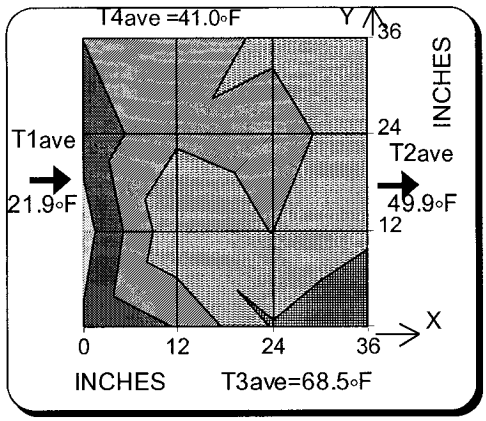

a) Cold air loop, top plane

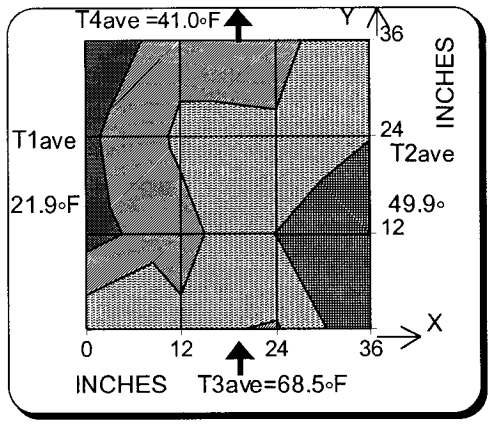

b) Hot air loop, top plane

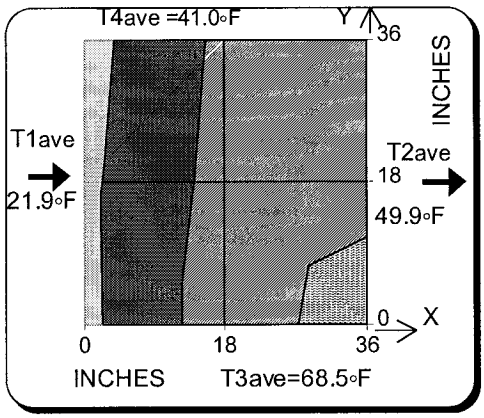

c) Cold air loop, middle plane

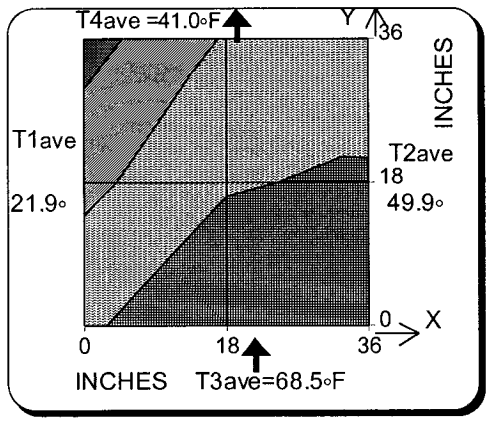

d) Hot air loop, middle plane

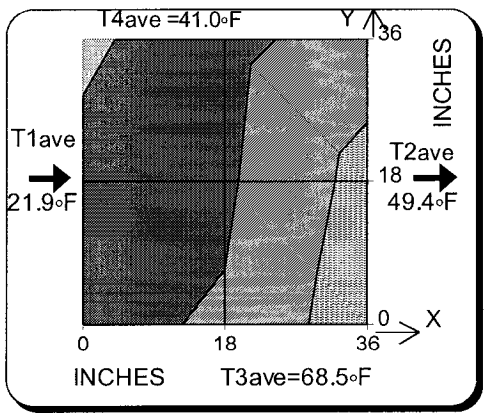

e) Cold air loop, bottom plane

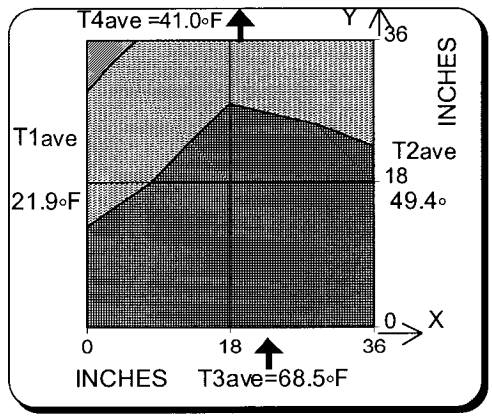

f) Hot air loop, bottom plane

Temperature distribution for balanced airflows, Qcal=1853 CFM (873 L/s) and Qhal=1869 CFM (882 L/s) at top, middle, and bottom planes on both the cold air and hot air loop side

APPENDIX E: TEMPERATURE DISTRIBUTIONS FOR ASSYMMETRIC OBSTRUCTIONS LOCATED ON HOT AIR LOOP

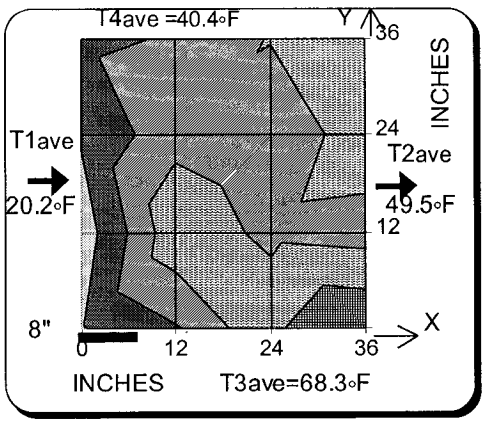

a) Cold loop temperature distribution

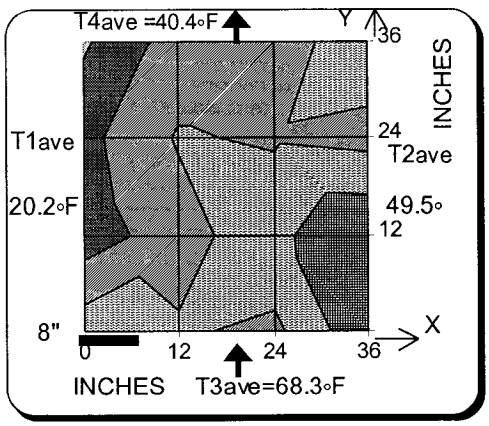

b) Hot loop temperature distribution

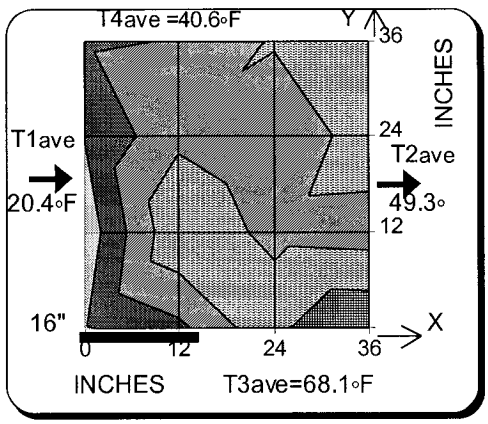

c) Cold loop temperature distribution

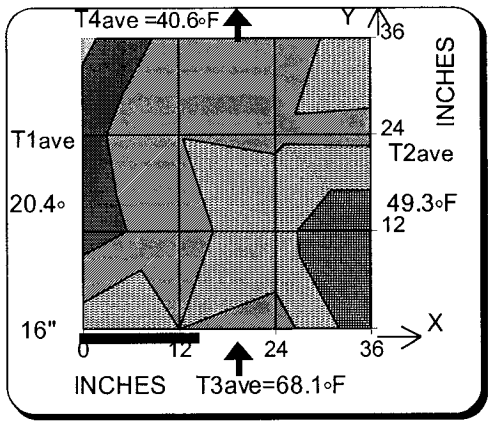

d) Hot loop temperature distribution

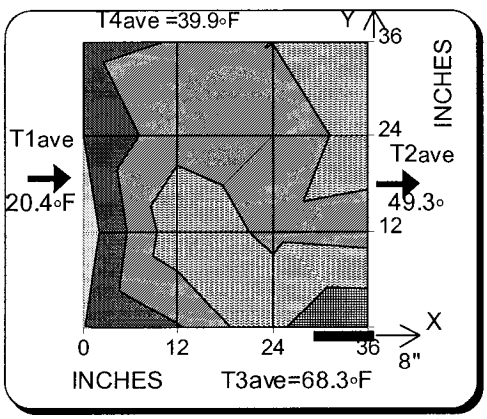

e) Cold loop temperature distribution

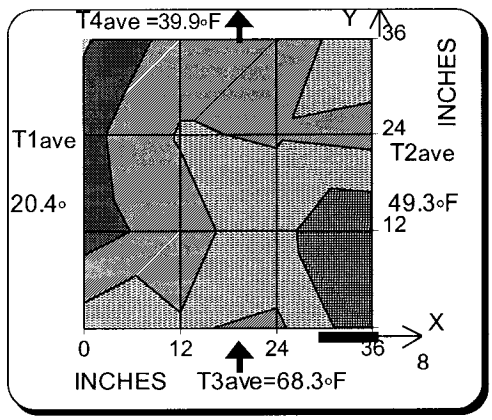

f) Hot loop temperature distribution

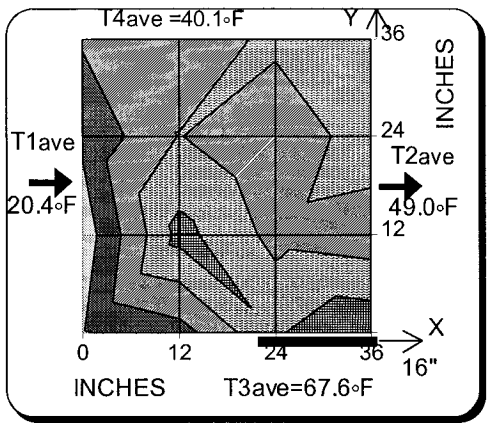

g) Cold loop temperature distribution

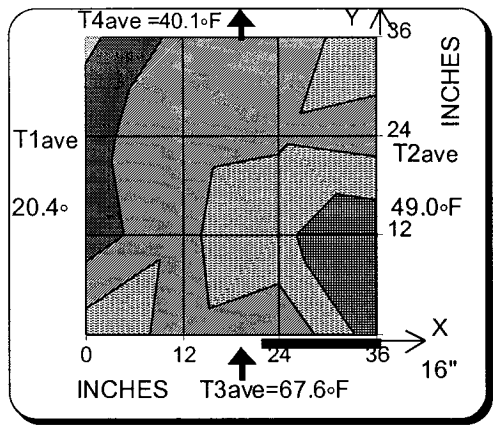

h) Hot loop temperature distribution

Temperature distributions within the plate heat exchanger for 8" (203 mm) and 16" (406mm) asymmetric obstructions located on the hot loop side for 1500 CFM (708 L/s) balanced airflow

APPENDIX F: POST TEST UNCERTAINTY ANALYSIS FOR UNBALANCED AIRFLOW EFFECTIVENESS TEST

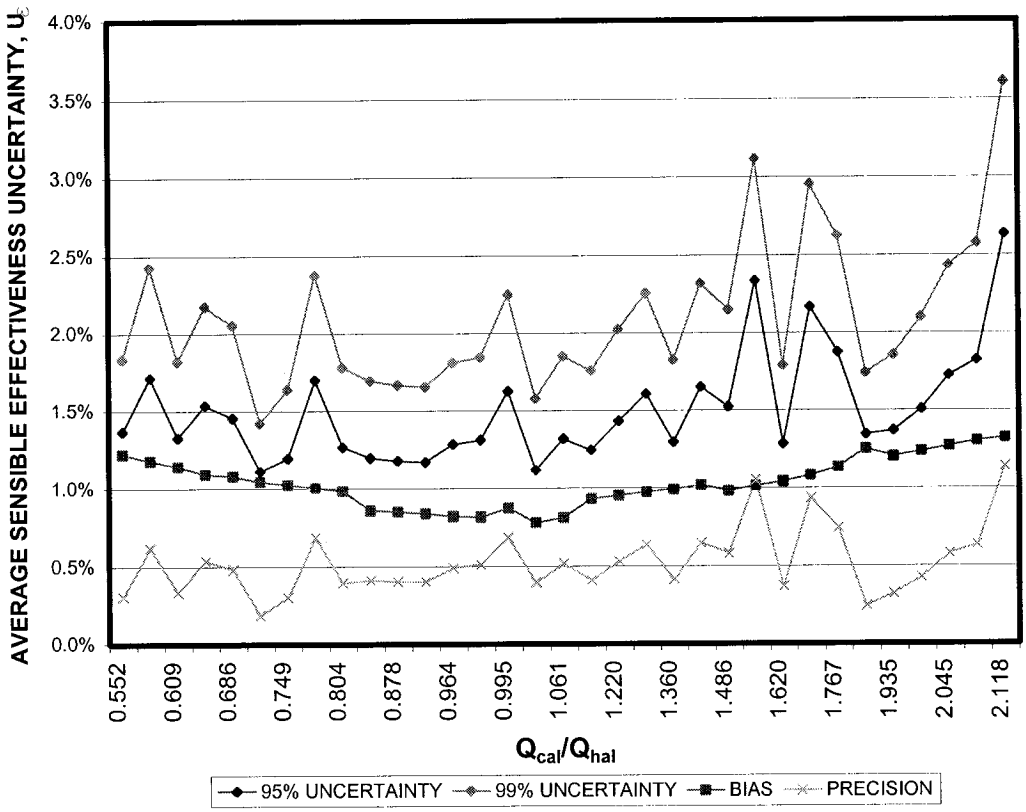

Sensible effectiveness uncertainty for unbalanced airflow tests ranging from Q_{cal}/Q_{cal} = 0.552 to Q_{cal}/Q_{cal} = 2.118